

NASA Conference Publication 10190

Computational Materials Research

Edited by

*Jeffrey A. Hinkley and Thomas S. Gates
Langley Research Center • Hampton, Virginia*

Proceedings of a workshop sponsored by the
National Aeronautics and Space Administration,
Washington, D.C., and held at
The College of William and Mary,
Williamsburg, Virginia
January 4–5, 1996

November 1996

Printed copies available from the following:

NASA Center for AeroSpace Information
800 Elkridge Landing Road
Linthicum Heights, MD 21090-2934
(301) 621-0390

National Technical Information Service (NTIS)
5285 Port Royal Road
Springfield, VA 22161-2171
(703) 487-4650

Table of Contents

| Title | Page |
|---|------------|
| Foreword | 2 |
| Molecular Modeling of Polyimides | 3 |
| Molecular Mechanics and Molecular Dynamics | 27 |
| Effect of Molecular Weight on Properties of LaRCTM - SI | 50 |
| Molecular Modeling of Novel Piezoelectric Polyimides | 77 |
| Monte Carlo Simulation of a Polyimide Melt | 98 |
| Equation of State Measurements: Thermal Pressure Coefficient of an Imide-Ketone Model Compound | 118 |
| Mechanical Properties from Acoustical Measurements on LaRCTM - SI | 124 |
| Predicting Bulk Polymer Properties from Molecular Structure | 155 |
| Multiaxial and Time Dependent Response of Rigid Polymers | 206 |
| Static and Viscoelastic Testing/ Modeling of LaRCTM - SI | 238 |

Foreword

NASA-Langley's Computational Materials program began in October 1994. The interdisciplinary team representing NASA Centers, universities, and industry met formally for the first time in January 1995 at LaRC.

One year later, with some changes in personnel, the group assembled again, this time at The College of William and Mary, to review the technical progress that had been made and to identify future directions. The present document is a collection of the technical charts presented at that two-day workshop.

The concept of Computational Materials requires model development at size scales ranging from atomic dimensions to the macroscopic, and times ranging from picoseconds to weeks. The LaRC program therefore adopts a hierarchical approach, with careful attention paid to the links between disciplines. This collection of papers is presented in order of increasing scale, as follows:

| Workshop Participant | Discipline | Scale |
|--|-----------------------------|-------------------------------|
| G. D. Smith, U. Missouri-Columbia | Quantum/molecular mechanics | Subatomic to molecular |
| B. L. Farmer U. Virginia | Molecular mechanics | Molecular |
| E. J. Siochi Lockheed | Physical chemistry | Molecular |
| J. A. Young U. Virginia | Molecular dynamics | Molecular assemblies |
| E. J. Dawnkaski College of William & Mary | Monte Carlo simulation | Molecular assemblies |
| R. A. Orwoll College of William & Mary | Chemical Thermodynamics | Liquids |
| T. Yost, J. Cantrell NASA LaRC | Physics | Solids |
| W. W. Welsh | Chemistry; statistics | Molecular to continuum |
| W. G. Knauss California Inst. of Tech. | Constitutive models | Continuum |
| T. S. Gates NASA LaRC | Viscoplasticity | Micromechanics to macroscopic |



Molecular Modeling of Polyimides

Grant D. Smith

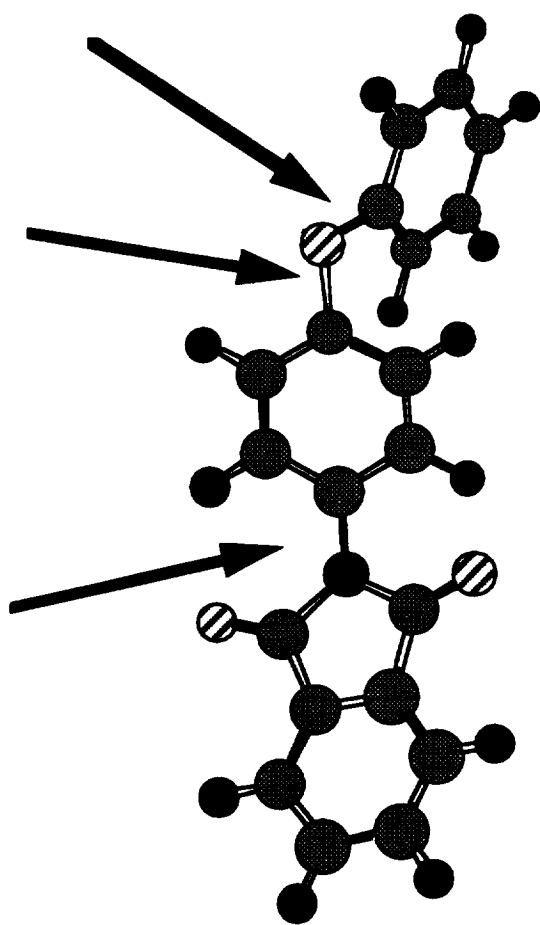
*Department of Chemical Engineering
University of Missouri-Columbia*

University of Missouri-Columbia

Outline

- Ab initio quantum chemistry studies of a model imide
- Force field for a model imide
- Molecular dynamics simulations of a model imide
- Future work and directions

Structure of the model ether-imide



Bonded parameters

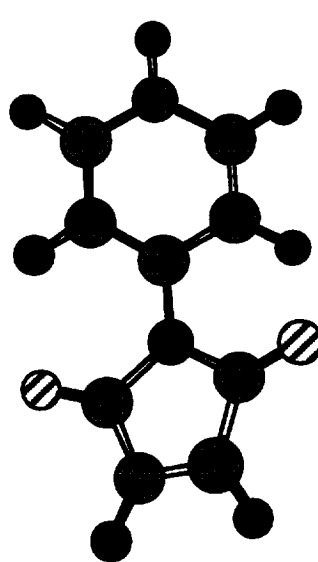
- From 6-31G** SCF optimized geometry

| σ | Bond Stretch | Constrained | (Å) |
|---|--------------|-------------|------|
| C _i =O (carbonyl) ^a | | | 1.19 |
| C-O (ether) | | | 1.38 |
| C-H | | | 1.07 |
| C=C | | | 1.38 |
| C _i -N | | | 1.43 |
| C-C _i | | | 1.49 |

Bonded parameters, cont.

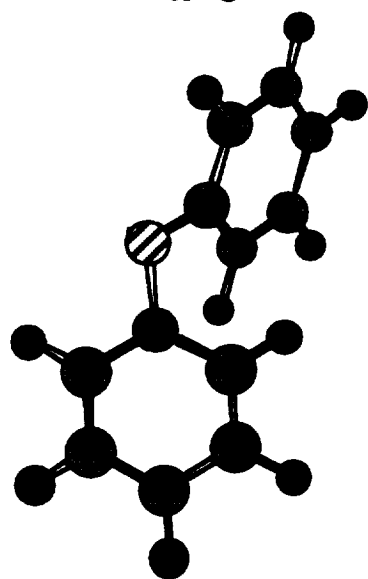
| Valence Bend | $E_{ijk} = 0.5 k_{ijk} (\theta_{ijl} - \theta_{ijl}^{\circ})^2$ | k_{ijk} (kcal/mol rad ²) | θ_{ijl}° |
|----------------------------------|---|--|------------------------|
| C-C-N | | 144. | 1.817 |
| C-C-C _i ^b | | 100.8 | 1.882 |
| C-C-C _i ^e | | 100.8 | 2.286 |
| C _i -N-C _i | | 115.2 | 1.988 |
| C-C _i -O | | 144. | 2.253 |
| C-C-C | | 144. | 2.094 |
| C-C-H | | 72. | 2.094 |
| C _i -N-C | | 115.2 | 2.148 |
| C-O-C | | 148.6 | 2.072 |
| C-C-O | | 100.8 | 2.094 |
| N-C _i -O | | 100.8 | 2.1991 |
| N-C-C | | 115.2 | 2.094 |

Torsional characteristics



6-31G+**

minimum = 52.4 °
perp = 0.38 kcal/mol (9.8)
planar = 3.03 kcal/mol (4.7)



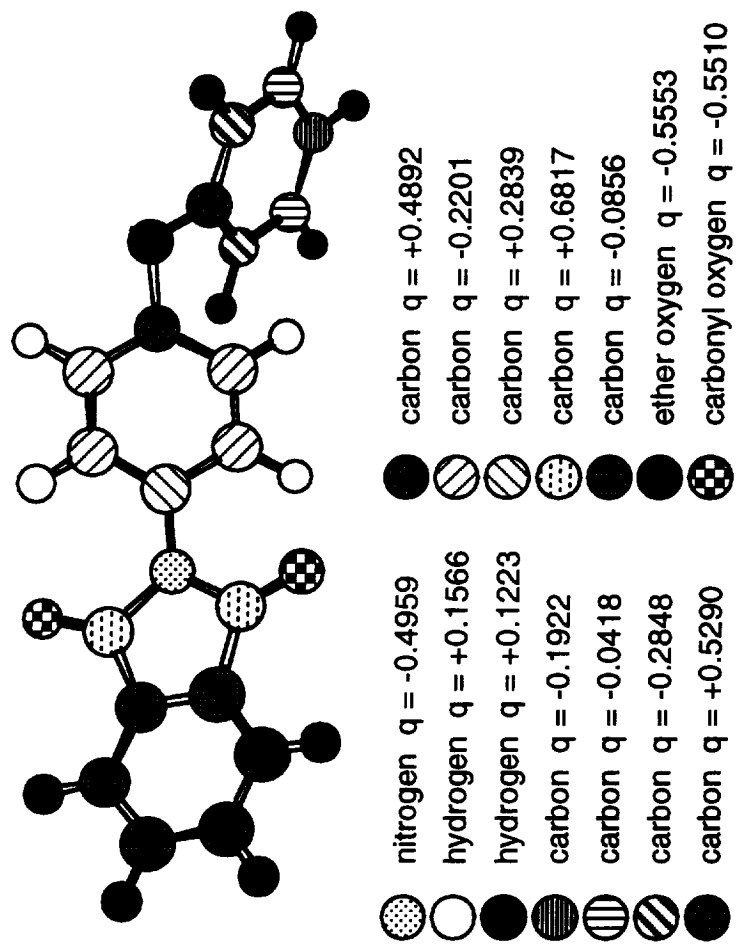
6-31G*

single = 2.5 kcal/mol (3.7)
double = 0.0 kcal/mol (1.2)

Partial atomic charges

- Charges were determined from electrostatic potential method--This method involves calculating the electrostatic potential for a grid of points around the molecule and best reproducing this with a distribution of partial atomic charges

Partial atomic charges, cont.

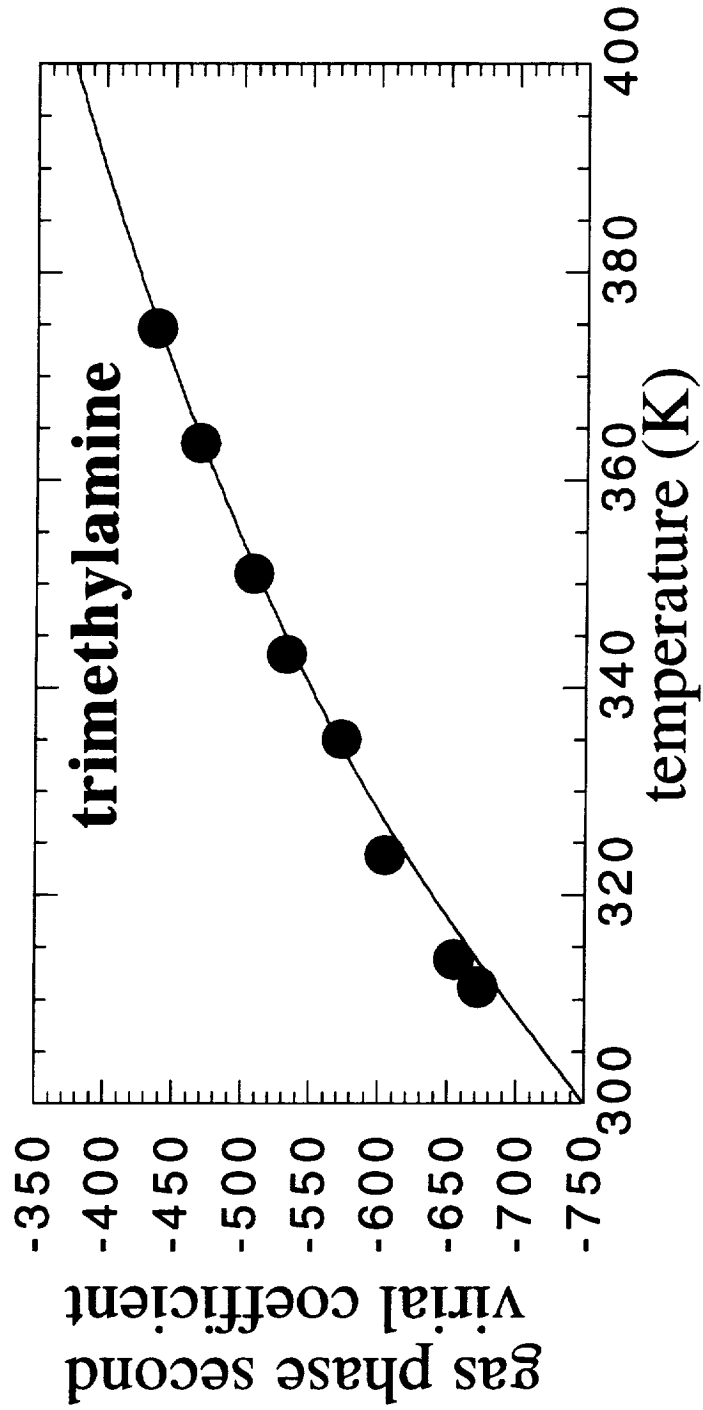


Nonbonded parameters

- Dispersion/repulsion parameters were mostly taken from our previous work
- Extensive quantum chemistry and MD studies of benzene revealed the importance of including hydrogen atoms
- Oxygen parameters were taken from our work with model ethers

Nonbonded parameters, cont.

- Nitrogen Parameters were adjusted to match second virial coefficient data



Nonbonded parameters

| Nonbonded Dispersion/Repulsion | $E_{ij} = A_{ij} \exp(-B_{ij}r_{ij}) - C_{ij}/r_{ij}^6$ (kcal/mol) | A_{ij} (kcal/mol) | B_{ij} (Å) | C_{ij} kcal/mol Å ⁶ |
|-----------------------------------|---|------------------------|-----------------|-------------------------------------|
| C-C | 78988. | 3.6 | 519.3 | |
| O-O | 75845. | 4.063 | 398.9 | |
| O-C | 77400.5 | 3.8315 | 455.1 | |
| O-H | 13448.4 | 3.902 | 99.1 | |
| O-N | 67926.0 | 3.922 | 446.6 | |
| C-H | 38888.0 | 3.415 | 124.416 | |
| C-N | 69323.6 | 3.69 | 509.6 | |
| H-H | 2384.6 | 3.74 | 24.624 | |
| H-N | 28122. | 4.252 | 127.7 | |
| N-N | 60833.9 | 3.780 | 500.0 | |

Out-of-plane deformation

- Parameters were taken from the empirical force field of Boyd

| Out-of-plane deformation | $E_{ijkl} = 0.5k_{ijkl}\delta^2$ | k_{ijkl} (kcal/mol rad ²) |
|------------------------------------|----------------------------------|---|
| C-C*H-C | | 41.76 |
| C-C*C _i -C | | 115.2 |
| C-C _i *O-N | | 115.2 |
| C _i -N*C-C _i | | 43.2 |
| C-C*N-C | | 115.2 |
| C-C*O-C | | 115.2 |

Molecular dynamics simulations

- 100 ether-imide molecules
- Ewald summation
- 5 fs time step (hydrogen atom positions constrained)
- Box = 36 Å

Density

- Experimental density measurements have been performed from 436 to 473 K.
- At 473 K, a constant volume simulation at experimental density yields a pressure of ~700 atmospheres.
- At 473 K, a constant pressure simulation at 1 atmosphere yields a density about 4% greater than experiment.

Thermal expansion

- At 1 atmosphere, thermal expansion over the experimental temperature range is $7.7 \times 10^{-4} /K$
- The experimental value is $6.8 \times 10^{-4}/K$

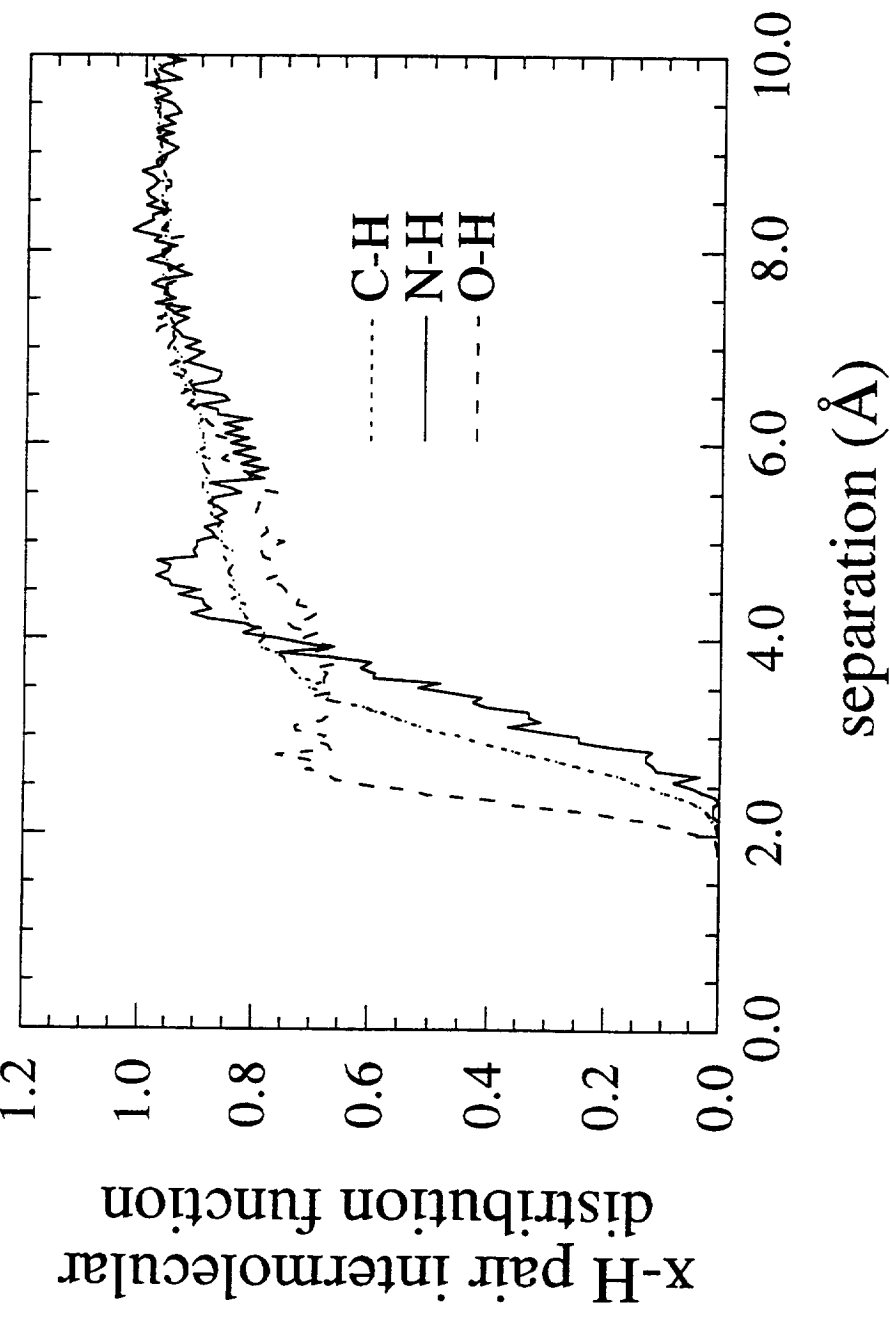
Sensitivity of density to force field parameters

- The density is insensitive to intramolecular parameters
- The density does is not very sensitive to electrostatic interaction*
- We are investigating the sensitivity of the density to nonbonded parameters

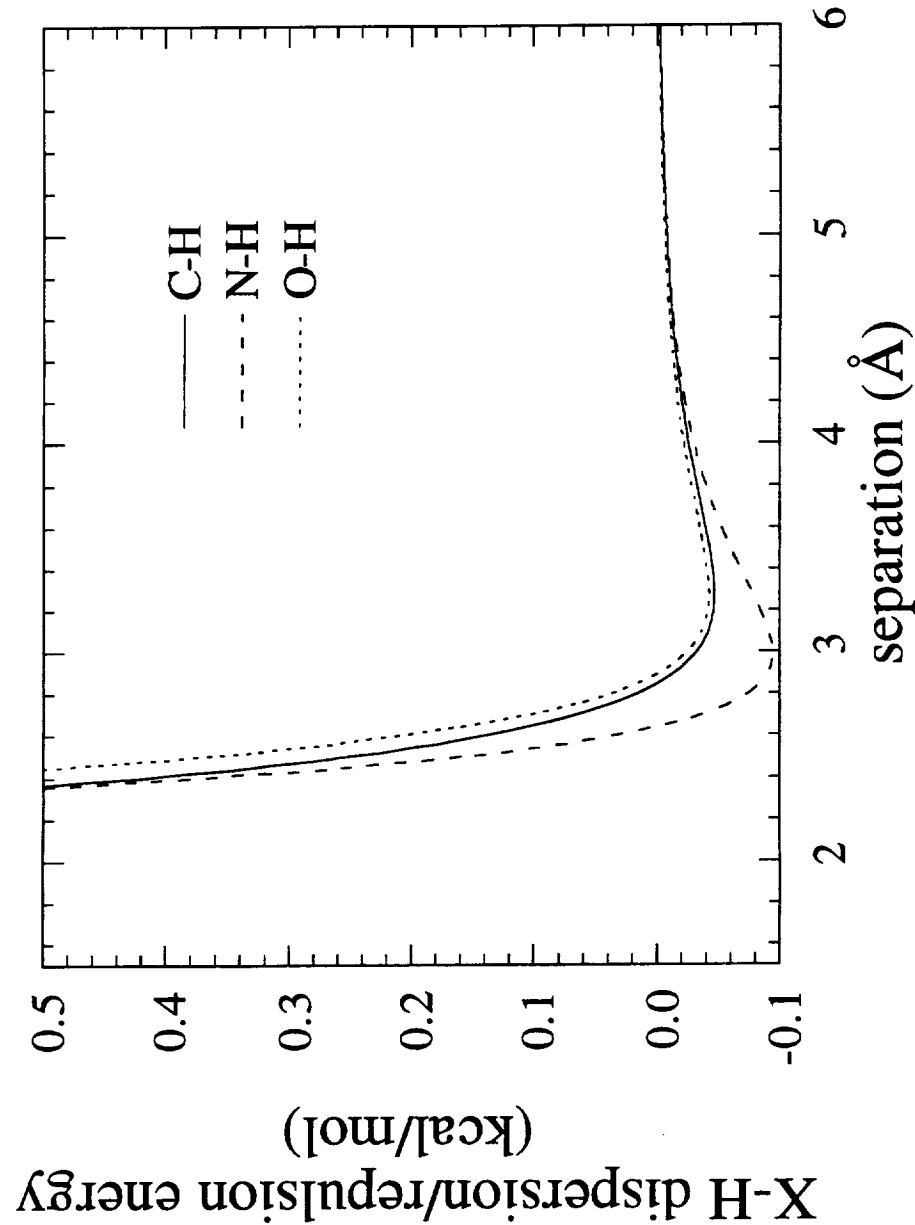
Pair distribution functions

- We have begun looking for important intermolecular interactions by examining pair distribution functions

Pair distribution functions, cont.



Pair distribution functions, cont.



Ongoing work

- PVT measurements of internal energy
- Force field parameterization for ketone-imide
- Fine-tuning of force fields
- MD simulation of model imide liquids

Key issues and future work

- Determine the most interesting chemical modifications to investigate
- Learn how to best interact with people further up the food chain-- including experimentalists and continuum models
- Apply techniques to interface, additives, etc.

Acknowledgments

- Dr. Richard Jaffe, NASA Ames Research Center
- Mr. Steven Shi

Table I
Quantum Chemistry Based Force Field for Ether-Imide

| Type | Energy Function | Parameters | |
|---|--|--|------------------------|
| <u>Bond Stretch</u> | <u>Constrained</u> | (Å) | |
| C _i =O (carbonyl) ^a | | 1.19 | |
| C-O (ether) | | 1.38 | |
| C-H | | 1.07 | |
| C=C | | 1.38 | |
| C _i -N | | 1.43 | |
| C- C _i | | 1.49 | |
| Valence Bend | $E_{ijk} = 0.5 k_{ijk}(\theta_{ijl} - \theta^{\circ}_{ijl})^2$ | k_{ijk} (kcal/mol rad ²) | θ°_{ijl} |
| C-C _i -N | | 144. | 1.817 |
| C-C-C _i ^b | | 100.8 | 1.882 |
| C-C-C _i ^c | | 100.8 | 2.286 |
| C _i -N-C _i | | 115.2 | 1.988 |
| C-C _i -O | | 144. | 2.253 |
| C-C-C | | 144. | 2.094 |
| C-C-H | | 72. | 2.094 |
| C _i -N-C | | 115.2 | 2.148 |
| C-O-C | | 148.6 | 2.072 |
| C-C-O | | 100.8 | 2.094 |
| N-C _i -O | | 100.8 | 2.1991 |
| N-C-C | | 115.2 | 2.094 |

| Torsion | $E_{ijkl} = 0.5[k^2_{ijkl} (1-\cos(2\phi_{ijll})) + k^4_{ijkl} (1-\cos(4\phi_{ijll}))]$ | k^2_{ijkl} (kcal/mol) | k^4_{ijkl} |
|-------------------------------------|---|-------------------------|--------------|
| C-C-C-C | | 25.92 | 0.00 |
| C-C-C-H | | 0.00 | 0.00 |
| H-C-C-H | | 0.00 | 0.00 |
| C _i -C-C-C | | 0.00 | 0.00 |
| C _i -C-C-H | | 0.00 | 0.00 |
| C _i -C-C-C _i | | 0.00 | 0.00 |
| O-C _i -C-C | | 0.00 | 0.00 |
| N-C _i -C-C | | 0.72 | 0.00 |
| C-N-C _i -C | | 0.00 | 0.00 |
| C-N-C _i -O | | 14.40 | 0.00 |
| C-C-O-C | | 0.86 | 0.00 |
| C-C-C-O | | 0.00 | 0.00 |
| H-C-C-O | | 0.00 | 0.00 |
| C-C _i -C-O | | 0.00 | 0.00 |
| C _i -N-C _i -O | | 7.06 | 0.00 |
| C-C-N-C _i | | 1.20 | 0.26 |
| N-C-C-C | | 0.00 | 0.00 |
| N-C-C-H | | 0.00 | 0.00 |

William & Mary Computational Materials Workshop

January, 1996

Barry L. Farmer

Retrospective Summary

(including both material presented and insight gained from resulting discussions)

The UVA (on-grounds) effort has focused on exploring the validity of the Tripos force field for computing the interactions between a graphite surface and a polyimide chain. Validation has proceeded along two paths.

The first validation path has involved comparison of calculations using the Tripos force field with the results of semiempirical molecular orbital and *ab initio* calculations for pairs of molecules, e.g. methane, formaldehyde, and trimethyl amine with benzene. The comparisons have not been good. However, rather than point to a deficiency in the empirical (Tripos) force field, the results underscore the inability of the molecular orbital and *ab initio* methods to properly represent dispersion interactions except when very extensive basis sets are employed. Thus the validation of the Tripos force field lies more correctly in the comparisons with experimental data than with the results with the more fundamental computational methods.

The second validation pathway involves calculations of the association between various small molecules (corresponding to representative fragments of polyimides) and a section of a graphitic surface (specifically, a coronene molecule) were made. These were compared with previous computational results based on more elegant treatments of the interaction potential developed to reproduce experimental data. Both the interaction energy *versus* distance curve and the geometry of the minimum energy association calculated using the Tripos force field for benzene on graphite were in good agreement with the previous model and data. In addition,

comparisons of the experimental heats of adsorption of other molecular fragments with graphitic substrates were generally in good agreement with the calculated interaction energies.

Another aspect of the semiempirical molecular orbital and *ab initio* calculations results however is both useful and interesting. Graphite, as a material, is electrically conductive. The effects of this conductivity on graphite's interactions with adsorbing material has apparently not been studied previously in the context of modern computational methods. (This neglect may arise in fact from the inability of molecular orbital calculations to provide a reasonable treatment of dispersion forces). A dipole in the vicinity of a conducting (metal) surface interacts electrostatically with an image dipole as well as through dispersion effects with the substrate atoms. The image interaction is about an order of magnitude smaller than the dispersive ones. This indicates that, overall, "summation of dispersion and repulsive energies" may indeed be a good approximation for computing the interaction energies of adsorbate molecules with graphite. At the same time, ignoring the image interactions may lead to underestimation of the role of the dipolar moieties of the polyimides on the interactions with the graphite substrate. The size of these effects will determine whether we will need to modify the potential function parameters to get a reasonable representation of the behavior of a polyimide on a graphite substrate. Since the interaction is electrostatic, the results of semiempirical molecular orbital and *ab initio* calculations should be valid in spite of the inability of these methods to properly account for dispersion interactions.

The calculations to date indicate that the partial charges in the adsorbing molecule and those on the atoms of the "substrate" molecule (benzene, naphthalene, coronene) change to a small extent as the separation distance changes. As expected, the charges on the substrate atoms nearest the adsorbate change individually more than those at greater distances, drawing upon contributions from its own several neighbors. The perturbations in electron distribution extend out from the location of the adsorbate, but they are damped in magnitude.

Figure Captions and Annotations

Note:

Sybyl does molecular mechanics calculations using a classical description of the force field.
Spartan does semiempirical molecular orbital (quantum mechanical) calculations.

1. Title
2. Polyimides of Interest
3. Energy (and partial atomic charge on methane hydrogen) versus separation distance between benzene and methane calculated using Spartan (semiempirical molecular orbital methods).
4. Energy (and partial atomic charge on fluorine) versus separation distance between benzene and perfluoromethane calculated using Spartan (semiempirical molecular orbital methods).
5. Energy (and partial atomic charge on nitrogen) versus separation distance between benzene and trimethylamine calculated using Spartan (semiempirical molecular orbital methods).
6. Energy (and partial atomic charge on oxygen) versus separation distance between benzene and formaldehyde calculated using Spartan (semiempirical molecular orbital methods).
7. Charges on the formaldehyde carbon and oxygen and three of the benzene carbons as a function of distance between benzene and formaldehyde (calculated using Spartan semiempirical molecular orbital methods).

These date show that the proximity of a polar (carbonyl) group perturbs the distribution of charges in the benzene molecule. What might be the effect of polar groups proximate to delocalized ring systems such as naphthalene, anthracene, coronene, and ultimately, graphite.

8. Charges on the formaldehyde carbon and oxygen and three of the naphthalene carbons in Ring 1 as a function of distance between naphthalene and formaldehyde (calculated using Spartan semiempirical molecular orbital methods). The formaldehyde molecule was centered over Ring 1 of the naphthalene molecule.
9. Charges on the formaldehyde carbon and oxygen and four of the naphthalene carbons in Ring 2 as a function of distance between naphthalene and formaldehyde (calculated using Spartan semiempirical molecular orbital methods). The formaldehyde molecule was centered over Ring 1 of the naphthalene molecule.
10. Charges on the formaldehyde carbon and oxygen and three of the anthracene carbons in Ring 1 as a function of distance between anthracene and formaldehyde (calculated using Spartan semiempirical molecular orbital methods). The formaldehyde molecule was centered over Ring 1 of the anthracene molecule.
11. Charges on the formaldehyde carbon and oxygen and three of the anthracene carbons in Ring 1 as a function of distance between anthracene and formaldehyde (calculated using Spartan semiempirical molecular orbital methods). The formaldehyde molecule was centered over Ring 2 of the anthracene molecule.

12. Charges on the formaldehyde carbon and oxygen and four of the anthracene carbons in Ring 2 as a function of distance between anthracene and formaldehyde (calculated using Spartan semiempirical molecular orbital methods). The formaldehyde molecule was centered over Ring 3 of the anthracene molecule.

These data show that a polar group does induce charge redistribution in rings sharing delocalized electronic structure with the ring closest to the approaching polar functionality. The effect, not surprisingly, dies out with distance. This can be attributed (in part if not totally) to the fact that there is an increasing number of atoms to contribute decreasing amounts of charge (per atom).

How do molecular mechanics (Sybyl) results compare with semiempirical (Spartan) results. Specifically, how do the energy versus distance curves compare?

13. Energy versus separation distance between coronene and methane calculated using Tripos force field and Sybyl for molecular mechanics.
14. Energy versus separation distance between coronene and methane calculated using Spartan semiempirical molecular orbital methods.
15. Energy versus separation distance between coronene and formaldehyde calculated using Tripos force field and Sybyl for molecular mechanics.
16. Energy versus separation distance between coronene and formaldehyde calculated using Spartan semiempirical molecular orbital methods.

The molecular mechanics results and semiempirical molecular orbital results are not in good agreement. Molecular mechanics methods compute van der Waals non-bonded interactions and Coulombic interactions as a matter of course. Semiempirical molecular orbital methods can account mainly for the Coulombic effects. Similarly, even ab initio methods cannot take into account non-bonded interactions (because they arise from electron correlation effects) unless prohibitively large, delocalized basis sets are used.

Comparisons with experimental data and other types of calculations in the literature might provide a better measure of the validity of the Tripos force field.

17. Orthogonal views of a benzene molecule proximate to a coronene molecule (representing a section of a graphite sheet).
18. Relative energy as a function of distance between benzene and coronene (in the positions shown in the previous figure).
19. Title and figures from a paper reporting calculations (and comparisons with experimental data) for the absorption of benzene on graphite.

The Sybyl results are in very nice agreement with the results in this paper, both in regard to the minimum energy orientation, the depth of the energy minimum, and the minimum energy separation distance.

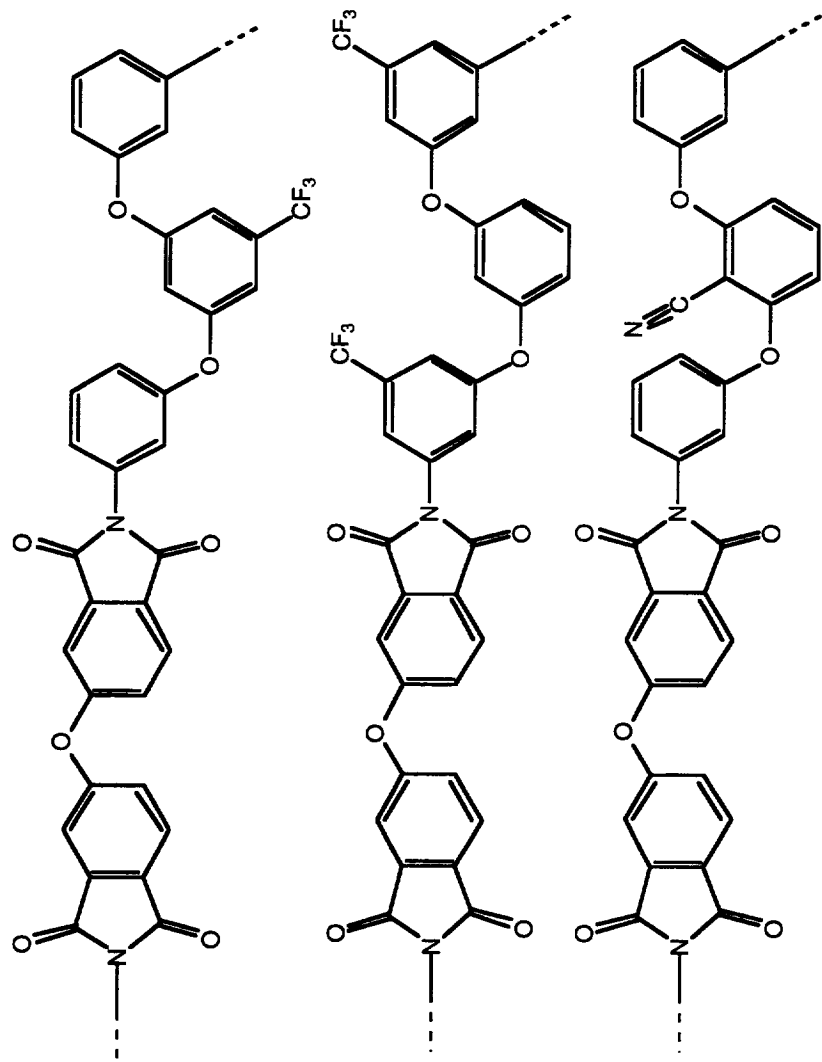
Molecular Mechanics and Molecular Dynamics

with applications to polyimides as
piezoelectric and composite materials

B. L. Farmer

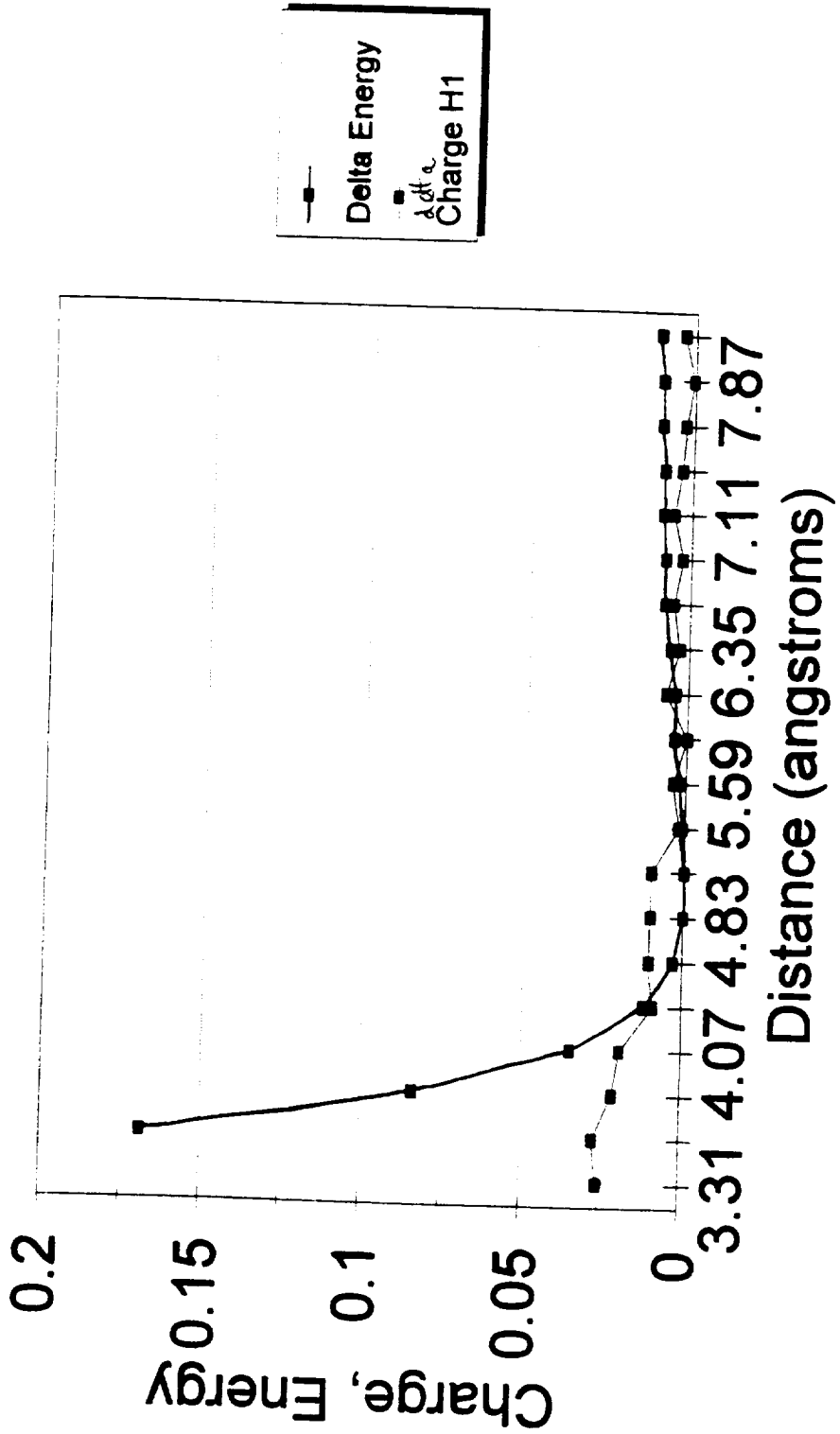
Materials Science and Engineering
University of Virginia

Piezoelectric Polyimides



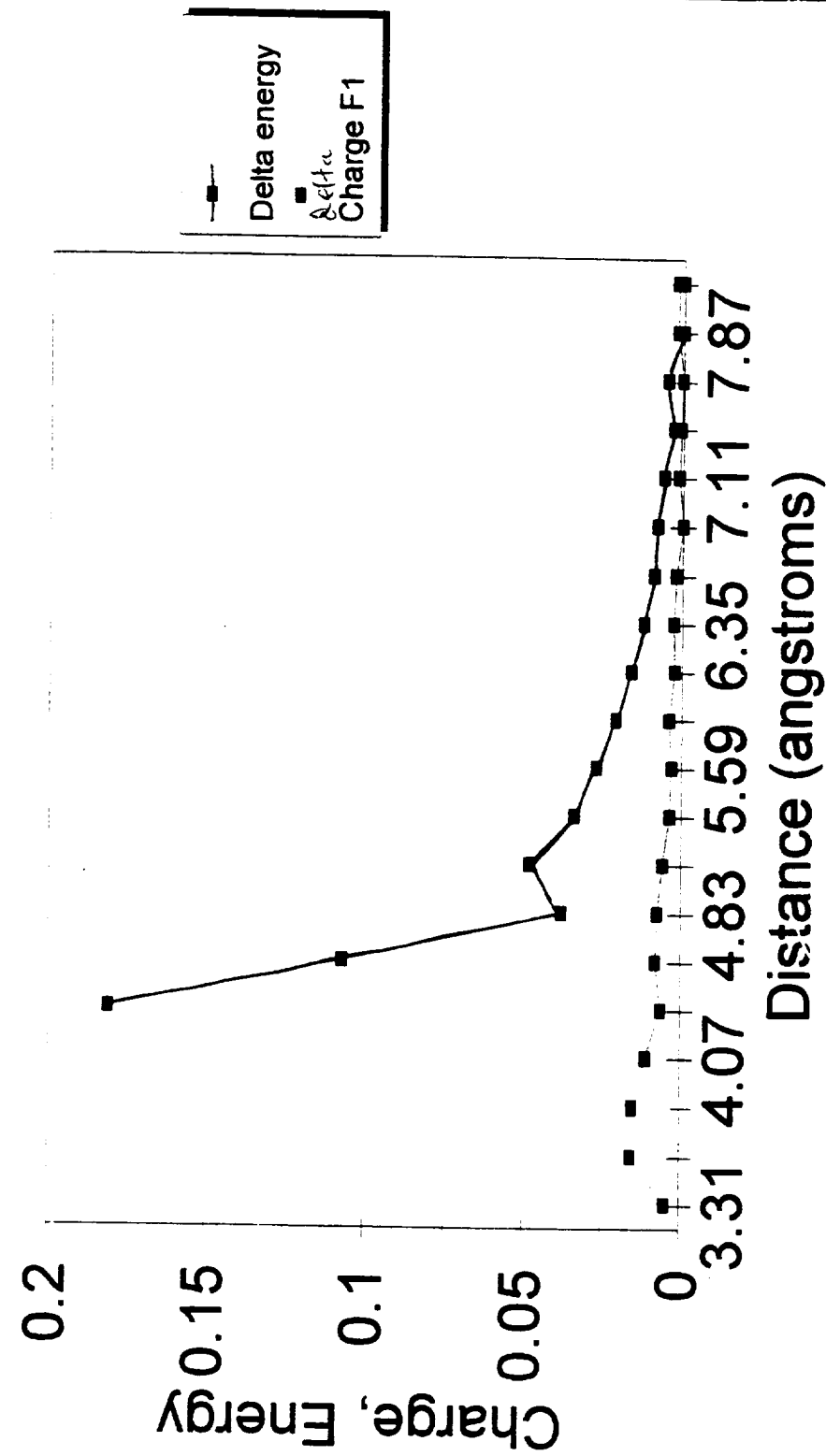
Energy and Charge Versus Distance

Phen_Meth Molecule



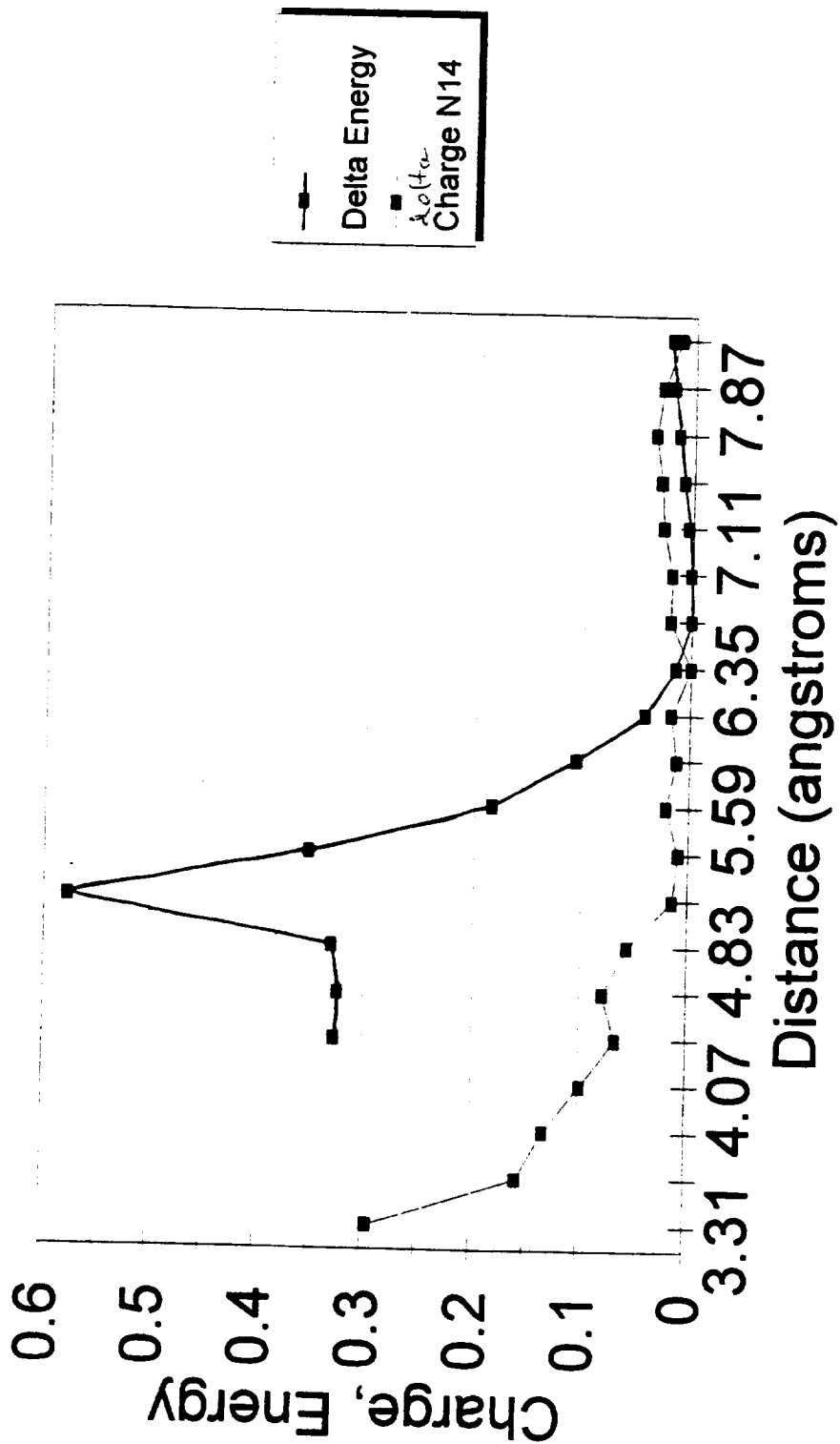
Energy and Charge Versus Distance

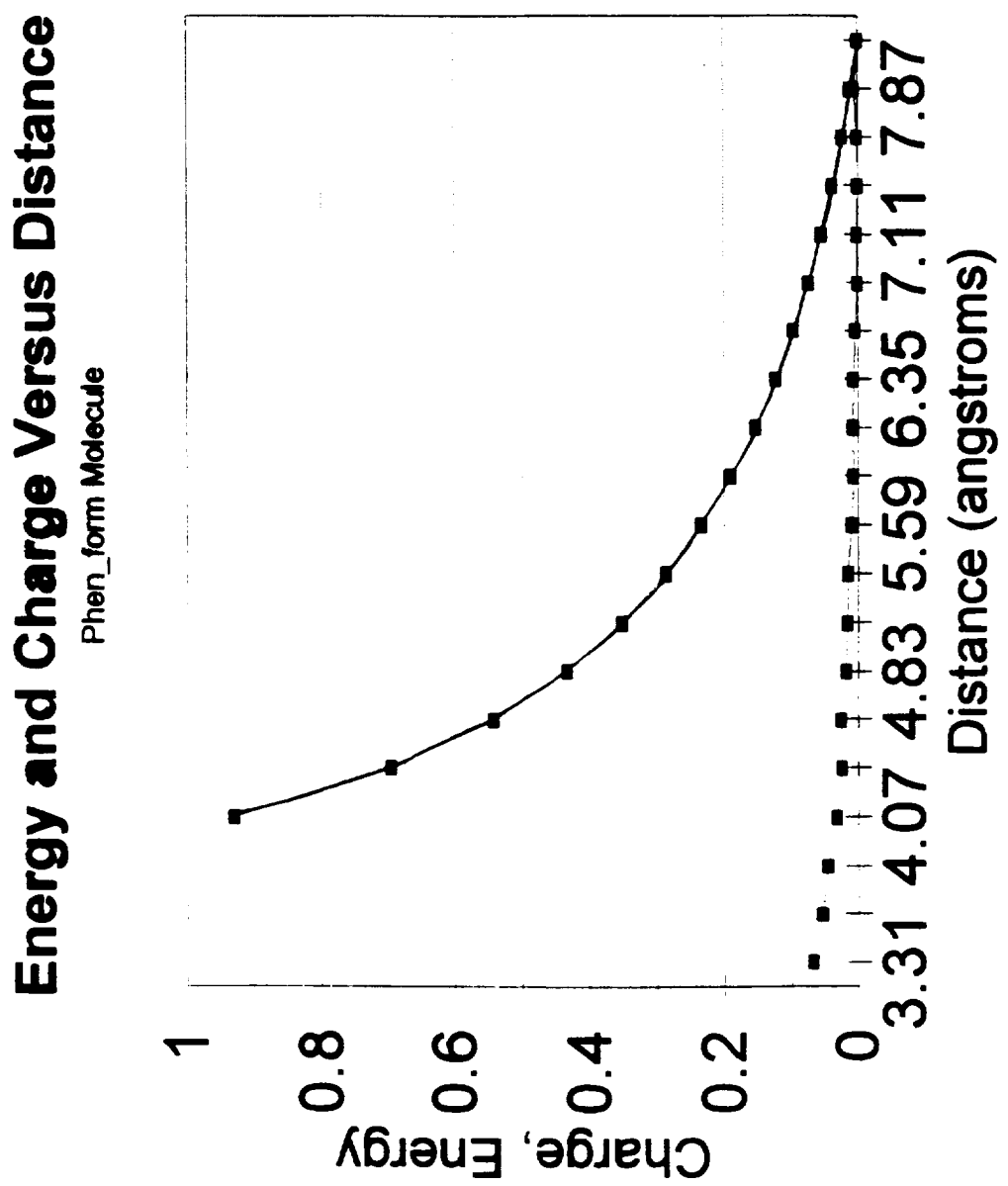
Phen_CF₄ Molecule

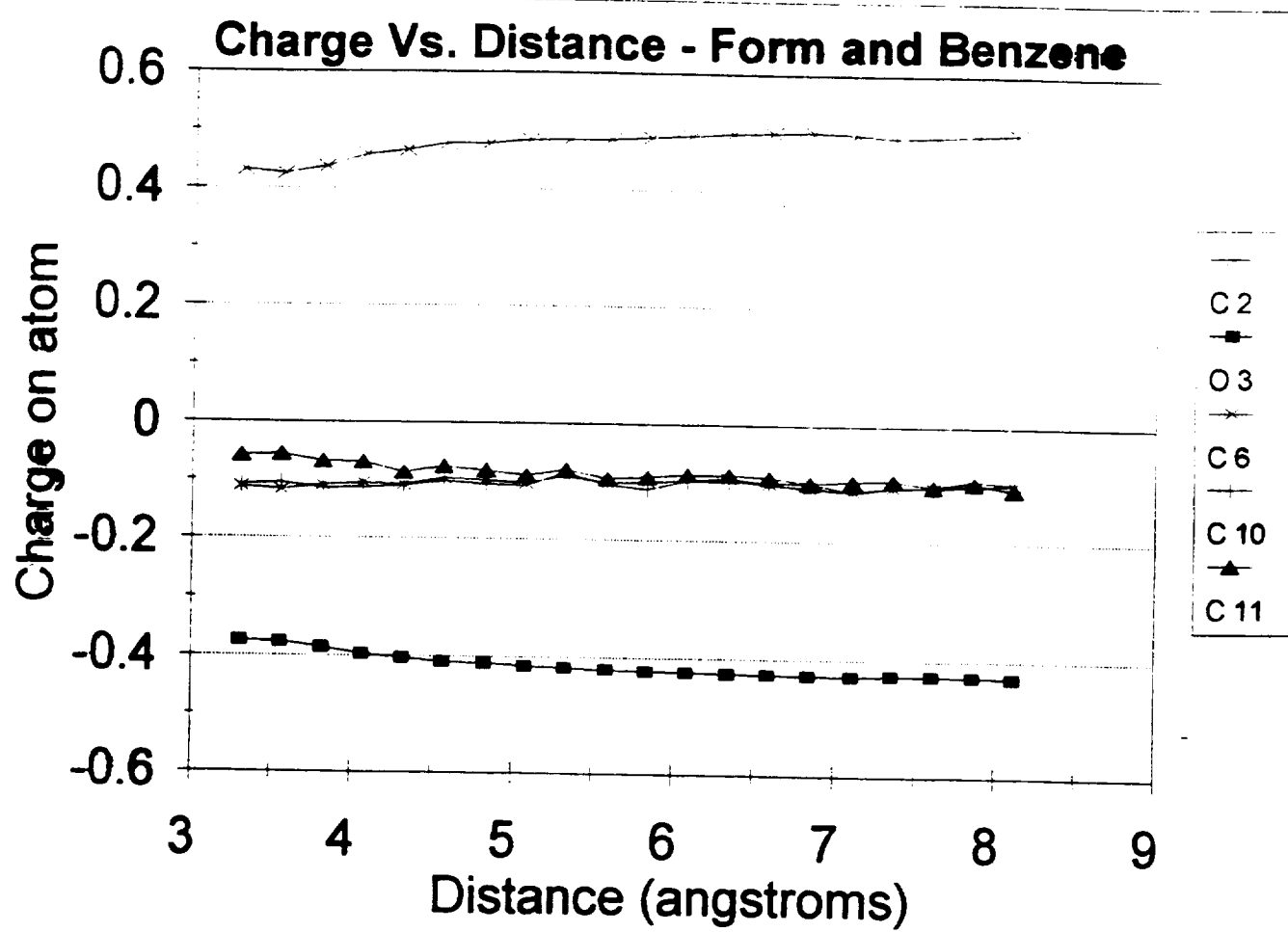


Energy and Charge Versus Distance

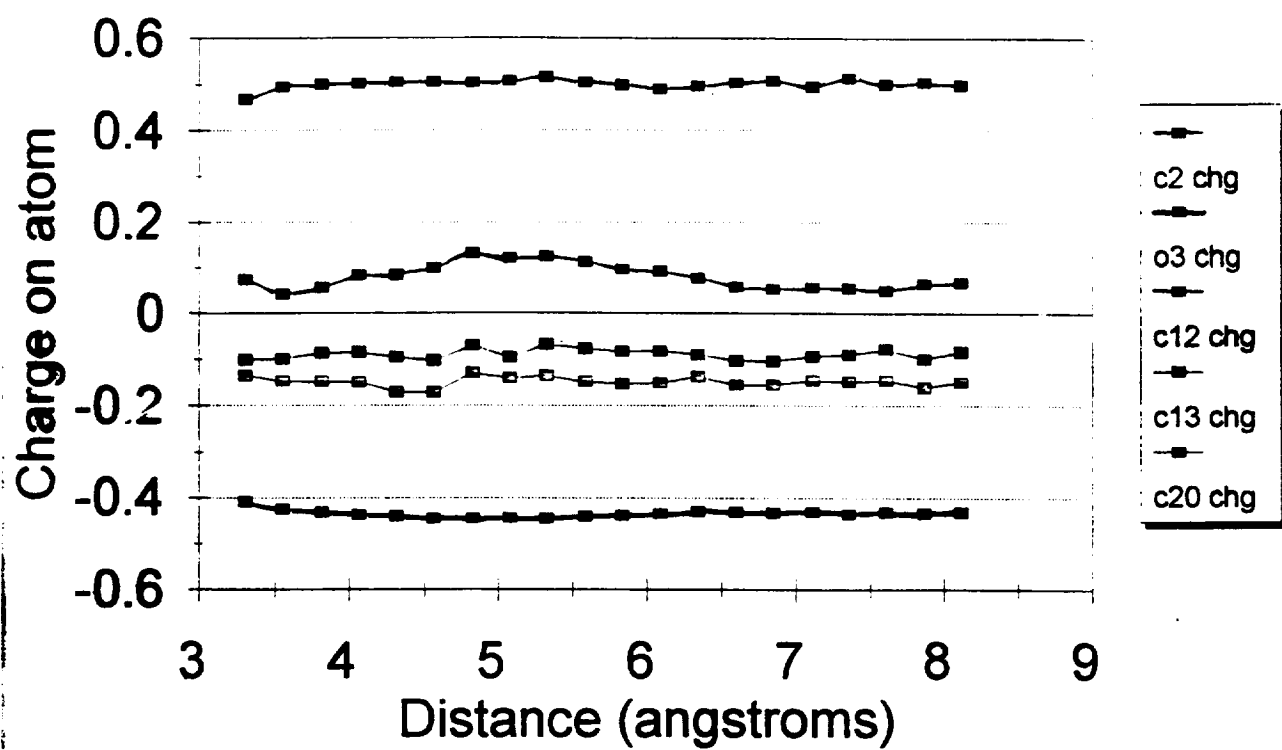
Phen_nndmn Molecule





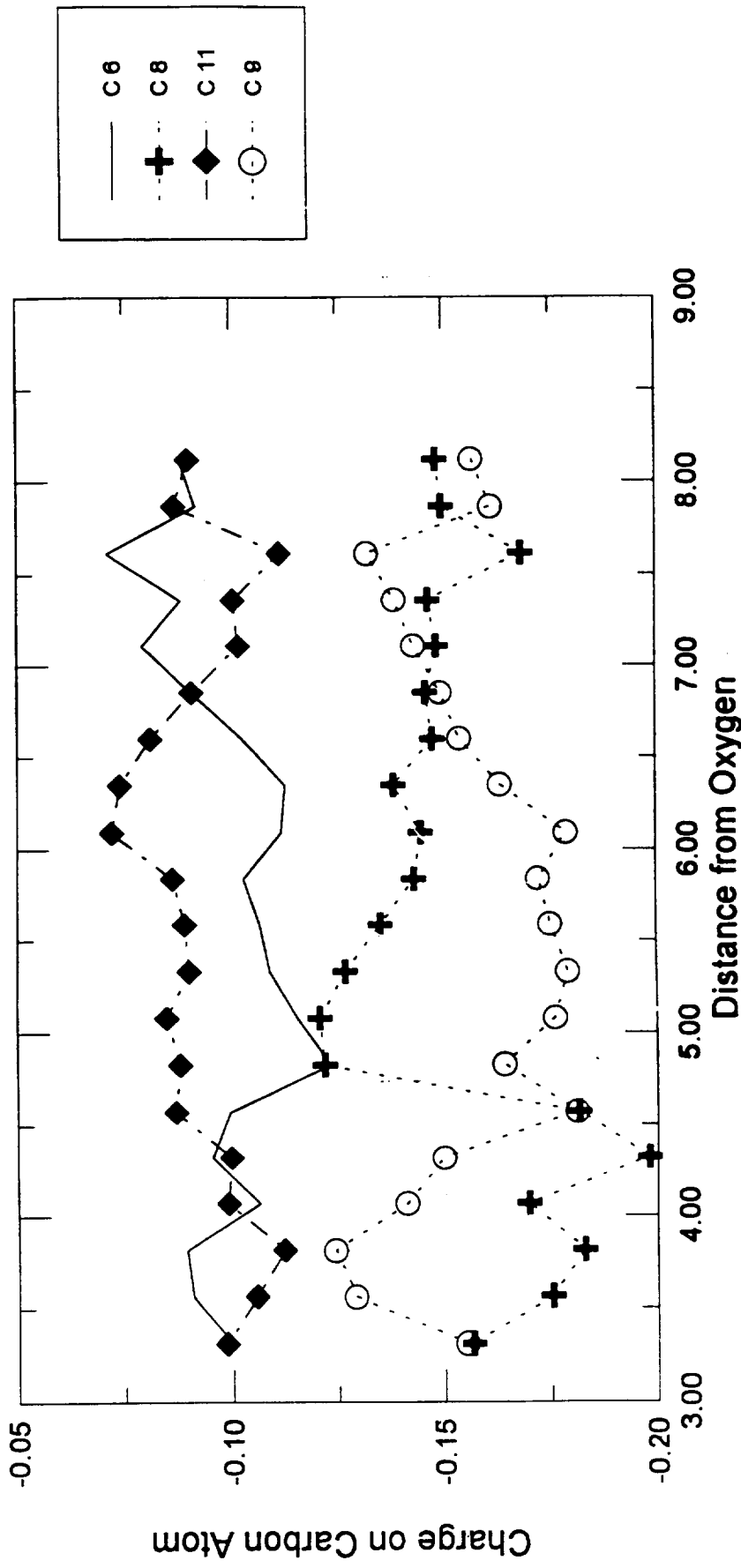


Charge Vs. Distance - Form and Nath



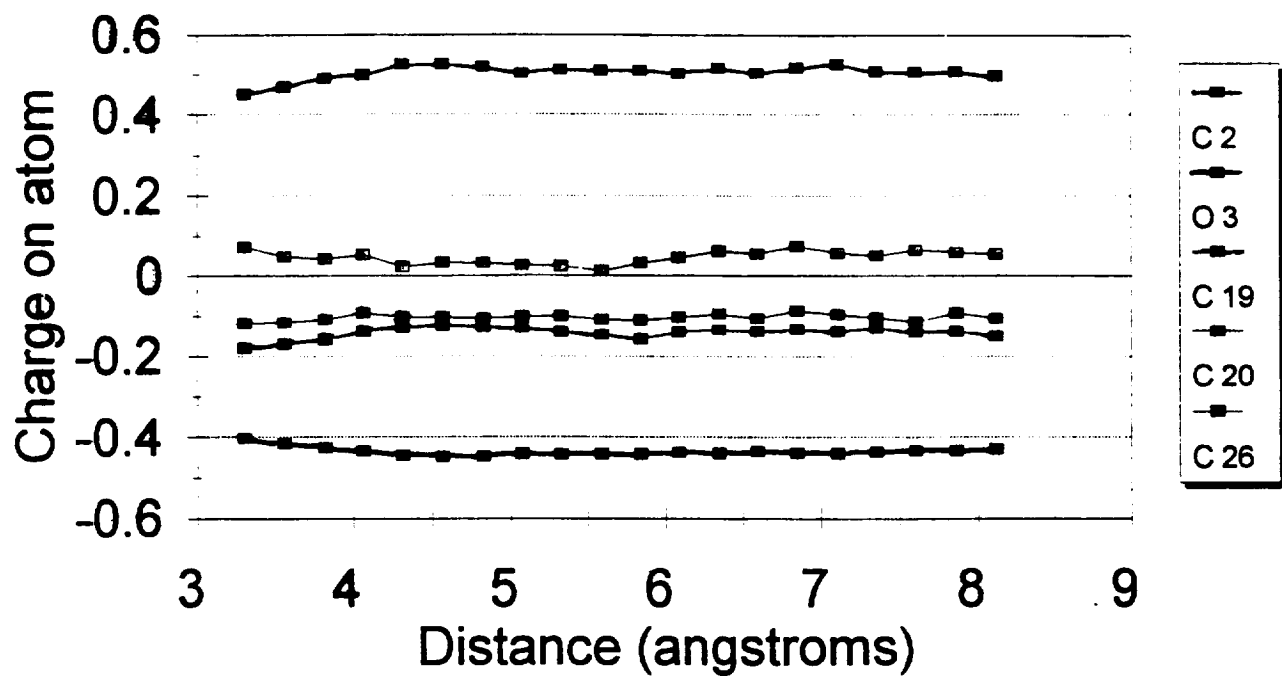
**Charge on Carbon Atoms Versus
Distance From Oxygen**

Formaldehyde and Naphthalene



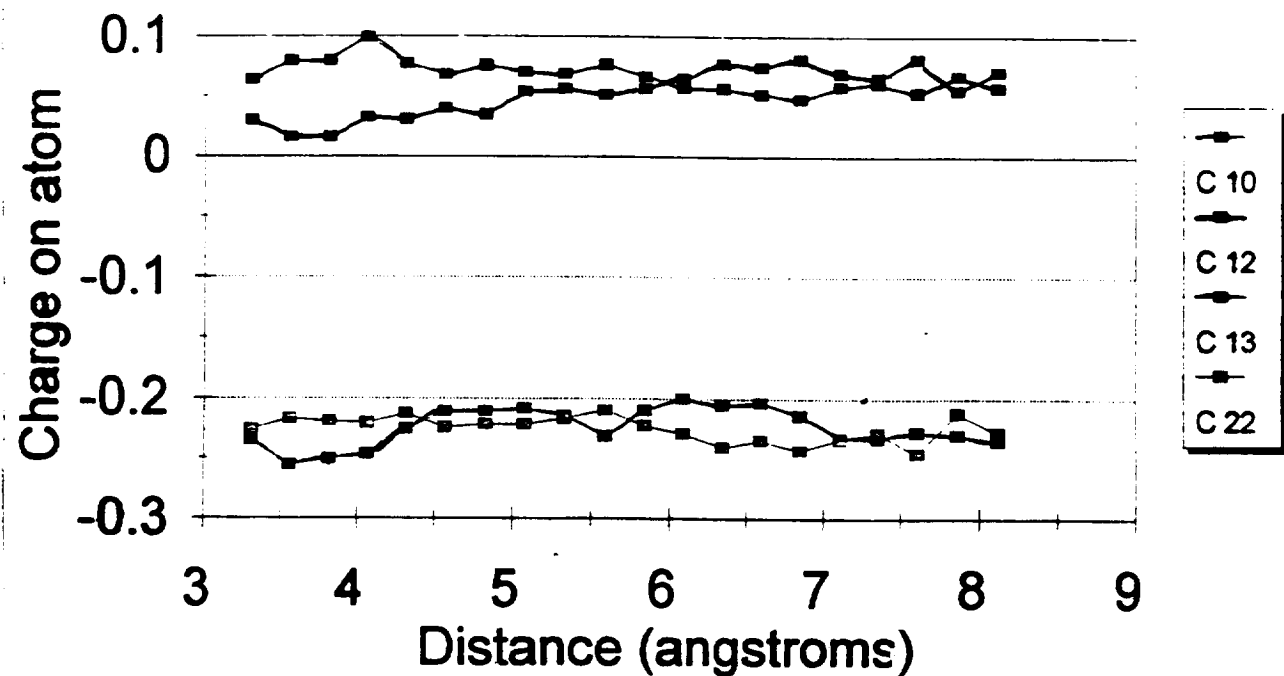
Charge Vs. Distance - Form and Anth

Ring 1



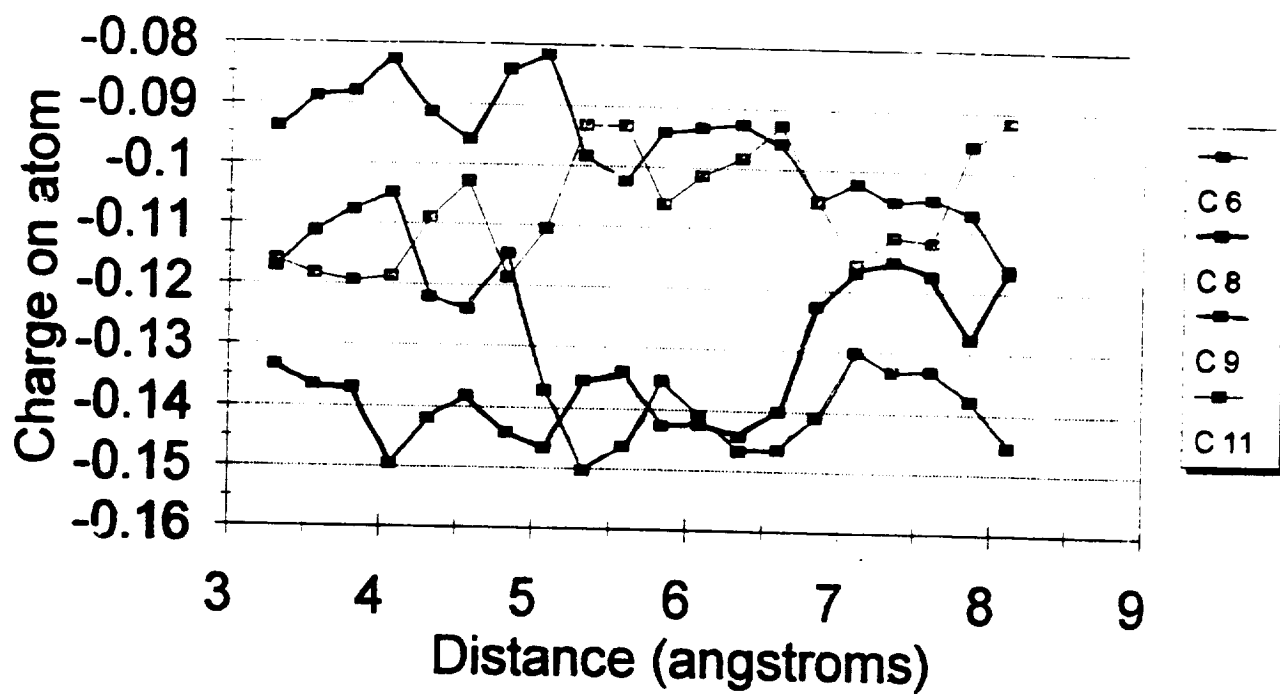
Charge Vs. Distance - Form and Anth

Ring 2

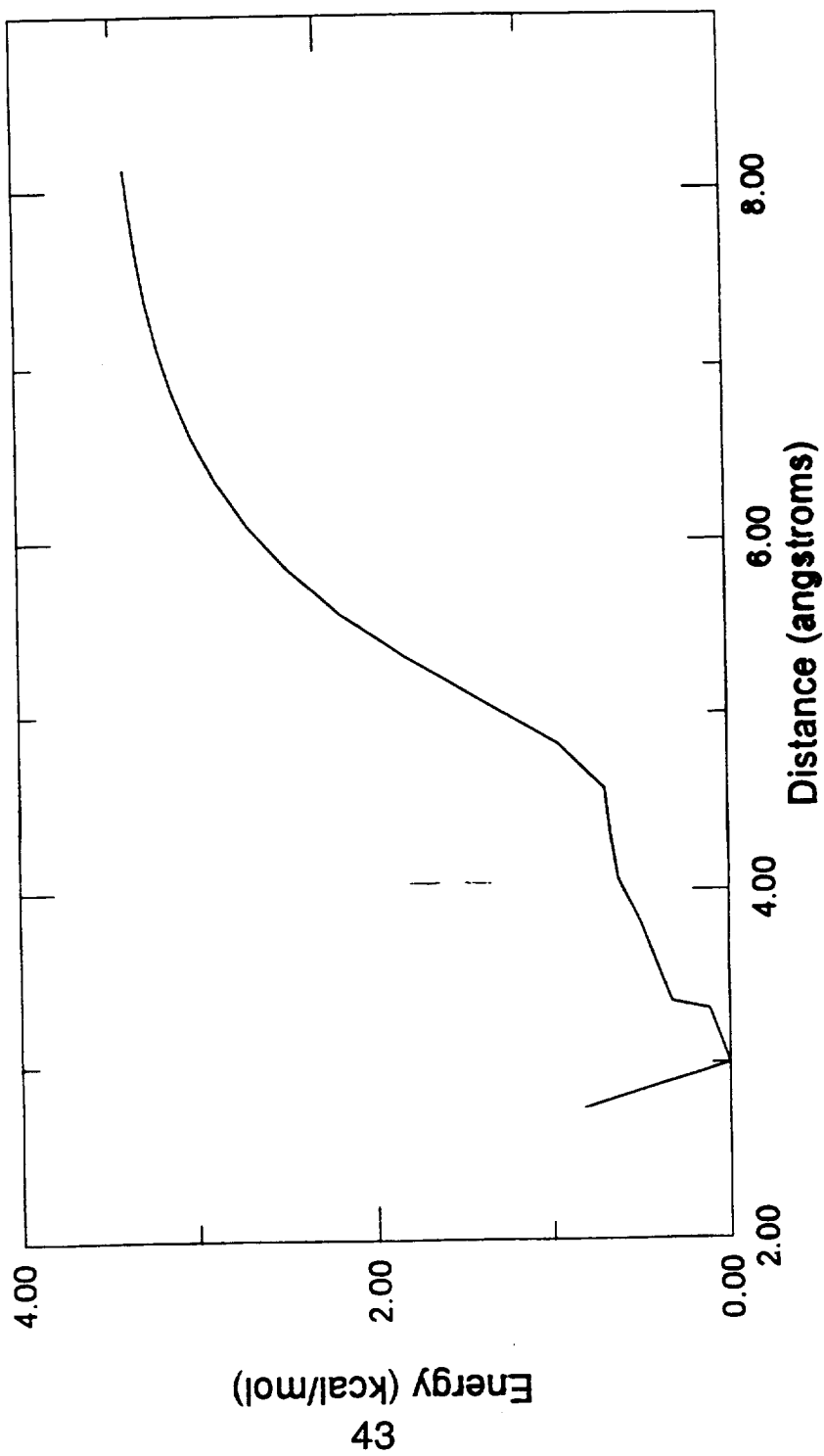


Charge Vs. Distance - Form and Anth

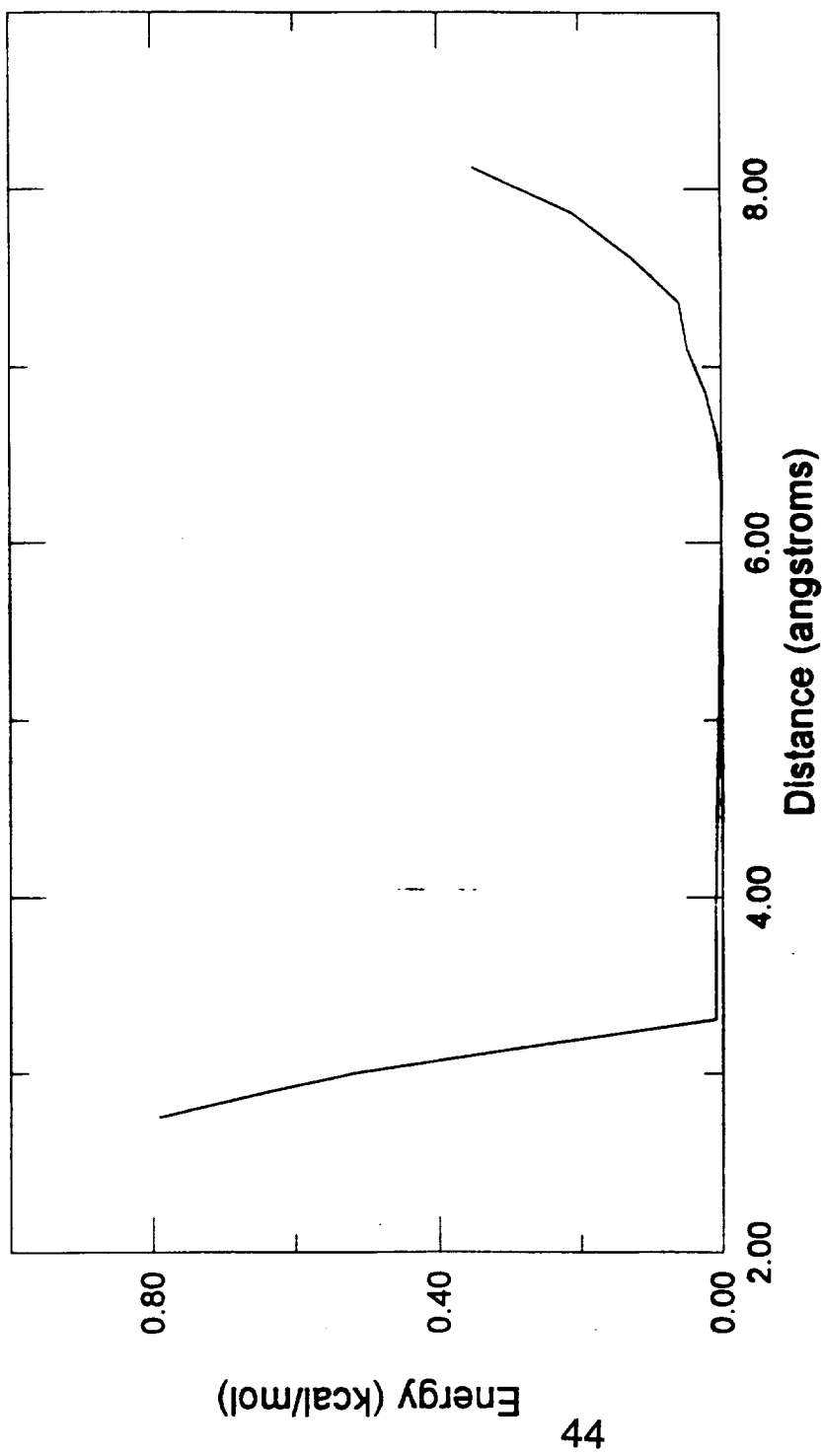
Ring 3



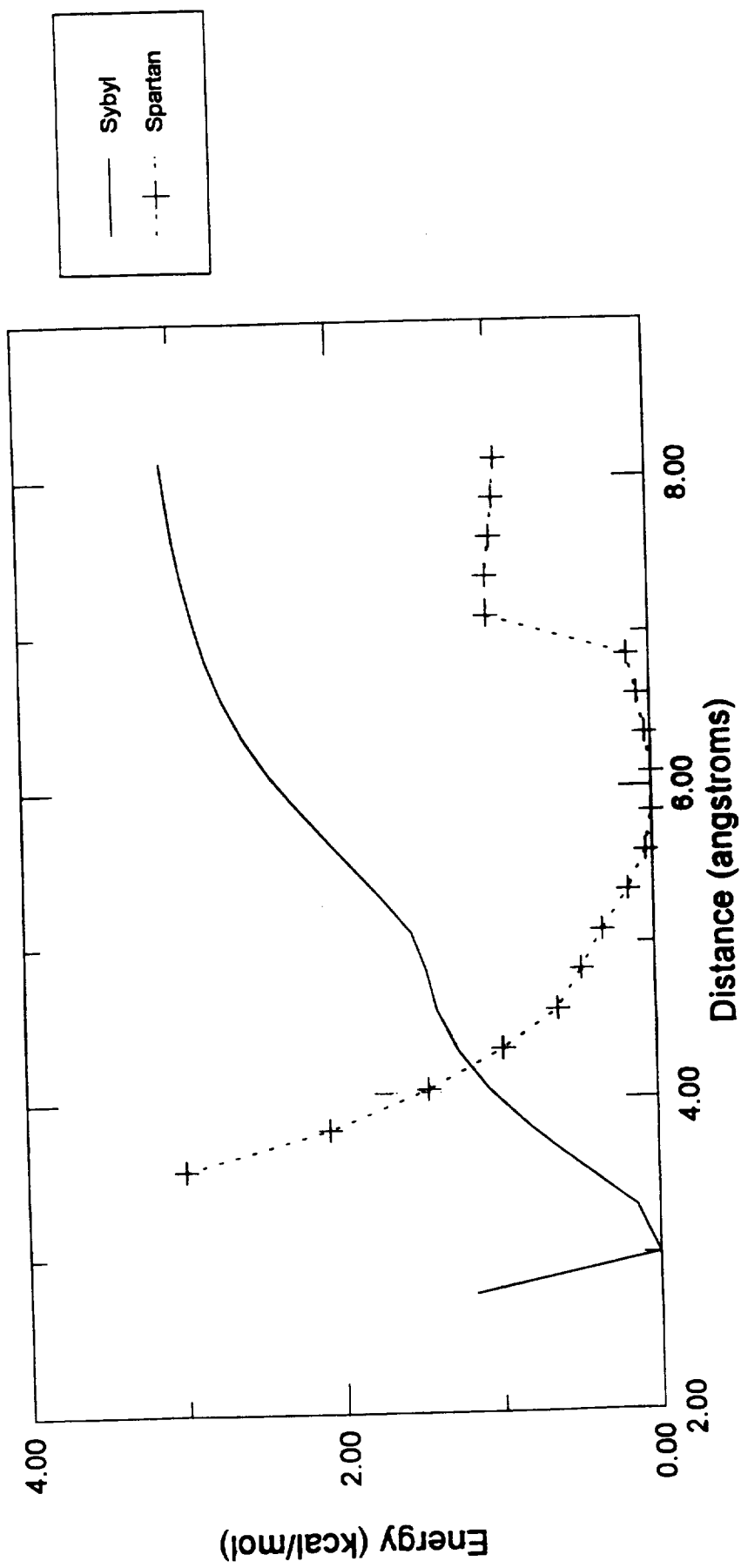
**Energy Calculated by Sybyl Versus Distance
Methane and Coronene Molecule**



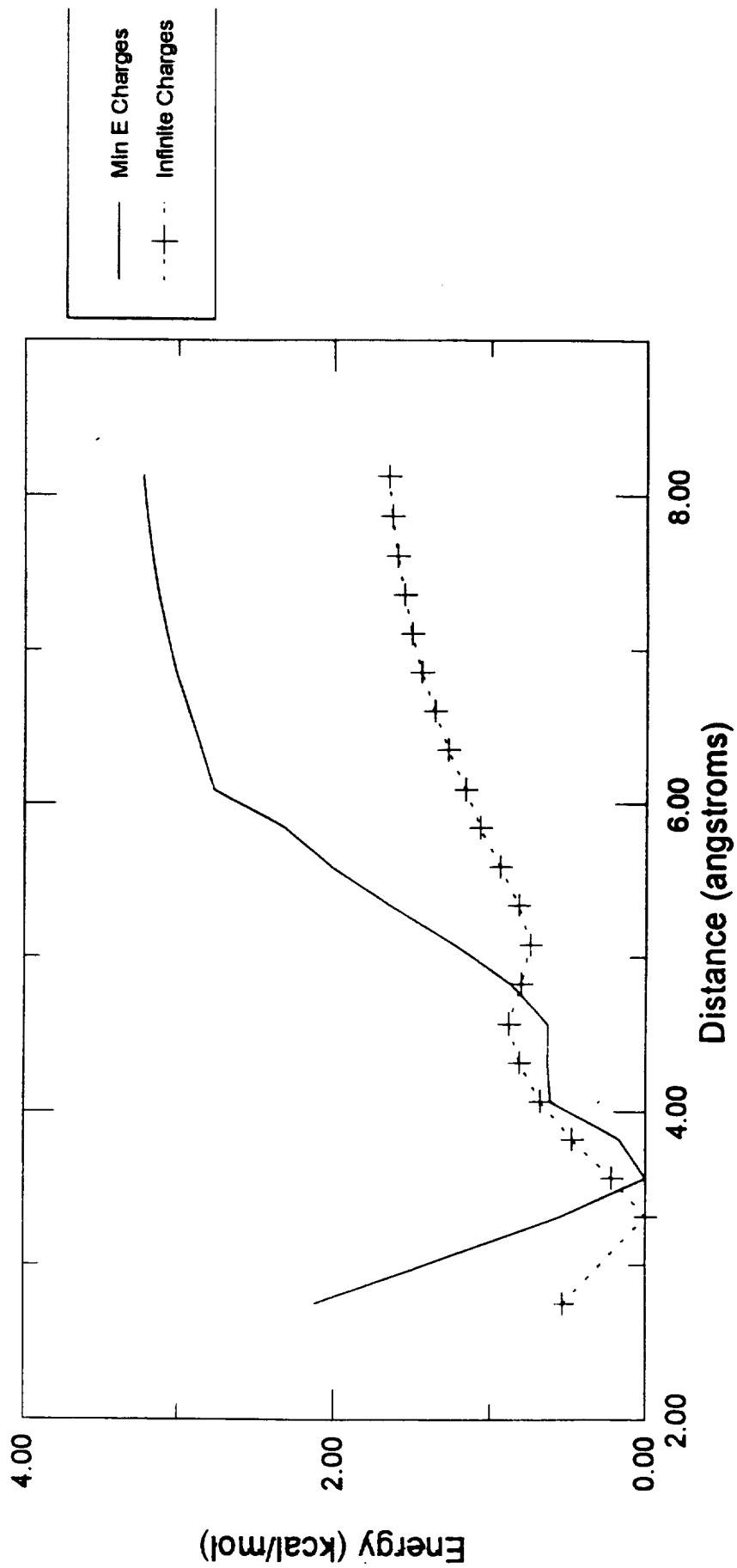
**Energy Calculated by Spartan Versus Distance
Methane and Coronene Molecule**

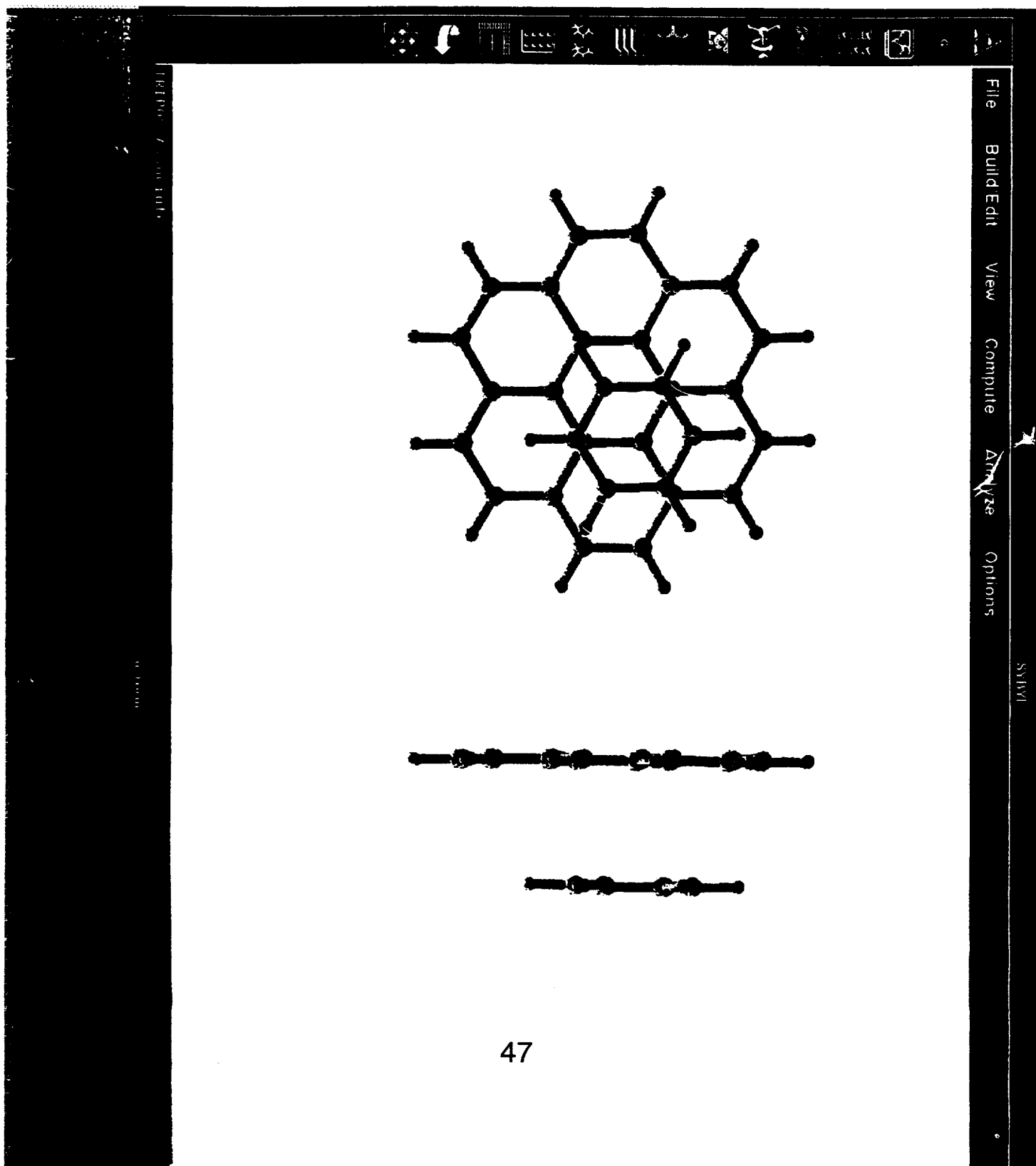


Energy Calculated by Sybyl and Spartan Versus Distance
Formaldehyde and Coronene Molecule



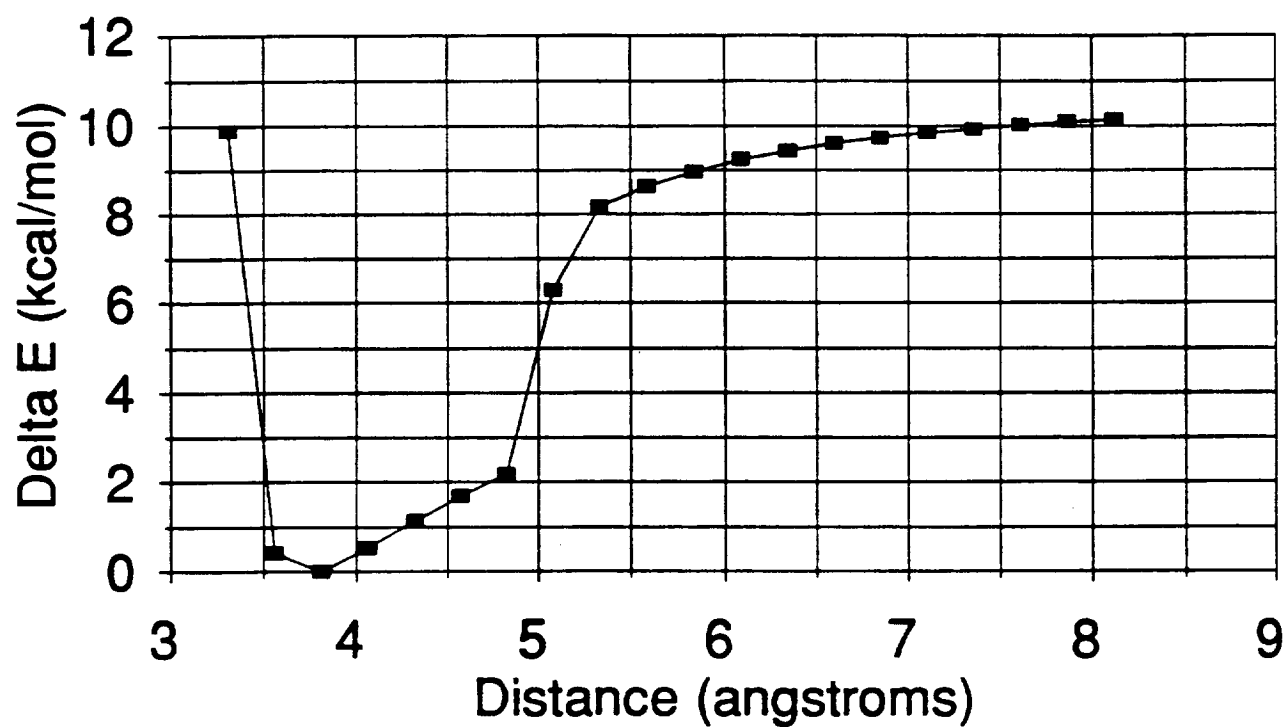
**Energy Calculated by Sybyl with Charges Versus Distance
Formaldehyde and Coronene**





Change in Strain Energy Vs. Distance

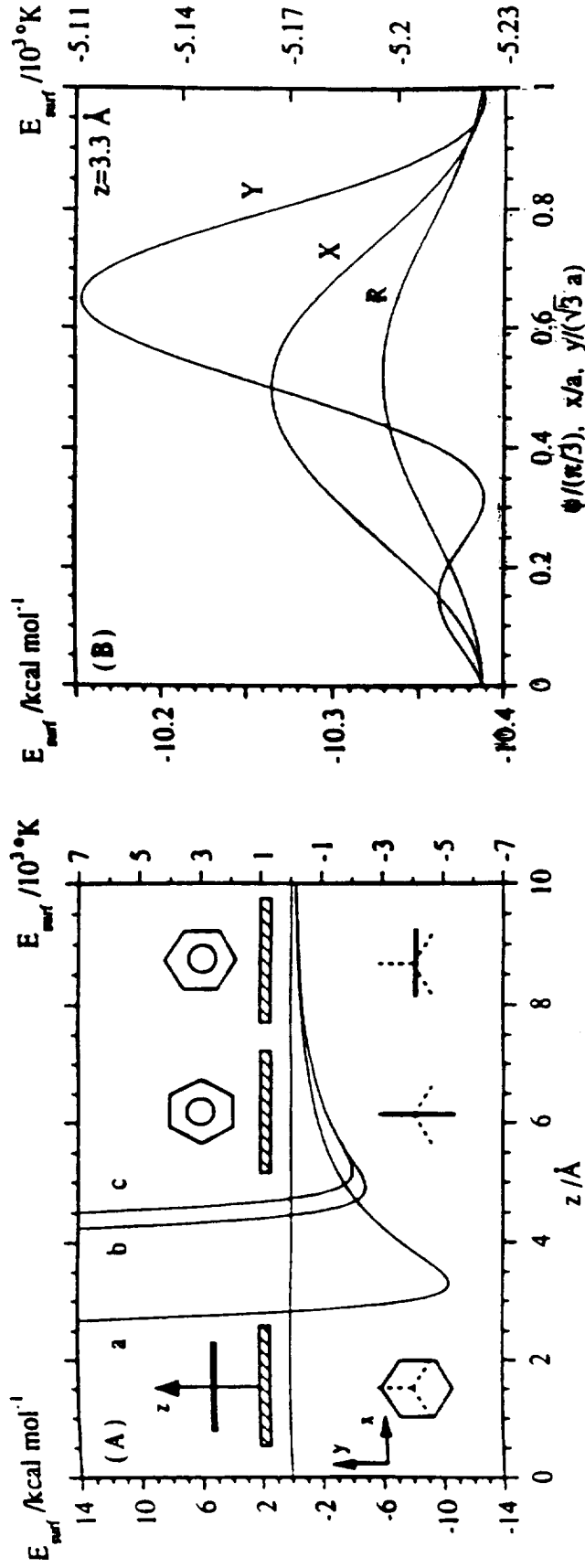
Benzene and Coronene



A molecular dynamics simulation of liquid benzene adsorbed on graphite

Reinhard Hentschke and Britta L. Schürmann
Max-Planck-Institut für Polymerforschung, Postfach 3148, D-6500 Mainz, Germany

Received 17 July 1991; accepted for publication 4 September 1991



EFFECT OF MOLECULAR WEIGHT ON PROPERTIES OF LARCTM-SI

E. J. Siochi
Lockheed Martin Engineering and Sciences Company
Hampton, VA 23666

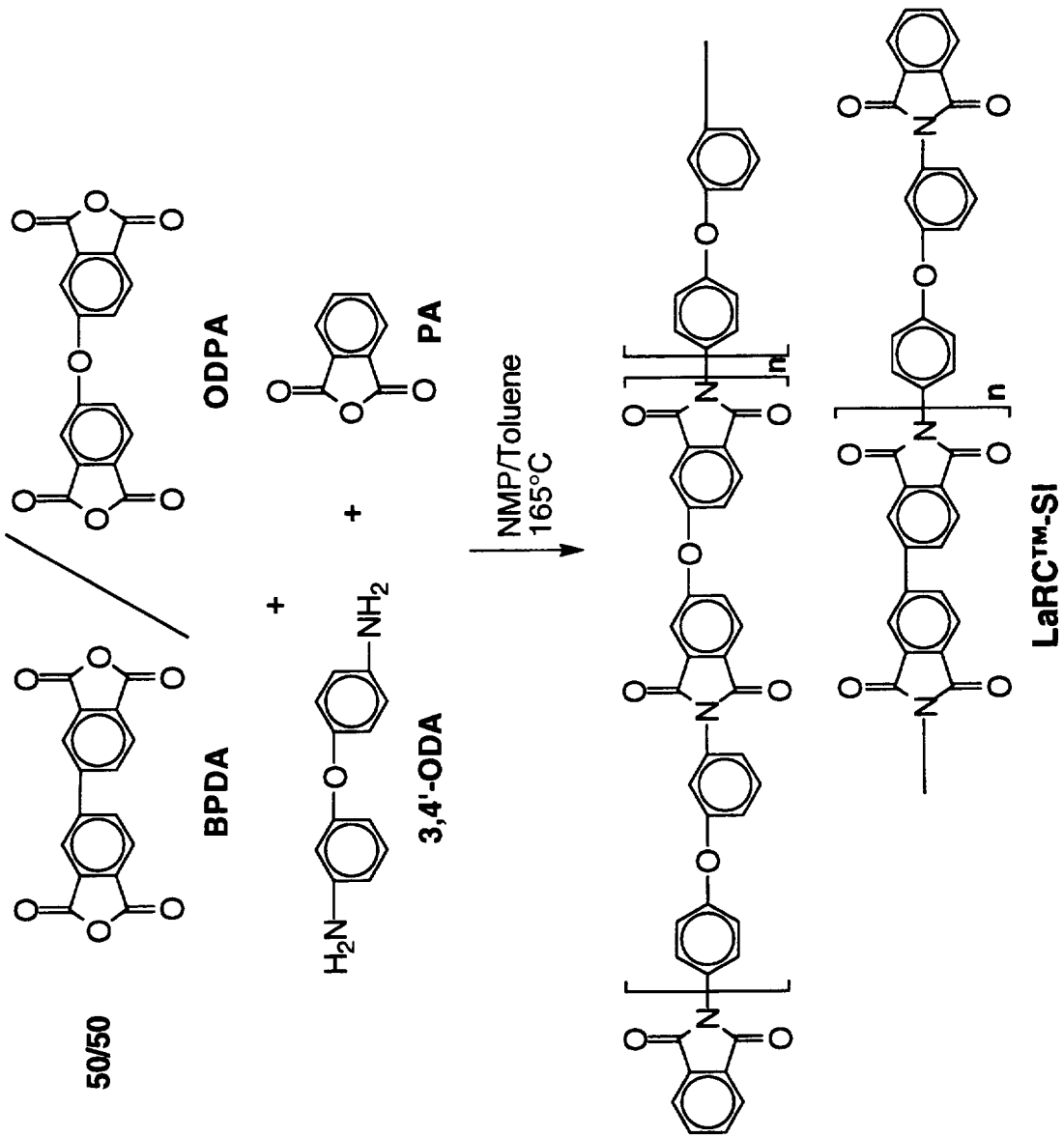
OUTLINE

- Introduction
- Objective
- Materials
- Characterization
 - ☒ Molecular Weight Determination
 - ☒ Thermal Analysis
 - ☒ Melt Viscosity
 - ☒ Density
 - ☒ Microhardness
 - ☒ Fracture Toughness
- Summary

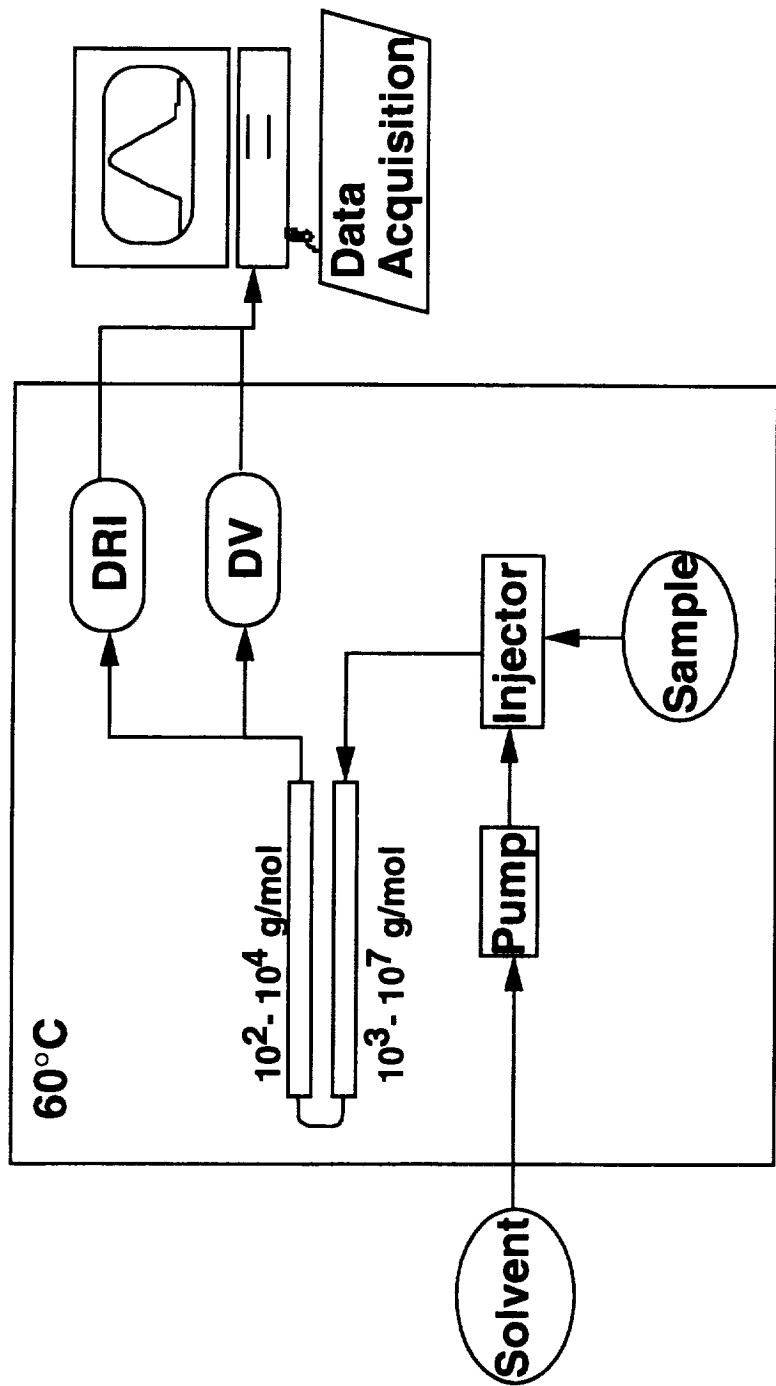
INTRODUCTION

- Polyimides as materials of choice
 - ☒ Excellent mechanical properties
 - ☒ Excellent thermooxidative stability
 - ☒ Good solvent resistance
- Tailoring of properties achieved using stoichiometric imbalance during synthesis
- Solubility of LARCTM-SI allows systematic investigation of the relationship of molecular weight to properties of interest

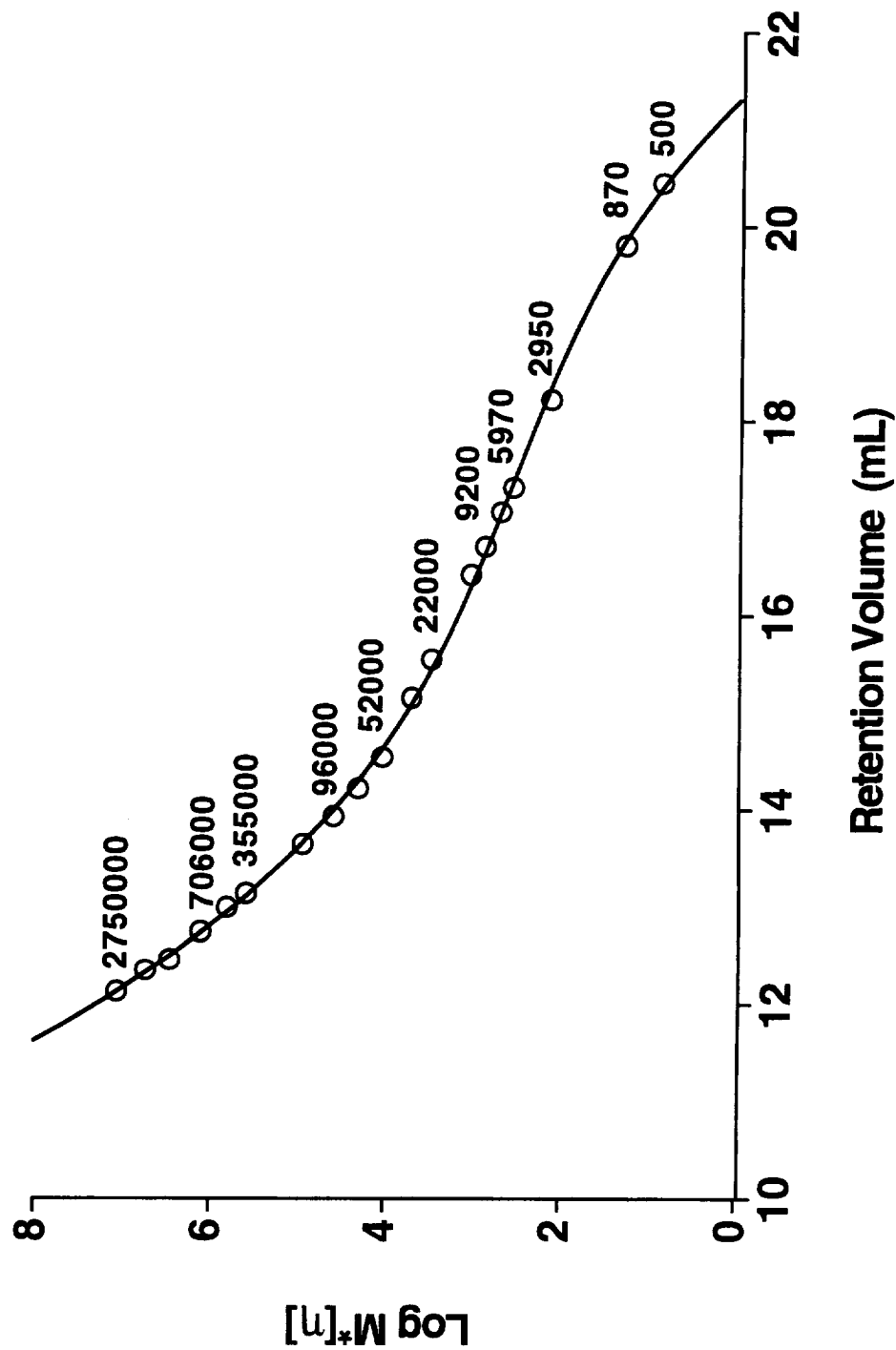
MATERIAL

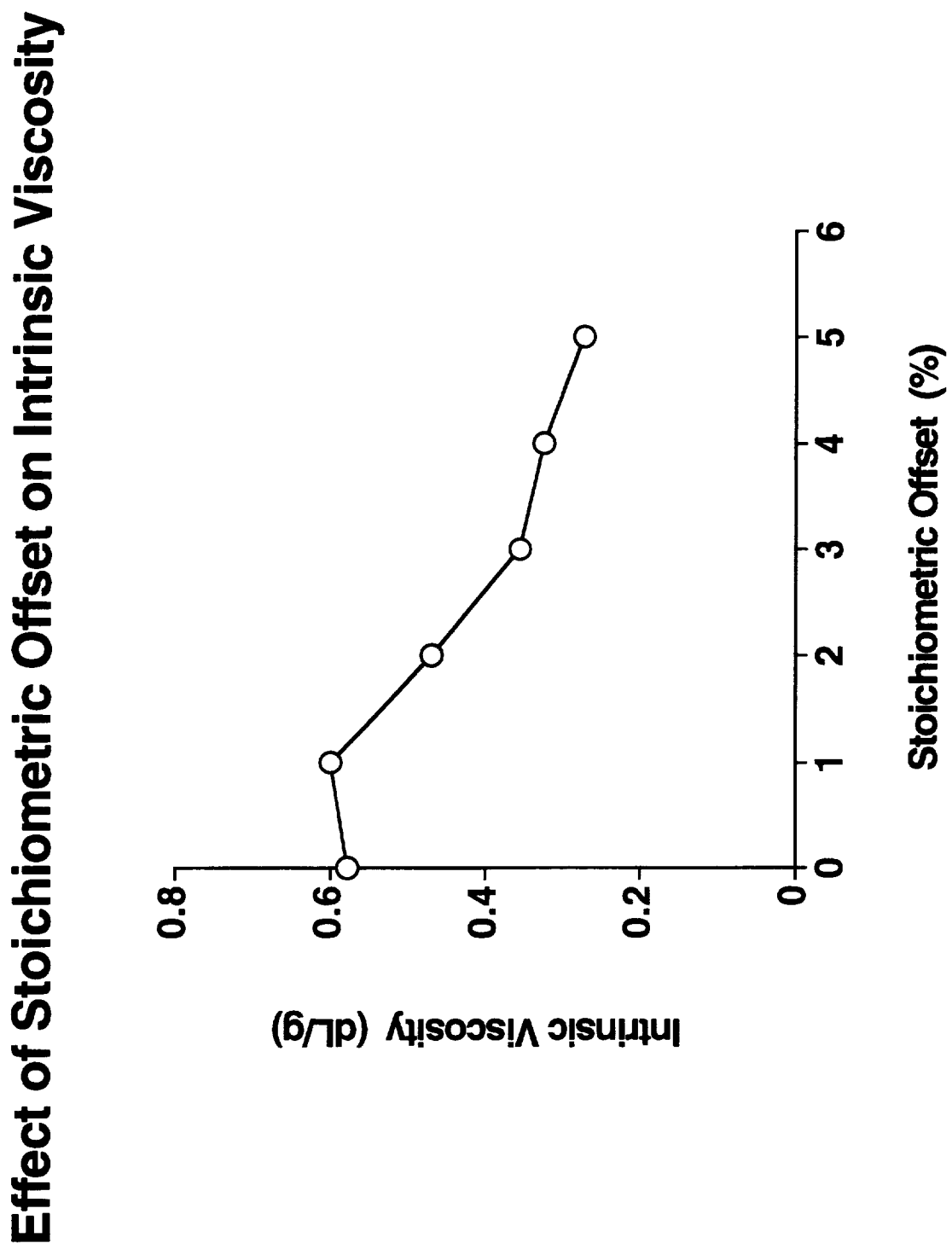


GPC/DV SCHEMATIC

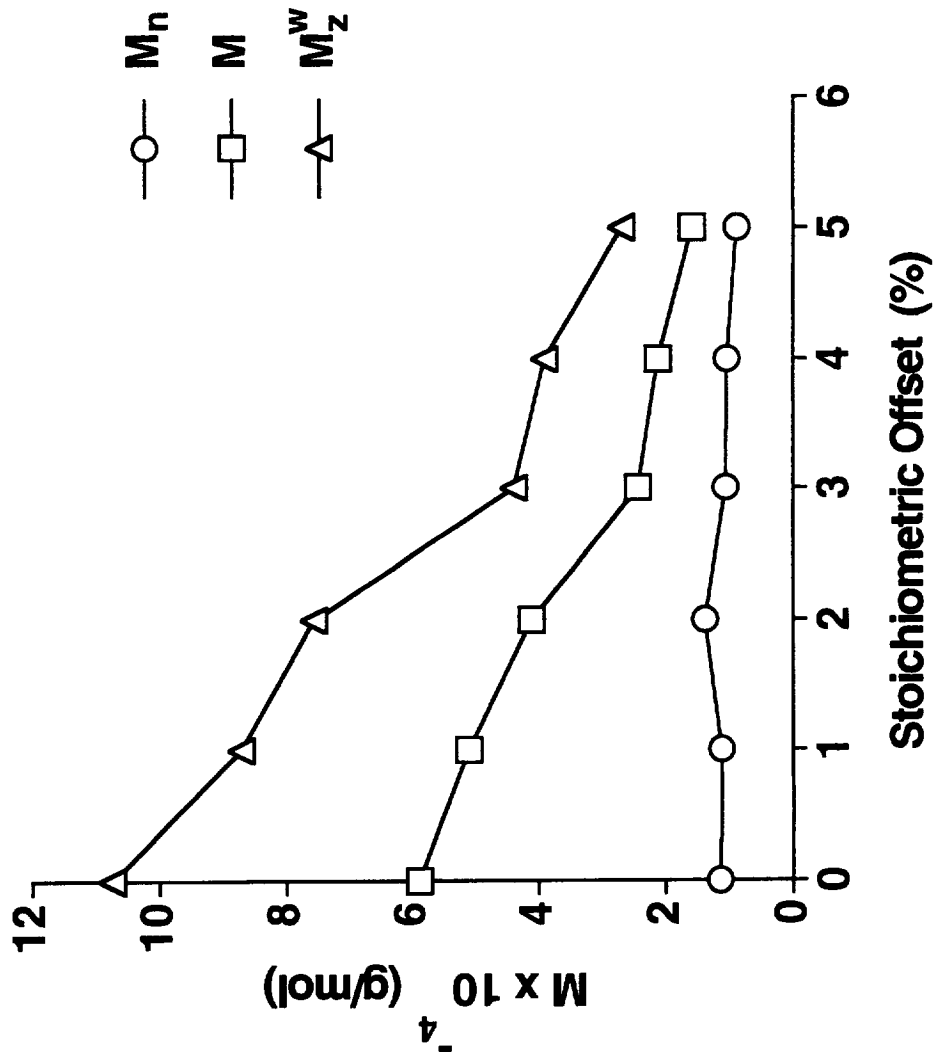


Universal Calibration Curve





Effect of Stoichiometric Offset on Molecular Weight Averages



Molecular Weight Characterization

| Sample Offset (%) | M_n (g/mol) | Theoretical M_n (g/mol) | M_w (g/mol) | M_z (g/mol) | M_v (g/mol) | Intrinsic Viscosity (dL/g) |
|-------------------|---------------|---------------------------|---------------|---------------|---------------|----------------------------|
| 0 | 11450 | ∞ | 58900 | 107350 | 43035 | 0.578 |
| 1 | 11180 | 44819 | 51070 | 87130 | 37530 | 0.600 |
| 2 | 13770 | 22297 | 41100 | 75703 | 31675 | 0.470 |
| 3 | 10560 | 14789 | 24290 | 43955 | 19170 | 0.356 |
| 4 | 10405 | 11036 | 21180 | 39110 | 17155 | 0.326 |
| 5 | 8882 | 8784 | 15880 | 26935 | 13690 | 0.273 |

Effect of Molecular Weight on the Properties of a Soluble Polyimide

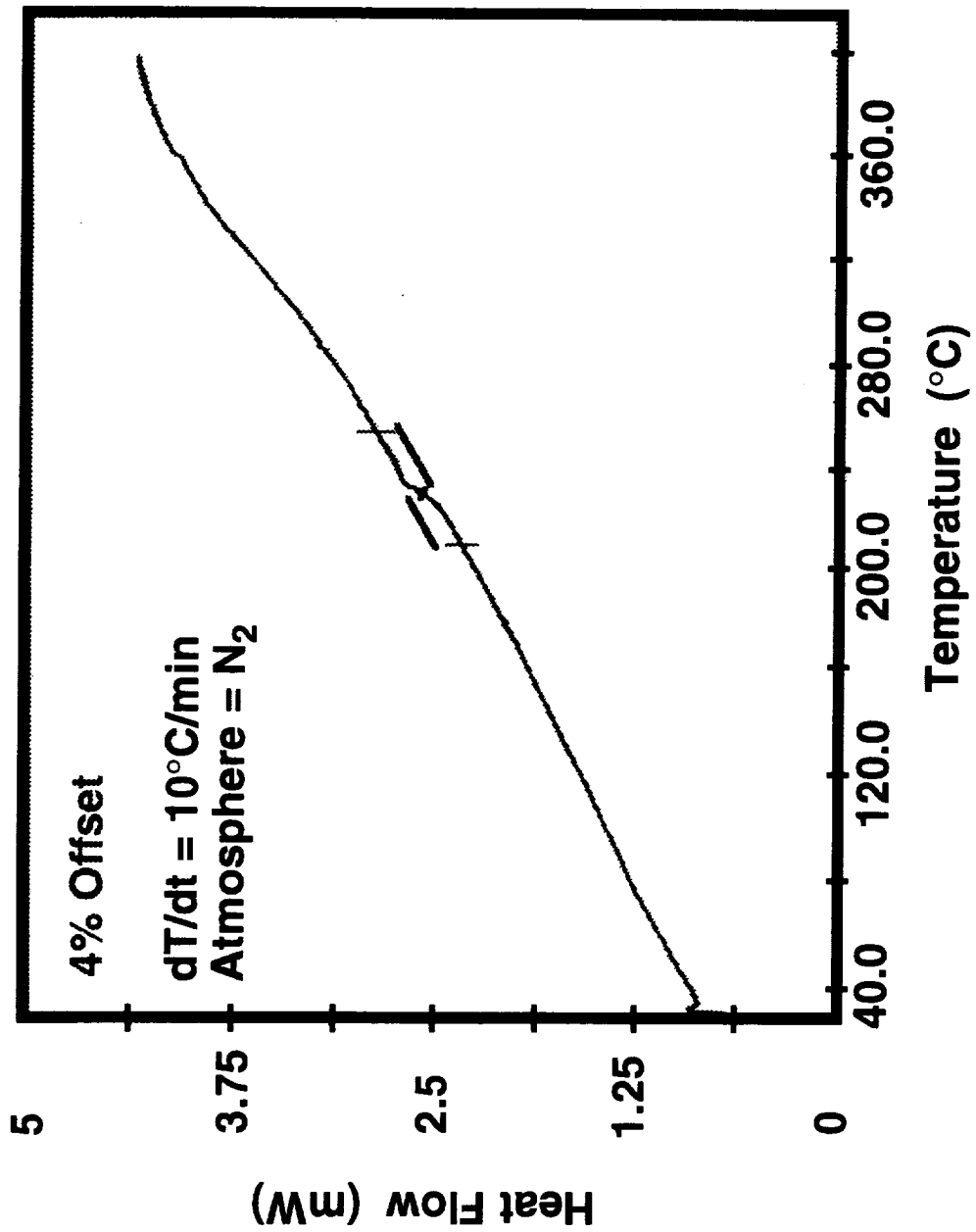
OBJECTIVE

- Quantitative understanding of how molecular weight characteristics influence selected properties of an advanced polymer matrix resin

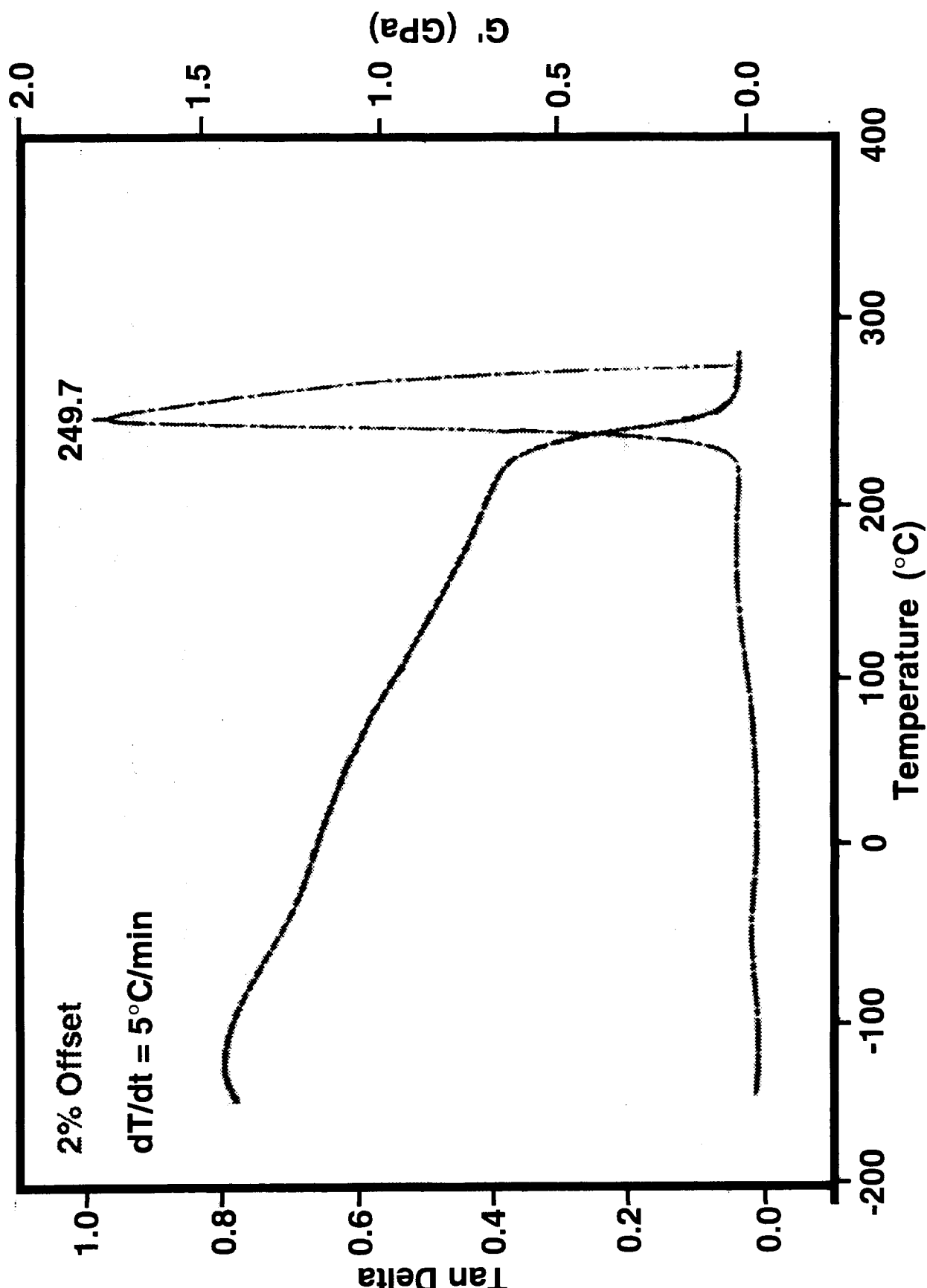
APPROACH

- Synthesize a series of soluble polyimides having controlled molecular weights
- Characterize polymer series with methods of analysis routinely practised by Composites and Polymers Branch
- Find relationships between physical properties of polymers and molecular weights

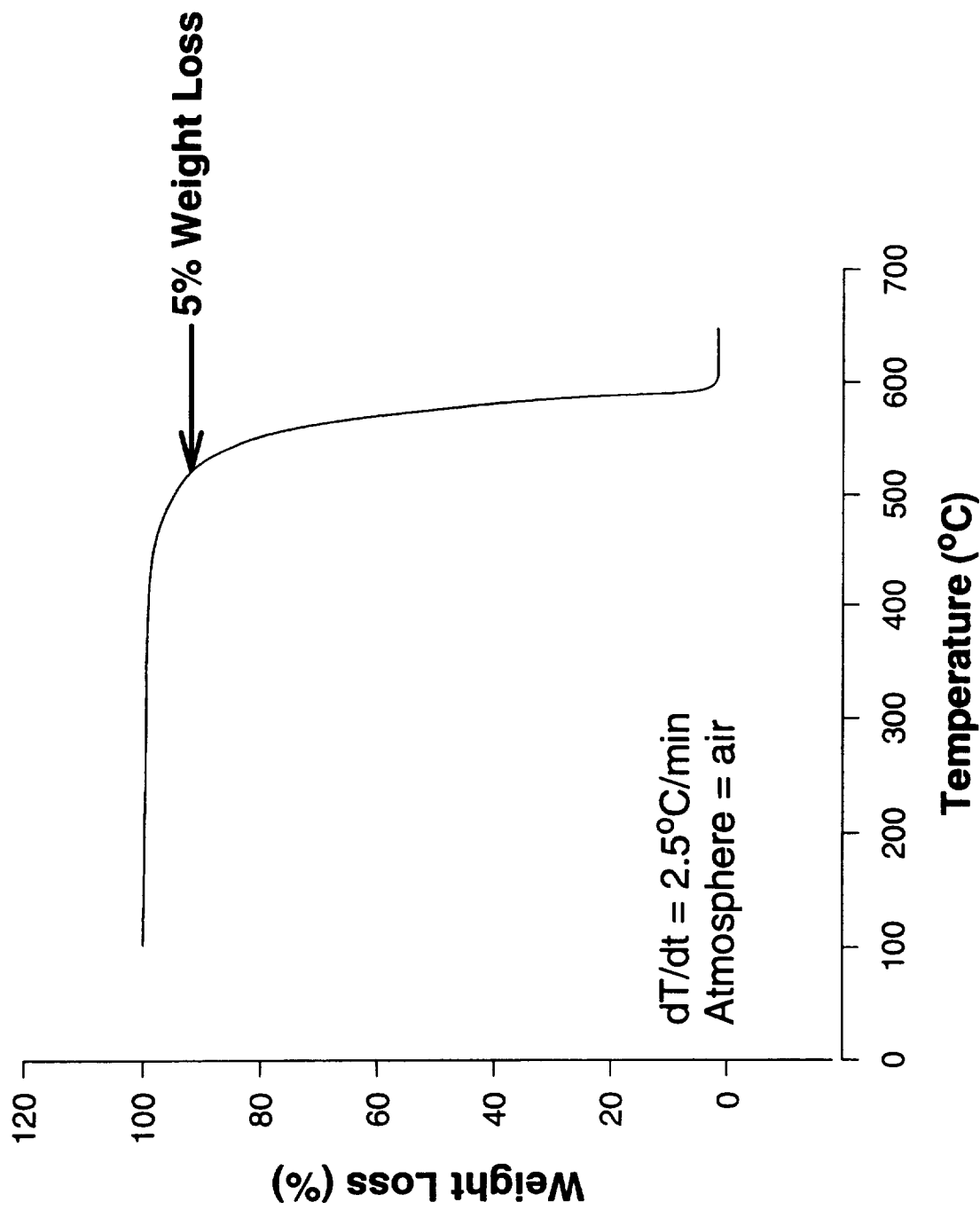
Differential Scanning Calorimetry



Dynamic Mechanical Spectrum



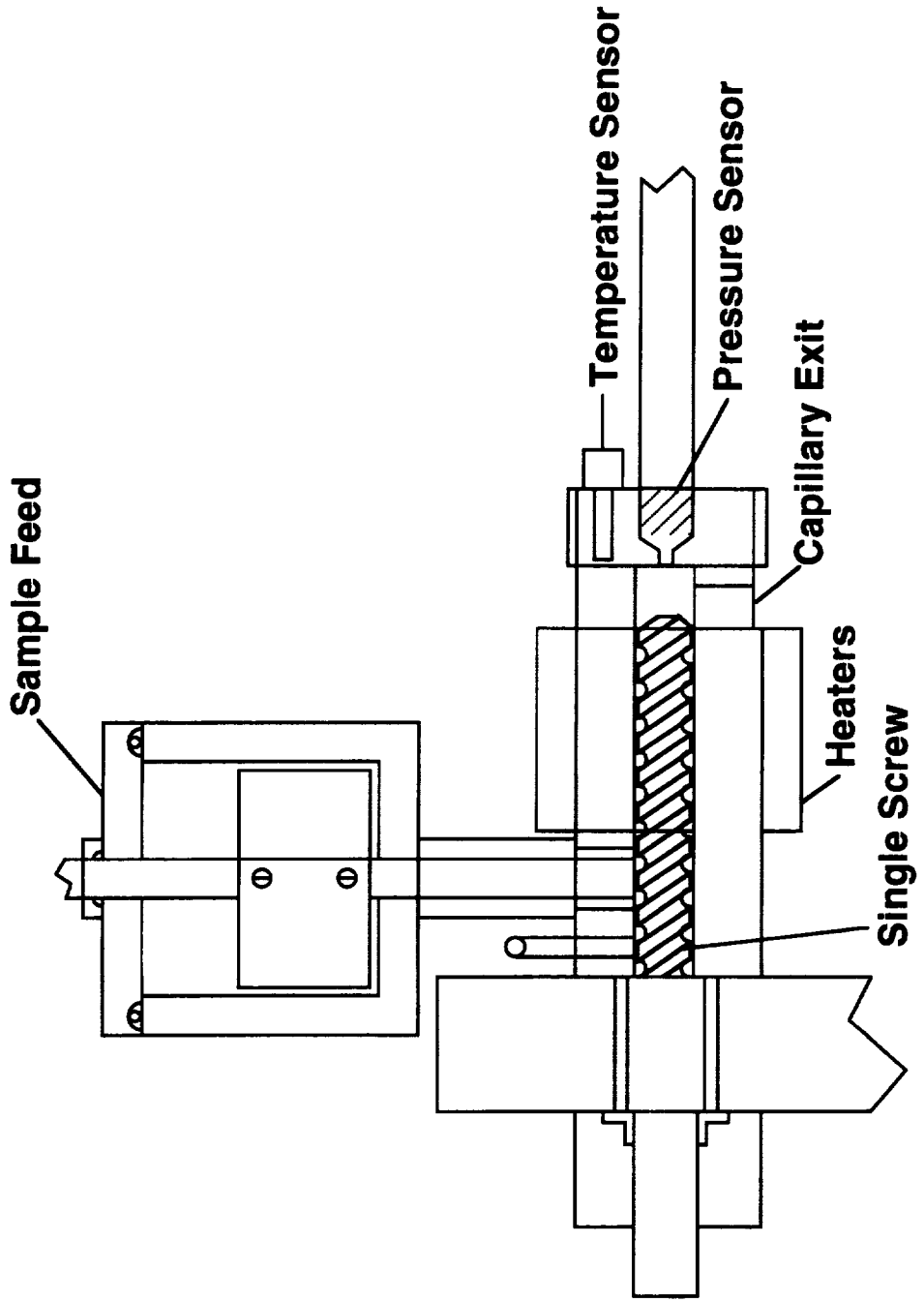
Thermogravimetric Analysis Data



Thermal Characterization

| Sample Offset (%) | Tg from DMA (°C) | Tg from DSC (°C) | 5% Weight Loss (°C) | Weight Change at 177°C After 100 Hours (%) |
|-------------------|------------------|------------------|---------------------|--|
| 0 | 253 | 239 | 498 | -0.2 |
| 1 | 258 | 248 | 523 | 0 |
| 2 | 250 | 248 | 467 | 0 |
| 3 | 249 | 242 | 527 | 0 |
| 4 | 246 | 230 | 505 | -0.2 |
| 5 | -- | 231 | 520 | 0 |

Profile of Vacuum Microextruder



Melt Viscosity Calculation

$$\eta = \tau_w / \dot{\gamma}_w$$

$$\tau_w = RP/2l$$

$$\dot{\gamma}_w = 4Q/\pi R^3$$

η = Melt Viscosity

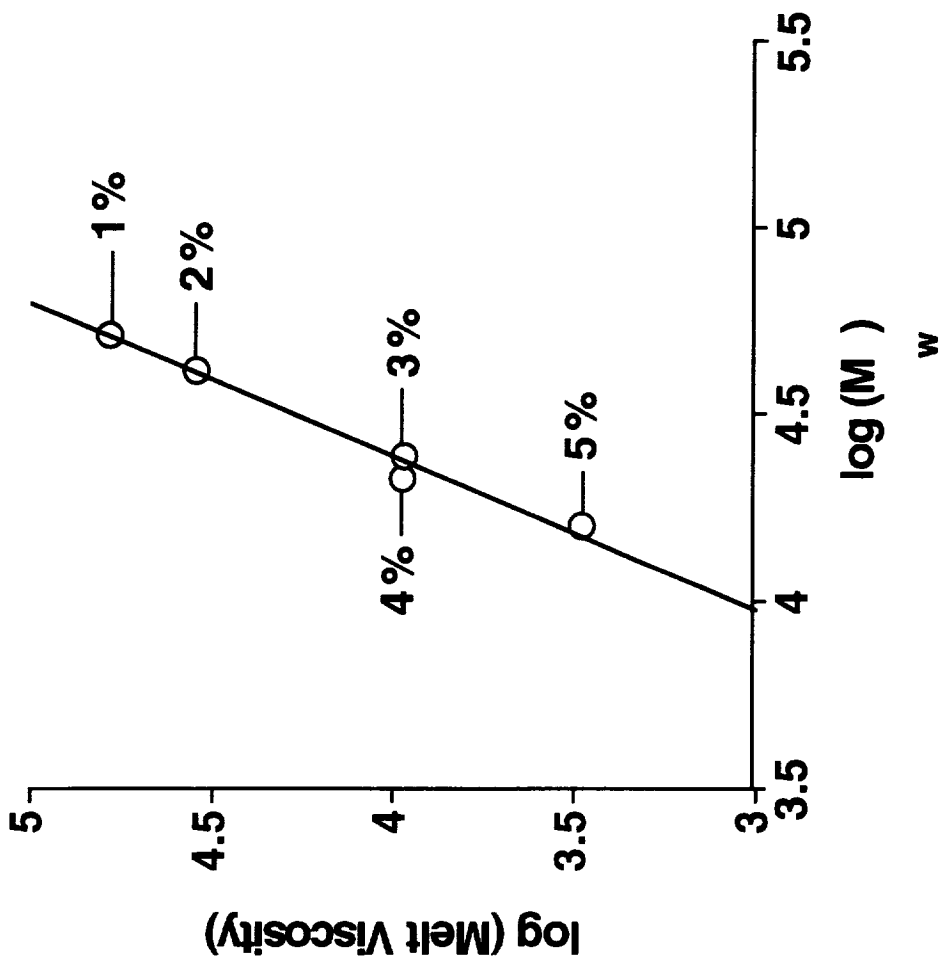
Q = Volume Flow Rate

R = Capillary Radius

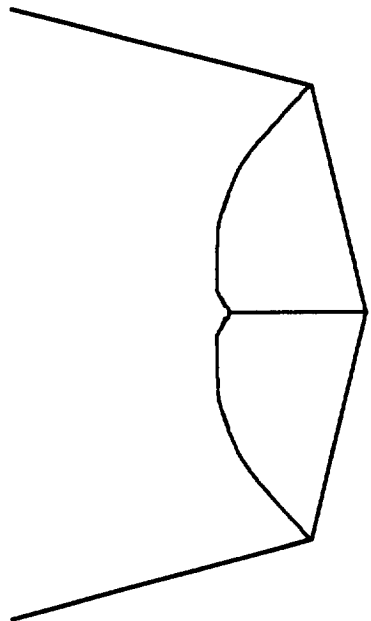
P = Pressure Drop

l = Capillary Length

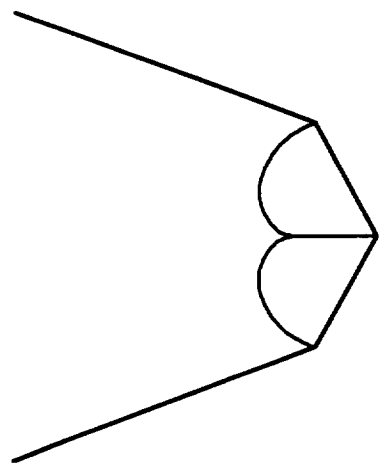
Relationship of Melt Viscosity to Molecular Weight



Microhardness Determination



Front View
($172^\circ 30'$)



Side View
(130°)

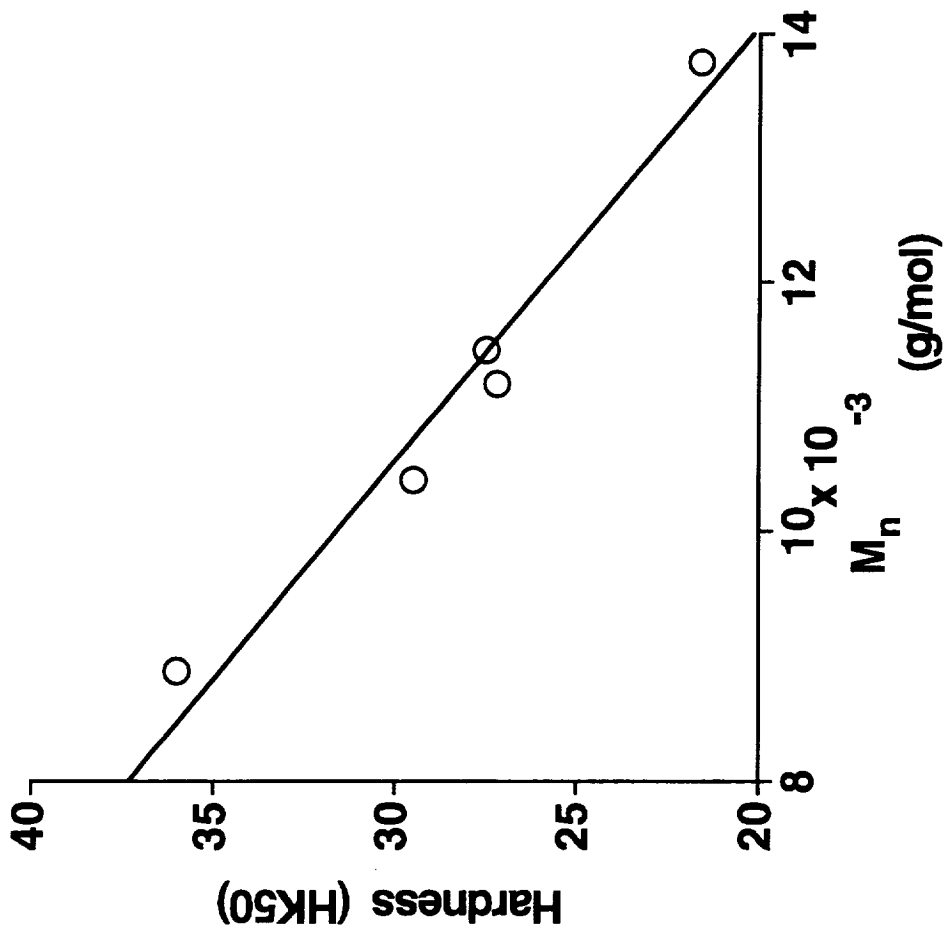
$$KHN = P/AP$$

KHN = Knoop Hardness

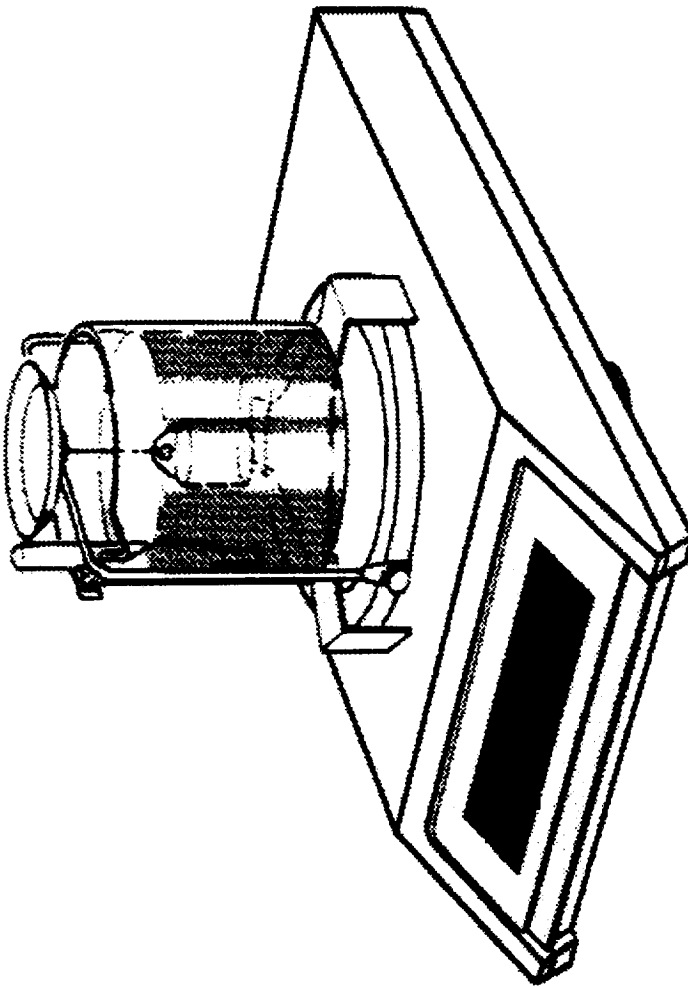
P = Load (kg)

AP = Area of the Impression

Relationship of Hardness to Molecular Weight



Density Determination Apparatus



$$\rho_2 = \frac{A}{P} \cdot \rho_0$$

ρ_2 = Density of Solid Body

A = Weight of Solid Body in Air

P = Buoyancy of Solid Body in Test Liquid

ρ_0 = Density of Test Liquid at a Given Temperature

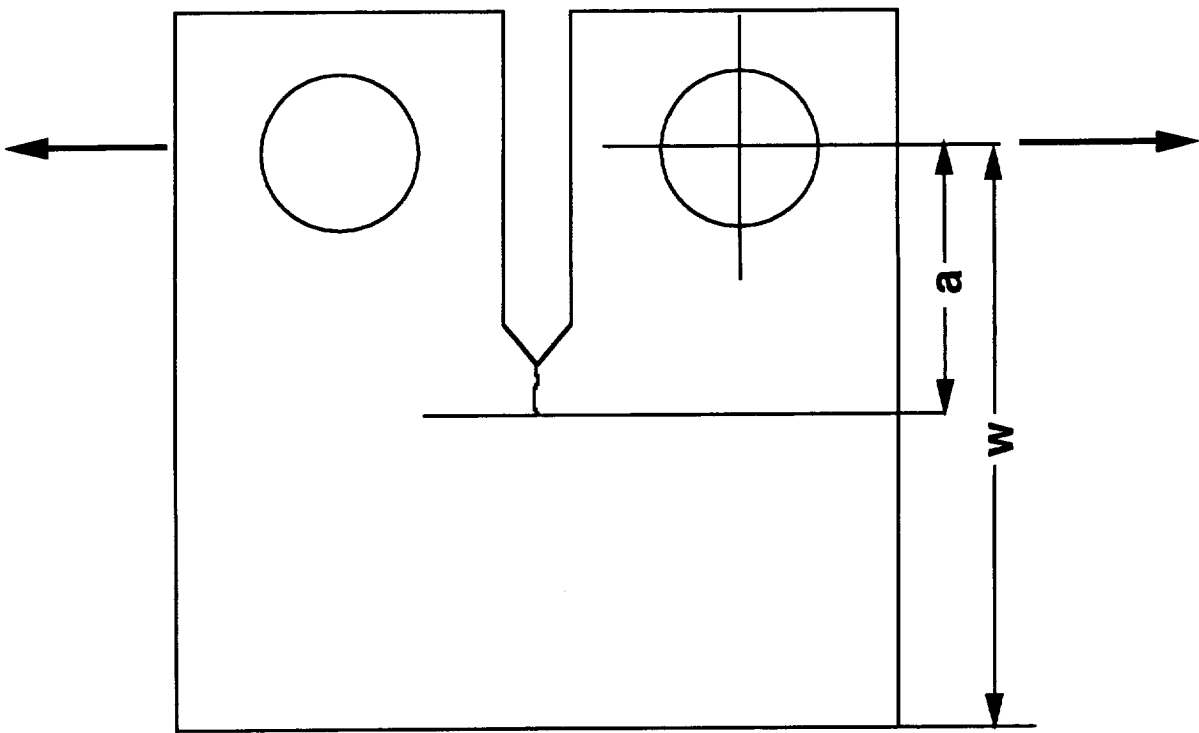
Density of LaRCTM-SI

| Stoichiometric Offset (%) | Density (g/cc) |
|---------------------------|----------------|
| 0 | 1.365 |
| 1 | 1.360 |
| 2 | 1.361 |
| 3 | 1.359 |
| 4 | 1.359 |

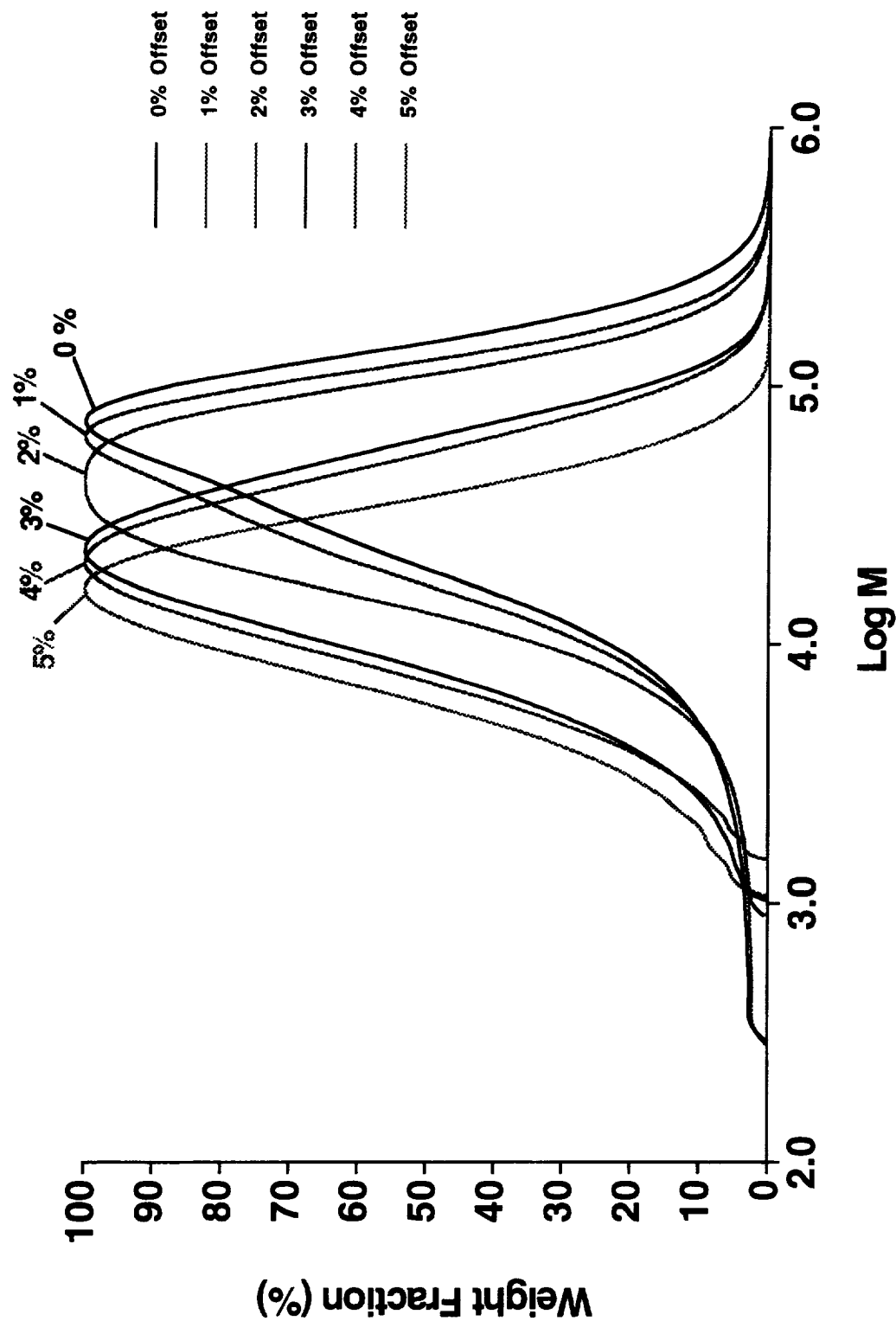
Compact Tension Configuration for Fracture Toughness

$$K_Q = (P_Q / BW^{1/2}) \cdot f(a/W)$$

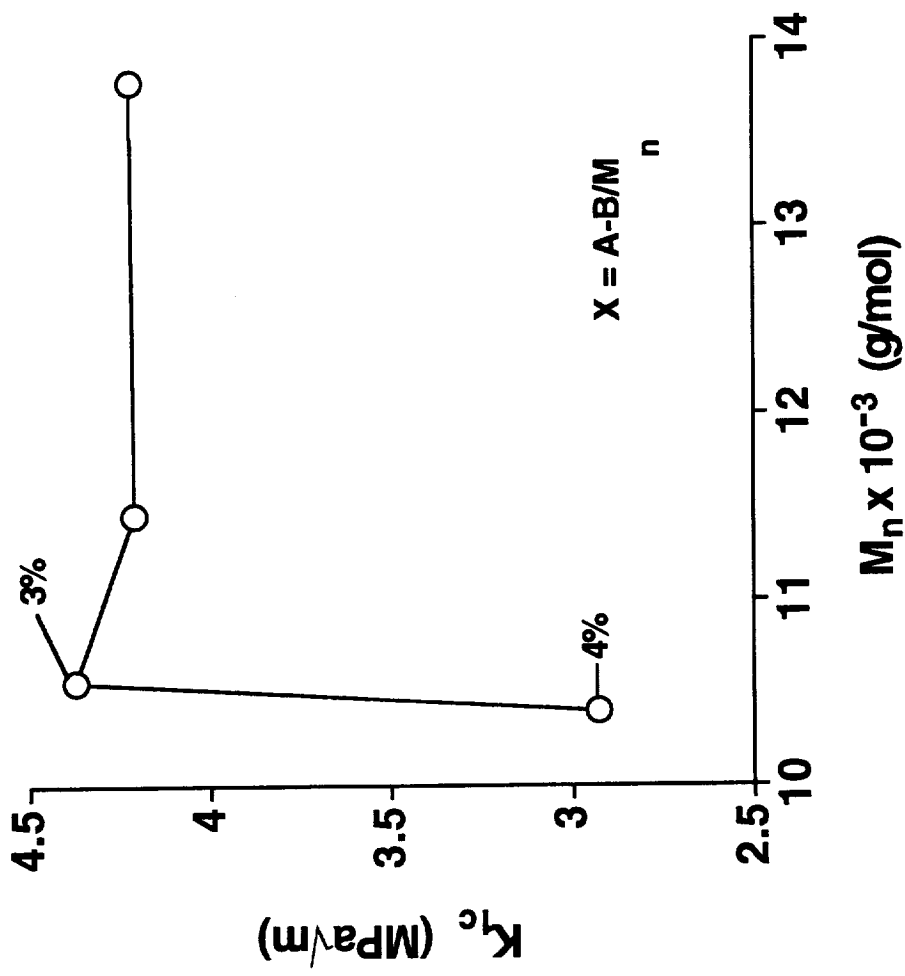
K_Q = Fracture Toughness
 P_Q = Maximum Load
B = Specimen Thickness
W = Specimen Width
a = Crack Length



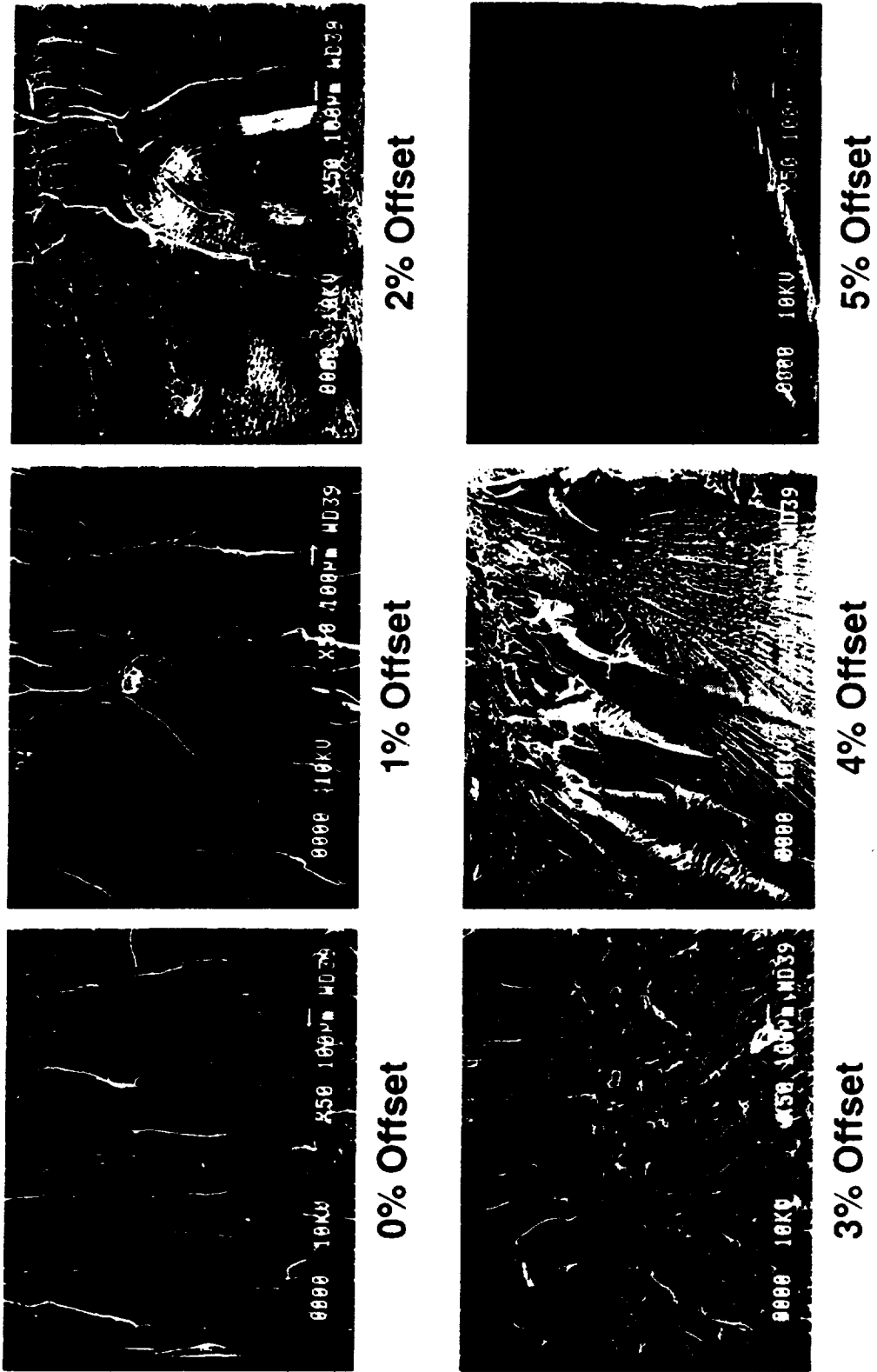
Effect of Stoichiometric Imbalance on Molecular Weight Distribution



Effect of Molecular Weight on Fracture Toughness



SEM Photomicrographs of LaRC™-Si Fracture Surfaces



SUMMARY

- Controlled molecular weight soluble polyimides were synthesized.
- Stoichiometric offsets were reflected in the higher moments of the molecular weight distribution.
- Glass transition temperatures ranged from 230-248°C for 0-5% offset in stoichiometry.
- Scatter in TGA data showed no clear dependence of thermooxidative stability on molecular weight.
- Melt viscosity varied logarithmically with M_w .
- Density was not affected by molecular weight.
- Hardness varied linearly with M_n .
- Fracture toughness decreased sharply for materials with greater than 3% offset in stoichiometry.

FUTURE WORK

- Moldings have been made for other members of the NASA LaRC Computational Materials group.
- A series of phenylethynyl terminated LARCTM-SI is being synthesized to examine the effect of crosslinking on properties.

*Molecular Modeling of Novel Piezoelectric
Polyimides*

by

J.A. Young and B.L. Farmer
Department of Materials Science and Engineering
University of Virginia
Charlottesville, VA

and

J.A. Hinkley
NASA Langley Research Center
Hampton, VA

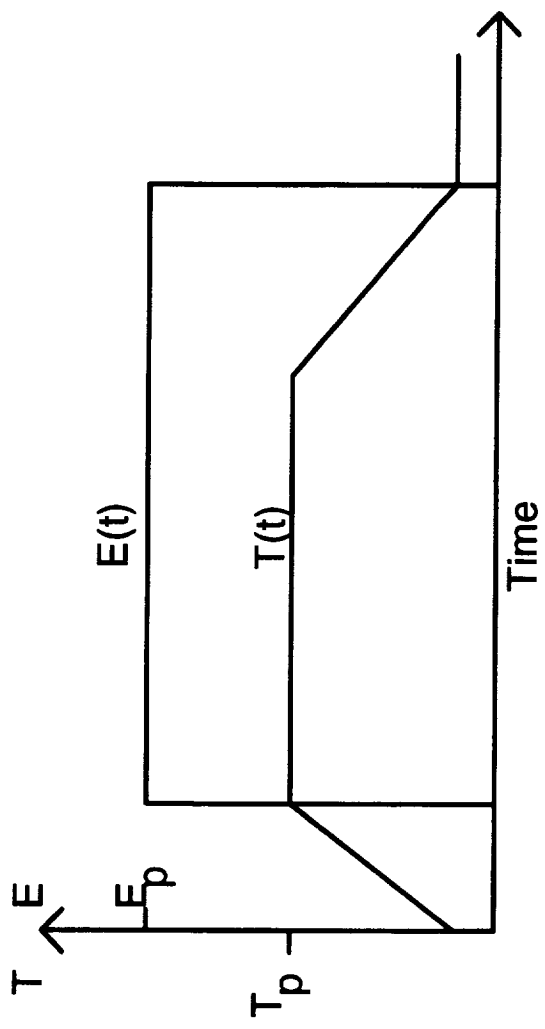
PURPOSE

Computational chemistry techniques are used to model the large piezoelectric responses seen in novel high temperature polyimides. Molecular orbital calculations and molecular dynamics on two dimensional systems are used to investigate the nature of the piezoelectric response by characterizing the underlying molecular physics of the process. This information will then be used to propose mechanisms for enhancing the response by maximizing the polymers ability to assume conformations that enhance the materials polarization and its electrical response to stress.

PIEZOELECTRICITY

Materials which electrically responded to mechanical deformations (or visa versa) are said to be piezoelectric. Piezoelectric materials are formed from polar amorphous polymers by:

- 1) inducing orientation polarization. Apply an electric field, E_p , at a temperature, T_p , near T_g to induce a remnant polarization, P_r in the material.



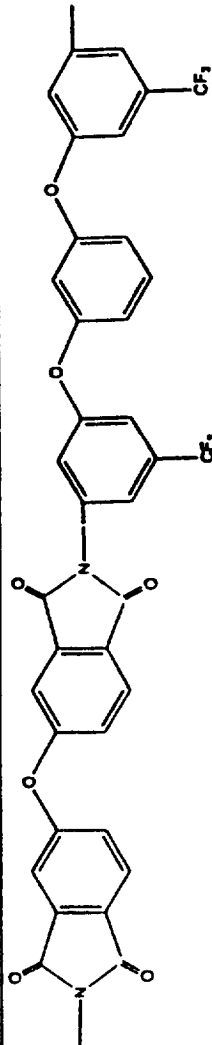
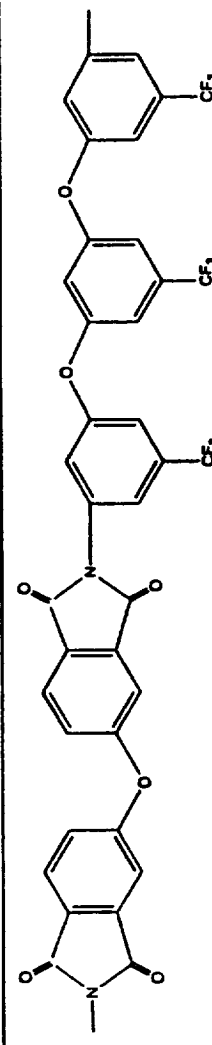
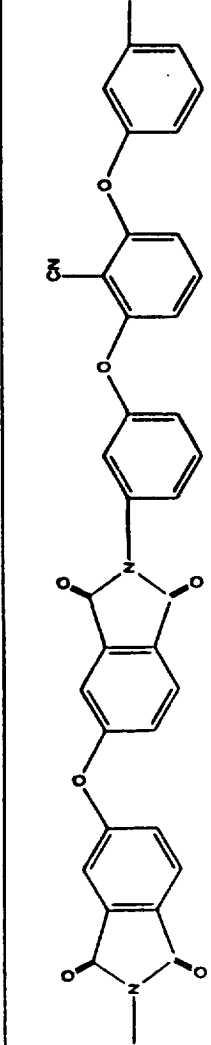
- 2) characterize the electrical response (electrical current, D or electric field, E) of the material as a function of mechanical deformation, T .

$d = (\delta D / \delta T)_E$ for closed circuit

or

$g = (\delta E / \delta T)_D$ for open circuit

MOLECULES OF INTEREST

| Polyimide Structure | Tg (K) | g_{33} (Vm/N) at 353 K * |
|---|--------|----------------------------|
|  | 449 | 8.0 |
|  | 453 | 8.5 |
|  | 493 | 13.5 |

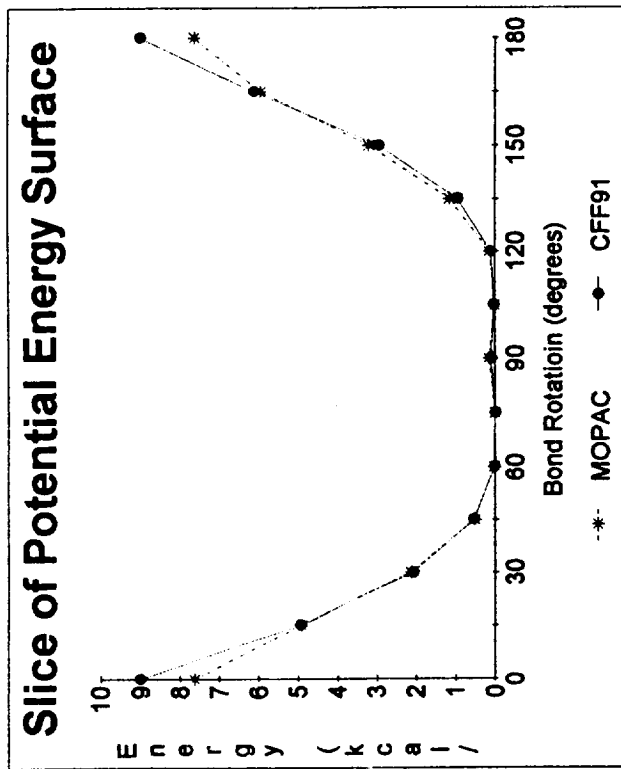
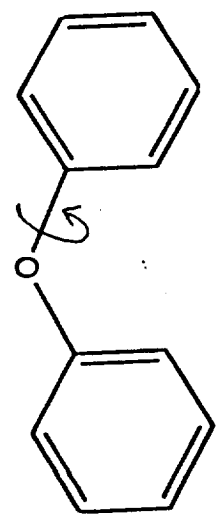
Note: for PVF₂ $g_{33} = 0.2$ Vm/N at 353 K.

* Joycelyn O. Simpson et al., Novel Piezoelectric Polyimides, Proceedings of the 1995 Fall Meeting of the Materials Research Society (November 27-December 1, 1995) Boston, Massachusetts.

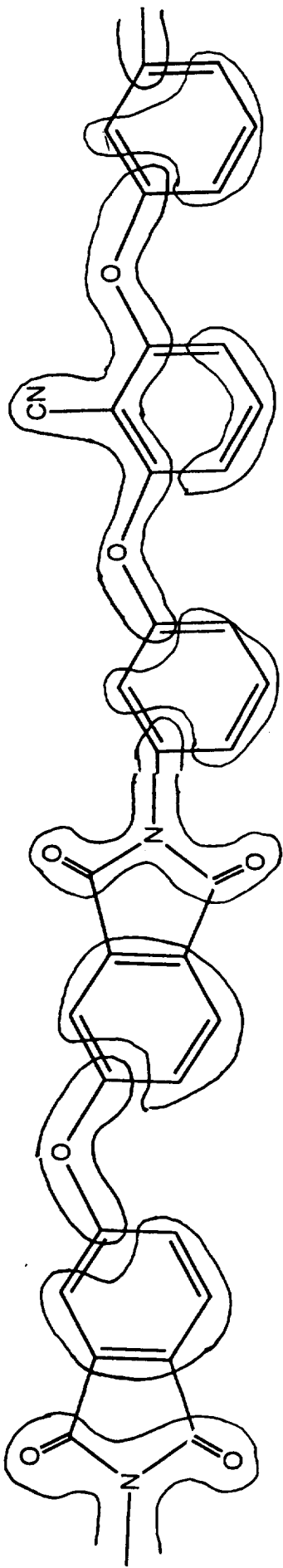
PARAMETERIZATION

Prior to being able to carry out force field based calculations (molecular mechanics or molecular dynamics) the proper force field parameters must be obtained.

- # Compare the potential energy surfaces of components of the polyimide backbone calculated via quantum mechanical methods and molecular mechanics with various force fields.
 - ❖ Modification of BIOSYM's CFF91 force field reproduced the MOPAC / Ab Initio surfaces.



¶ MOPAC with the AM1 parameterization was used to generate partial atomic charges for the polyimides. Charge neutral groups were then formed while maintaining the original dipole moment.



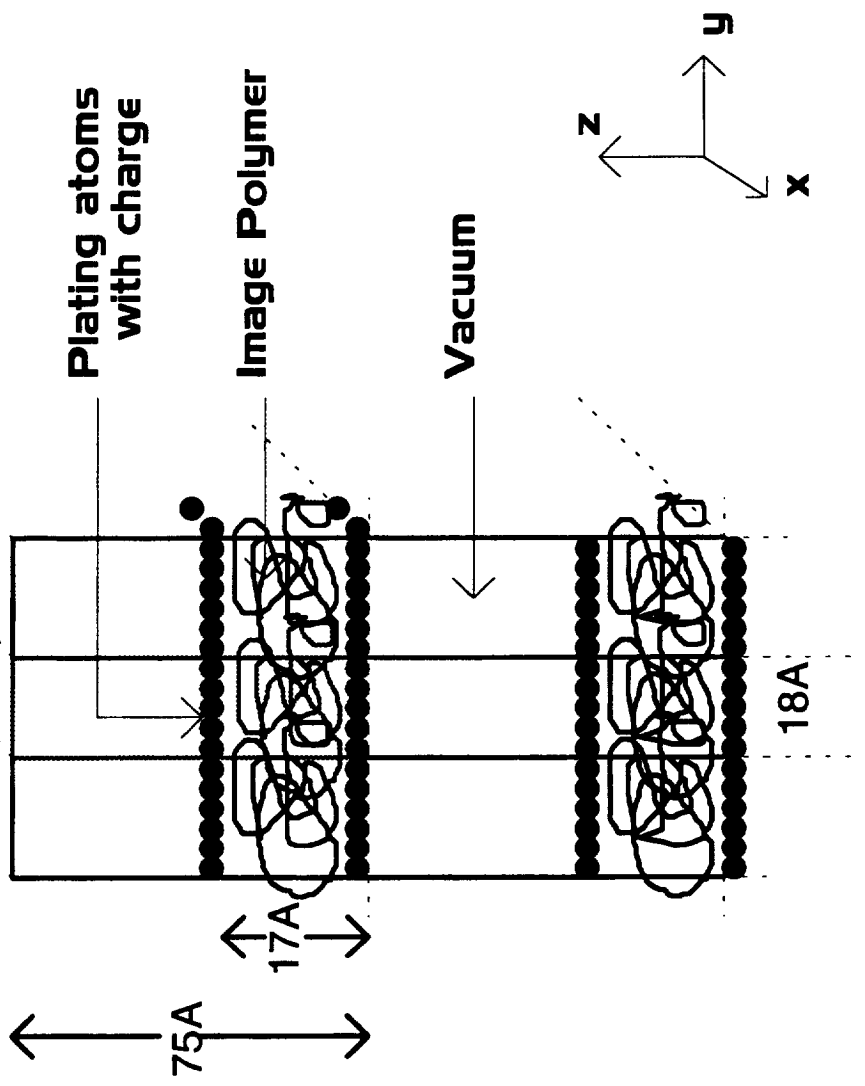
GENERATE AMORPHOUS CELL

Construction of a two dimensionally periodic amorphous box was done via the Amorphous Cell module in BIOSYM.

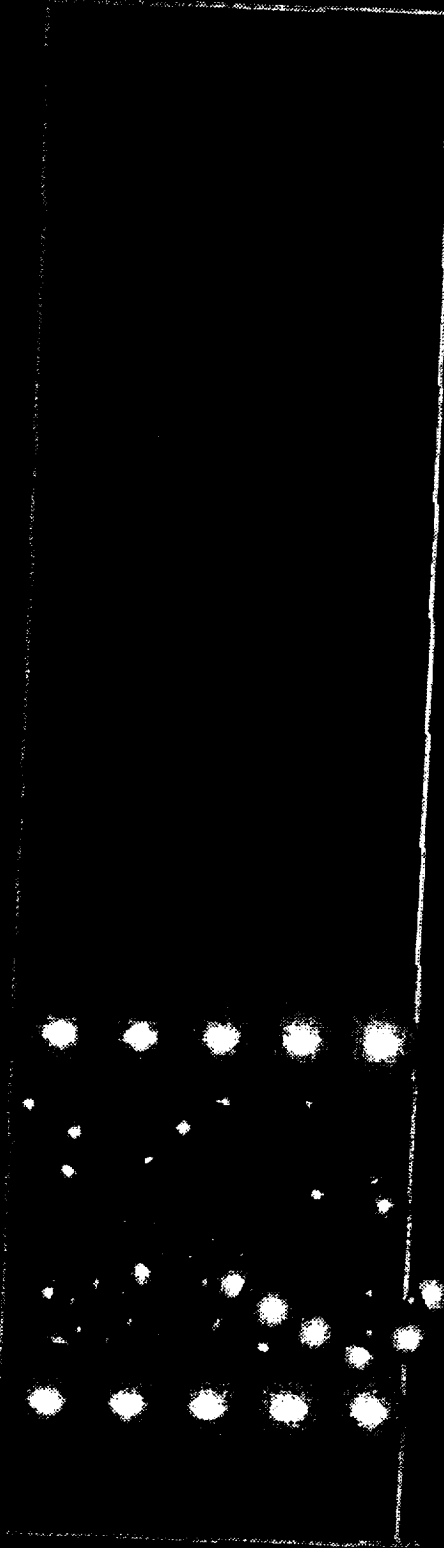
⌘ Build a low density (0.2 g/cm³) five-mer polyimide cell.

⌘ Run high pressure (5000 bar) molecular dynamics until system reaches experimental density (1.34 g/cm³).

⌘ Merge plates of tightly packed 'dummy atoms' to x-y faces of polymer cell. Placing charges on these plates will simulate the electric poling field.



View of parent box (red) within the systems periodic boundaries.



The parent cell containing a five-mer polyimide and plating atoms.

❖ Molecular dynamics was done to obtain a starting configuration.

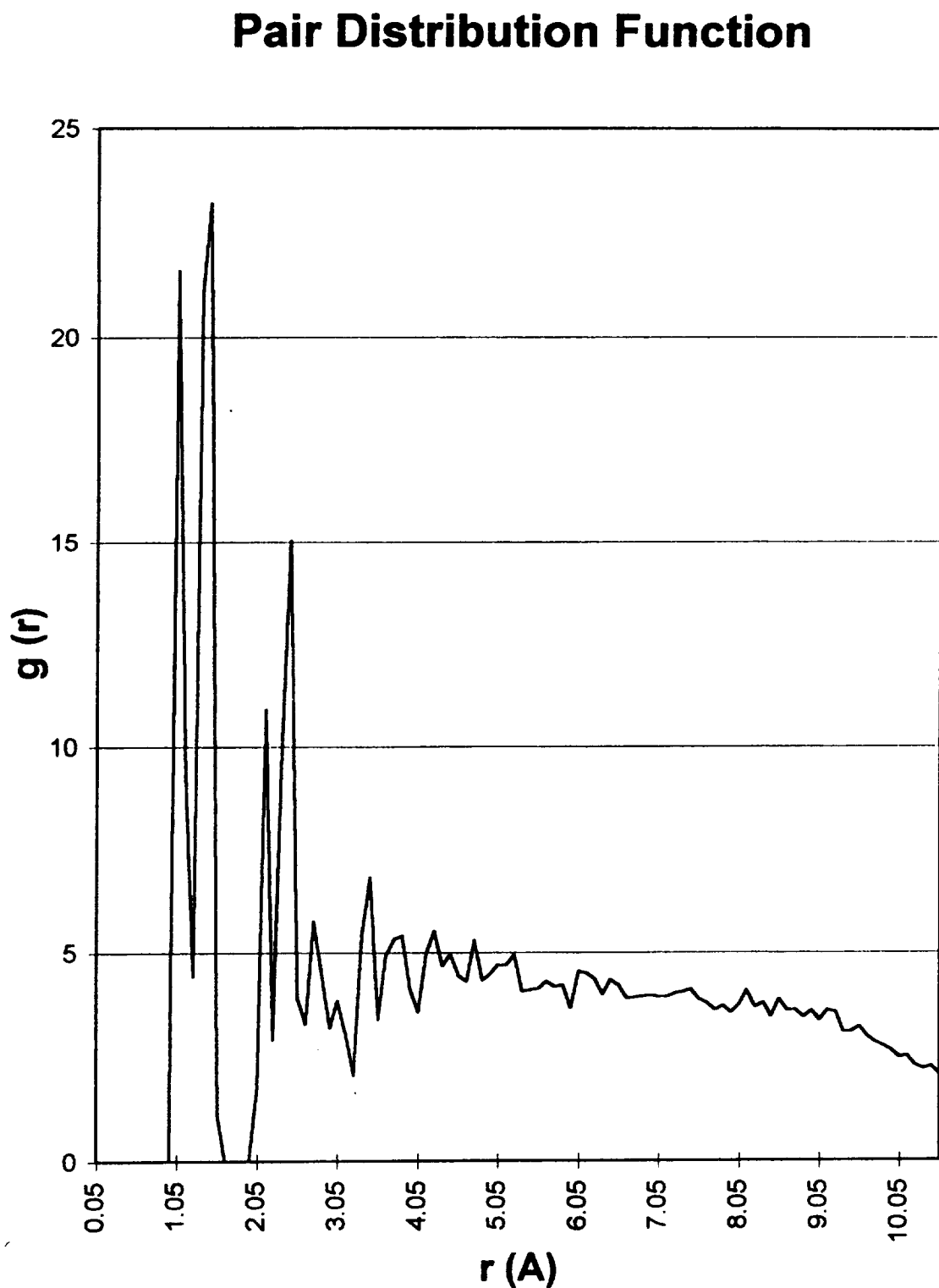
- ❖ The plates of dummy atoms were fixed in space.
- ❖ Group based non-bonded cutoffs of 9.5 Å for the Lennard Jones contribution and 17.5Å (the distance between the plates) for the Coulombic terms were used.

❖ The total pair distribution function is the probability of finding any two atoms at a distance r apart relative to the expected probability for a homogeneous system with random atoms.

$$g(r) = (N_r * V) / (N * 4 * \pi * r^2 * dr)$$

- ❖ The peaks are associated with specific covalent bonds and interatomic distances along the rings. The absence of peaks at long distances, $r > 5\text{Å}$, indicates the lack of long range order in the system.

Chart1



POLE MATERIAL

Molecular dynamics was used to simulate the poling of the material.

Following Experimental Variables

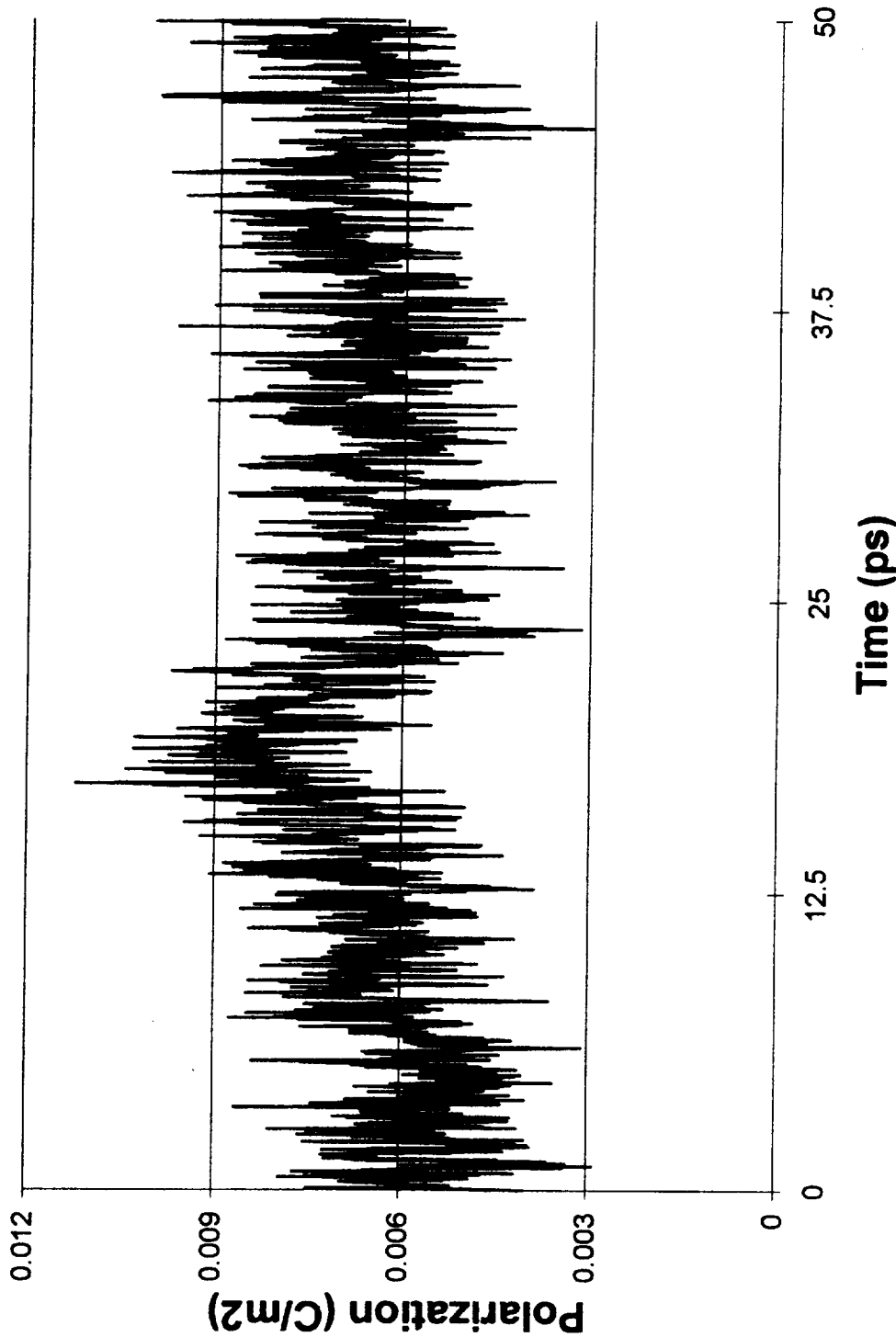
⌘ A poling field of 150 MV/m ($+/- 0.013 e^-/\text{plating atom}$) was placed on the system at $T_p=500\text{K}$.

⌘ 50ps for dynamics were run at 500K.

⌘ System was cooled to 300 K in 10 K steps each lasting 10 ps. Once at 300 K the system was simulated for 50 ps.

Char2

Polarization of Cell



A small polarization of $0.006 \text{ C}/\text{m}^2$ was obtained when using experimental parameters.

Collapse Time Scale

- ⌘ Dipole relaxation times are of the order of micro-seconds.
Molecular dynamics calculations cover only the pico-second / nano-second range.
- ⌘ Collapse the time scale of the polarization process into the pico-second range.
 - ❖ Translate time and temperature.

$$\tau = [3\epsilon_s/(2\epsilon_s + \epsilon_\alpha)]^* [h/kT]^* [\exp(\Delta F/kT)]$$

- ❖ Maintain the population densities of the dipoles.

$$mE / kT$$

⌘ Collapsed parameters for dynamics simulation.

- ❖ $T_p = 2100 \text{ K}$
- ❖ $E_p = 700 \text{ MV/m}$ (i.e. +/- 0.052 e⁻/plating atom)

The calculated polarization of 0.02 C/m^2 is obtained when using the parameters obtained after collapsing the time scale.

Dipole Reorientation

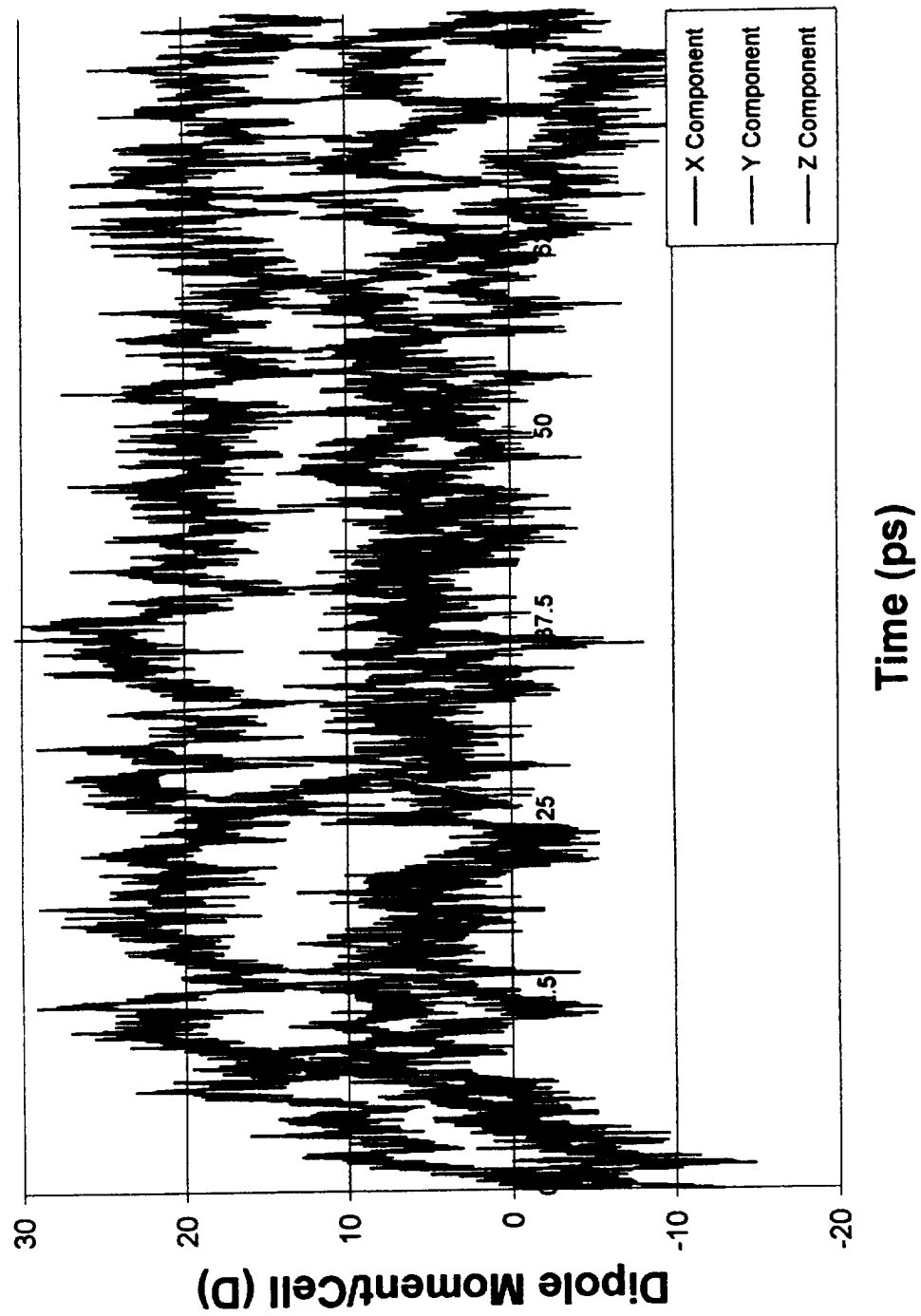
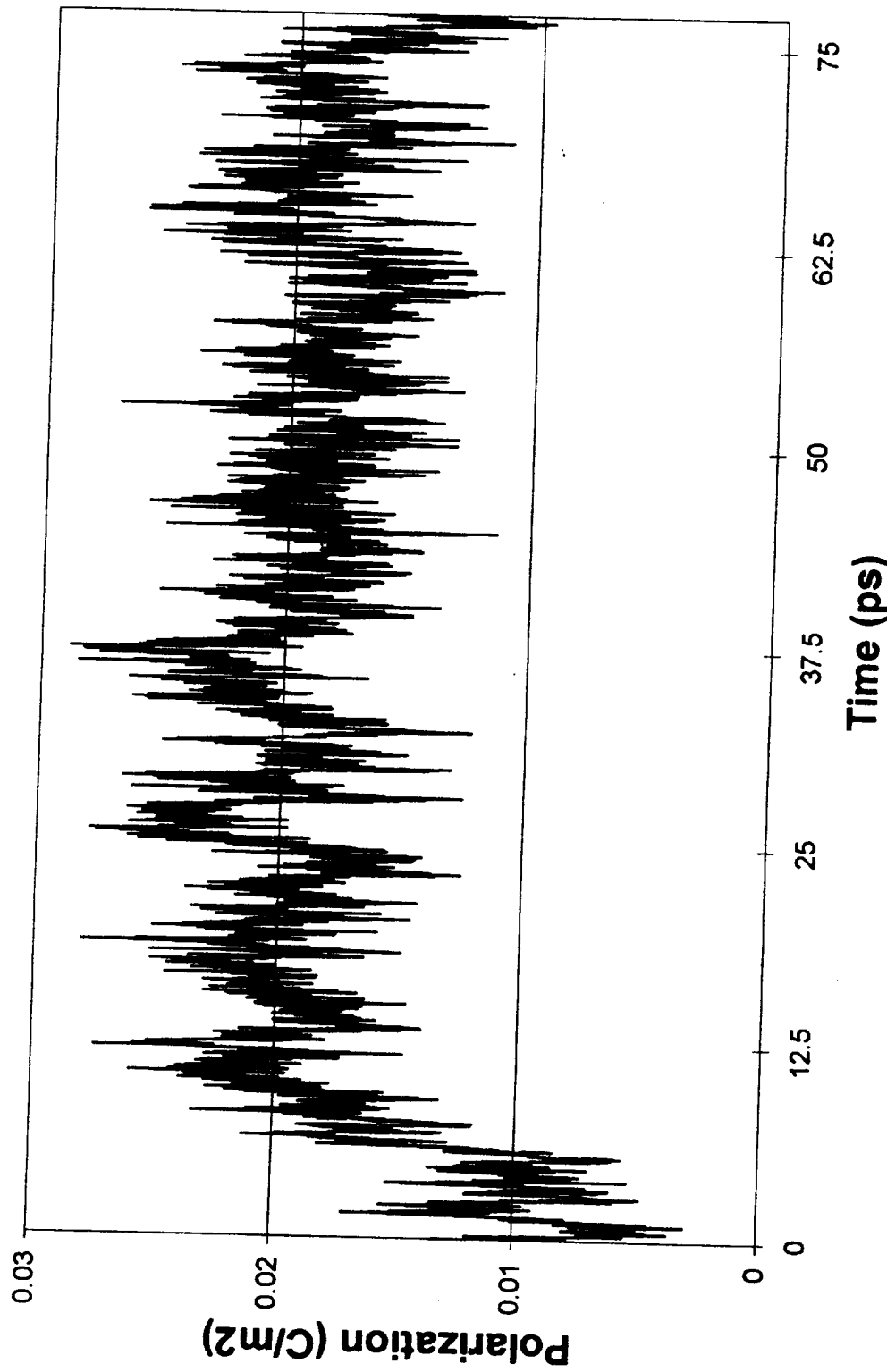


Chart2

Polarization of Cell



A polarization of $0.02\text{C}/\text{m}^2$ was obtained when using the collapsed time scale parameters

CONCLUSIONS

- ⌚ Force field parameters were corrected then validated to give agreement with quantum mechanical results.
- ⌚ The bulk polyimide was modeled by creating a two dimensionally periodic amorphous cell.
- ⌚ Computer simulation techniques have been developed to model the poling of amorphous polyimides.
- ✖ High temperatures and high poling fields were used to account for the long relaxation times.
- ✖ Polarizations of 0.02 C/m^2 were calculated for the polyimide.

FUTURE WORK

- ⌚ Construct and simulate several initial configurations to achieve better statistics.
- ⌚ Calculate piezoelectric response by monitoring dipole orientation during constant stress dynamics.
- ⌚ Analyze molecular motions which occur as a result of the poling and deformation processes.
- ⌚ Propose novel polyimide structures and rank their piezoelectric responses, calculation of absolute values is not the focus of this research.

ACKNOWLEDGMENTS

We would like to thank the following:

NASA Langley the sponsor of this project:
The Graduate Student Researchers Program

Joycelyn O. Simpson of NASA Langley Research Center,
Hampton, VA for providing the experimental input.

Fiona Case of BIOSYM Technologies, San Diego, CA for
providing software support.

Monte Carlo Simulation

of a

Polyimide Melt

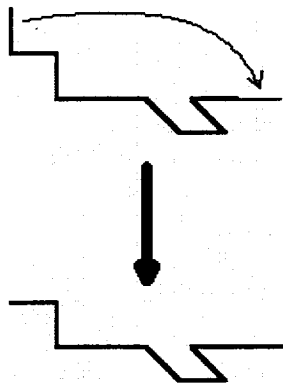
Monte Carlo

- Bridge the gap between sub-microscopic and macroscopic
 - Retain knowledge and detail of sub-microscopic system
 - Determine macroscopic quantities
- Larger system sizes
- Faster simulations (larger time frame available)

Types of Monte Carlo

- Slithering Snake
- Kink-Jump
- Bond Fluctuation

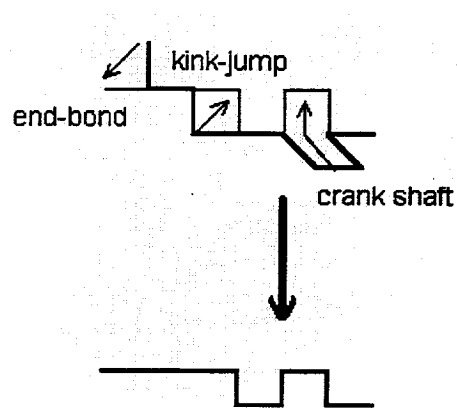
Slithering Snake Monte Carlo



- One move type
- Unrealistic on local scale

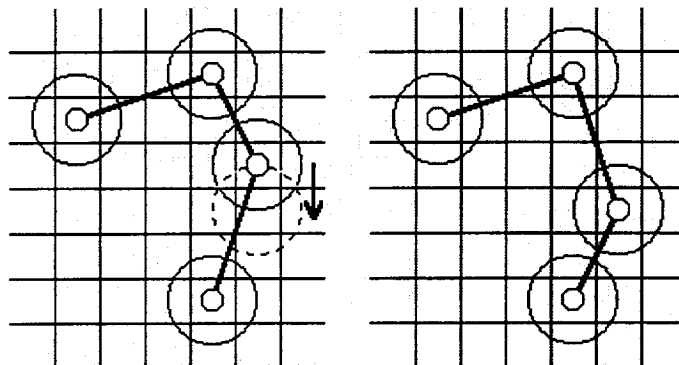
T. Wall and F. Mandel, *J. Chem. Phys.* **63**, 4592 (1975)

Kink Jump Monte Carlo



H. Verdier and W. H. Stockmayer, *J. Chem. Phys.* **36**, 227 (1962).

Bond Fluctuation Monte Carlo



1. H. P. Deutsch and K. Binder, *J. Chem. Phys.* **94**, 2294 (1991).
2. W. Paul, K. Binder, J. Batoulis, B. Pittel and K. H. Sommer, *Makromol. Chem., Macromol. Symp.* **65**, 1 (1993).
3. M. Schulz and J. U. Sommer, *J. Chem. Phys.* **96**, 7102 (1992).
4. J. U. Sommer, M. Schulz and H. L. Trautenberg, *J. Chem. Phys.* **98**, 7515 (1993).

Bond Fluctuation vs Kink-Jump

BFMC

KJMC

ADVANTAGES

- | | |
|--|---|
| <ul style="list-style-type: none"><input type="checkbox"/> Computationally more efficient<input type="checkbox"/> One move type<input type="checkbox"/> Acceptance probability higher<input type="checkbox"/> Faster equilibration in dense systems | <ul style="list-style-type: none"><input type="checkbox"/> Longer move length<input type="checkbox"/> Faster equilibration in less dense systems |
|--|---|

DISADVANTAGES

- | | |
|--|--|
| <ul style="list-style-type: none"><input type="checkbox"/> Short move length<input type="checkbox"/> More steps to reach equilibrium<input type="checkbox"/> Slower equilibration time in less dense systems | <ul style="list-style-type: none"><input type="checkbox"/> Three types of motion<input type="checkbox"/> Lower acceptance probabilities<input type="checkbox"/> Computationally less efficient<input type="checkbox"/> Slower equilibration time in dense systems |
|--|--|

Bond Fluctuation Monte Carlo: The details

Allowed motion:

$P(1,0,0)$

Allowed bond vectors:

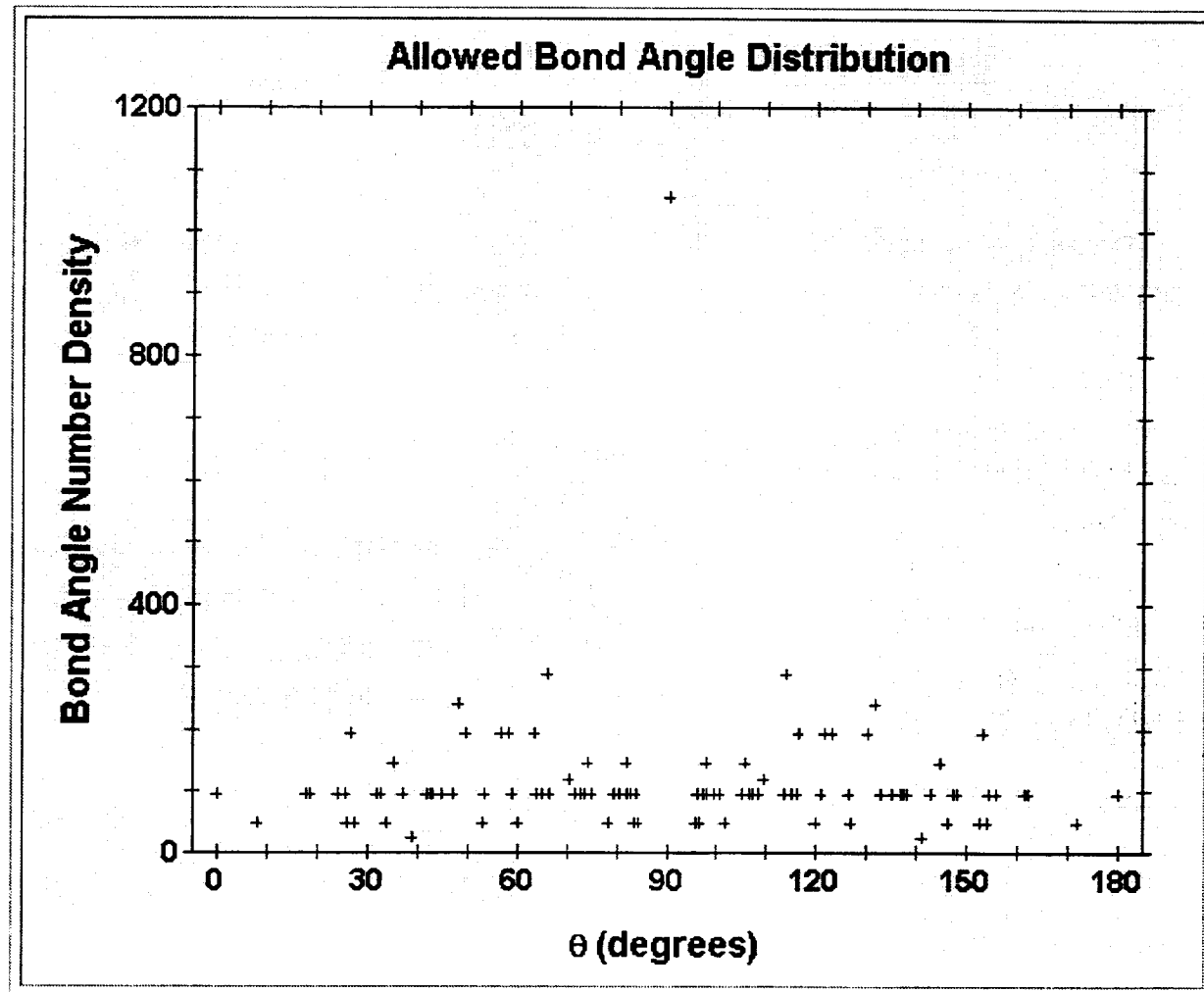
Union of:

$p(2,0,0), p(2,1,0),$
 $p(2,1,1), p(2,2,1),$
 $p(3,0,0), p(3,1,0)$

This yields 108 Bonds with 5 different bond lengths

$b = 4^{1/2} (2), 5^{1/2}, 6^{1/2}, 9^{1/2} (3),$
 $10^{1/2}$

Two successive bonds may have up to 87 different angles over the interval [0-180] degrees.



Summary of Restrictions

Excluded Volume:

The surrounding 26 grid locations must be vacant.

Bond Vector:

Set of allowed bond vectors prevents intrachain crossing.

Allows only 5 bond lengths.

Allows only 87 bond angles.

What About Energetics?

Metropolis Transition Probability: $w = \min[1, e^{(-E/kT)}]$

Energy Restrictions

Psuedo Bond Length

No Restrictions

Bond Angles

Restricted by bond bend stiffness (calculated via biosym)

"Long Range Torsions"

Calculate Energies for torsions and restrict accordingly

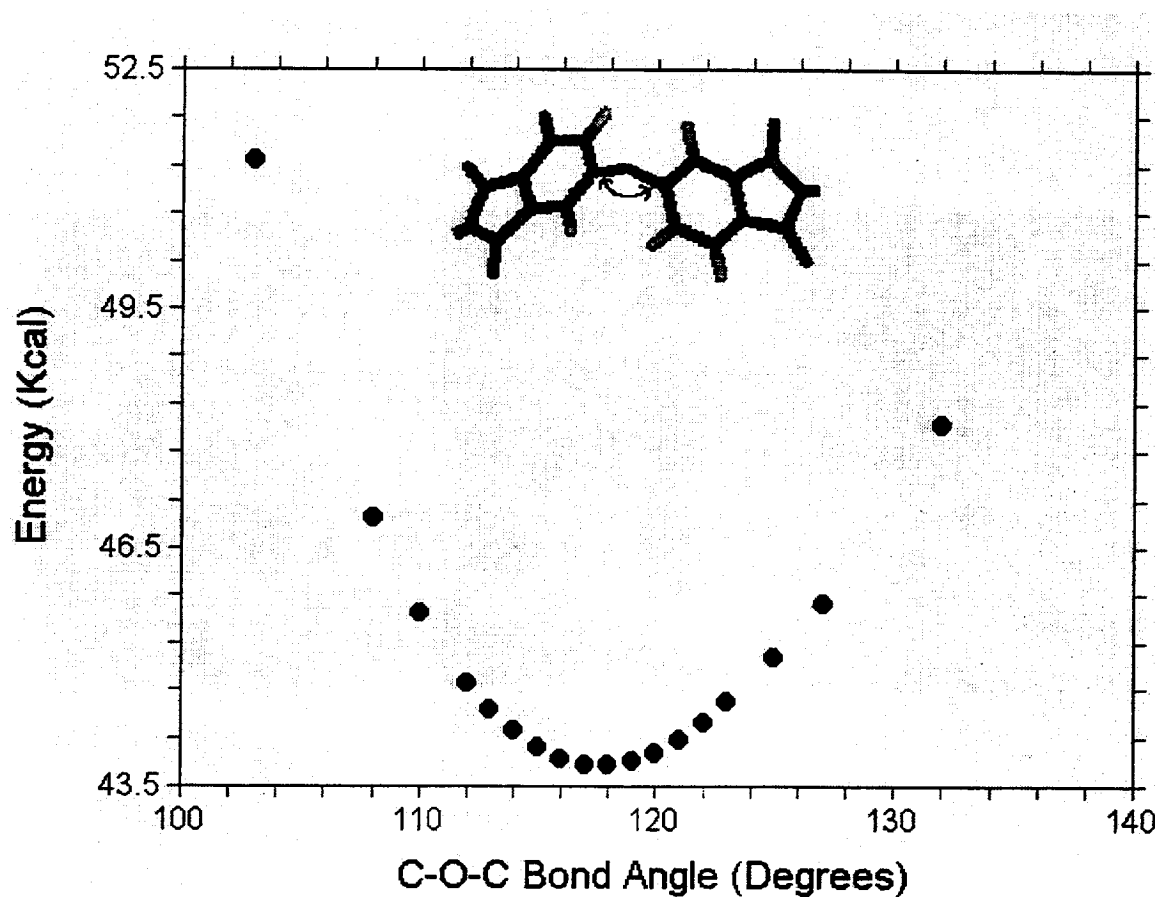
Inter-chain interactions:

Not accounted for as of yet

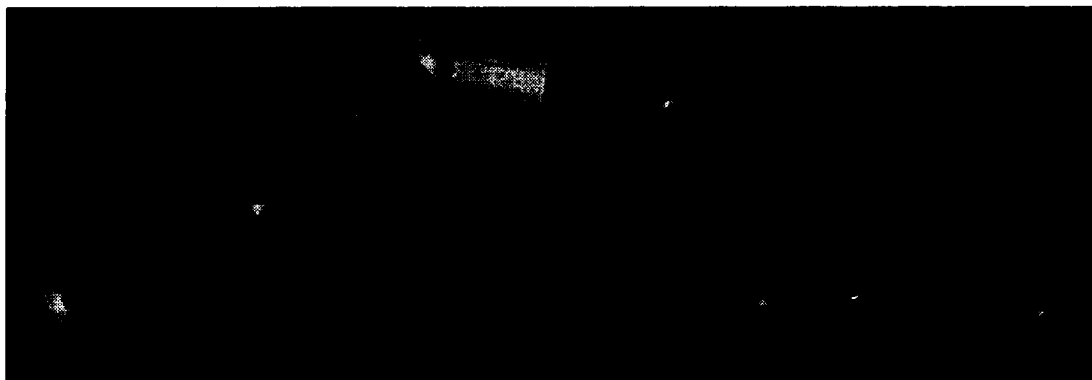
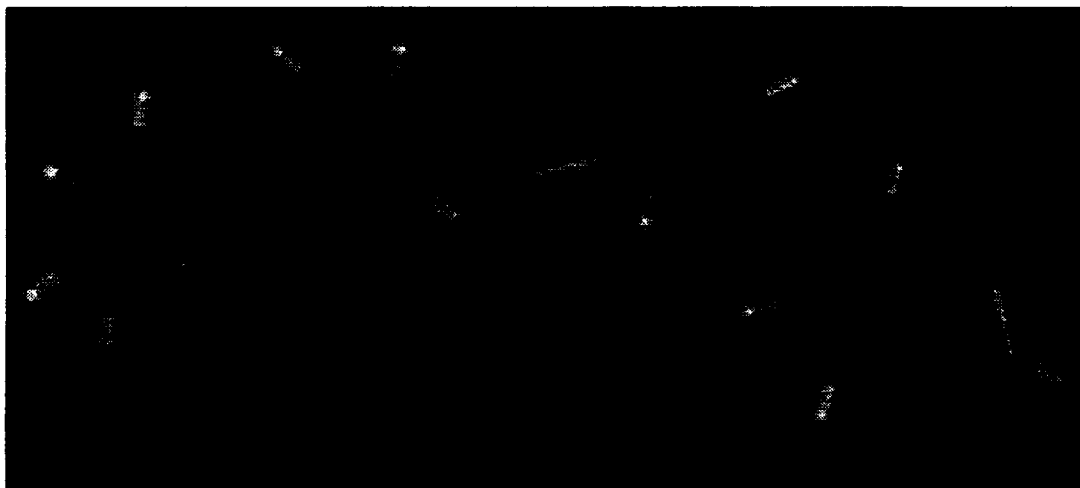
[Go to Page Seven](#)

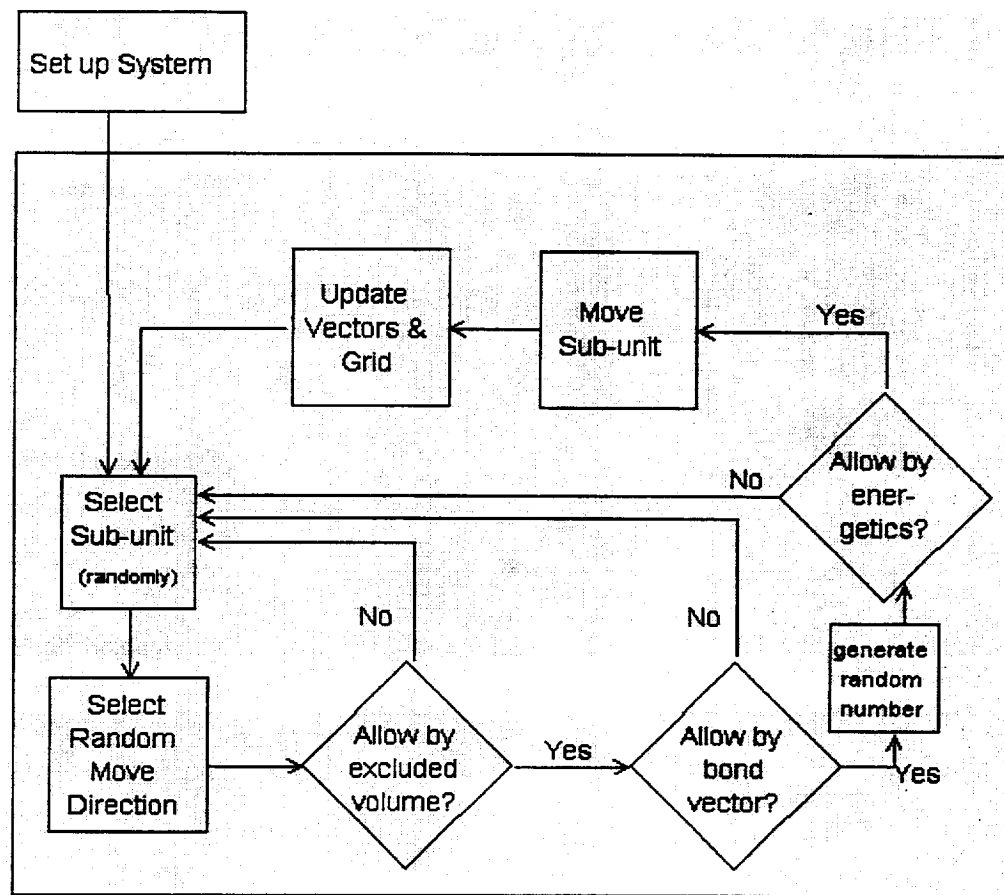
LARC-IA

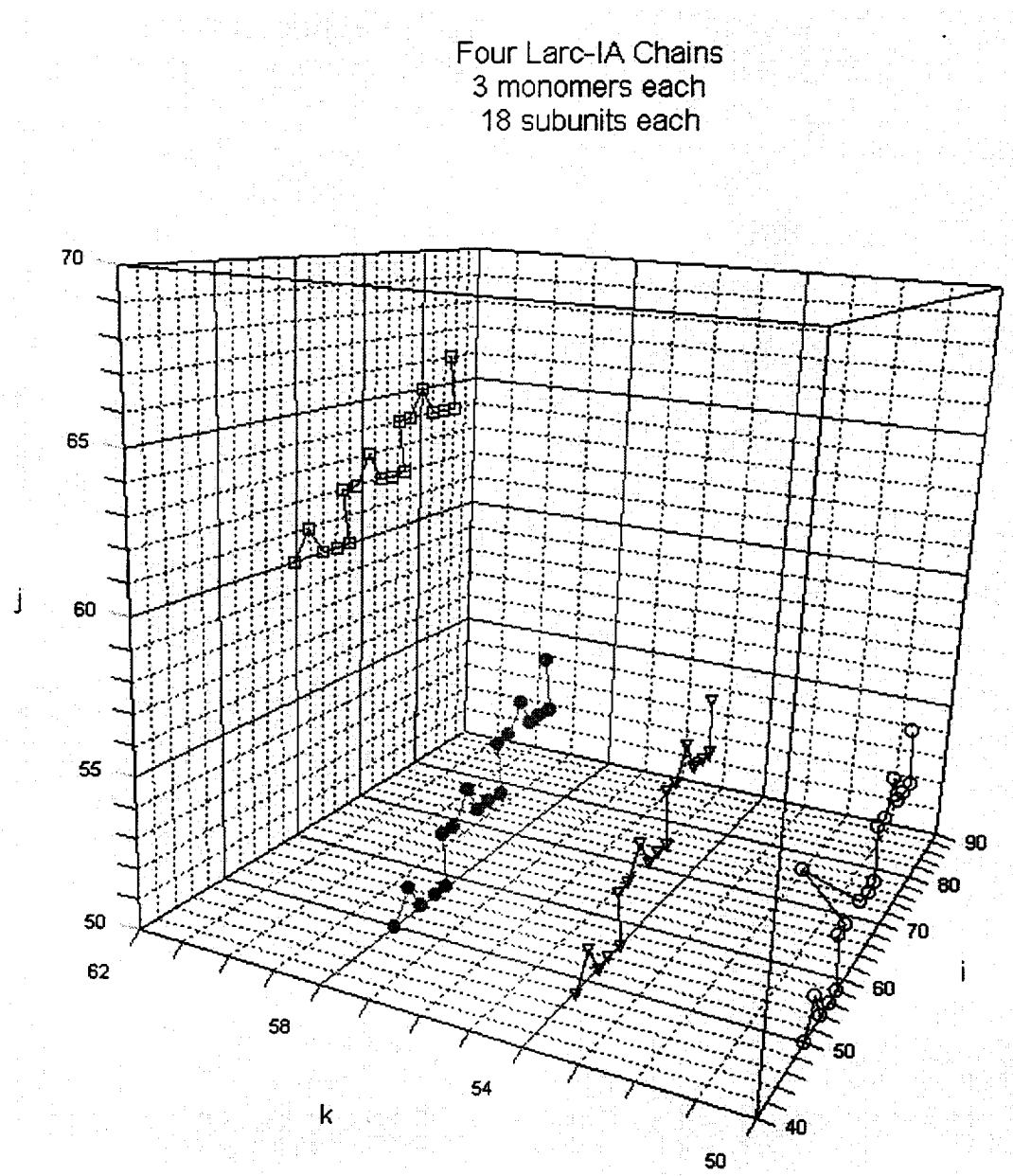




Bond Fluctuation representation of LARC-IA



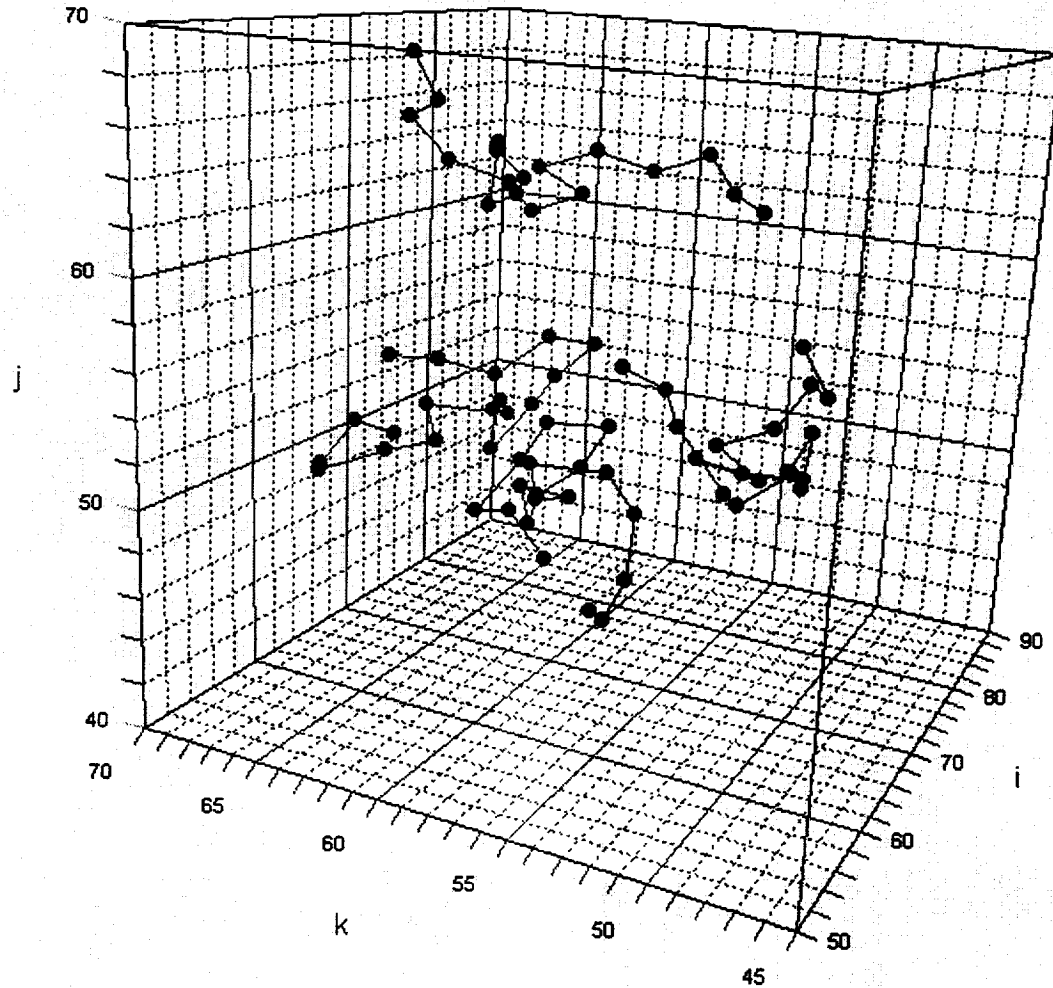




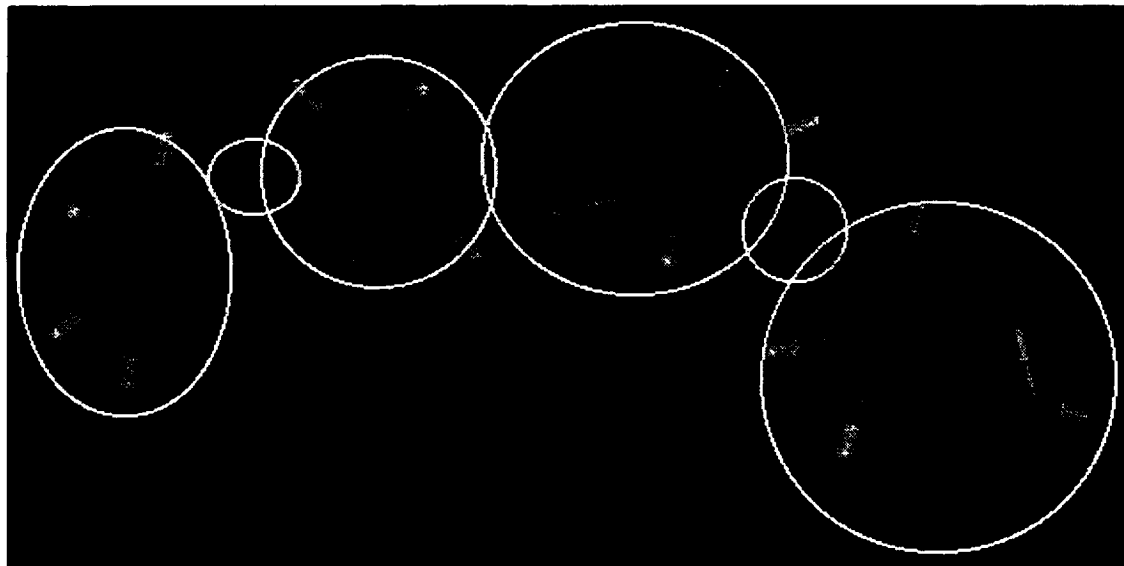
Four Larc-IA Chains

3 monomers each

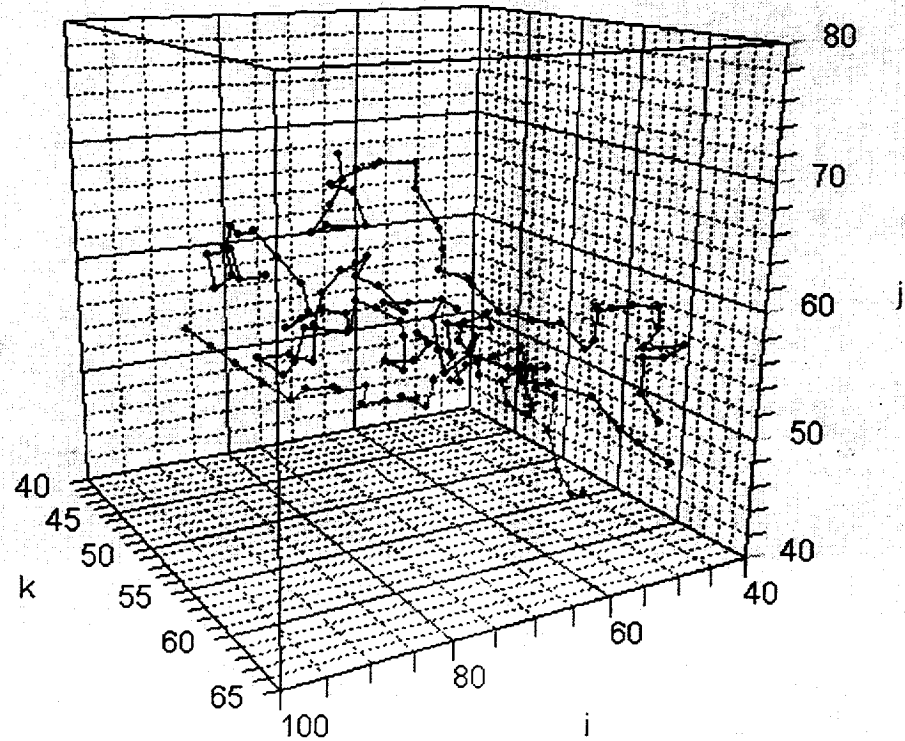
18 subunits each



Six sub-units of one monomer of LARC-IA



**4 Chains of Larc-IA
(6 monomers, 6 subunits)
after 50,000 MC steps**



Cross Linking

- Allow only end cross linking.
- Chain Ends will be allowed to cross link with other chain ends.
- All restrictions must still be met.
- Cross link kinetics as function of MC step (and also Time?).

Computational Materials Workshop, January 4-5, 1996

Equation of State Measurements: Thermal Pressure Coefficient of an Imide-Ketone Model Compound

**Robert Orwoll and Rachel Ward
Department of Chemistry
College of William and Mary
Williamsburg, VA 23187**

$$\frac{\Delta E_{vap}}{V_{liq}} = \text{Cohesive Energy Density}$$

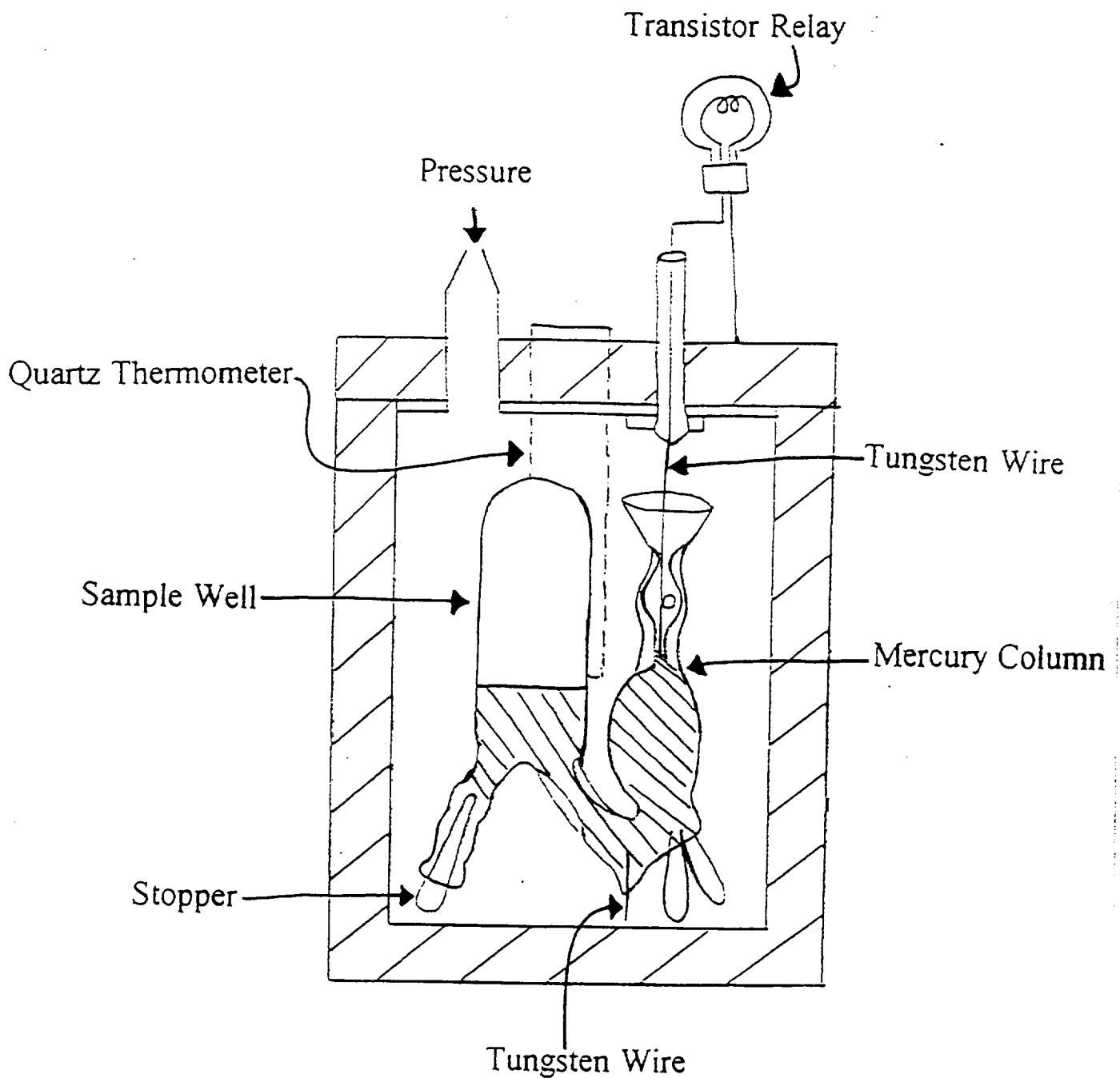
$$p = T \left(\frac{\partial p}{\partial T} \right)_V - \left(\frac{\partial E}{\partial V} \right)_T$$

$$\text{Internal Pressure} = \left(\frac{\partial E}{\partial V} \right)_T = T \left(\frac{\partial p}{\partial T} \right)_V - p$$

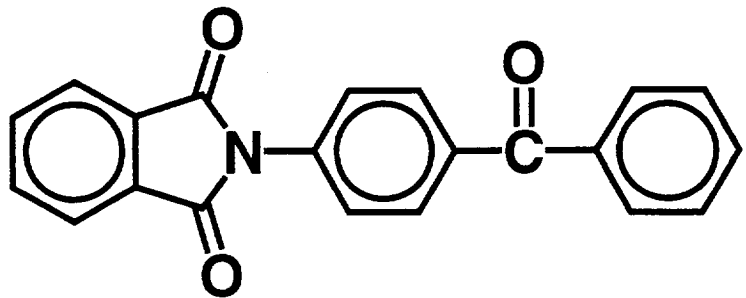
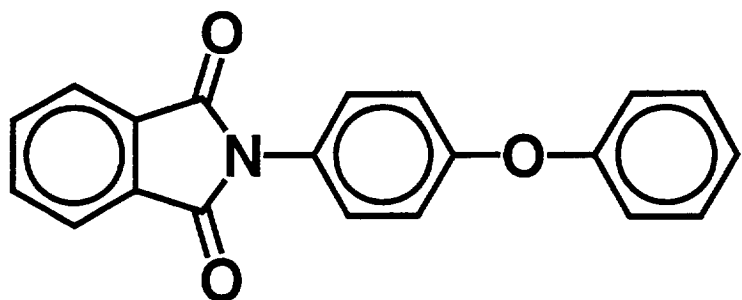
$$\left(\frac{\partial p}{\partial T} \right)_V = \frac{\frac{1}{V} \left(\frac{\partial V}{\partial T} \right)_p}{-\frac{1}{V} \left(\frac{\partial V}{\partial p} \right)_T}$$

$$\text{Thermal Pressure Coefficient} = \gamma_V = \frac{\alpha_p}{\kappa_T}$$

THERMODYNAMIC RELATIONSHIPS CONNECTING THE DESIRED $(\partial E / \partial V)_T$ AND THE MEASURED THERMAL PRESSURE COEFFICIENT $(\partial p / \partial T)_V$

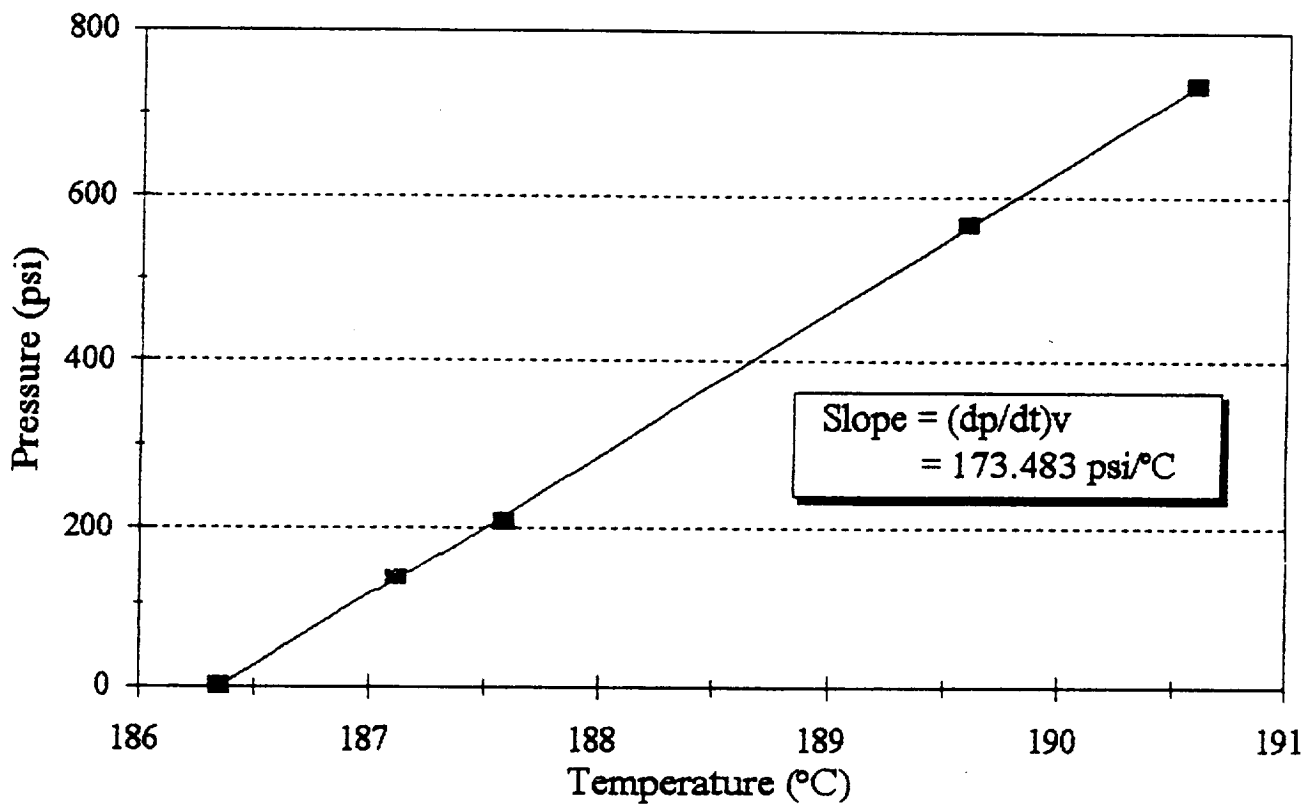


"CONSTANT" VOLUME CELL FOR MEASURING THE THERMAL PRESSURE COEFFICIENT



MOLECULAR STRUCTURES FOR THE MODEL ETHER-IMIDE (TOP) AND KETONE-IMIDE (BOTTOM)

Pressure vs Temperature of a Model Imide-Ketone



RESULTS FOR THE KETONE-IMIDE (BEFORE CORRECTION FOR THE EXPANSION
AND COMPRESSION OF THE MERCURY AND GLASS)

Comparison with Other Amorphous Compounds

| | $(\partial E / \partial V)_T, J/cm^3$ | Temp, °C |
|-------------------------|---------------------------------------|----------|
| <i>n</i> -octane | 265 | 25 |
| benzene | 379 | 25 |
| cyclohexanone | 413 | 25 |
| poly(dimethyl siloxane) | 145 | 180 |
| polyethylene | 275 | 180 |
| polyethylene oxide | 433 | 100 |
| imide ketone | 440 | 186 |

p-V-T Results to Date

| Model Cmpd | $CTE = (1/V)(\partial V / \partial T)_p, K^{-1}$ | $(\partial E / \partial V)_T, J/cm^3$ |
|--------------|--|---------------------------------------|
| imide ketone | $6.59 \times 10^{-4} (\pm 3 \times 10^{-6})$ | 440 ± 10 |
| imide ether | $6.83 \times 10^{-4} (\pm 3 \times 10^{-6})$ | next measurement |

Mechanical Properties from Acoustical Measurements on LaRC-SI

Tom Yost and John Cantrell

Outline

1. Relationship between acoustical measurements and mechanical properties. The application of $F=ma$ to the material, the results from which elastic constants and engineering moduli can be determined.
2. Thermodynamic definitions for major concepts in above.
3. Schematic view of ultrasonic measurement system.
4. Measurements to determine the effects of molecular weight on engineering moduli, and discussion.
5. Future Plans

1. Relationship between Acoustical Measurements and Moduli

Relationship between Acoustical Measurements and Mechanical Properties

- We begin with the force acting on a small segment of isotropic material. We apply $F=ma$ to the segment.
- This leads to the equation

$$\frac{\partial \sigma_{sk}}{\partial x_k} = \rho \ddot{u}_s$$

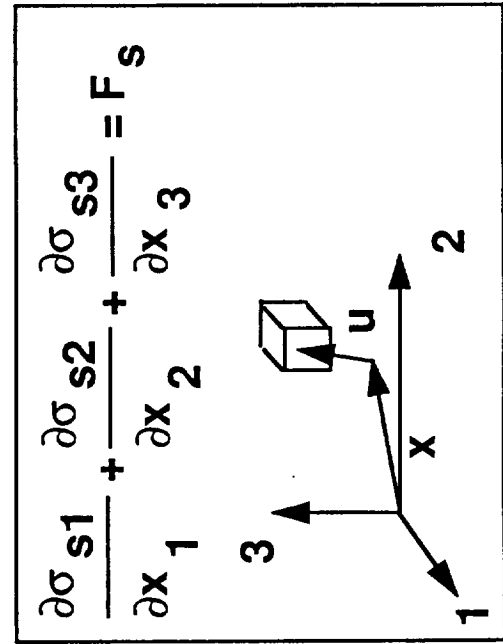
where

u is the particle displacement,

ρ is the density

x_k is the particle location (at rest)

σ_{sk} is the stress acting on the segment



Hooke's Law

- For the general case Hooke's Law can be expressed as

$$\sigma_{sk} = c_{sklm} \epsilon_{lm}$$

where the c_{sklm} are the second-order elastic constants

- The strain is expressed as

$$\epsilon_{lm} = \frac{1}{2} \left(\frac{\partial u_l}{\partial x_m} + \frac{\partial u_m}{\partial x_l} + \frac{\partial u_p}{\partial x_m} \frac{\partial u_p}{\partial x_l} \right)$$

The Wave Equation

- Combining Eq. 1 with Hooke's Law we obtain

$$\rho \ddot{u}_s = c_s k l m \frac{\partial^2 u}{\partial x_k \partial x_l} m$$

- Consider a plane harmonic travelling wave of the form

$$i(k_j x_j - \omega t)$$

$$u_s = A_s e$$

where A_s are the amplitudes of the displacement components

k_j are the components of the wave vector
(magnitude of wave vector = $2\pi/\lambda$)

ω is the angular frequency of the wave
(= $2\pi f$, f is frequency)

i is the square root of -1

Wave Speed and Elastic Constants

- We substitute the expression for the wave into the equation of motion and obtain

$$\rho \omega^2 u_{\bar{s}} - c_s k_m k_l u_m$$

which gives

$$(\rho \omega^2 \delta_{sm} - c_s k_m k_l) u_m = 0$$

and finally to the relationship between the elastic constants and the wave velocity

$$| c_s k_m k_l - \rho c^2 \delta_{sm} | = 0$$

Elastic Constants and Engineering Moduli

- Once the elastic constants are determined the engineering moduli (Young's Modulus, E, Poisson's contraction, μ , and bulk modulus, K, can be determined. For an isotropic material with Lame' constants, λ and G, we have

$$\begin{aligned} E &= \frac{G(3\lambda + 2G)}{\lambda + G} && \text{where } \lambda = c_{1122} = c_{1133} = c_{2233} \\ \mu &= \frac{\lambda}{2(\lambda + G)} && G = \frac{1}{2}(c_{1111} - c_{1122}) \\ &&& = c_{2323} = c_{3131} = c_{1212} \\ K &= \lambda + \frac{2}{3}G \end{aligned}$$

2. Thermodynamic Basis

Thermodynamic Definitions of Elastic Constants

- The elastic constants can also be defined in terms of thermodynamic variables

$$c_{ijkl} = \rho \left. \frac{\partial^2 U}{\partial \epsilon_{ijkl} \partial \epsilon} \right|_{\text{Im}} \quad (\text{adiabatic conditions})$$

0 stress

where U is the internal energy

- These are the elastic constants used in this study

Thermodynamic Definitions of Stresses and Strains

We start with the second law of thermodynamics and write the differential work in terms of stress and strain. This gives

$$dU = \sigma_{ik} d\varepsilon_{ik} + T dS$$

The Helmholtz free energy is given as

$$F = U - TS$$

$$dF = \sigma_{ik} d\varepsilon_{ik} - SdT$$

The Gibbs free energy is given as

$$\Phi = F - \sigma_{ik} \varepsilon_{ik}$$

$$d\Phi = - SdT - \varepsilon_{ik} d\sigma_{ik}$$

$$\text{Hence } \sigma_{ik} = \left(\frac{\partial U}{\partial \varepsilon_{ik}} \right)_S = \left(\frac{\partial F}{\partial \varepsilon_{ik}} \right)_T \quad \& \quad \varepsilon_{ik} = - \left(\frac{\partial \Phi}{\partial \sigma_{ik}} \right)_T$$

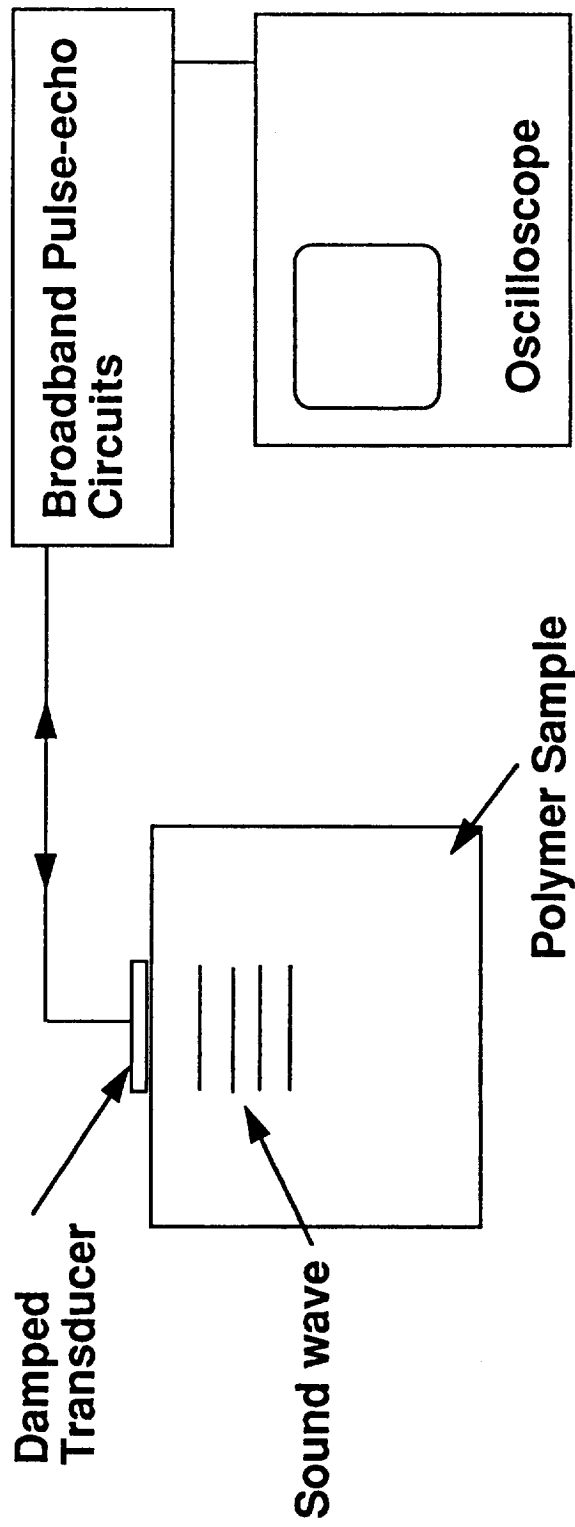
Thermodynamic Definition of Elastic Constants

$$c_{ijkl}^s = \rho_0 \left(\frac{\partial^2 U}{\partial n_{ij} \partial n_{kl}} \right)$$

The elastic constants used in this study
are isentropic elastic constants

3. Overview of Ultrasonic Measurements

Viscoelastic Materials and Ultrasonic Measurements (Linear Moduli)



Before measurement the sample thickness is determined. The oscilloscope measures the transit time. From these two measurements the sound velocity can be determined.

This ultrasonic technique measures the unrelaxed second-order moduli of the LaRC-SI sample

4. Sample Set Preparation and Measurements

Five sample sets were prepared from each of the molecular weight offset stocks. Each set consisted of one sample from each molecular weight offset. Every sample was lapped and polished so that the surfaces were flat (to one band of green light) and parallel to better than 20 Arc sec. The following measurements include:

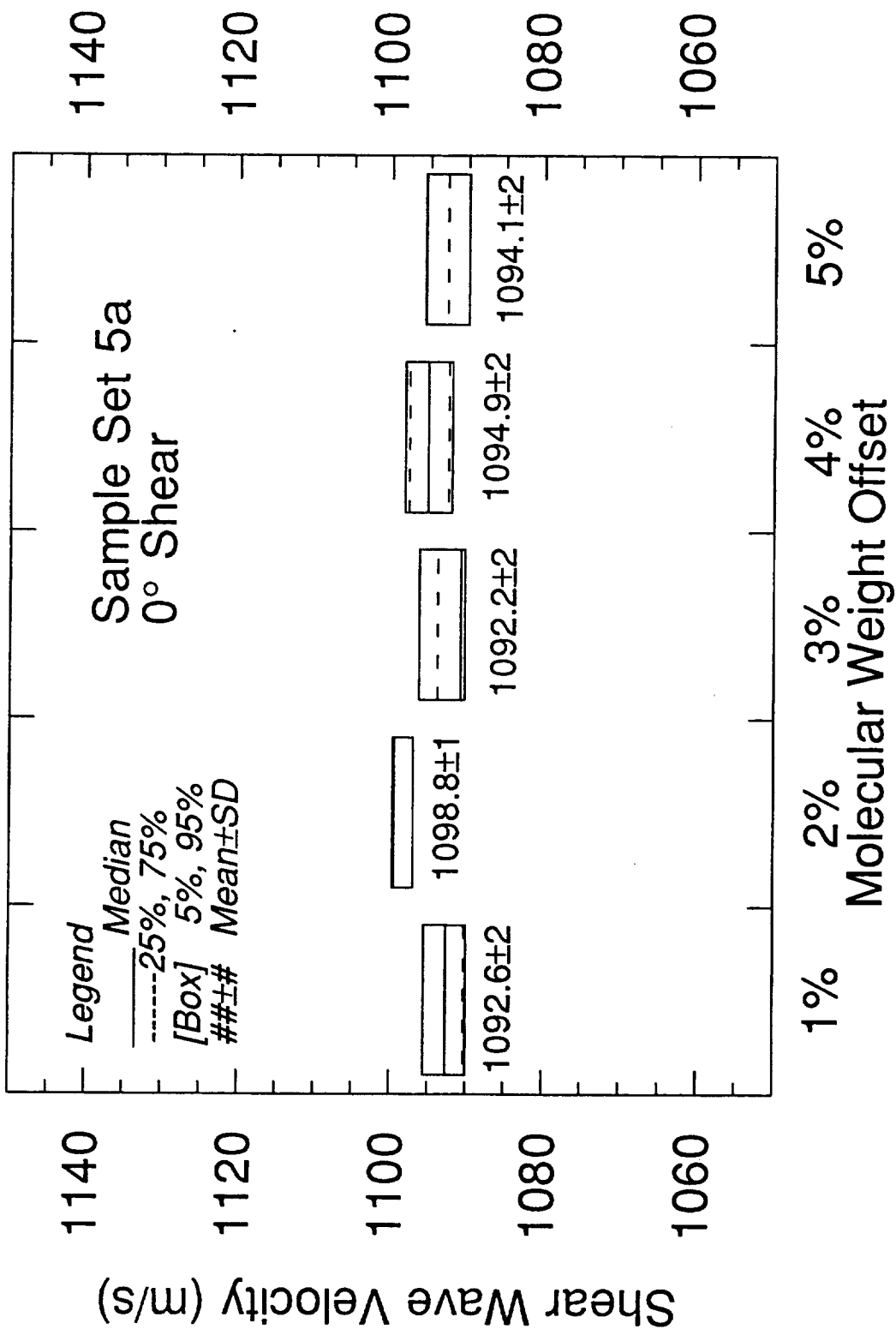
- Density measurements on 5 sample Sets
- Ultrasonic Wave Velocities (Set 5a and Averages)
- Moduli of LaRC-SI at room temperature (Set 5a and Averages)

4. Summary of Measurements

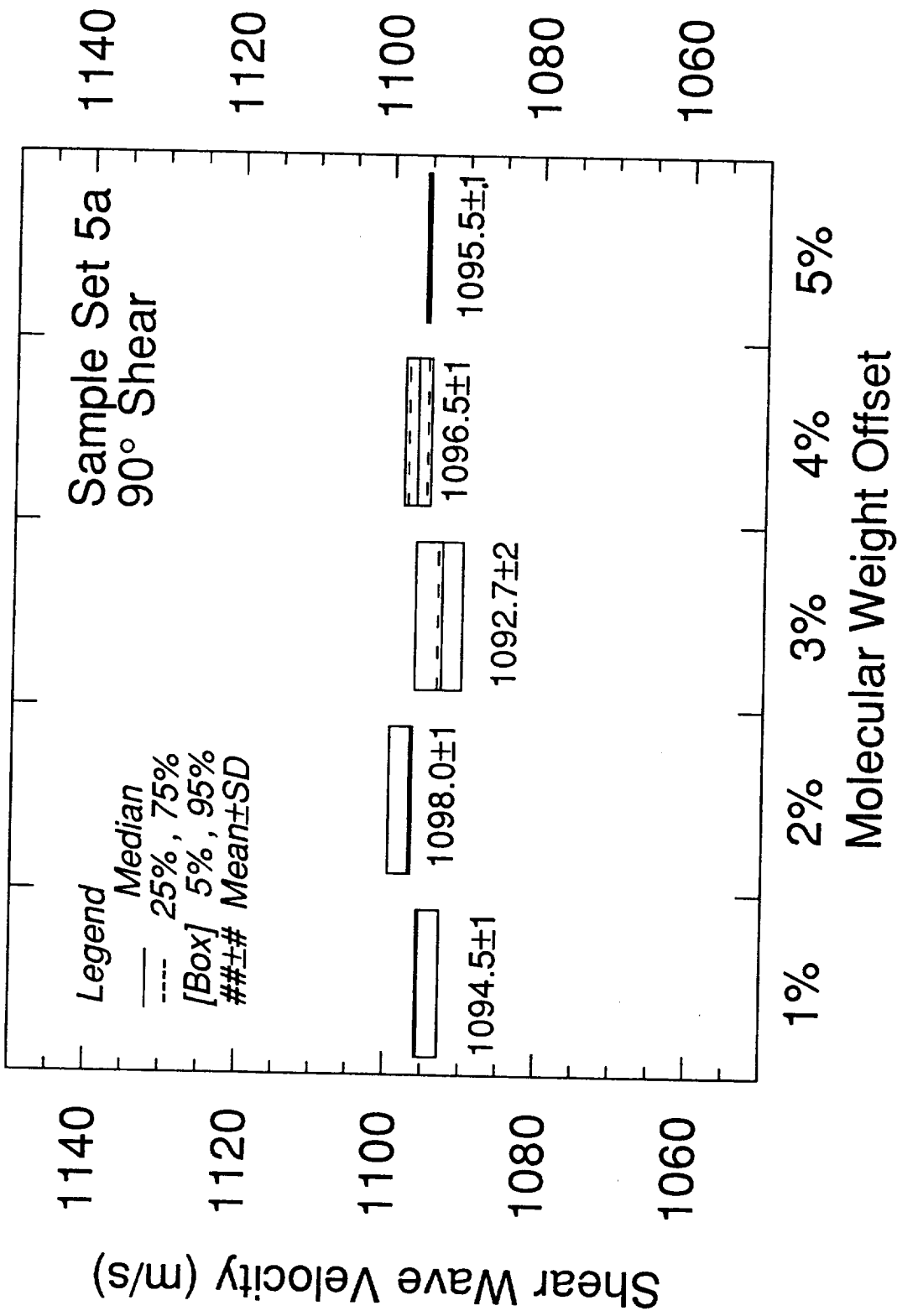
Measurements on a Typical Sample Set

Graphs show compressional and shear velocities as well as moduli calculated from them. Enclosed is a chart of measured densities.

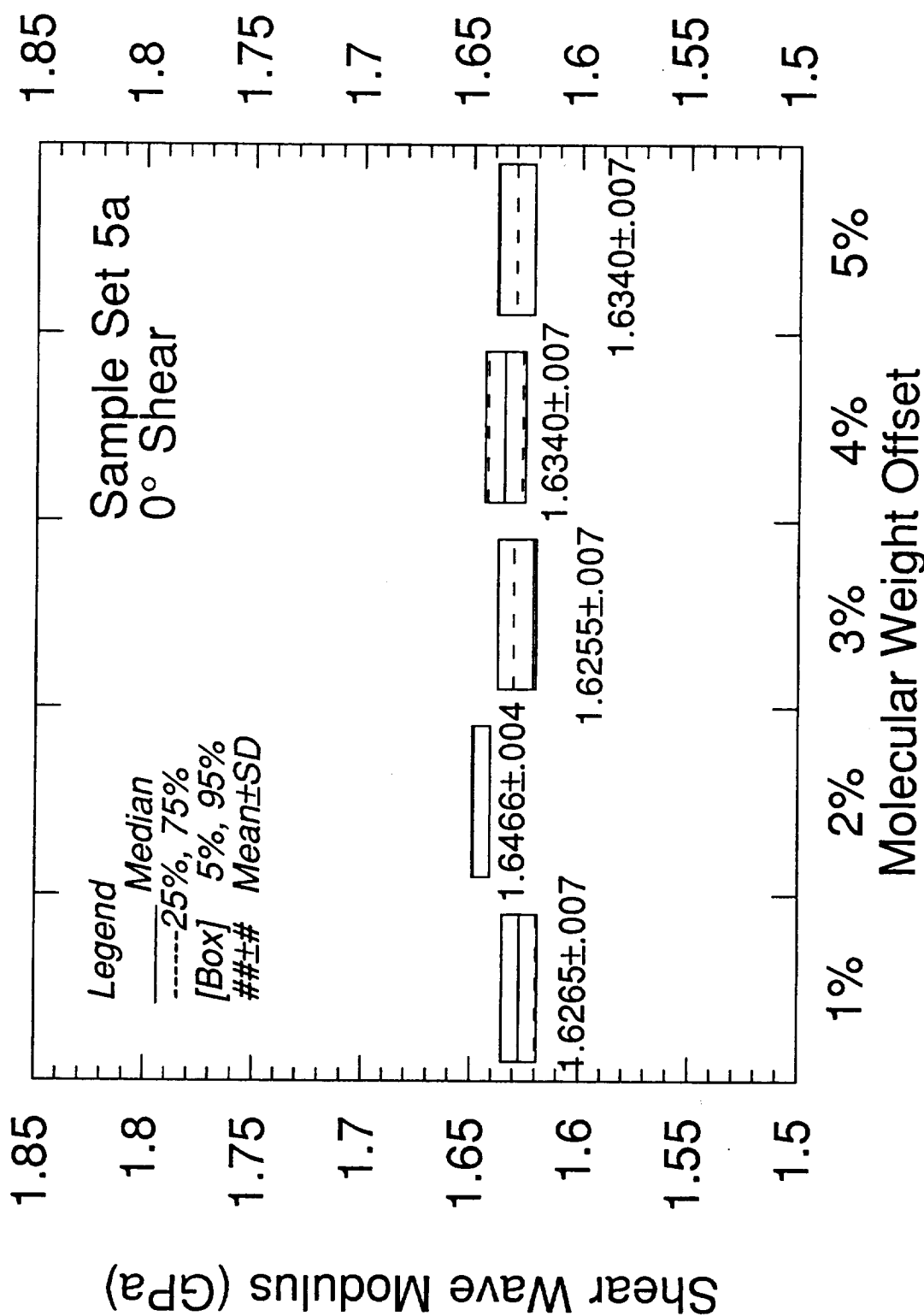
Ultrasonic Shear Wave Velocity in LARC-SI



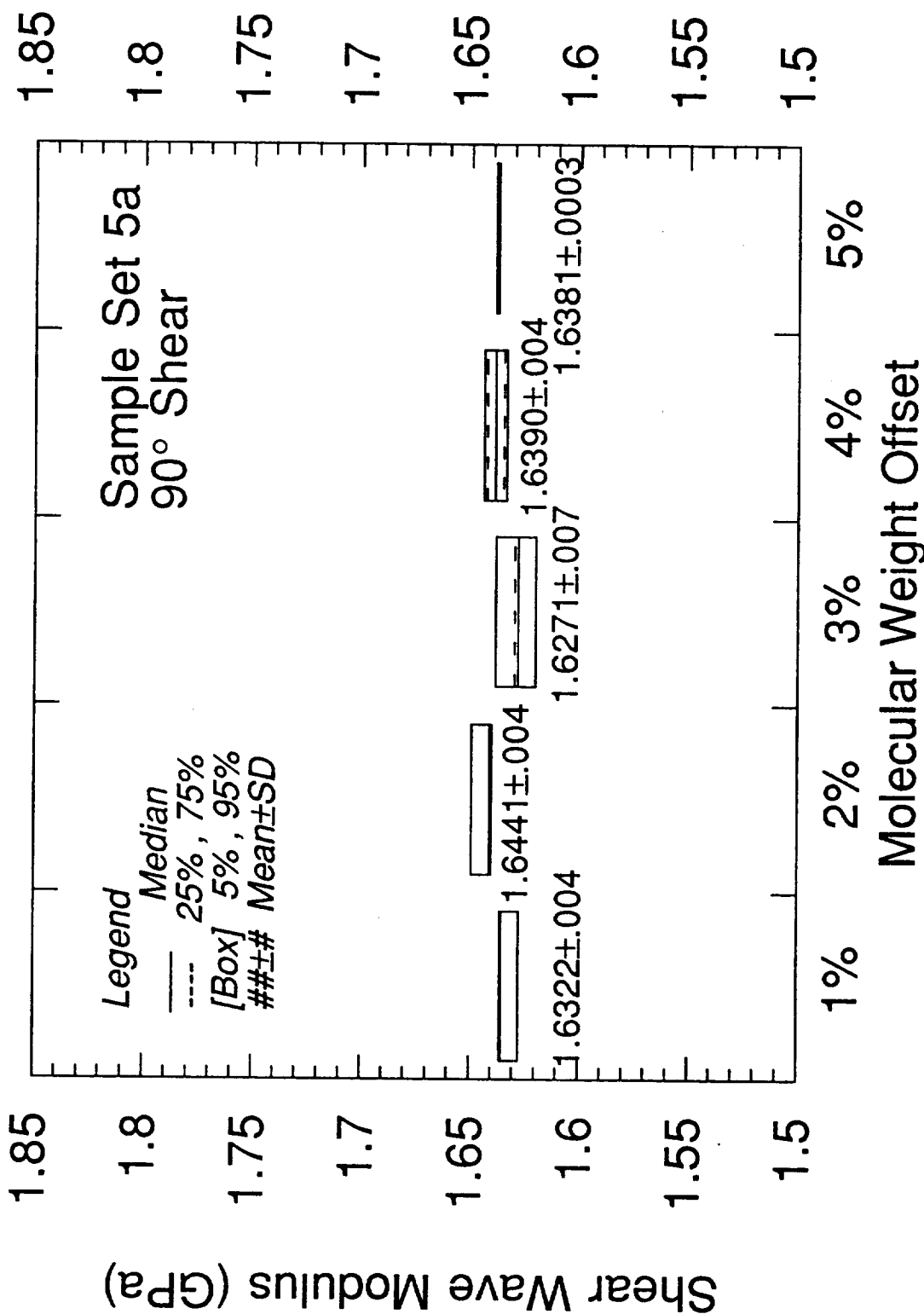
Ultrasonic Shear Wave Velocity in LaRC-SI



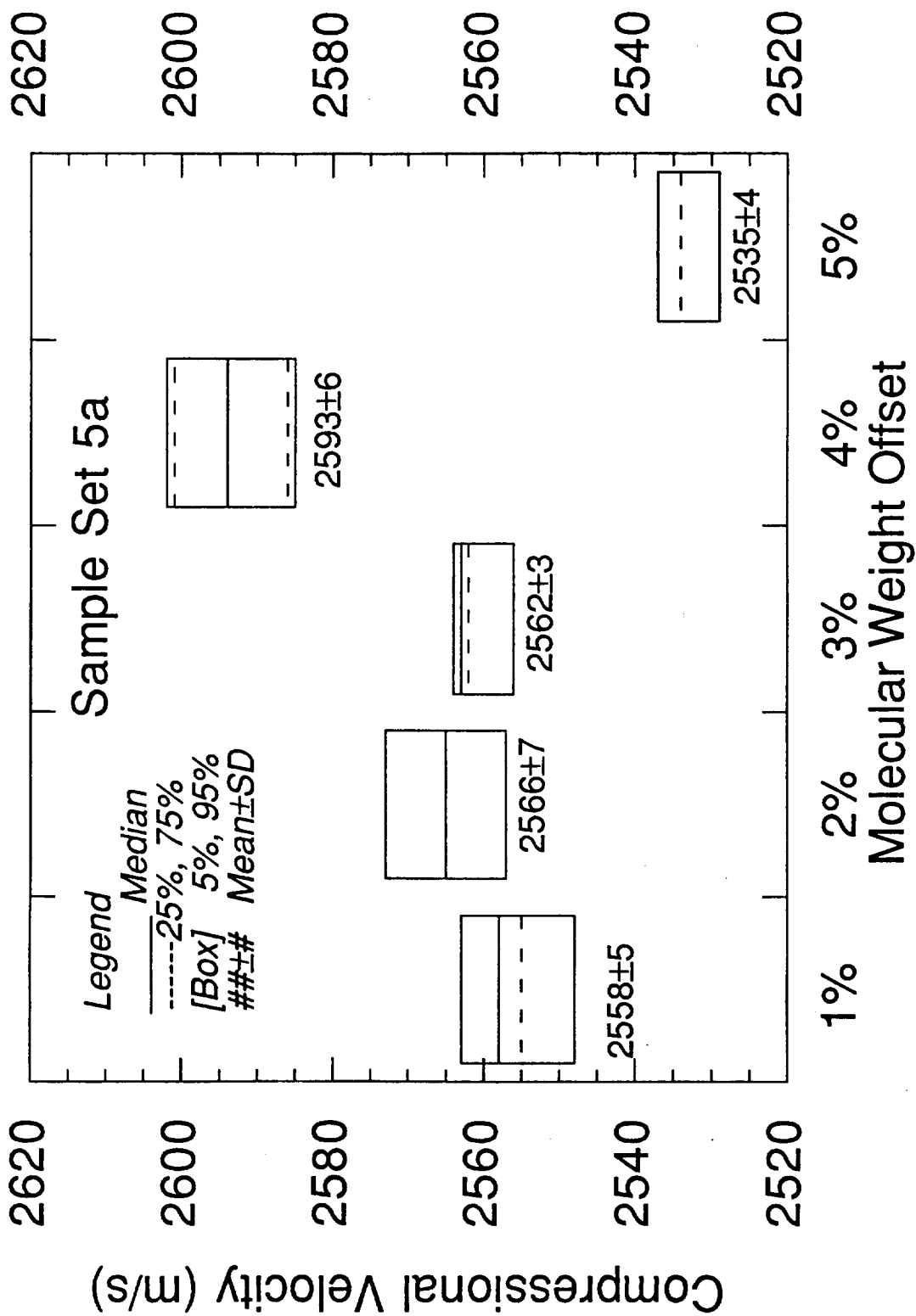
Isentropic Shear Wave Modulus in LaRC-SI



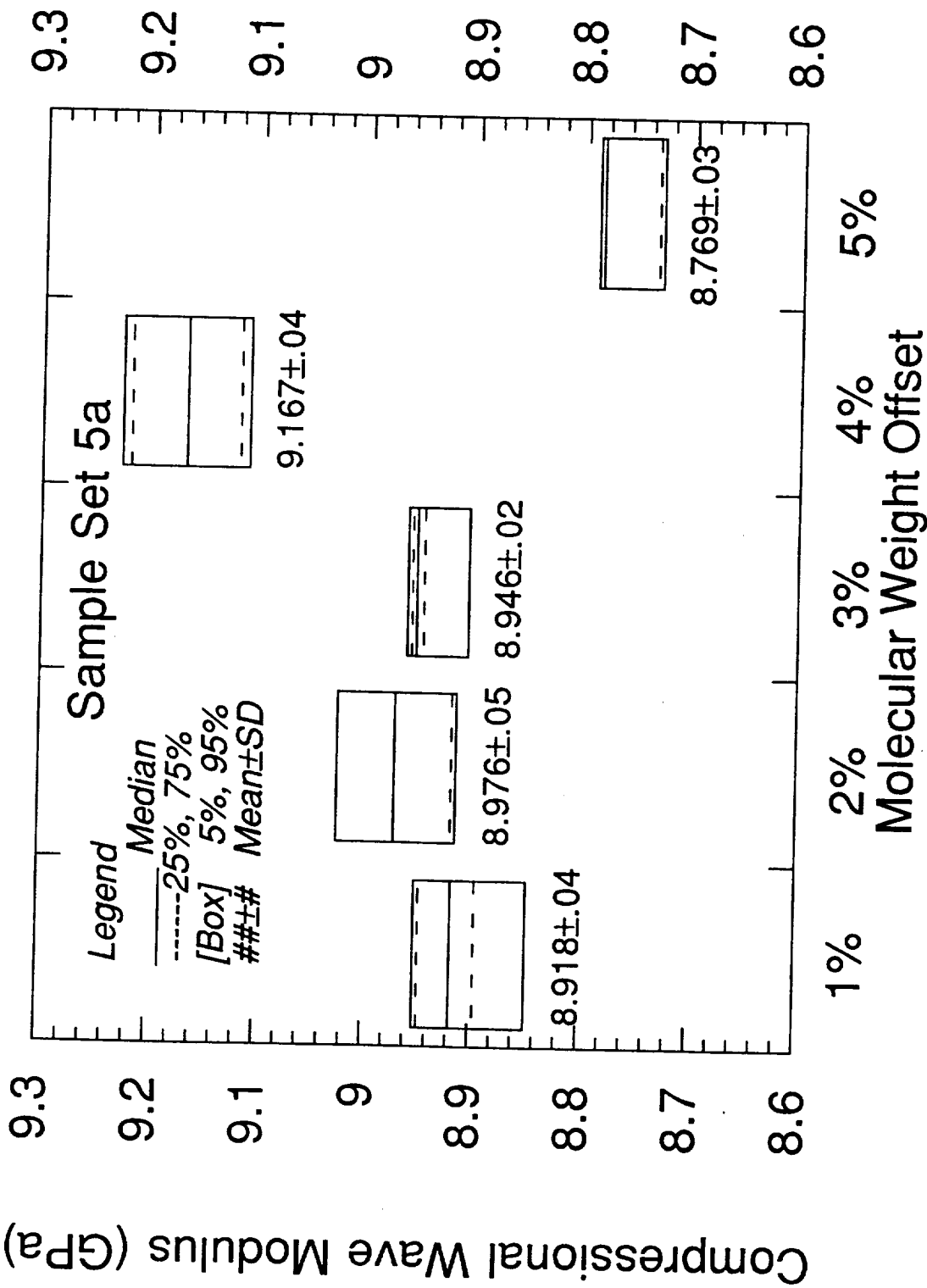
Isentropic Shear Wave Modulus in LaRC-SI



Ultrasonic Wave Compressional Velocity LaRC-SI



Isentropic Compressional Wave Modulus in LARC-SI



Measured Density of Molded Samples Using Archimede's Principle

Molecular Weight % Offset

| | <u>Density (x 10³ Kg/m³)</u> |
|---|--|
| 1 | 1.3624±0.0003 |
| 2 | 1.3635±0.0003 |
| 3 | 1.3628±0.0002 |
| 4 | 1.3612±0.004 |
| 5 | 1.3648±0.0002 |

Elastic Properties

- Unrelaxed moduli, linear
- Elastic constants, Young's modulus, shear modulus, Poisson's ratio, bulk modulus

Wave Velocities as a Function of Molecular Weight Offset

| Molecular Weight Offset | Shear Velocity(m/s) | | Compressional Velocity (m/s) |
|-------------------------|---------------------|-------------------|------------------------------|
| | 0° | 90° | |
| 1% | $1.0927 \pm .001$ | $1.0935 \pm .001$ | $2.5589 \pm .005$ |
| 2% | $1.0984 \pm .001$ | $1.0986 \pm .001$ | $2.5659 \pm .003$ |
| 3% | $1.0928 \pm .0007$ | $1.0940 \pm .001$ | $2.5623 \pm .0007$ |
| 4% | $1.0943 \pm .0002$ | $1.0949 \pm .002$ | $2.5657 \pm .002$ |
| 5% | $1.0942 \pm .0002$ | $1.0948 \pm .002$ | $2.5660 \pm .003$ |

Moduli from Wave Velocities

| Molecular Weight Offset | Shear Modulus (GPa) | Compressional Modulus (GPa) |
|-------------------------|---------------------|-----------------------------|
| | 0° | 90° |
| 1% | $1.6266 \pm .004$ | $1.6290 \pm .004$ |
| 2% | $1.6451 \pm .003$ | $1.6456 \pm .003$ |
| 3% | $1.6277 \pm .002$ | $1.6311 \pm .004$ |
| 4% | $1.6301 \pm .007$ | $1.6319 \pm .006$ |
| 5% | $1.6341 \pm .006$ | $1.6358 \pm .006$ |

Moduli Derived from Ultrasonics Results: Engineering Moduli (Isentropic)

| Molecular Weight Offset | Shear Modulus (GPa) | Young's Modulus (GPa) | Poisson's Ratio |
|-------------------------|---------------------|-----------------------|-------------------|
| 1% | $1.6278 \pm .004$ | $4.5199 \pm .046$ | $0.3860 \pm .007$ |
| 2% | $1.6453 \pm .003$ | $4.5667 \pm .026$ | $0.3878 \pm .003$ |
| 3% | $1.6294 \pm .004$ | $4.5265 \pm .013$ | $0.3887 \pm .001$ |
| 4% | $1.6320 \pm .007$ | $4.5324 \pm .062$ | $0.3886 \pm .004$ |
| 5% | $1.6350 \pm .006$ | $4.5409 \pm .041$ | $0.3887 \pm .004$ |

Moduli Derived from Ultrasonics

Isentropic Bulk Modulus

| Molecular Weight Offset | Isentropic Bulk Modulus (GPa) |
|-------------------------|-------------------------------|
| 1% | $6.7504 \pm .04$ |
| 2% | $6.7836 \pm .03$ |
| 3% | $6.7751 \pm .02$ |
| 4% | $6.781 \pm .05$ |
| 5% | $6.798 \pm .05$ |

Conclusions

- Molding of LaRC Samples affected the densities of the samples
- Samples have inclusions and show evidence of residual stresses under polarized light. We think that this is responsible for some of the data scatter.
- The 0° and 90° shear measurements show that the assumption of isotropy is a valid one in this case, even with the residual effects left from the moulding process.
- It is possible to calculate the significant engineering moduli from ultrasonic measurements.

Future Planned Activities

- Measurement of the nonlinear moduli
- Measurement of coefficients of linear expansion
- Measurements of effects on moduli (linear and nonlinear) of raising LaRC to glass transition temperature and beyond to

PREDICTING BULK POLYMER PROPERTIES FROM MOLECULAR STRUCTURE

Elizabeth Collantes, Tamara Gahimer, and William Welsh
University of Missouri

Michael Grayson
McDonnell Douglas Aerospace-St. Louis

GOALS & OBJECTIVES

- **DEVELOP AND APPLY METHODS IN COMPUTATIONAL CHEMISTRY FOR FAST, RELIABLE, PREDICTION OF POLYMER PROPERTIES**
- **RELATE BULK MACROSCOPIC POLYMER PROPERTIES TO MICROSCOPIC MOLECULAR STRUCTURE AND PROPERTIES**
- **DEVELOP STRUCTURE-PROPERTY RELATIONSHIPS**

COMPUTATIONAL APPROACHES

- **QUANTITATIVE STRUCTURE-PROPERTY RELATIONSHIPS (QSPR)**
 - Group-Additivity Techniques (van Krevelen, Dow)
 - Connectivity Indices (Bicerano's Synthia)
- **MULTIVARIATE REGRESSION**
 - Partial Least Squares (PLS)
- **ARTIFICIAL NEURAL NETWORKS (ANNs)**
- **ATOMISTIC MOLECULAR MODELING**
 - Cerius² Mechanical Properties Module

DESCRIPTION OF METHODS

QSPR Approaches

QSPR Approaches

The van Krevelen Method

D. W. van Krevelen, Properties of Polymers: Their Estimation and Correlation with Chemical Structure (Elsevier, 1976)

- assumes that the physiochemical properties of a polymer can be obtained by adding contributions from the constituent chemical groups
- this approach is commonly known as Group Additivity (GA)
- based on empirical and semi-empirical fitting to expt'l data
- relies on large database containing group contributions, typically one for each property of interest (e.g., T_g , α_T)
- property values apply to bulk amorphous and semi-crystalline homopolymers, statistical polymers, and for polymer solutions

Advantages

- fast
- easy to use
- applicable to many properties
- usually reliable

Disadvantages

- depends on chemical-fragment library
- theoretically less rigorous than atomistic methods
- do not account for special interactions (e.g., solvent)
- do not provide insight into mechanism

Table 9–12. QSPR Groups (Page 1 of 3)

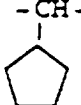
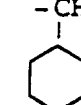
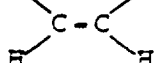
| | | | |
|--|---|--|--|
| $-\text{CH}_2-$ | $-\text{CH}-$ CH_3 | $-\text{CHi}-$ $i\text{-Prop}$ | $-\text{CH}-$ $t\text{-But}$ |
| 1. methylene | 2. methylmethylen | 3. isopropylmethylen | 4. <i>t</i> -butylmethylen |
| $-\text{CH}-$  | $-\text{CH}-$  | $-\text{CH}-$  | $-\text{CH}-$  |
| 5. cyclopentylmethylen | 6. cyclohexylmethylen | 7. phenylmethylen | 8. <i>p</i> -methoxyphenylmethylen |
| $-\text{CH}-$ O H | $-\text{CH}-$ OCH_3 | $-\text{CH}-$ O $\text{O}=\text{C}-\text{CH}_3$ | $-\text{CH}-$ $\text{C}=\text{O}$ OCH_3 |
| 9. hydroxymethylen | 10.methethermethylen | 11.acetylmethylen | 12.methacrylmethylen |
| $-\text{CH}-$ $\text{C}=\text{N}$ | $-\text{CH}-$ F | $-\text{CH}-$ Cl | $\begin{matrix} \text{CH}_3 \\ \\ -\text{CH}- \\ \\ \text{CH}_3 \end{matrix}$ |
| 13.cyanomethylen | 14.fluoromethylen | 15.chloromethylen | 16.dimethylmethylen |
| $\begin{matrix} \text{CH}_3 \\ \\ -\text{C}- \\ \\ \text{C}_6\text{H}_5 \end{matrix}$ | $\begin{matrix} \text{CH}_3 \\ \\ -\text{C}- \\ \\ \text{C}=\text{O} \\ \\ \text{CH}_3 \end{matrix}$ | $\begin{matrix} \text{F} \\ \\ -\text{C}- \\ \\ \text{F} \end{matrix}$ | $\begin{matrix} \text{Cl} \\ \\ -\text{C}- \\ \\ \text{F} \end{matrix}$ |
| 17.phenylmethylen | 18.methmethacrylmethylen | 19.difluoromethylen | 20.chlorfluoromethylen |
| $\begin{matrix} \text{Cl} \\ \\ -\text{C}- \\ \\ \text{Cl} \end{matrix}$ | $\begin{matrix} \text{H} & & \text{H} \\ & \text{---} & \\ -\text{C} & \text{---} & \text{C}- \\ & & \\ \text{H} & & \text{H} \end{matrix}$ |  |  |
| 21.dichloromethylen | 22.paraxylylene | 23.transcyclobutyl | 24.cisethene |

Table 9-12. QSPR Groups (Page 2 of 3)

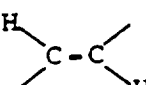
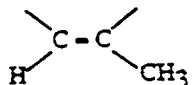
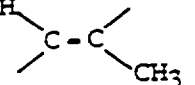
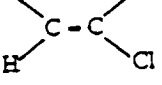
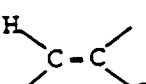
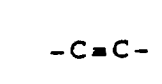
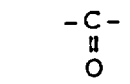
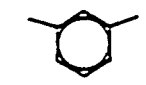
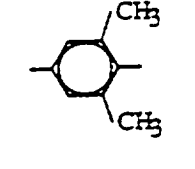
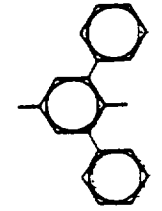
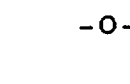
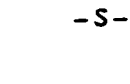
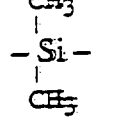
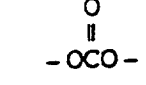
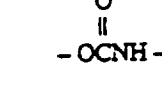
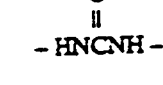
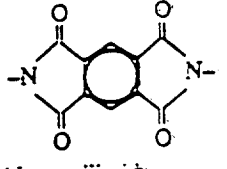
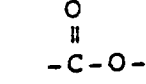
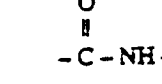
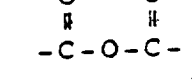
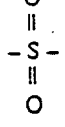
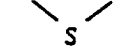
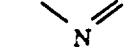
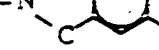
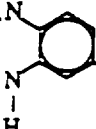
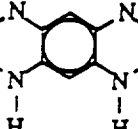
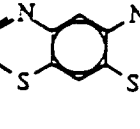
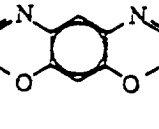
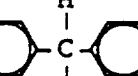
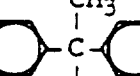
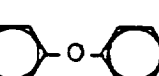
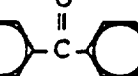
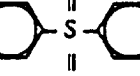
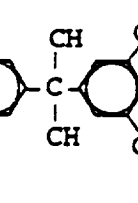
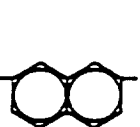
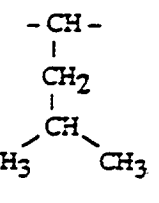
| | | | |
|---|---|---|---|
|  |  |  |  |
| 25.transethene | 26.cismethylethene | 27.transmethylethene | 28.cischloroethene |
|  |  |  |  |
| 29.transchloroethene | 30.ethyne | 31.carbonyl | 32.orthophenylenes |
|  |  |  |  |
| 33.metaphenylenes | 34.paraphenylenes | 35.3,6-dimethoxyphenylene | 36.3,6-di phenylphenylene |
|  |  |  |  |
| 37.2,6naphthalene | 38.oxide | 39.sulfide | 40.dimethylsilane |
|  |  |  |  |
| 41.carbonate | 42.urethane | 43.urea | 44.benzimidazole |
|  |  |  |  |
| 45.estер | 46.amide | 47.anhydride | 48.sulfonyl |

Table 9–12. QSPR Groups (Page 3 of 3)

| | | | |
|---|---|--|---|
|  |  |  |  |
| 49. oxadiazole | 50. thiadiazole | 51. 25thiazole | 52. phthalimide |
|  |  |  |  |
| 53. benzoimidazole | 54. benzodiiimidazole | 55. benzodithiazole | 56. benzodioxazole |
|  |  |  |  |
| 57. parabiphenylene | 58. pbisphenylmethlene | 59. pbisphenylA | 60. pbisphenylether |
|  |  |  |  |
| 61. pbisphenylS | 62. pbisphenylcarbonyl | 63. pbisphenylsulphone | 64. pbisphenylmethphemeth |
|  |  |  |  |
| 65. pbisphenidiphenemeth | 66. p-tetmethbisphenolA | 67. 27naphthalene | 68. iburyimethylene |

van Krevelen Methodology

The polymer properties that can be calculated with the van Krevelen methodology are:

Thermophysical Properties

- glass transition temperature
- crystalline melt transition temperature
- attainable degree of crystallinity
- maximum linear growth rate of spherulitic crystallites
- density of glassy, rubbery and crystalline phases
- volume coefficients of thermal expansion
- volume change on melting
- molar heat capacity at constant pressure
- molar heat capacity at constant volume
- molar entropy of fusion
- molar latent heat of fusion
- cohesive energy
- solubility parameter
- surface tension

Mechanical Properties

- bulk modulus
- Poisson's ratio
- longitudinal velocity of sound
- shear modulus of an amorphous or semicrystalline polymer
- tensile modulus of an amorphous or semicrystalline polymer

Ultimate Mechanical Properties

- tensile yield strength
- compressive strength
- flexural strength
- indentation hardness

Transport Properties

Permeation of a Gas

- specific permachor
- permeability of a gas

Viscoelastic Properties of a Polymer Melt

- activation energy of viscous flow
- Newtonian viscosity
- characteristic deformation time
- non-Newtonian viscosity

Dilute Solution Properties in a theta Solvent

- Mark-Houwink prefactor
- intrinsic viscosity
- radius of gyration
- critical molecular mass for entanglement

Dilute Solution Properties in a Good Solvent

- Mark-Houwink prefactor and exponent
- excluded volume expansion factor
- intrinsic viscosity
- radius of gyration

Concentrated Solution Property in a Good Solvent

- Newtonian viscosity

Electrical, Optical, and Magnetic Properties

- dielectric constant
- resistivity
- refractive index
- magnetic susceptibility

Properties Relating to Thermal Stability

- free enthalpy of formation
- temperature at half thermal decomposition
- char residue
- oxygen index

The van Krevelen methodology relies on the calculation of various molar properties of the average repeat unit. These molar properties are denoted here by enclosure in braces $\{ \}$. The molar properties are then used in the calculation of the macroscopic properties of the polymer. The molar properties that are calculated are listed below:

- mass $\{M\}$
- number of QSPR groups $\{N\}$
- number of backbone atoms $\{Z\}$
- van der Waals volume $\{V_w\}$
- glass transition temperature $\{Y_g\}$
- melt transition temperature $\{Y_m\}$
- volume at 298 K in the amorphous phase $\{V_a\}$
- heat capacity of the solid $\{C_{p,s}\}$
- heat capacity of the liquid $\{C_{p,l}\}$
- entropy of melting $\{\Delta S_m\}$
- cohesive energy $\{E_{coh}\}$
- interaction $\{F\}$
- parachor $\{P_s\}$
- permachor $\{\Pi\}$
- elastic wave velocity $\{U\}$
- intrinsic viscosity $\{J\}$
- viscosity-temperature gradient $\{H_h\}$
- polarization $\{P_{LL}\}$
- optical refraction $\{R_{GD}\}$
- magnetic susceptibility $\{\chi\}$
- enthalpy of formation $\{\Delta G_a\}$
- entropy of formation $\{\Delta G_b\}$
- half thermal decomposition temperature $\{Y_{d,1/2}\}$
- char forming tendency $\{C_f\}$

QSPR Approaches

The Dow Method

J. Seitz, J. Appl. Polym. Sci., 49, 1331 (1993)

- adopts group-additivity (GA) concept, but uses only six group contributions of the repeat unit to predict polymer properties: (1) molecular weight; (2) length; (3) vdW volume; (4) cohesive energy; (5) rotational df of the backbone; and (6) T_g
- focuses on mechanical properties
- limited to amorphous (not semi-crystalline) polymers

Advantages

- same advantages as van Krevelen: fast, reliable
- less dependent on large database of group contributions
- better fitted to high-performance engineering polymers
- conceptually more rigorous than van Krevelen

Disadvantages

- same disadvantages as van Krevelen
- restricted to amorphous polymers
- depends on library of group contributions, although smaller

Properties Calculable

Dow Methodology

With the Dow methodology implemented within the QSPR module it is possible to predict 17 different properties of amorphous thermoplastic polymers. These are:

- Molar volume per repeat unit
- Density
- Thermal expansion coefficient
- Cohesive energy
- Solubility parameter
- Surface tension
- Dielectric constant
- Average molecular cross-sectional area
- Glass transition temperature
- Poisson's ratio
- Tensile modulus
- Tensile yield strength
- Brittle strength
- Crazing strength
- Entanglement molecular weight
- Distance between entanglements
- Plateau modulus

In addition, if $T_g > 300$ K, many of these properties may be calculated as a function of temperature.

The group parameters required to predict these properties are:

- Molecular weight
- Length per repeat unit
- van der Waals volume
- Cohesive energy
- Molar glass transition temperature
- Number of backbone rotatable units

QSPR Approaches

Bicerano's Synthia Method

J. Bicerano, Prediction of Polymer Properties (Marcel Dekker, 1993)

- circumvents reliance on group contributions by relating polymer properties to topological information about polymers using connectivity indices derived from graph theory
- useful for any polymer comprised of the following elements: C, H, N, O, Si, S, F, Cl, Br
- applicable to bulk amorphous homopolymers and statistical copolymers

Advantages

- independent of large group-contribution library
- thermodynamic, mechanical, and transport properties

Disadvantages

- restricted to nine atom-types
- restricted to amorphous polymers
- does no account for special interactions

Table 11-1. Properties Calculable By the Synthia Module

| Thermophysical Properties | Electrical, Optical and Magnetic Properties |
|---|---|
| Glass transition temperature | Refractive index |
| Temperature of half decomposition | Molar refraction |
| Coefficient of volumetric thermal expansion | Dielectric constant |
| Molar volume | Volume resistivity |
| Density | Diamagnetic susceptibility |
| Molar heat capacity at constant pressure | Chain Stiffness and Entanglement Properties |
| Cohesive energy | Steric hindrance parameter |
| Solubility parameter | Characteristic ratio |
| Surface tension | Molar stiffness function |
| Thermal conductivity | Entanglement molecular weight |
| <hr/> | |
| Mechanical Properties | Critical molecular weight |
| Bulk modulus | Entanglement length |
| Shear modulus | Transport Properties |
| Young's modulus | Activation energy for viscous flow |
| Poisson's ratio | Permeability of gases |
| Shear yield stress | |
| Brittle fracture stress | |

DESCRIPTION OF METHODS

Multivariate PLS Approach

Multivariate PLS Approach

Attempts to eliminate any dependence on group contributions or connectivity indices

- relate bulk polymer properties to specific molecular descriptors associated with the repeat unit
- focused on two polymer properties: T_g and Tensile Modulus
- selected seven easily-obtainable molecular descriptors: (1) molecular weight; (2) length; (3) number of atoms; (4) number of non-H atoms; (5) vdW volume; (6) rotational df, and (7) number of backbone atoms
- develops linear regression equation to map bulk polymer property onto calculable descriptors thereby allowing prediction of polymer property solely from knowledge of descriptors

$$\text{property value} = a_1 (PC_1) + a_2 (PC_2) + a_3 (PC_3) + \dots$$

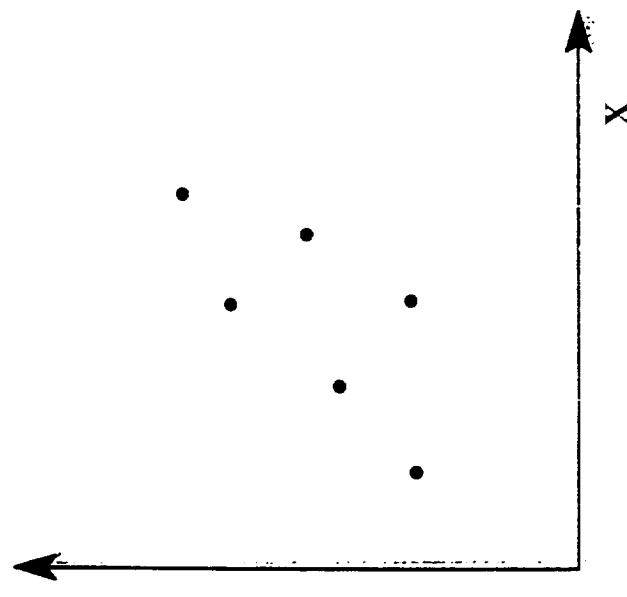
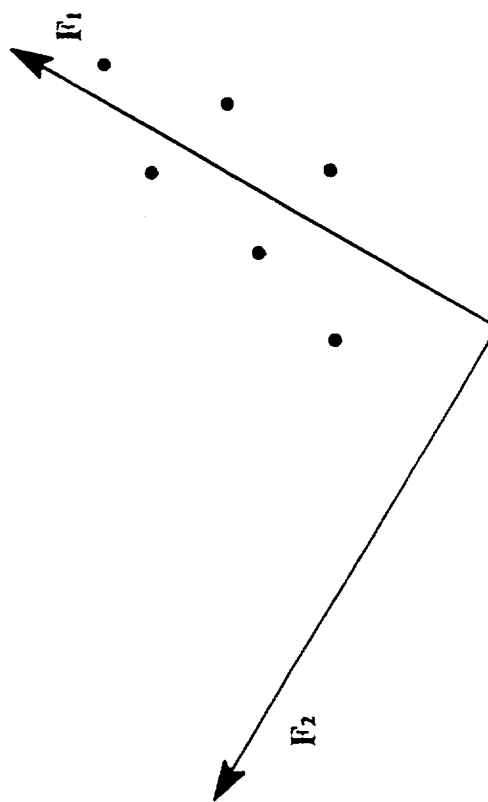
- applicable to any series of polymers for which experimental data is available

Advantages

- totally independent of any database library
- generally applicable to any property and any polymer
- from Loadings, evaluates contribution by each descriptor to property of interest

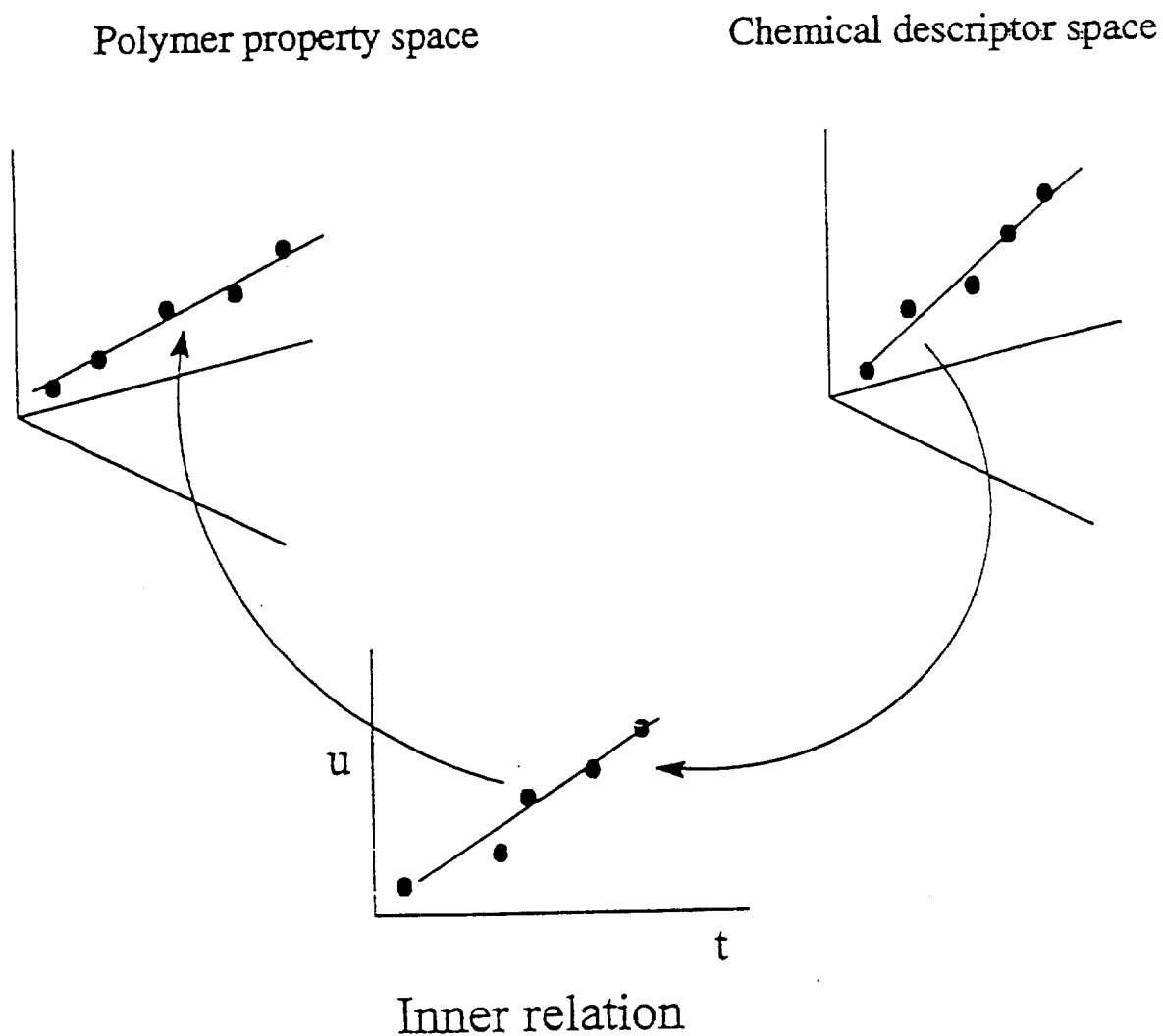
Disadvantages

- assumes linear relationship between property and descriptors
- need expt'l data on related polymers to develop regression equation



172

PLS: GRAPHICAL REPRESENTATION

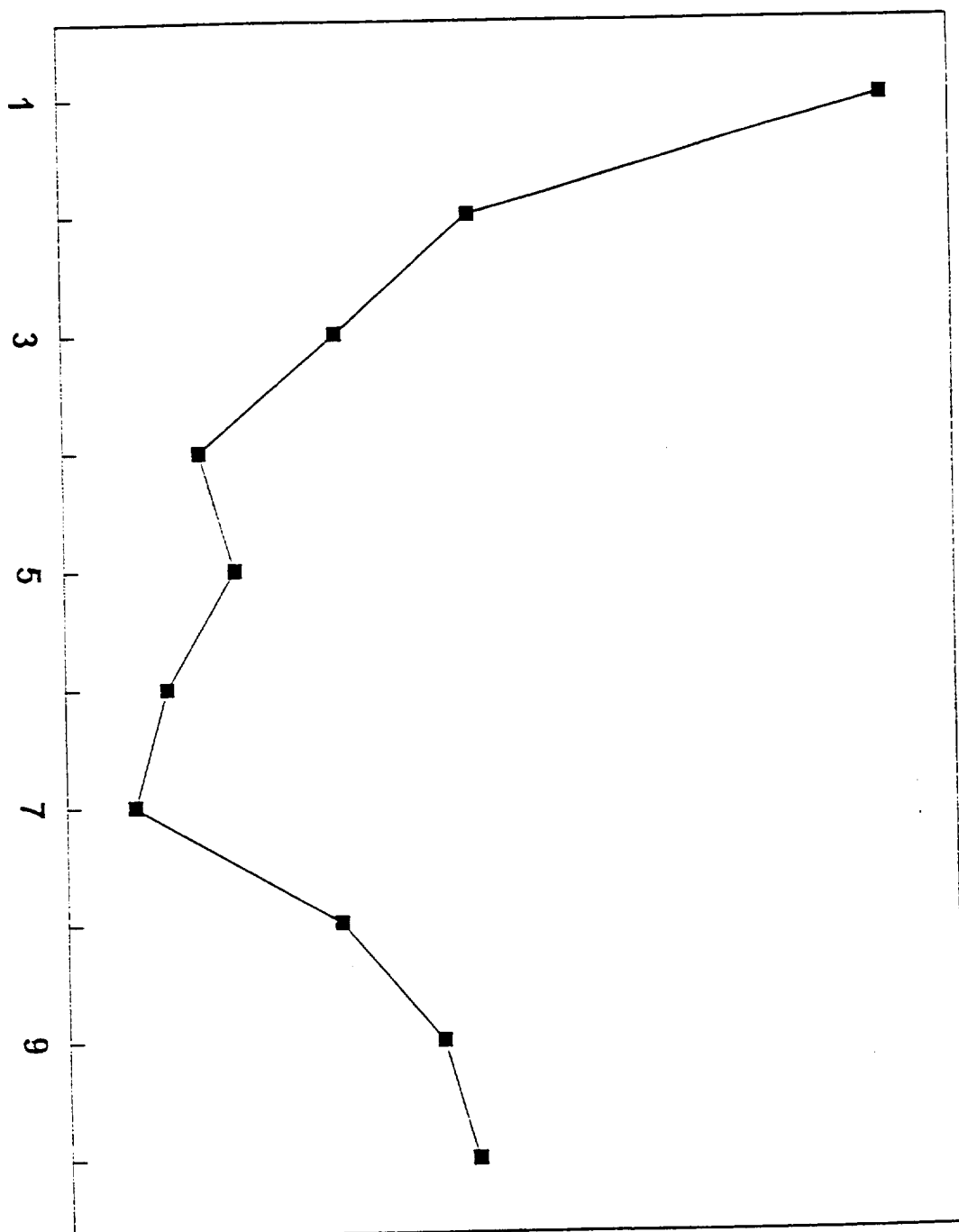


*Determining the number of
significant components*

- cross-validation

PRESS

NUMBER OF COMPONENTS



DESCRIPTION OF METHODS

Artificial Neural Networks

Artificial Neural Networks (ANN)

paradigm based on architecture of biological network of neurons in human brain

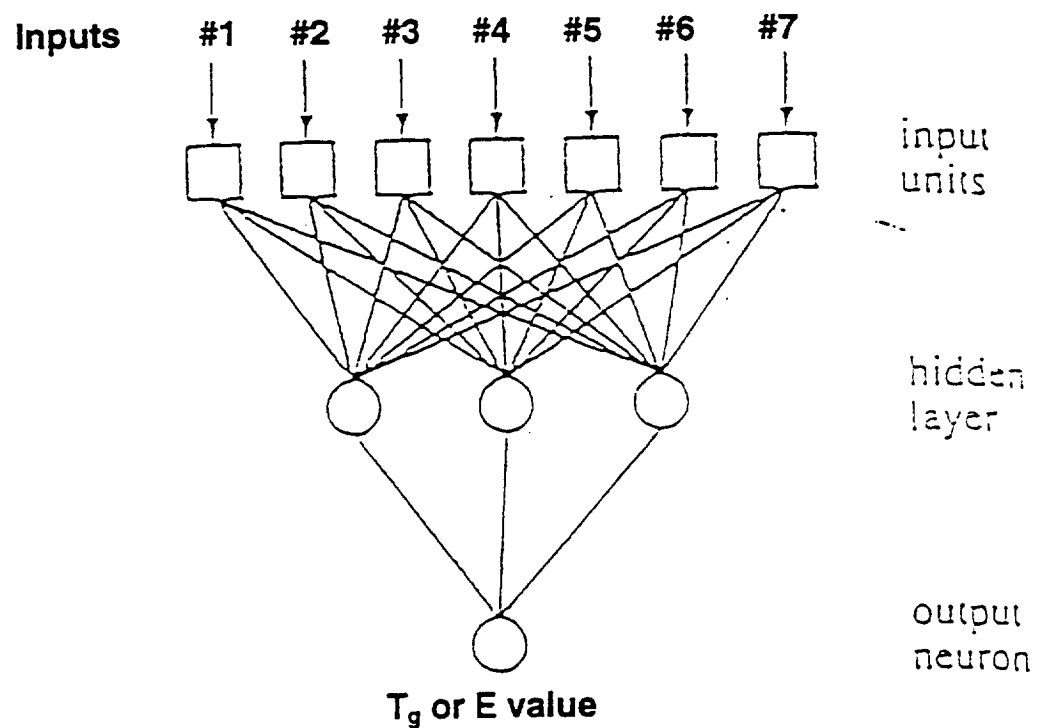
- **ANNs learn by repetition (like a child) to generate a desired response (output) based on knowledge of specific stimuli (inputs)**
- **learns to map bulk polymer property (output) onto calculable molecular descriptors (inputs), thereby allowing prediction of polymer properties solely from knowledge of these descriptors**
- **applicable to any series of polymers for which experimental data is available**
- **focused on same two polymer properties as outputs: T_g and Tensile Modulus**
- **selected identical seven molecular descriptors as inputs: (1) molecular weight; (2) length; (3) number of atoms; (4) number of non-H atoms; (5) vdW volume; (6) rotational df, and (7) number of backbone atoms**

Advantages

- **totally independent of any fragment database**
- **generally applicable to any property and to any polymer**
- **inherently nonlinear and tolerant of noisy data**

Disadvantages

- **requires expt'l data on related polymers to train the network prior to making predictions**



List of Inputs (per repeat unit)

- #1 molecular weight
- #2 end-to-end length
- #3 number of atoms
- #4 number of non-H atoms
- #5 vdW volume
- #6 rotational degrees of freedom
- #7 number of backbone atoms

SUMMARY OF RESULTS

Figure 1. Repeat units of polymers included in this QSPR study

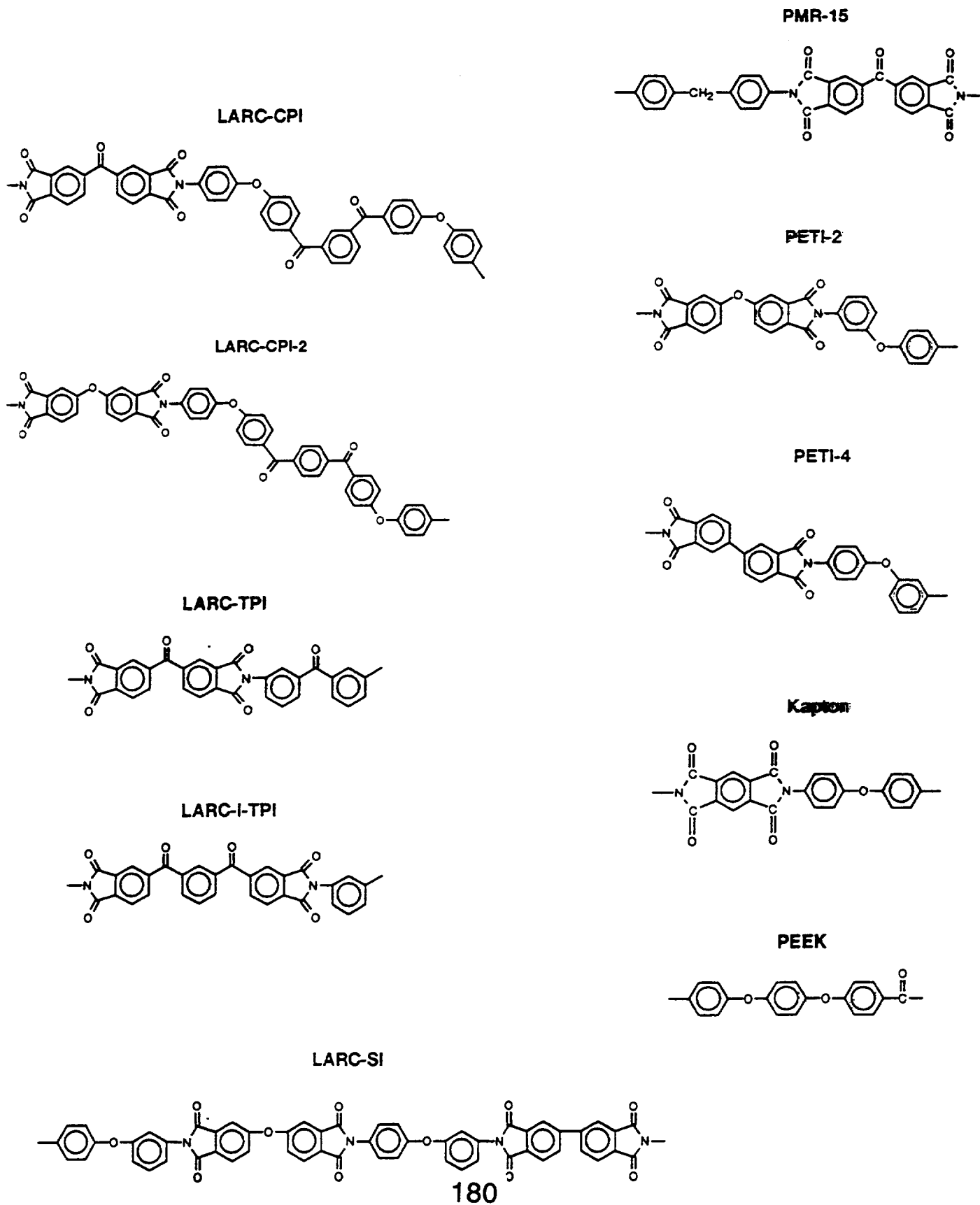


Table I
Abbreviated List of Calculated Properties of Polyimides and PEEK

| PROPERTY ^a | UNIT | LARC-CPI | LARC-CPI2 | LARC-TPI | LARC-TPI | LARC-SI | PMR-15 | PETI-2 | PETI-4 | KAPTON | PEEK |
|--|--------------------|----------|-----------|----------|----------|---------|--------|--------|--------|--------|--------|
| THERMOPHYSICAL PROPERTIES | | | | | | | | | | | |
| Glass Transition Temperature, T_g | K | 486 | 488 | 532 | 534 | 520 | 518 | 516 | 522 | 628 | 411 |
| Melt Transition Temperature ^b , T_m | K | 707 | 726 | 744 | 746 | 755 | 733 | 754 | 850 | 650 | 627 |
| Coef. of Thermal Expansion ^c , α | ppm/K | 206 | 204 | 192 | 187 | 183 | 186 | 190 | 177 | 147 | 227 |
| Density, ρ , at 298 K | g/cm ³ | 1.36 | 1.36 | 1.43 | 1.43 | 1.43 | 1.40 | 1.44 | 1.43 | 1.38 | 1.25 |
| Solubility Parameter, δ | MPa ^{1/2} | 25.6 | 25.3 | 27.2 | 27.2 | 26.5 | 26.6 | 26.5 | 26.6 | 25.3 | 22.8 |
| Cohesive Energy, E_{coh} | kJ/mole | 378.5 | 364.5 | 258.6 | 258.6 | 457.8 | 246.2 | 230.6 | 227.2 | 177.2 | 119.9 |
| Attainable Degree of Crystallinity, X_c | vol frac | 0.43 | 0.46 | 0.37 | 0.37 | 0.42 | 0.39 | 0.43 | 0.42 | 0.32 | 0.49 |
| Free Enthalpy of Formation ^b , ΔG_f | kJ/mole | -1046 | -1046 | -686.0 | -686.0 | -1224 | -600.0 | -686.0 | -538.0 | -565.0 | -360.0 |
| MECHANICAL PROPERTIES at 298 K | | | | | | | | | | | |
| Tensile Modulus, E | GPa | 3.63 | 3.41 | 4.24 | 4.13 | 4.46 | 4.03 | 4.02 | 3.90 | 3.93 | 2.42 |
| Tensile Yield Strength, σ_y | MPa | 90.8 | 85.3 | 105.9 | 103.2 | 111.5 | 100.8 | 100.4 | 97.4 | 98.3 | 60.4 |
| Poisson's Ratio, μ | MPa | 0.406 | 0.410 | 0.408 | 0.411 | 0.397 | 0.407 | 0.406 | 0.410 | 0.407 | 0.414 |
| Ultimate Compressive Strength ^b , σ_{comp} | MPa | 235.7 | 237.9 | 283.1 | 284.8 | 270.2 | 268.4 | 266.5 | 272.3 | 394.0 | 168.9 |
| Brittle Strength, σ_b | MPa | 124.4 | 134.3 | 128.7 | 135.1 | 104.7 | 126.8 | 124.2 | 134.4 | 128.1 | 142 |

^a Based on DOW QSPR method, unless otherwise noted.

^b Based on van Krevelen QSPR method.

^c Based on Synthia method.

Table II. Expanded List of Calculated Properties of Polyimides and PEEK

| PROPERTY ^a | UNIT | LARC-CPI | LARC-CPI ₂ | LARC-TPI | LARC-TPI ₁ | LARC-SI | PNMR-15 | PETI-2 | PETI-4 | MAPPON | PEEK |
|---|----------------------|----------|-----------------------|----------|-----------------------|---------|---------|--------|--------|--------|--------|
| THERMOPHYSICAL PROPERTIES | | | | | | | | | | | |
| Glass Transition Temperature, T _g | K | 486 | 468 | 532 | 534 | 520 | 516 | 516 | 522 | 628 | 411 |
| Melt Transition Temperature ^b , T _m | K | 707 | 726 | 744 | 746 | 755 | 733 | 755 | 754 | 850 | 627 |
| Coeff. of Thermal Expansion ^c , α | ppm/K | 206 | 204 | 192 | 187 | 183 | 186 | 190 | 177 | 147 | 227 |
| Molar Volume at 298 K | cm ³ /mol | 579.2 | 569.2 | 348.4 | 348.3 | 651.0 | 347 | 329.4 | 321.7 | 277.5 | - |
| Density, ρ , at 298 K | g/cm ³ | 1.36 | 1.36 | 1.43 | 1.43 | 1.43 | 1.40 | 1.44 | 1.43 | 1.36 | 1.25 |
| Solubility Parameter, δ | MPa ^{1/2} | 25.6 | 25.3 | 27.2 | 27.2 | 26.5 | 26.6 | 26.5 | 26.6 | 25.3 | 22.6 |
| Cohesive Energy, E _{coh} | kJ/mol | 378.5 | 364.5 | 258.6 | 258.6 | 457.8 | 246.2 | 230.6 | 227.2 | 177.2 | - |
| Molar Heat Capacity ^d : at constant P, at constant V, | J/mol-K | 766.0 | 760.5 | 473.7 | 473.7 | 905.6 | 476.1 | 461.2 | 444.4 | 365.0 | - |
| Surface Tension, γ | J/Kms | 674.9 | 661.9 | 419.6 | 419.6 | 781.7 | 410.4 | 399.1 | 382.7 | 330.2 | - |
| Thermal Conductivity ^e : at 298 K at T _g | W/mK | 56.48 | 55.72 | 61.49 | 61.50 | 59.31 | 59.66 | 59.13 | 59.49 | 55.62 | - |
| Attainable Degree of Crystallinity ^f , X _c | vol frac | 0.43 | 0.46 | 0.37 | 0.37 | 0.42 | 0.39 | 0.43 | 0.42 | 0.32 | 0.49 |
| Av. Molecular Cross Sectional Area | A ² | 20.21 | 18.71 | 19.63 | 18.70 | 24.11 | 19.90 | 20.30 | 18.78 | 19.89 | - |
| PROPERTY RELATING TO THERM. STABILITY | | | | | | | | | | | |
| Free Enthalpy of Formation ^g , ΔG_f | kJ/mol | -1046 | -1046 | -686.0 | -686.0 | -1224 | -600.0 | -606.0 | -538.0 | -565.0 | -360.0 |

Table II (continued)

| PROPERTY ^a | UNIT | IARC-CPI | IARC-CPI2 | IARC-TPI | IARC-TPI | PMR-15 | PETI-2 | PETI-4 | KAPTON | PEEK |
|--|---------------------|----------|-----------|----------|----------|--------|--------|--------|--------|--------|
| MECHANICAL PROPERTIES at 298 K | | | | | | | | | | |
| Tensile Modulus, E | GPa | 3.63 | 3.41 | 4.24 | 4.13 | 4.46 | 4.03 | 4.02 | 3.90 | 3.93 |
| Tensile Yield Strength, σ_y | MPa | 90.8 | 85.3 | 105.9 | 103.2 | 111.5 | 100.8 | 100.4 | 97.4 | 98.3 |
| Bulk Modulus ^b | GPa | 6.055 | 5.875 | 6.855 | 6.94 | 6.355 | 6.483 | 6.172 | 6.382 | 7.115 |
| Shear Modulus ^c | GPa | 1.329 | 1.258 | 1.492 | 1.387 | 1.463 | 1.392 | 1.368 | 1.343 | 1.369 |
| Poisson's Ratio, μ | | 0.406 | 0.410 | 0.408 | 0.411 | 0.397 | 0.407 | 0.406 | 0.410 | 0.407 |
| Ultimate Compressive Strength ^b , | MPa | 235.7 | 237.9 | 263.1 | 284.8 | 270.2 | 268.4 | 266.5 | 272.3 | 394.0 |
| Brittle Strength, σ_b | MPa | 124.4 | 134.3 | 128.7 | 135.1 | 104.7 | 126.8 | 124.2 | 134.4 | 126.1 |
| Crazing Strength, σ_c | MPa | 93.2 | 92.4 | 132.0 | 133.0 | 110.5 | 118.7 | 116.1 | 120.1 | 160.0 |
| Ultimate Flexural Strength ^b , σ_f | MPa | 123.7 | 123.3 | 128.3 | 128.5 | 125.9 | 125.4 | 125.7 | 126.0 | 136.7 |
| Shear Yield Stress ^c | MPa | 104.0 | 98.64 | 116.8 | 109.2 | 114.2 | 109.2 | 107.0 | 105.4 | 108.1 |
| Hardness ^d , H _p | MPa | 15.2 | 15.2 | 15.9 | 15.9 | 15.5 | 15.5 | 15.5 | 15.6 | 17.0 |
| Plateau Modulus, G_N^0 | MPa | 1.75 | 2.01 | 2.31 | 2.52 | 1.53 | 2.17 | 2.05 | 2.56 | 2.89 |
| ELECTRICAL, OPTICAL AND MAGNETIC | | | | | | | | | | |
| Refractive Index, n | | 1.643 | 1.644 | 1.657 | 1.657 | 1.664 | 1.66 | 1.661 | 1.667 | 1.663 |
| Molar Refraction (Lorentz and | | 215.7 | 213.1 | 133.3 | 133.3 | 251.4 | 133.2 | 128.1 | 125.8 | 103.07 |
| Dielectric Constant, ϵ | | 3.42 | 3.36 | 3.65 | 3.65 | 3.46 | 3.49 | 3.48 | 3.44 | 3.60 |
| Volume Resistivity ($\times 10^{14}$) | ohm-cm | 1.45 | 1.89 | 0.49 | 0.49 | 1.20 | 1.03 | 1.12 | 1.29 | 0.641 |
| Diamagnetic Susceptibility ($\times 10^6$) | cm ³ /mo | 423.8 | 422.5 | 254.6 | 254.6 | 497.9 | 258.6 | 251.9 | 245.9 | 196.0 |

Table II (continued)

| PROPERTY | UNIT | VTC CP | VTC CP | LARC- III | LARC- III | LARC- II | LARC- II | PEI-2 PPH | PEI-4 PPH | KAPTON | PEEK |
|---|----------------------|-----------|-----------|--------------|--------------|-------------|-------------|--------------|--------------|--------|--------|
| MECHANICAL PROPERTIES AT INCEPTION OF RUBBER PLATEAU^a | | | | | | | | | | | |
| | | | | | | | | | | | |
| Temperature | K | 512 | 517 | 549 | 564 | 576 | 566 | 555 | 594 | 717 | 463 |
| Molar Volume | cm ³ /mol | 626.41 | 618.41 | 382.06 | 382.52 | 715.92 | 381.10 | 365.57 | 357.41 | 296.56 | 244.33 |
| Density | g/cm ³ | 1.256 | 1.253 | 1.305 | 1.303 | 1.303 | 1.271 | 1.298 | 1.283 | 1.289 | 1.180 |
| Bulk Modulus | MPa | 2766 | 2604 | 3121 | 3074 | 3000 | 2917 | 2598 | 2721 | 2344 | 2301 |
| Shear Modulus | MPa | 1.59 | 1.72 | 2.06 | 2.70 | 1.61 | 2.17 | 1.86 | 2.59 | 3.96 | 1.31 |
| Tensile Modulus | MPa | 4.78 | 5.15 | 6.17 | 6.11 | 5.42 | 6.51 | 5.58 | 7.76 | 11.89 | 3.92 |
| Poisson's Ratio | | 0.50 | 0.50 | 0.50 | 0.50 | 0.50 | 0.50 | 0.50 | 0.50 | 0.499 | 0.500 |
| TRANSPORT PROPERTIES^b | | | | | | | | | | | |
| Activation Energy for Viscous Flow | kJ/mol | 69.55 | 68.87 | 70.96 | 70.96 | 69.80 | 69.91 | 68.81 | 70.83 | 69.70 | 67.14 |
| Permeability at 298 K : O ₂ | Dow Units | 23.2 | 34.1 | 10.9 | 10.9 | 33.5 | 24.3 | 39.0 | 39.3 | 32.4 | 71.6 |
| N ₂ | | 5.1 | 7.8 | 2.3 | 2.3 | 7.6 | 5.4 | 6.9 | 9.0 | 7.3 | 17.2 |
| CO ₂ | | 89.6 | 136.2 | 39.4 | 39.4 | 133.4 | 94.1 | 157.2 | 156.7 | 126.9 | 305.0 |

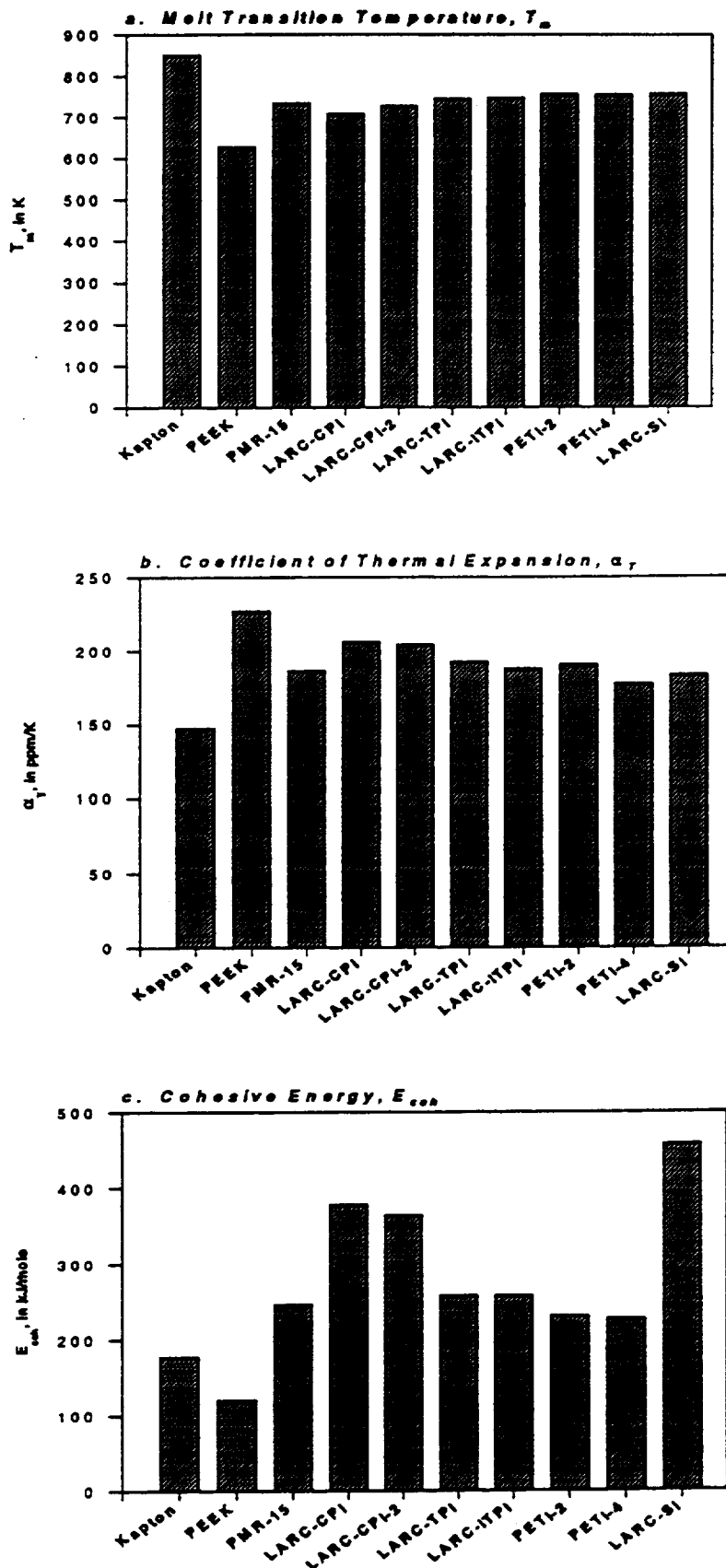
^a Based on DOW QSPR method, unless otherwise noted.^b Based on van Krevelen QSPR method.^c Based on Synthia method.

Table III. List of Experimental Properties of Polyimides and PEEK

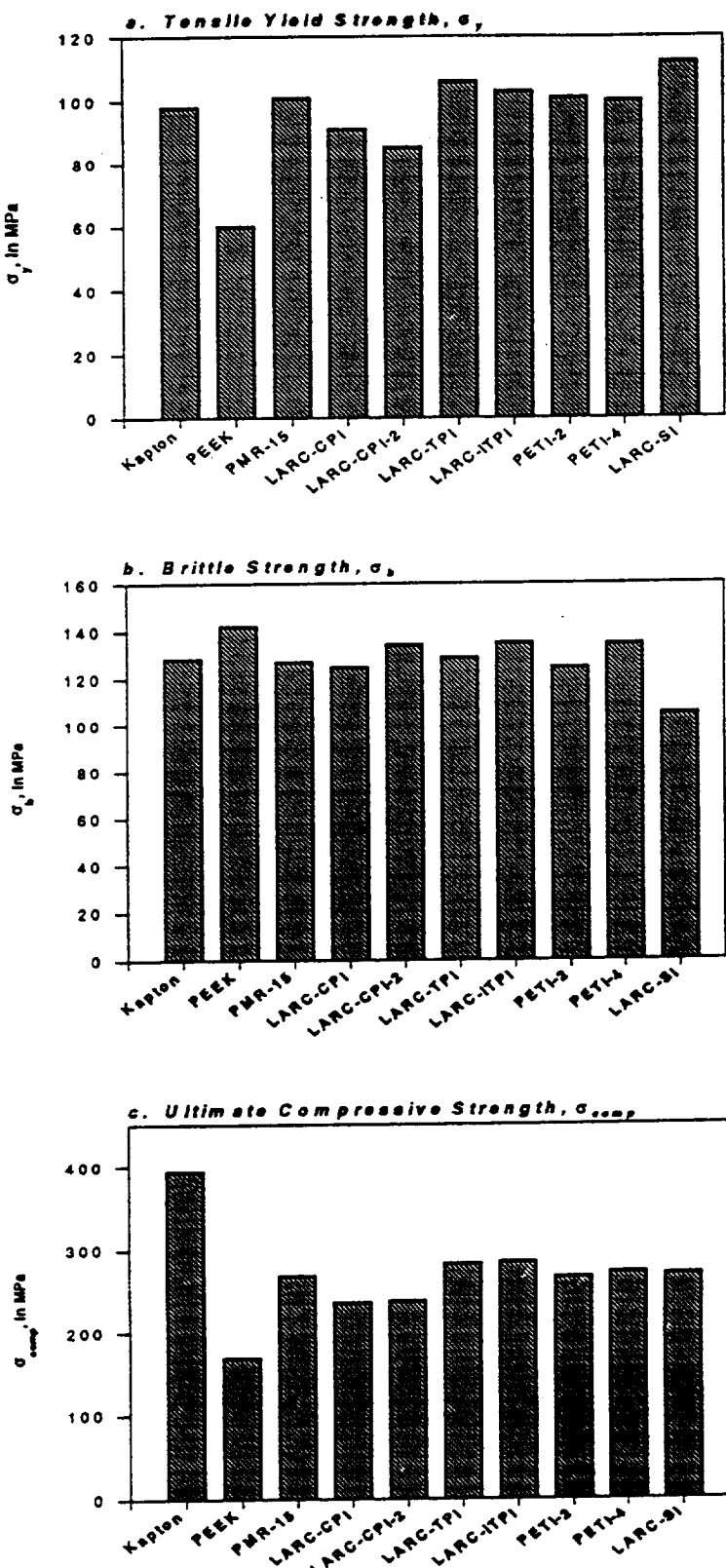
| PROPERTY | UNIT | LARC-CPI | LARC-CPI2 | LARC-TPI | LARC-TPI1 | LARC-SI | PMR-15 | PEI-2 | PEI-4 | KAPTON | PEEK |
|--------------------------------------|---|---|------------------|--|---|--|---|-------------------|--|---|--------------------|
| Glass Transition Temperature, T_g | K | 495. ^a 493. ¹⁰ | 490 ^c | 513 ^c | 532. ¹¹ 523. ¹⁰ | 533. ¹⁰ | 600 ^c | 611. ² | 656. ¹ | 418. ¹ | 416. ² |
| Melt Transition Temperature, T_m | K | 623. ⁴ | | 548. ^c | 533. ¹¹ | 578 ^c | 613. ⁹ | | 770. ¹ | 597. ¹ | 417. ² |
| Coef. of Thermal Expansion, α | $\text{In}/\text{In}^{\circ}\text{F}$ g/cm^3 | | | | | | $28(10^{-4})^e$ | | | | $22(10^{-4})^f$ |
| Density, ρ | | | | | 1.55 ^c 1.37 ^c | | 1.58 ^c 1.32. ⁹ | | 1.42. ¹ | 1.20. ⁴ | |
| Tensile Modulus, E | GPa (kN) | 4.27. ¹⁰ | | 3.5 ^c 3.7. ¹¹ | 3.70. ¹¹ (465) ^c | | 3.2 ^c 3.9 ^c | | 2.10 ^c (430) ¹¹ | 3.7. ¹ (550) ^c | 1.26. ⁷ |
| Tensile Yield Strength, σ | | | | | 103.4 ^c 3.30 ^c | 96.6 ^c 3.29 ^c | | | 3.5 ¹ | 3.3 ⁷ | 1.31. ² |
| Dielectric Constant, ϵ | | | | | | | | | 3.2 ^c ^e | | |

References

- van Krevelen, D.W. *Properties of Polymers: Their Correlation with Chemical Structure; Their Additive Group Contributions*; Elsevier: Amsterdam, 1990.
- Proceedings of the Interdisciplinary Symposium on Recent Advances in Polyimides and other High Performance Polymers, San Diego, CA, January 22-25, 1990.
- Hergenrother, P.M. *Angew. Chem. Int. Ed. Eng.* **1990**, *29*, 1262-1268.
- Wilkes, G.L. *Polymer* **1994**, *35*, 5672-5677.
- Fetters, L.J.; Lohse, D.; Richter, D.; Witten, T.; Zikoli, A. *Macromolecules* **1994**, *27*, 4439-4647.
- Croall, C.I.; St. Clair, T.L. Technical Memorandum NASA TM-104202, NASA Langley Research Center, January 1992.
- Data Sheet for STABAR K200.
- Data Sheet for Fibelite®966C.
- Scola, D.A.; Vontell, J.H. *Polymer Composites* **1988**, *9*, 443-452.
- Hergenrother, P.M.; Rogalski, M.E. *Composites for High Speed Commercial Transports*. pp. 354-366.
- Prahl, J.R.; St. Clair, T.L. *SAMPE Journal* **1990**, *26*, 29-34.
- Prahl, J.F.; Krueger, W.H.; Chang, I.Y. *34th International SAMPE Symposium and Exhibition*, Reno, NV, May 8-11, 1989.
-

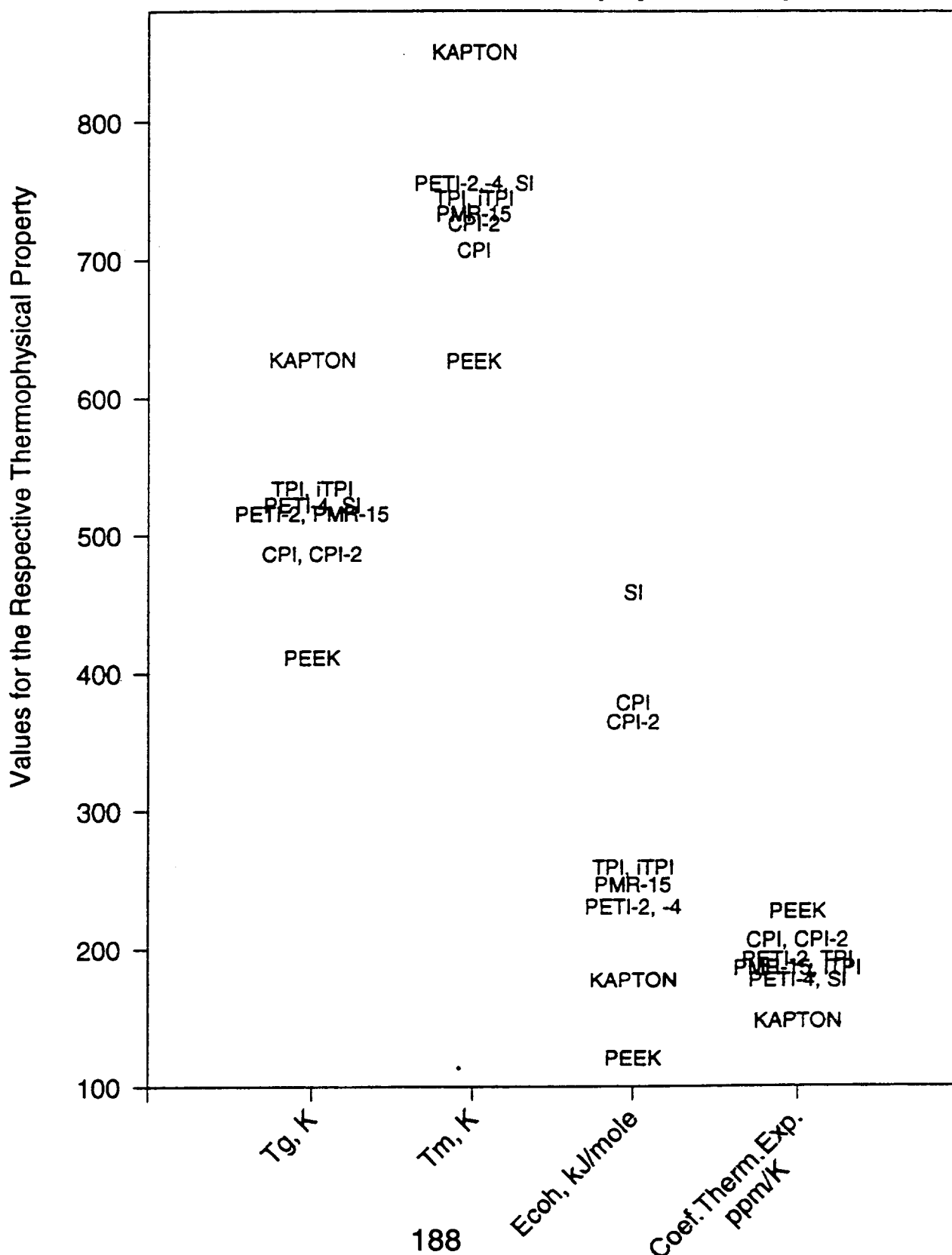


QSPR-calculated Thermophysical Properties for Various Polyimides

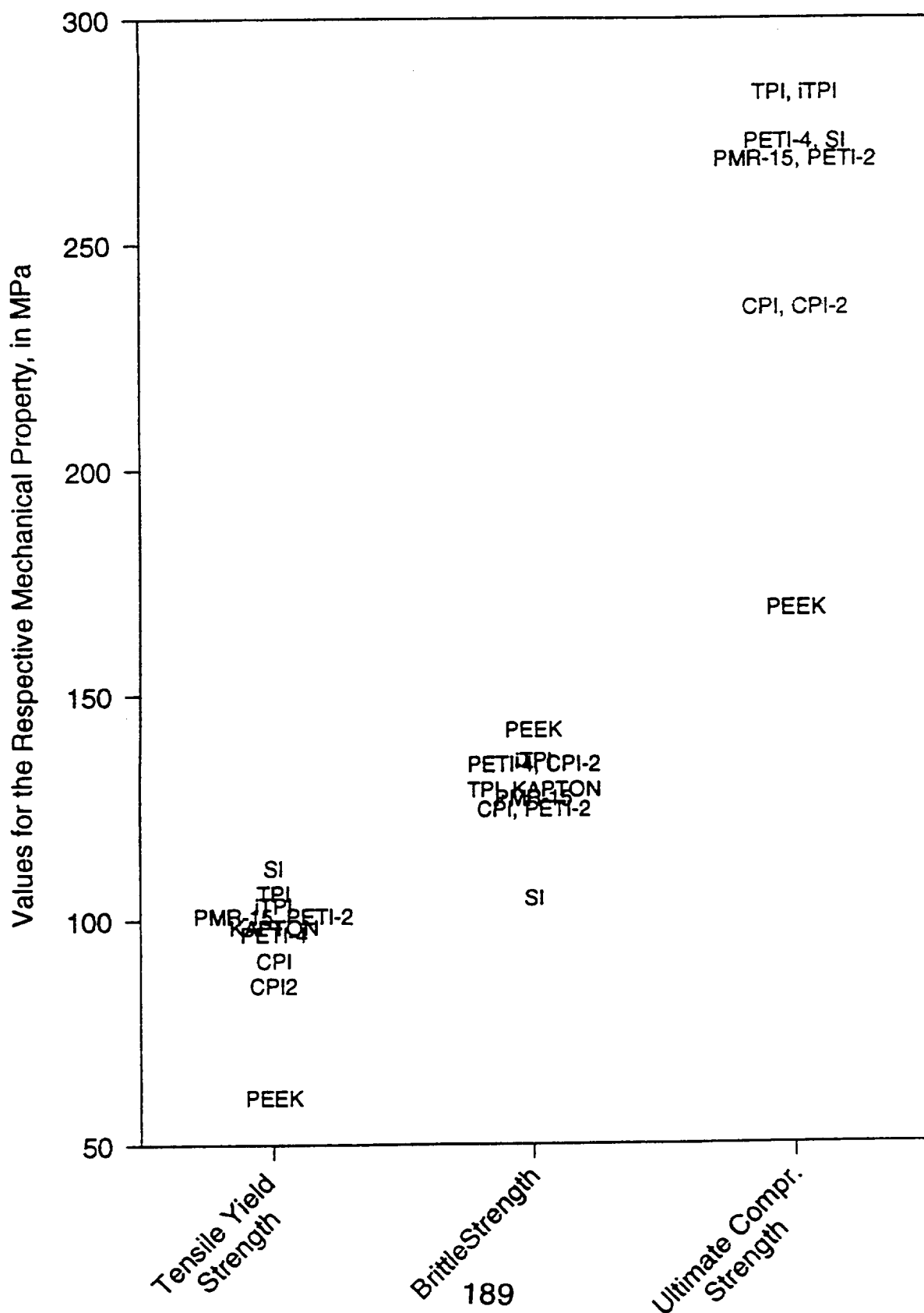


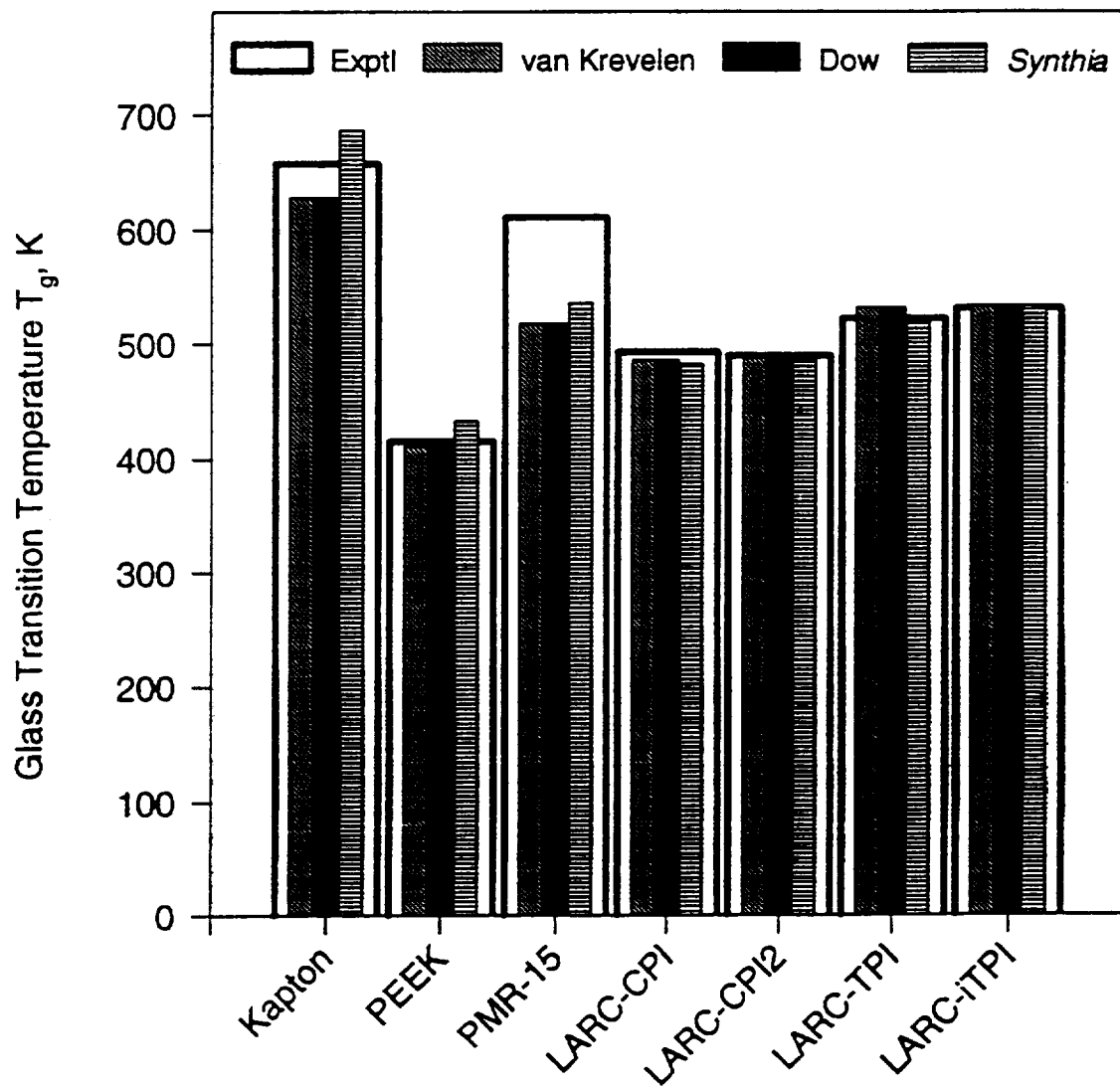
QSPR-calculated Mechanical Properties for Various Polyimides

QSPR-calculated Thermophysical Properties



QSPR-calculated Mechanical Properties

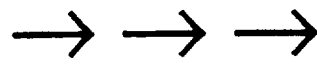


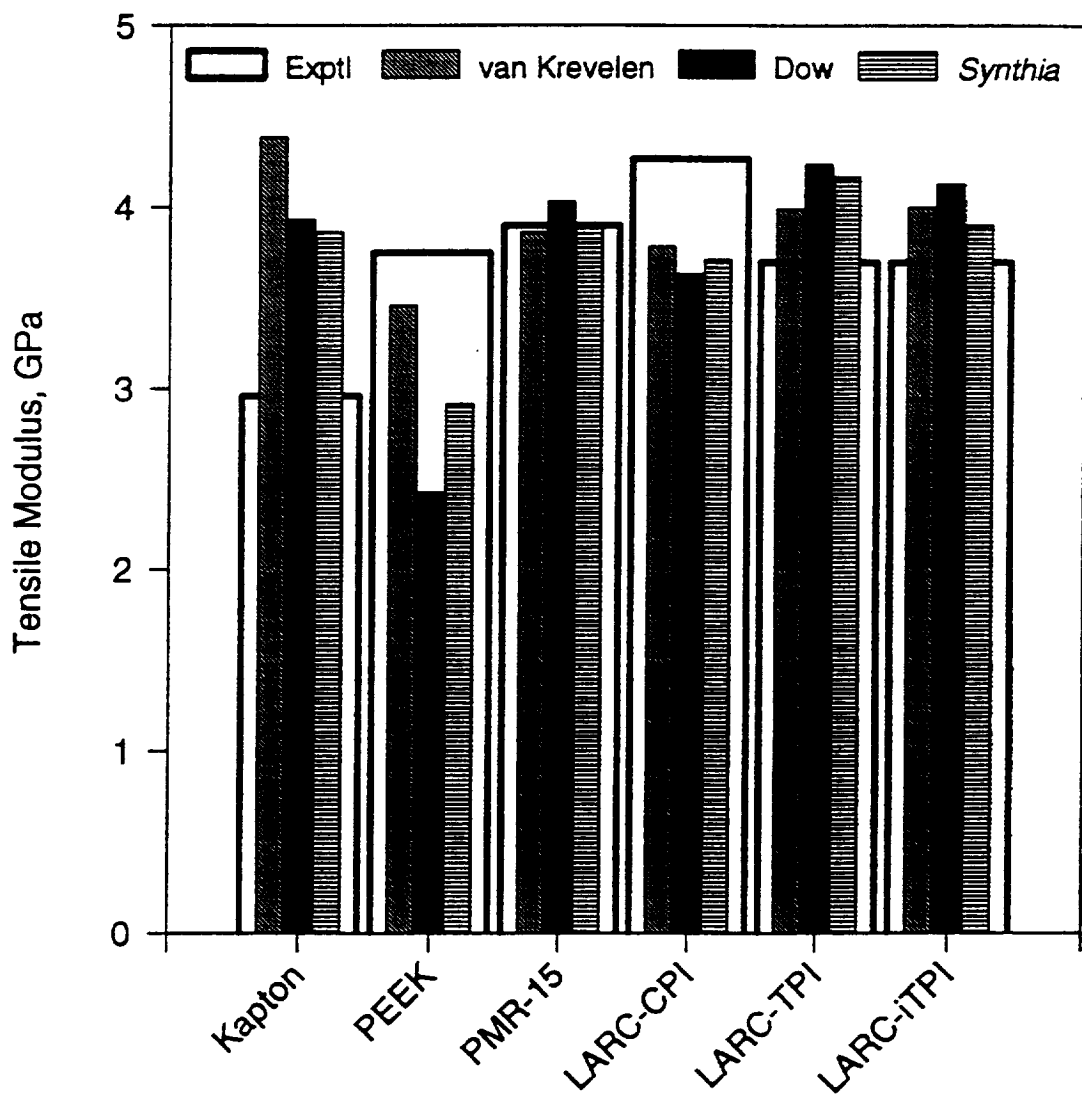


EXPERIMENTAL POLYMER PROPERTIES

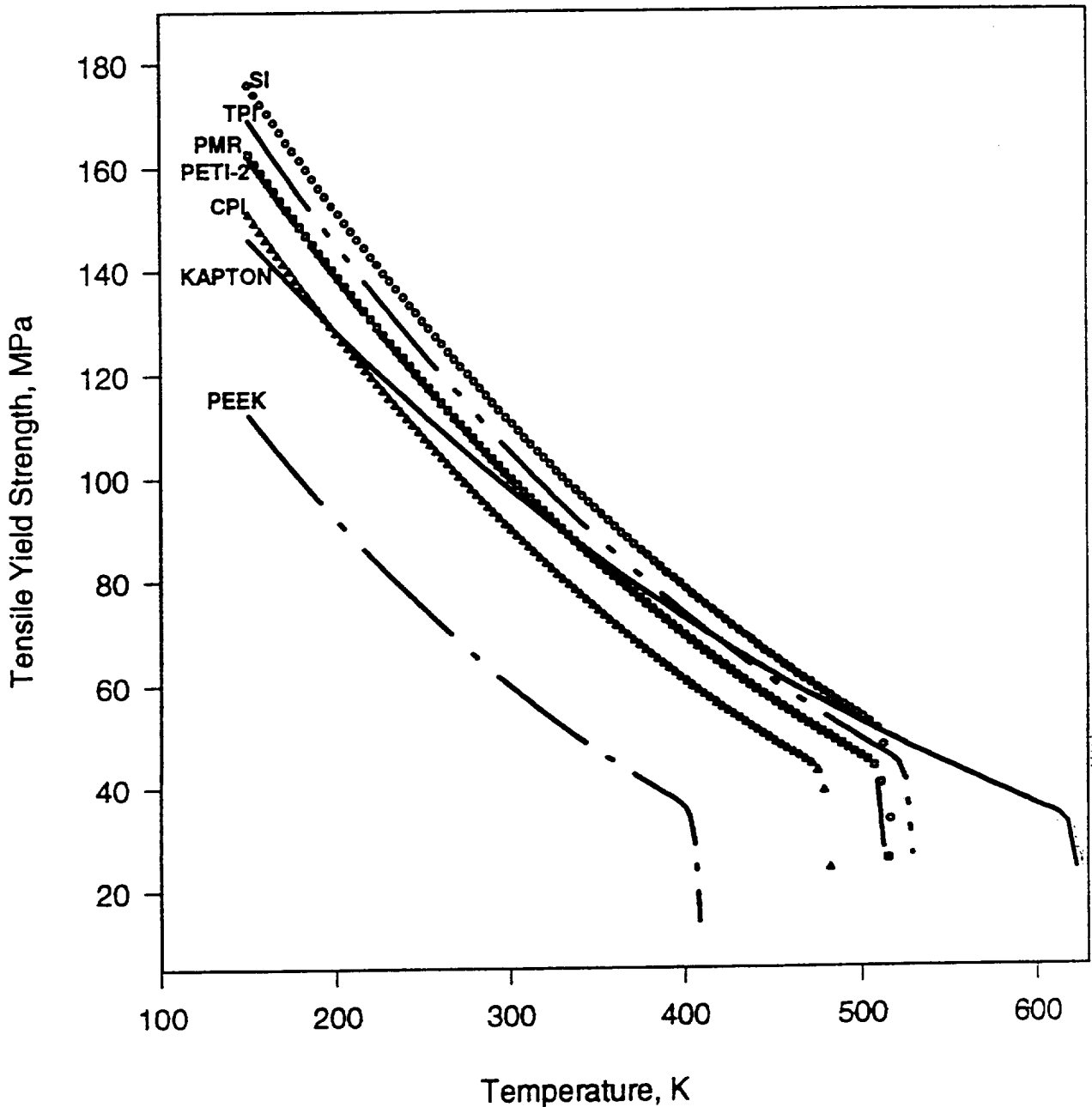
+

NEURAL NETS QSPR METHODS REGRESSION METHODS ATOMISTIC METHODS

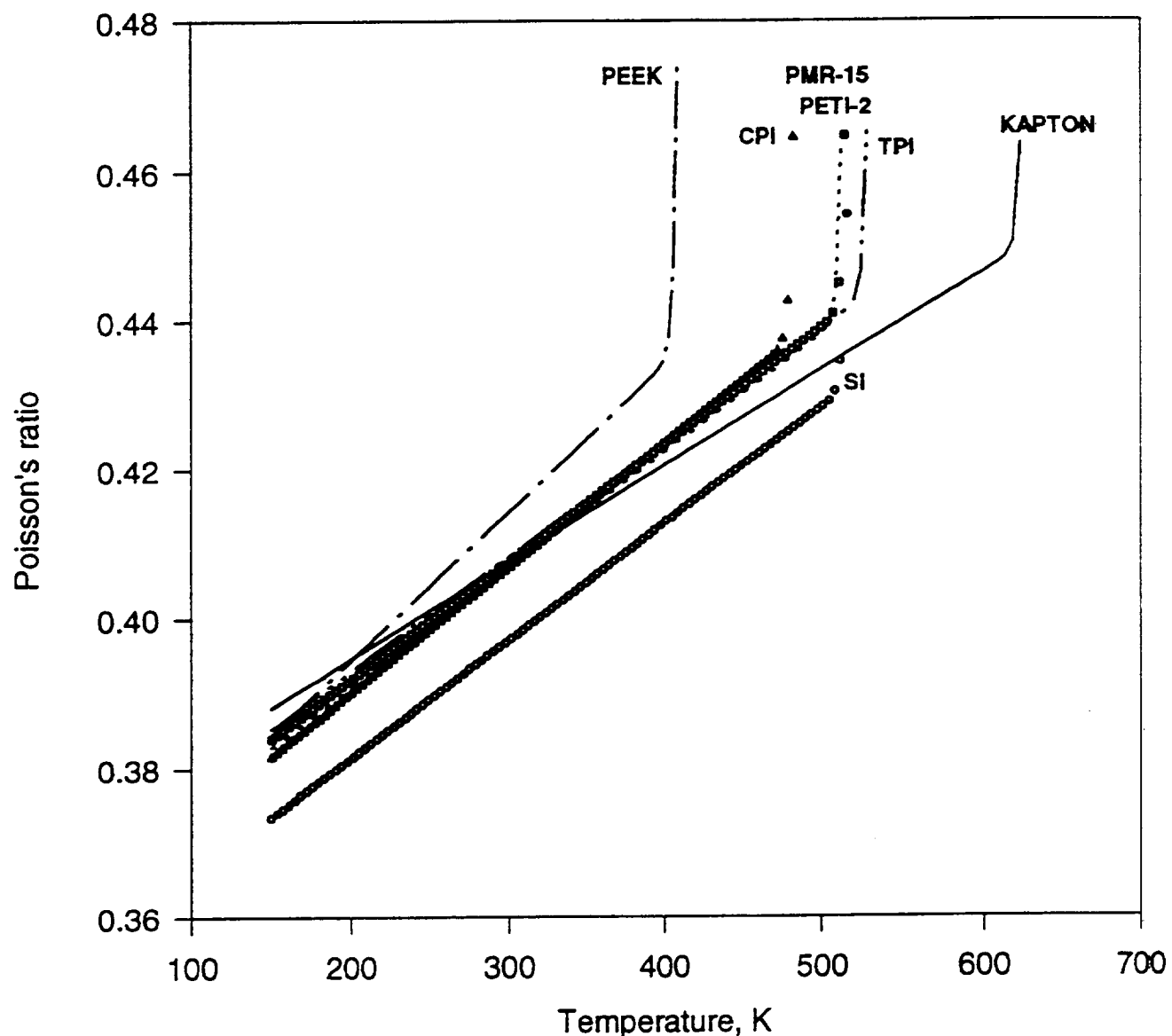




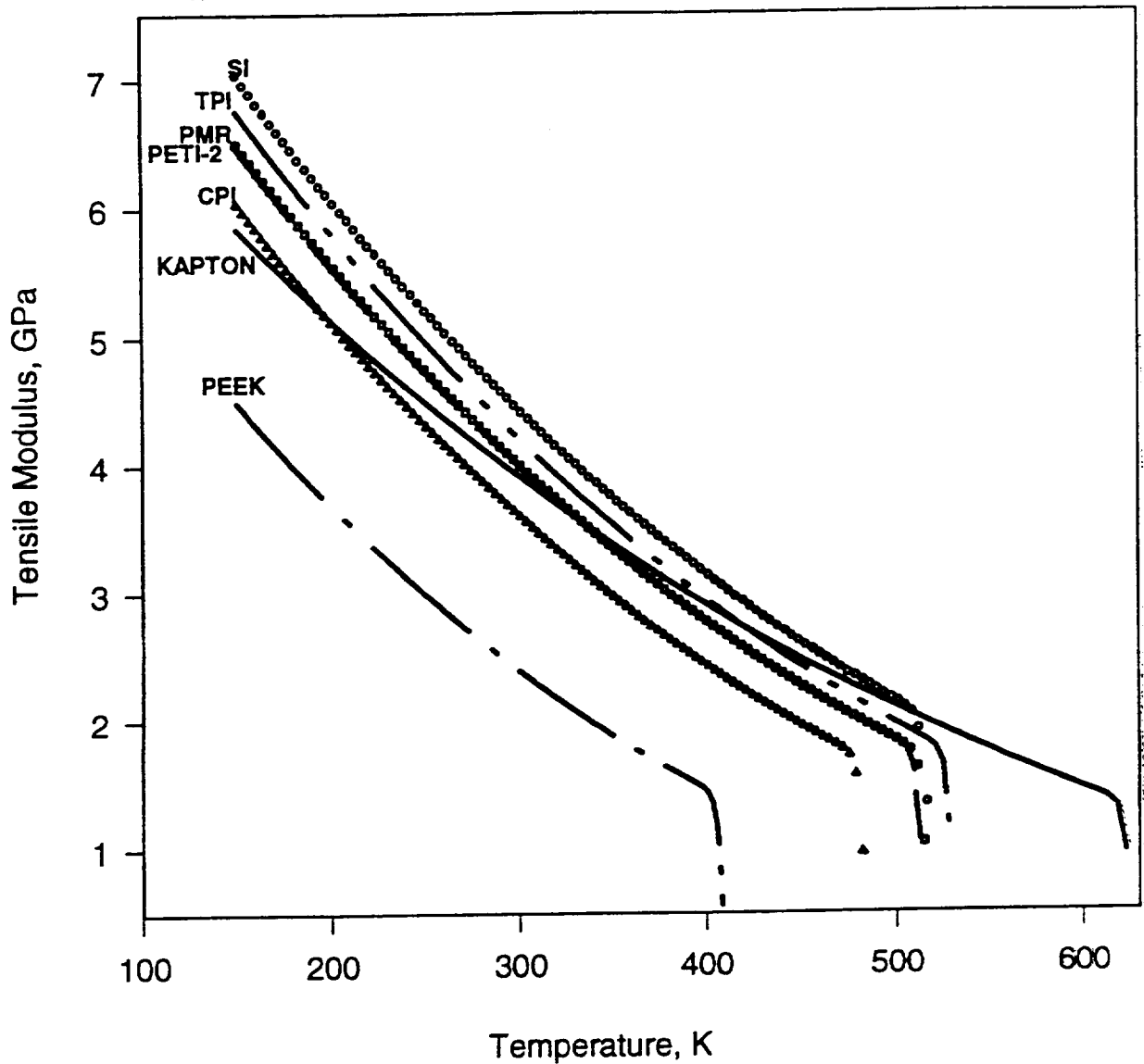
QSPR-calculated Tensile Yield Strength vs. Temperature



QSPR-calculated Poisson's Ratio vs. Temperature



QSPR-calculated Tensile Modulus vs. Temperature

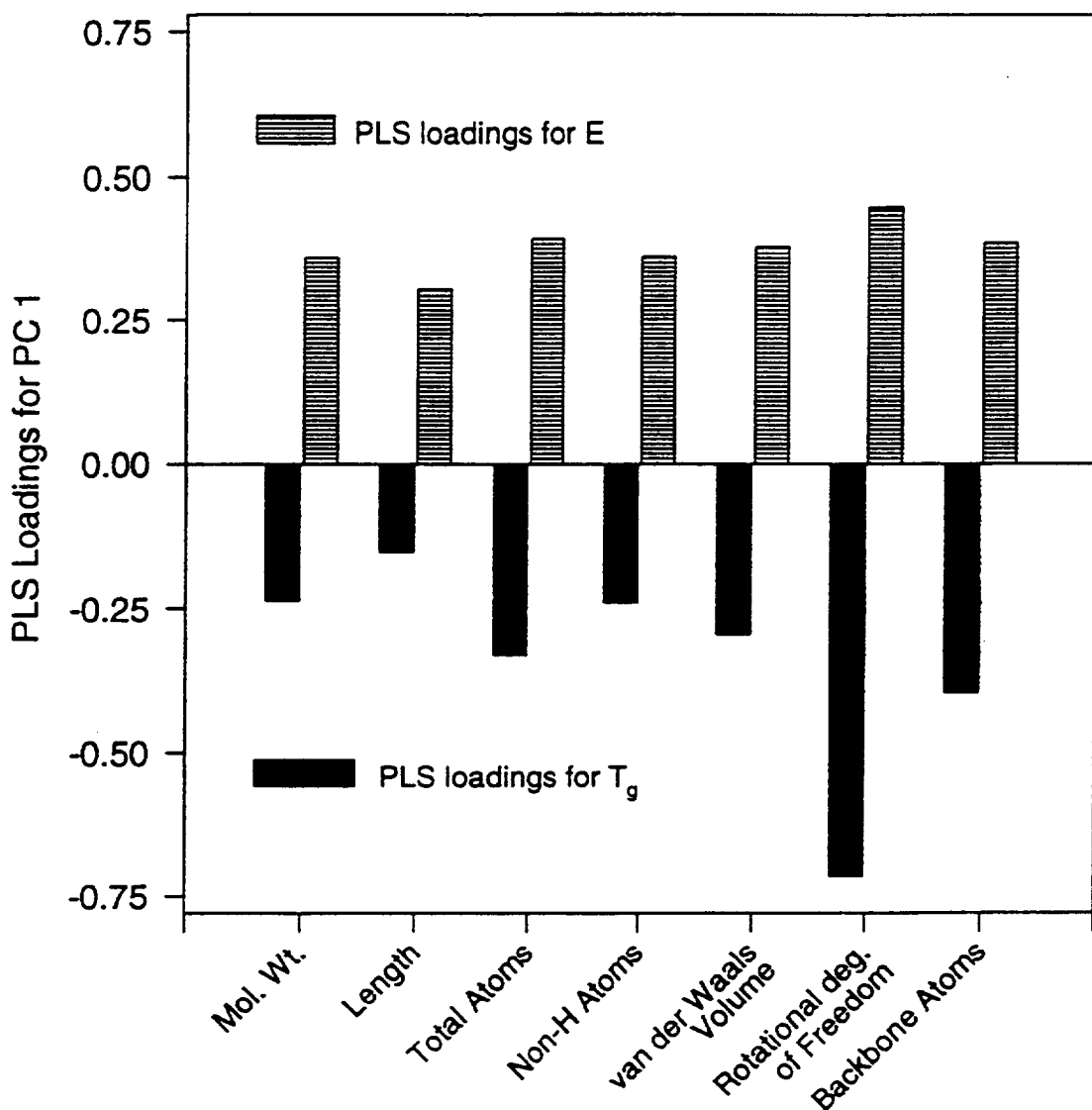


ANN and PLS Calculated T_g vs. Experimental Values

| | <u>Expt'l</u> T _g , K | <u>Calculated/Predicted T_g, K</u> | | | |
|--------|-------------------------------------|--|----------|-----|----------|
| | | ANN | Residual | PLS | Residual |
| CPI | 493 | 506 | -13 | 473 | 20 |
| TPI | 523 | 546 | -23 | 520 | 3 |
| Kapton | 658 | 634 | 24 | 664 | -6 |
| PMR-15 | 611 | 587 | 24 | 583 | 28 |
| CPI-2 | 490 | 513 | -23 | 513 | -23 |
| iTPI | 532 | 556 | -24 | 550 | -18 |
| PEEK | 416 | 440 | -24 | 420 | -4 |
| PETI-2 | | 562 | | 540 | |
| PETI-4 | | 620 | | 617 | |
| SI | | 519 | | 633 | |

ANN and PLS Calculated Tensile Modulus (E)
vs. Experimental Values

| | <u>Expt'l</u> | <u>Calculated/Predicted E, GPa</u> | | | |
|--------|---------------|------------------------------------|-------|----------|-------|
| | | E, GPa | ANN | Residual | PLS |
| CPI | 4.27 | 4.15 | 0.12 | 4.39 | -0.12 |
| TPI | 3.7 | 3.83 | -0.13 | 3.62 | 0.08 |
| Kapton | 2.96 | 3.09 | -0.13 | 3.32 | -0.36 |
| PMR-15 | 3.9 | 3.77 | 0.13 | 3.65 | 0.25 |
| CPI-2 | 3.7 | 3.7 | 0 | 3.53 | 0.17 |
| iTPI | 3.75 | 3.62 | 0.13 | 3.77 | 0.02 |
| PEEK | | 3.77 | | 3.68 | |
| PETI-2 | | 3.4 | | 3.49 | |
| PETI-4 | | 3.97 | | 4.26 | |
| SI | | 4.13 | | 4.38 | |



CURRENT WORK

- Atomistic Cerius² calculations of polymer properties: tensile modulus, bulk modulus, speed of sound, Poisson's ratio, density
- EGAMS of neat LaRC-SI resin (with Mike Grayson): experimental and theoretical investigation of thermal degradation
- Dynamic mechanical analysis (DMA) of LaRC-SI resin (with Mike Grayson): measure T_g , characterize sub- T_g transitions
- Extend multivariate regression and neural network analysis relating bulk polymer properties to molecular descriptors

SUMMARY AND CONCLUSIONS

QSPR

- ALL THREE QSPR METHODS AGREE WITH EACH OTHER REASONABLY WELL IN PREDICTING MECHANICAL AND THERMOPHYSICAL POLYMER PROPERTIES
- VALUES OF T_g AND E PREDICTED BY ALL THREE QSPR METHODS AGREE REASONABLY WELL (WITHIN 15%) WITH THE CORRESPONDING EXPT'L VALUES
- COMPARING THE POLYIMIDES, KAPTON RANKS HIGH IN T_g AND T_m BUT LOW IN α_t ; T_g IS SLIGHTLY HIGHER FOR PARA OVER META CATENATION (488K FOR CPI2 VS. 486K FOR CPI)
- HIGH T_g AND E ARE INVERSELY RELATED TO α_t ; KAPTON VS. PEEK
- LARC-SI EXHIBITS HIGH VALUES OF TENSILE MODULUS AND TENSILE YIELD STRENGTH (AND LOW VALUES OF POISSON'S RATIO) ACROSS THE $T = 100\text{-}600$ K TEMPERATURE RANGE

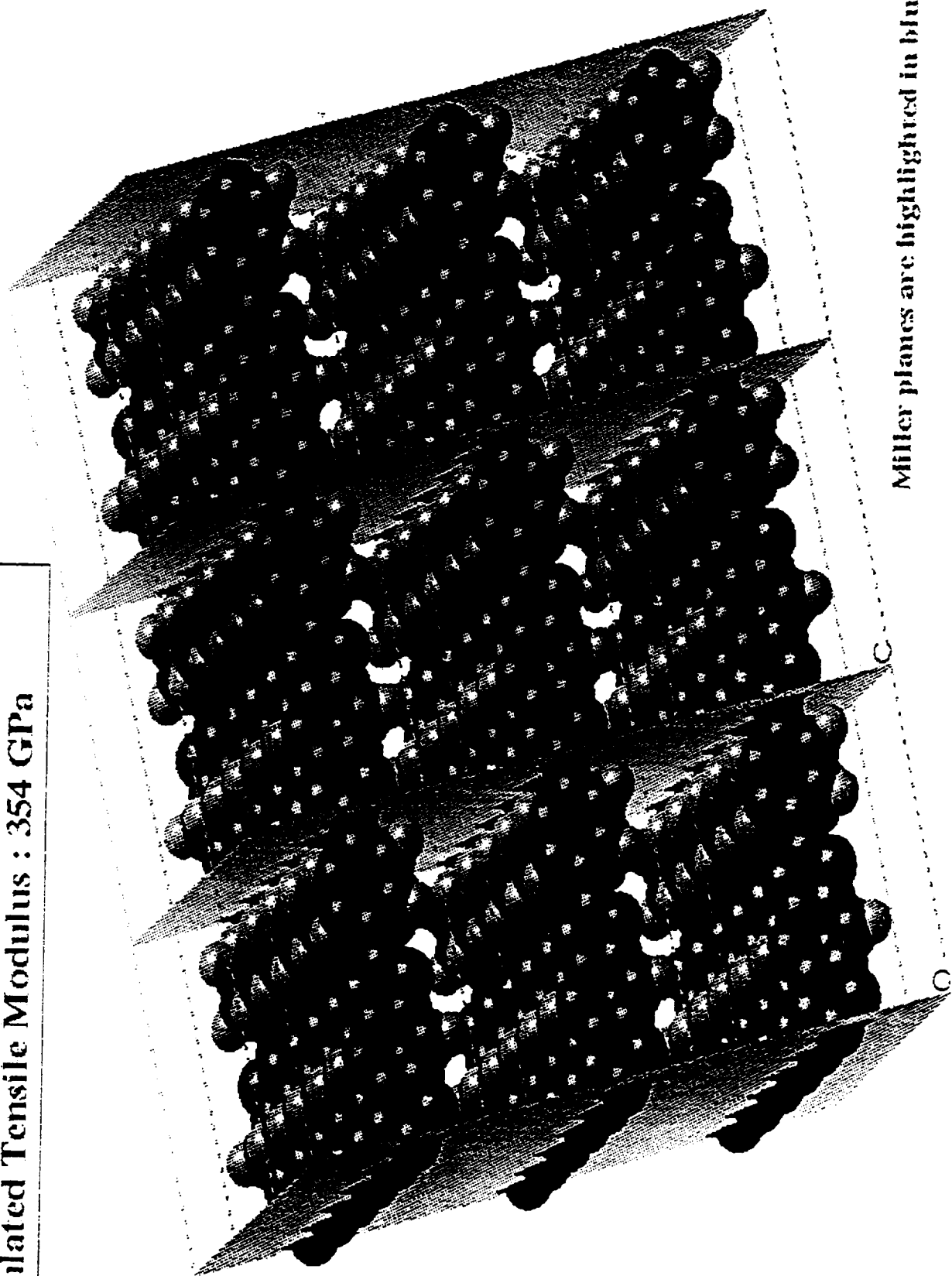
PLS REGRESSION AND NEURAL NETS (ANN)

- FOR T_g , THE RESIDUAL STANDARD DEVIATION (RSR) WAS 18K FOR PLS, 20K FOR ANN, AND 37K FOR QSPR
- FOR E , THE RSD WAS 0.20 GPA FOR PLS, 0.12 GPA FOR ANN, AND 0.91 GPA FOR QSPR-DOW
- THE MOLECULAR DESCRIPTOR WITH THE HIGHEST PLS LOADING WAS THE ROTATIONAL DEGREES OF FREEDOM FOR BOTH T_g AND E

RESULTS OF ATOMISTIC CERIUS² CALCULATIONS

cis – PBO

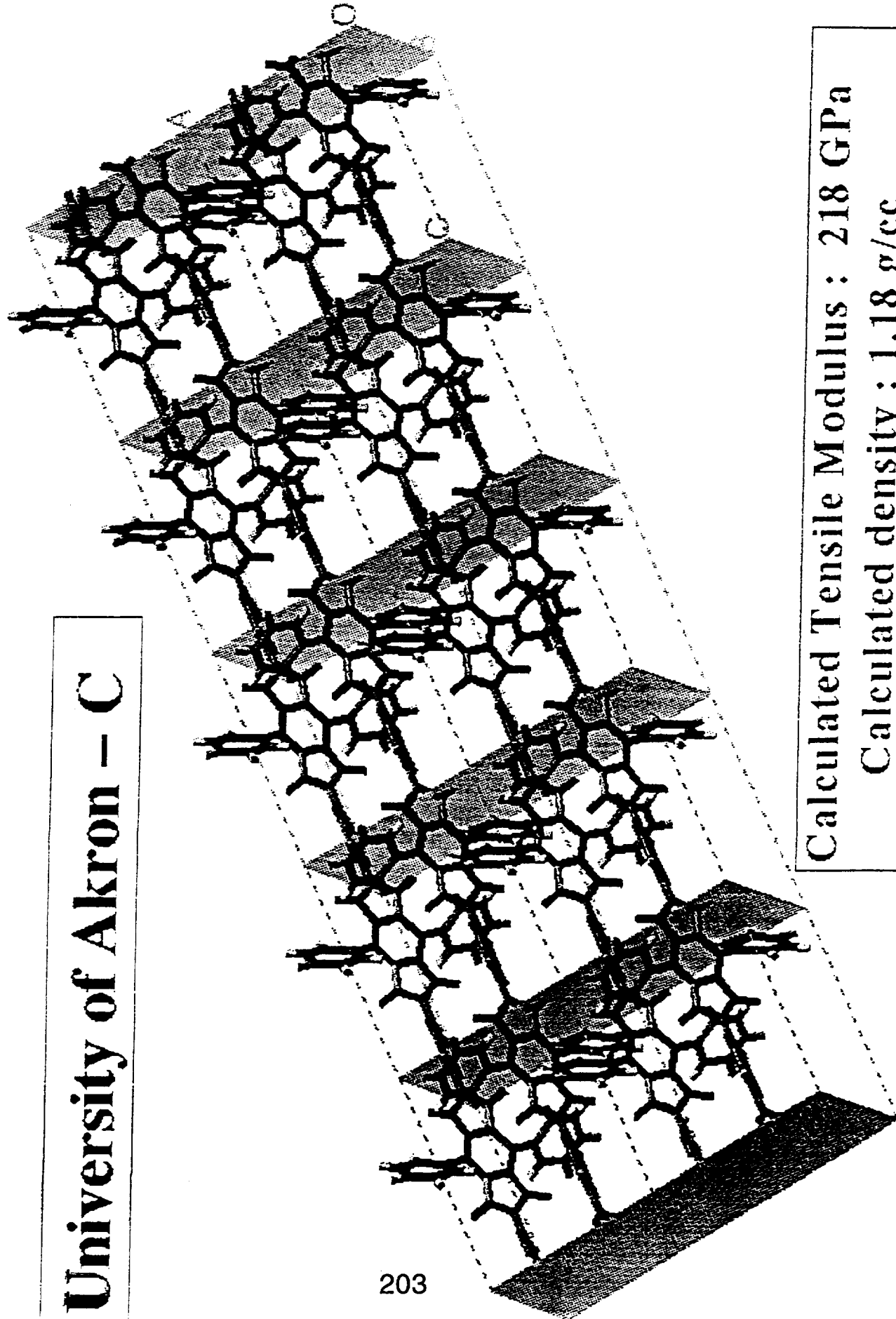
Calculated Tensile Modulus : 354 GPa



Miller planes are highlighted in blue

University of Akron - C

203



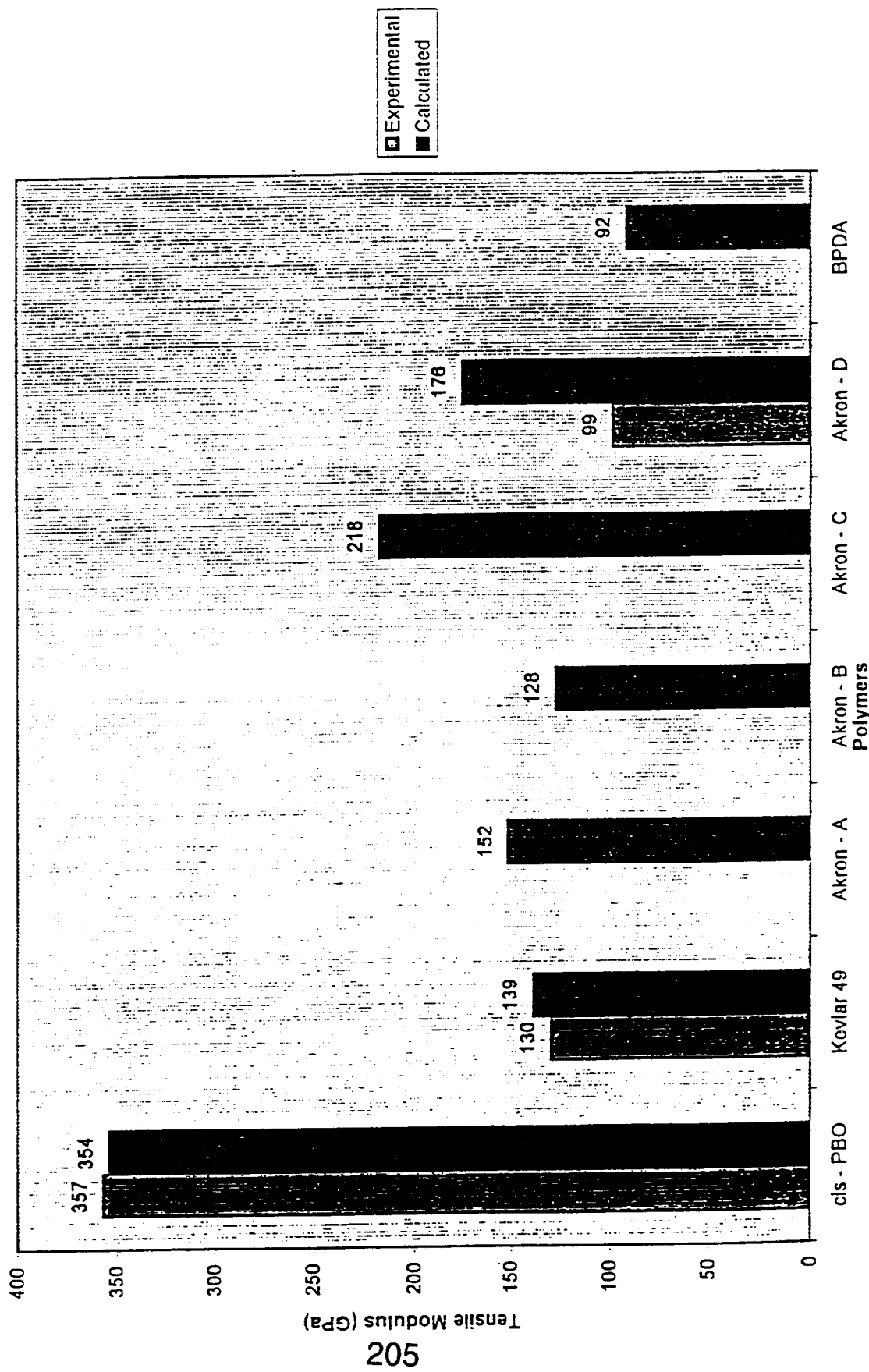
Calculated Tensile Modulus : 218 GPa

Calculated density : 1.18 g/cc

Table C: University of Akron - C Cerius² Data

| <u>Structure</u> | <u>Energy</u> | <u>density</u> | <u>Tensile Modulus (GPa)</u> |
|------------------|-----------------|----------------|------------------------------|
| | kcal/mol | g/cc | Z axis |
| a | 145.0534 | 1.1860 | 221.3720 |
| b | 144.7304 | 1.1840 | 217.1443 |
| c | 144.9722 | 1.1830 | 222.4243 |
| d | 144.6897 | 1.1840 | 219.5773 |
| e | 144.6852 | 1.1830 | 215.7280 |
| f | 144.6677 | 1.1840 | 219.6206 |
| g | 145.0247 | 1.1860 | 219.7376 |
| h | 145.0469 | 1.1860 | 200.7676 |
| i | 144.7431 | 1.1840 | 217.9189 |
| j | 145.0385 | 1.1860 | 233.4200 |
| Average | | | 218.195 |

Chart 1: Predicted Tensile Modulus for Control and Experimental Polymers



**Multiaxial and
Time Dependent Response
of
Rigid Polymers**

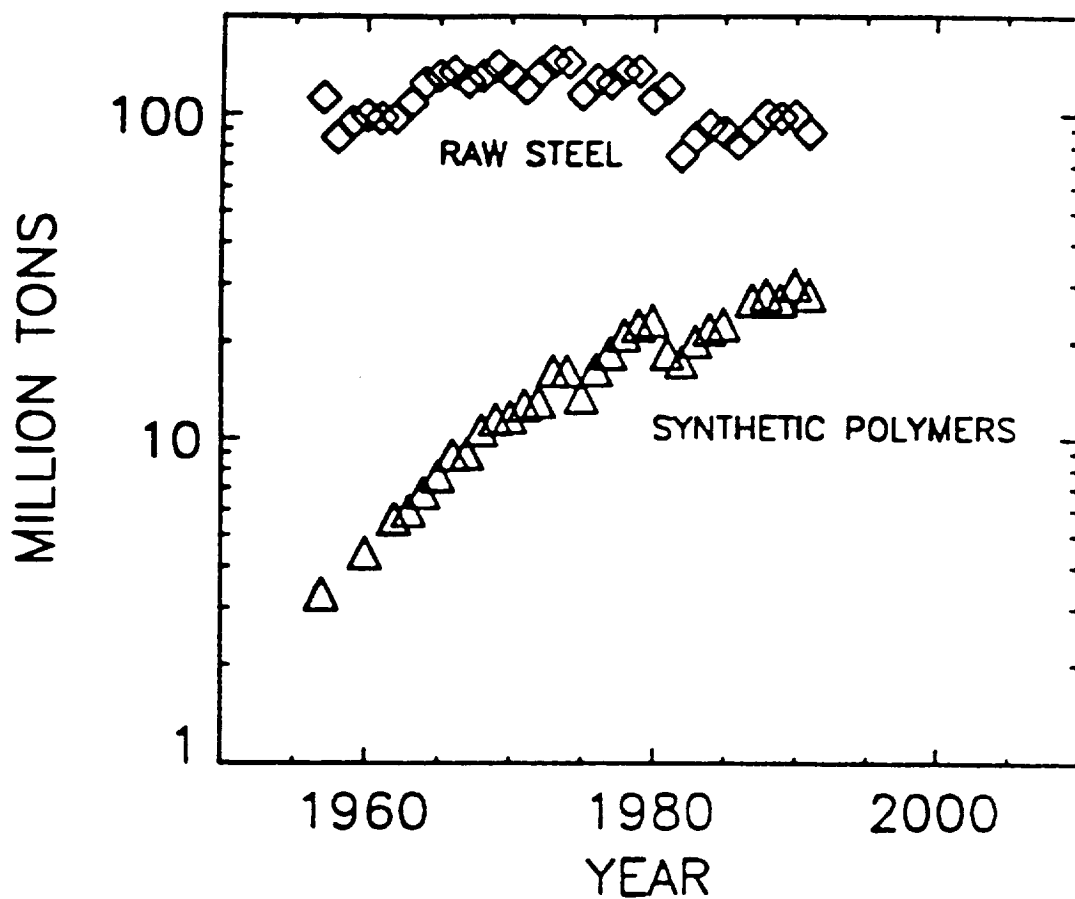
W.G. Knauss

**California Institute of Technology
Pasadena, California**

Supported in part by the Materials Branch at NASA, Langley

The following are the captions for the figures.

1. Title
2. Productions of steel and polymer during last 35 years
3. Long range objectives
4. Constitutive Interest
5. Range of Issues
6. Yield-like behavior
7. Experimental Approaches to Physical Characterization
8. A free volume based constitutive model
9. Comparison of material responses between the free volume model prediction and experimental observation for uniaxial loading and unloading
10. Comparison of material responses between the free volume model prediction and experimental observations for relaxation at different small strain levels
11. Simulation of yield-like behavior from the free volume model
12. Free volume model for large uniaxial strains (polymide)
13. Creep compliance at different stress levels measured by Govaert
14. Master creep compliance curve shifted by Govaert. The master curve is not smooth
15. Comparison of the master creep compliance curve shifted by Govaert and that shifted by H. Lu and W.G. Knauss
16. Zoom of a portion of the master curve "shifted" by Govaert. (The curves do not really fit a shift.)
17. The shift factors measured by Govaert
18. The shift factors measured by H. Lu and W.G. Knauss
19. Displacement measurement resolution of the digital image correlation
20. Shear relaxation modulus measured at 0.2% of shear strain
21. Shear relaxation master curve
22. Young's relaxation modulus measured at 0.2% of axial strain
23. Young's relaxation master curve
24. Shift factors for the Young's and shear modulus master curves
25. Superposed tension or compression increases the shear creep rate under pure torsion well below glass transition (results at 22°C)
26. Superposed tension or compression increases the shear creep rate under pure torsion well below glass transition (results at 50°C)
27. Shear stress also controls the shear creep rate - shear creep compliances at different stress levels
28. Superposed tension or compression increases the shear creep rate under pure torsion well below glass transition (results at 80°C)
29. Under the same torque, a superposed tension increases the torsional creep rate while a superposed compression decreases it in the vicinity of the glass transition (results at 100°C)
30. Under the same torque, a superposed tension increases the torsional creep rate while a superposed compression decreases it in the vicinity of the glass transition (results at 110°C)
31. Under the same shear stress, a superposed tension has a much higher creep rate than a superposed compression, indicating free volume plays a major role in the glassy state
32. Some thoughts on an "activation" rate model incorporating the coupling of volumetric deformation and shear deformation



Annual Tonnage of Steel and Polymer produced
during the last 35 years

Long range objectives:

**Establish general polymer
constitutive behavior and**

Analytically model this behavior

Constitutive behavior must incorporate

**Linear and nonlinear viscoelasticity at
small and moderate strains
(yield-like response)**

**Nonlinear viscoelasticity at
very large strains**

**under arbitrary load histories, including
ageing and "recovery"**

Environmental factors:

**Temperature dependence, including the
range around the glass transition**

Solvent influence, including water

Constitutive Interest

Physical properties descriptions involve the whole spectrum of size scales and approaches to analytical formulation

- 1) Model material behavior for engineering analyses:
Application oriented and global view**

- 2) Structure - property relationships:
Molecular science orientation and microscopic view**

Physics-based Observation and Issues

Yield-like behavior is physically different from yielding in metals. In thermoplastic solids it is not necessarily associated with crazing

"Yield-like behavior" occurs at small strains ($\mathcal{E}_{\text{uniaxial}} < 5\%$)

"Yield-deformations" are usually recoverable under thermal control

Yield-like behavior does not involve large scale molecular re-orientation and organization unless it is associated with very localized shear bands

Molecular orientation occurs in uniaxial deformation at extension ratios exceeding 100%

Very small changes in volume ($>0.1\%$) have a disproportionate effect on the time-temperature trade-off

To what degree is yield-like behavior the result of local material instability augmented or controlled by small volume changes?

To what degree is yield-like response controlled or influenced by organized molecular rearrangement

Range of Issues

- 1) Time and rate dependence**
- 2) Nonlinear response**
- 3) Thermorheology**
- 4) Glass transition behavior**
- 5) Physical ageing**

Experimental Approaches to Physical Characterization

Different stress state histories

There is a lot of data on pressure superposed on uniaxial tension in the literature

There is no data on biaxial stress states shear-plus-tension or shear-plus-compression

There is virtually no data on time-dependent bulk behavior

Constitutive Model (Emri and Knauss, 1981)

Free volume

$$f = f_o + A\alpha(t) * dT + \delta\epsilon_{kk}$$

Time-shift factor, ϕ

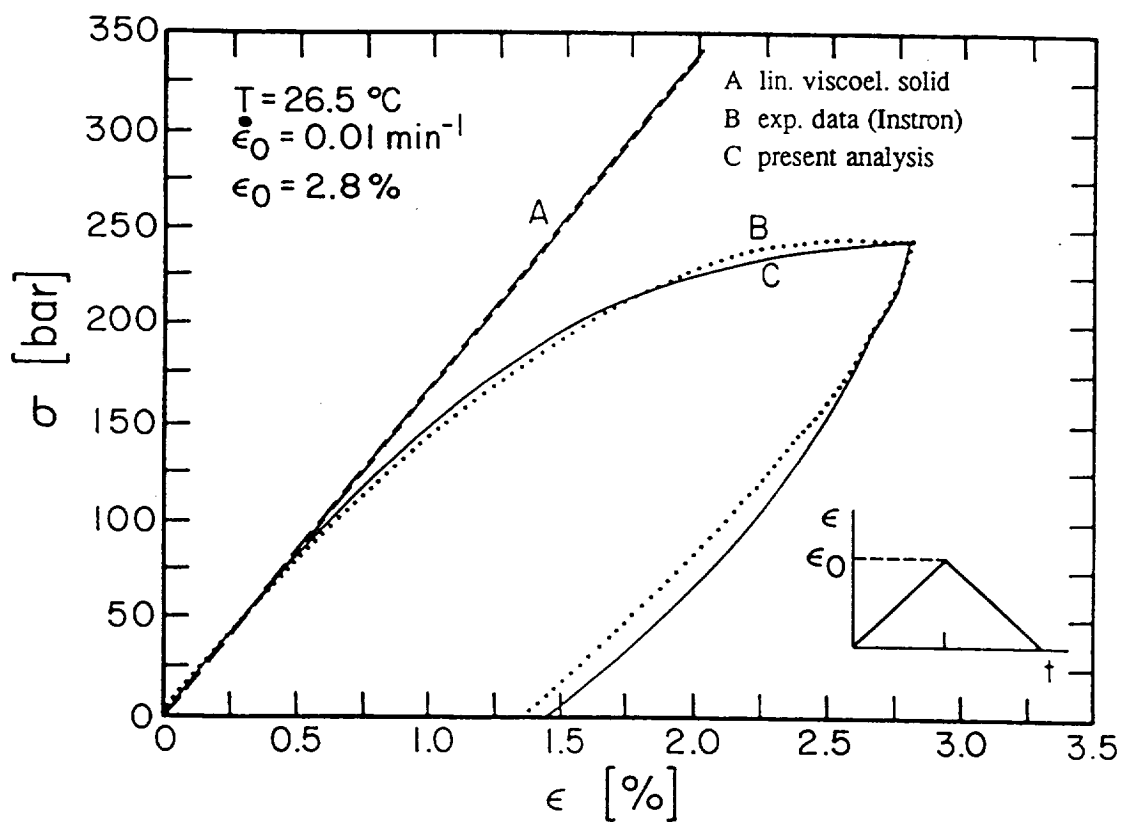
$$\log \phi = \frac{b}{2.303} \left(\frac{1}{f} - \frac{1}{f_o} \right)$$

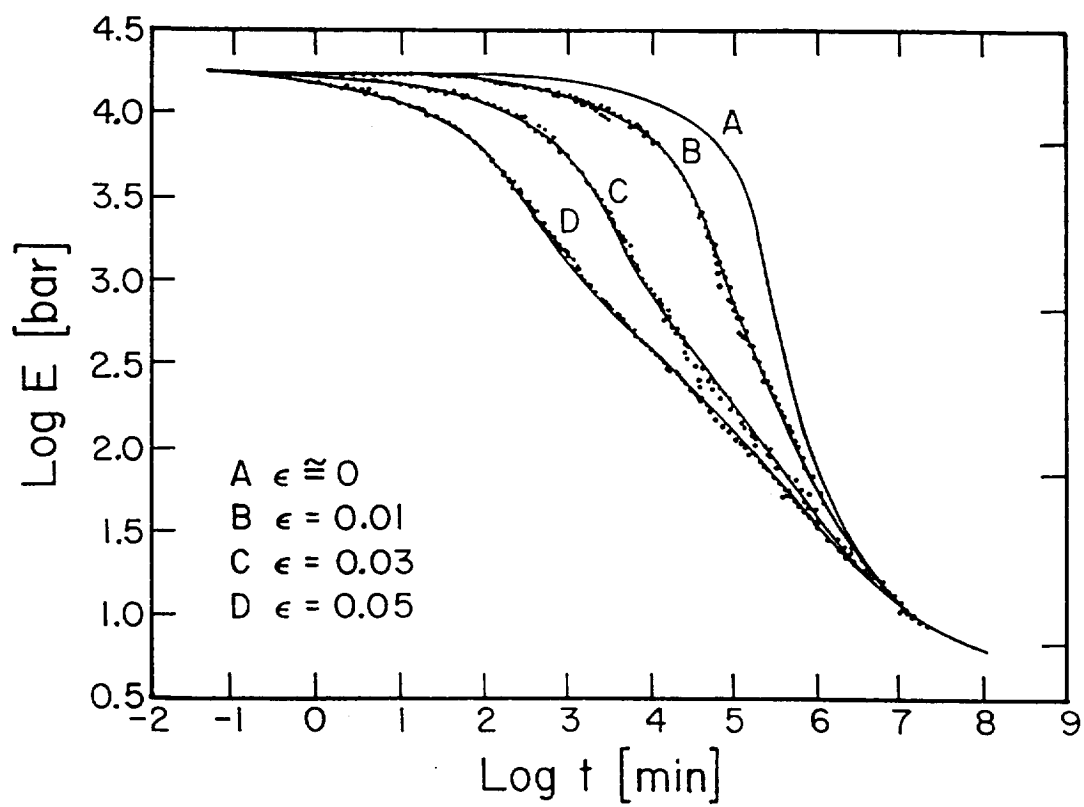
Internal (reduced) time

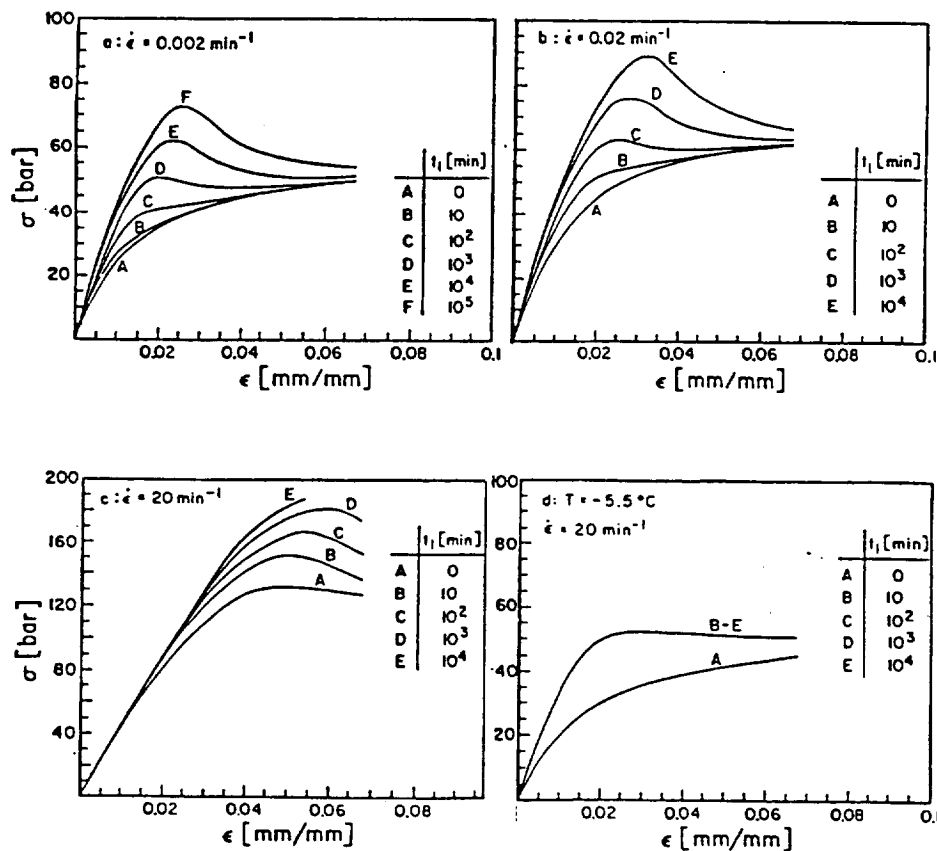
$$d\xi(t) = \frac{dt}{\phi(t)} \quad \text{or} \quad \xi(t) = \int_0^t \frac{du}{\phi[T(u), \theta(u)]}$$

Thermorheologically simple material

$$S_{ij} = 2 \int_{-\infty}^t \mu(\xi - \xi') \frac{\partial e_{ij}(t')}{\partial t'} dt'$$
$$\sigma_{kk} = 3 \int_{-\infty}^t K(\xi - \xi') \frac{\partial \epsilon_{kk}(t')}{\partial t'} dt'$$







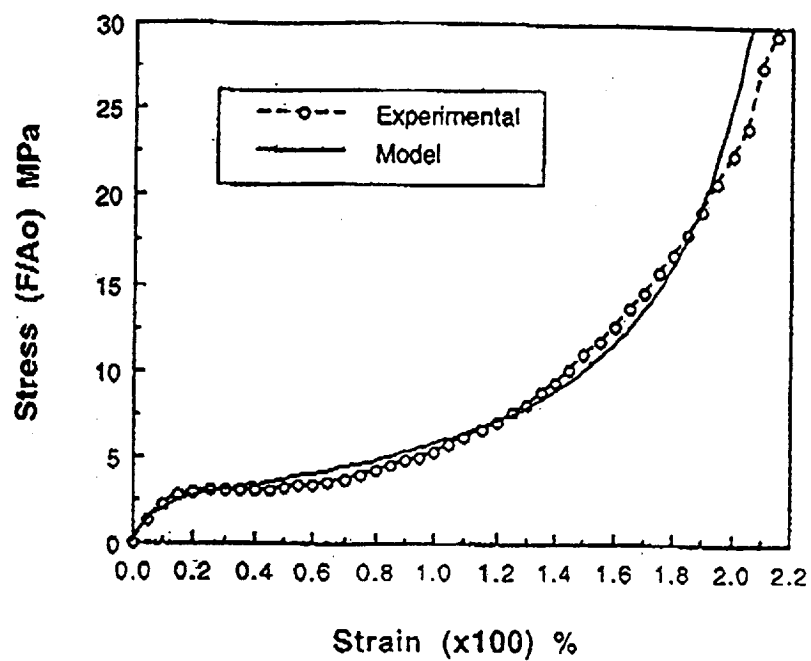


Figure 4.6 Three Term Model Tensile Response

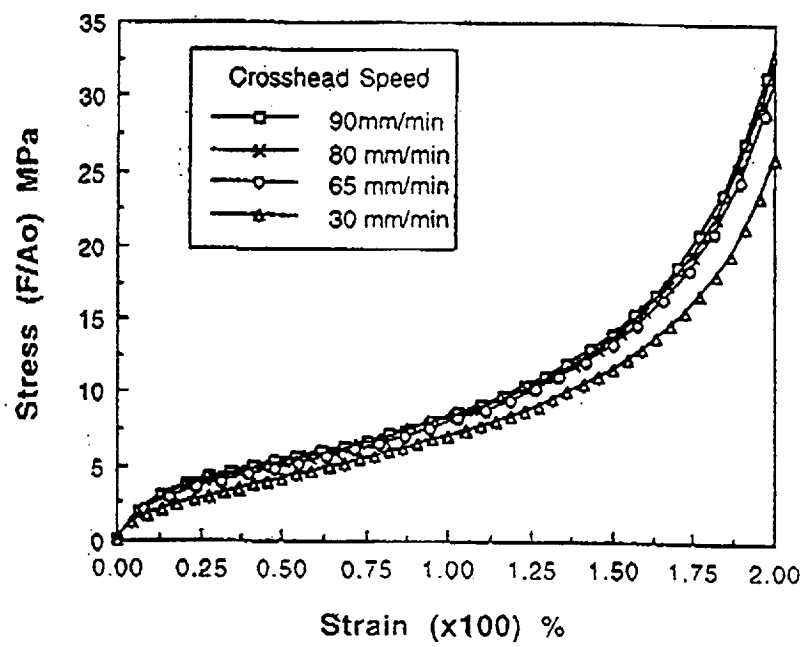
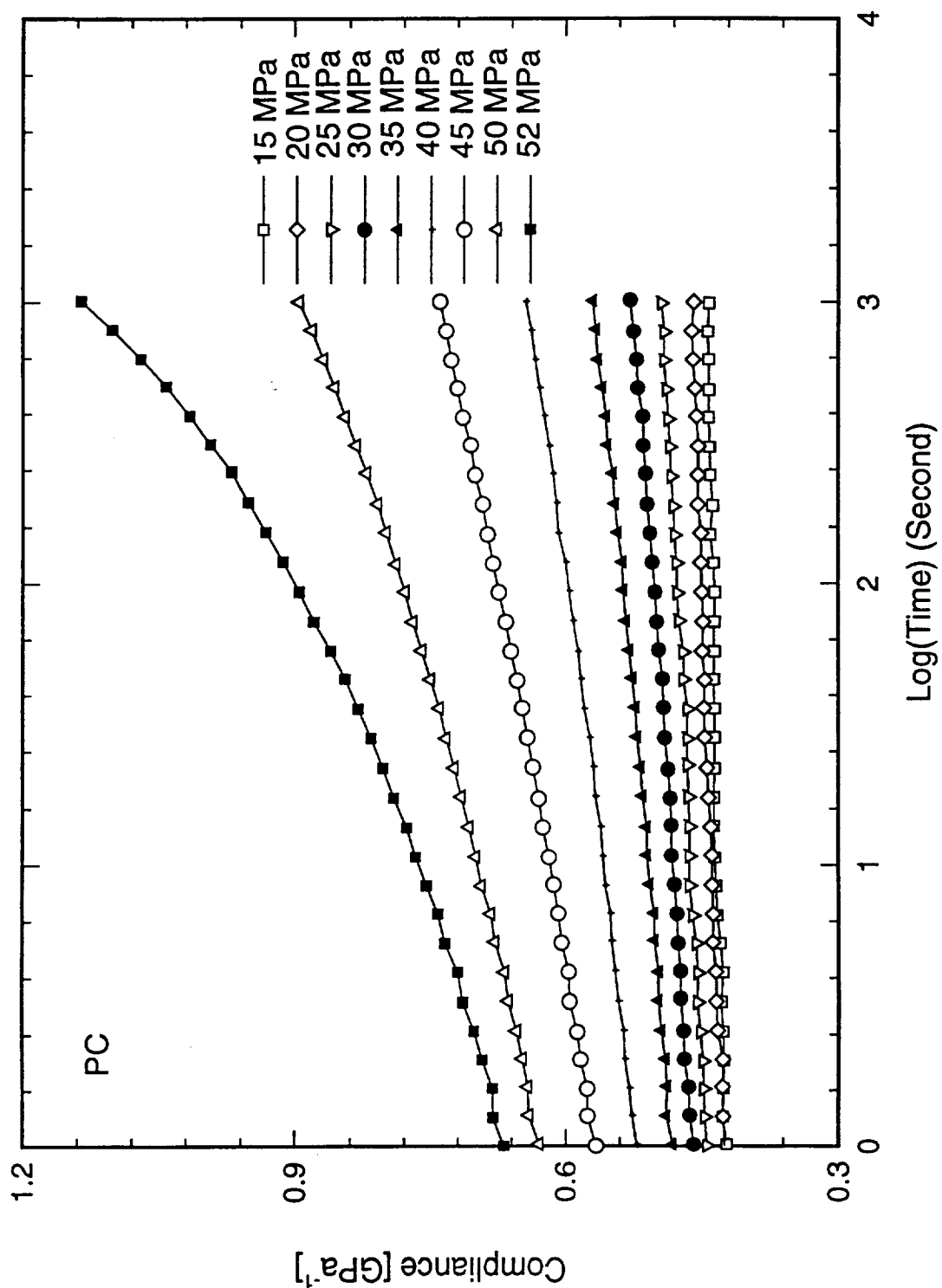
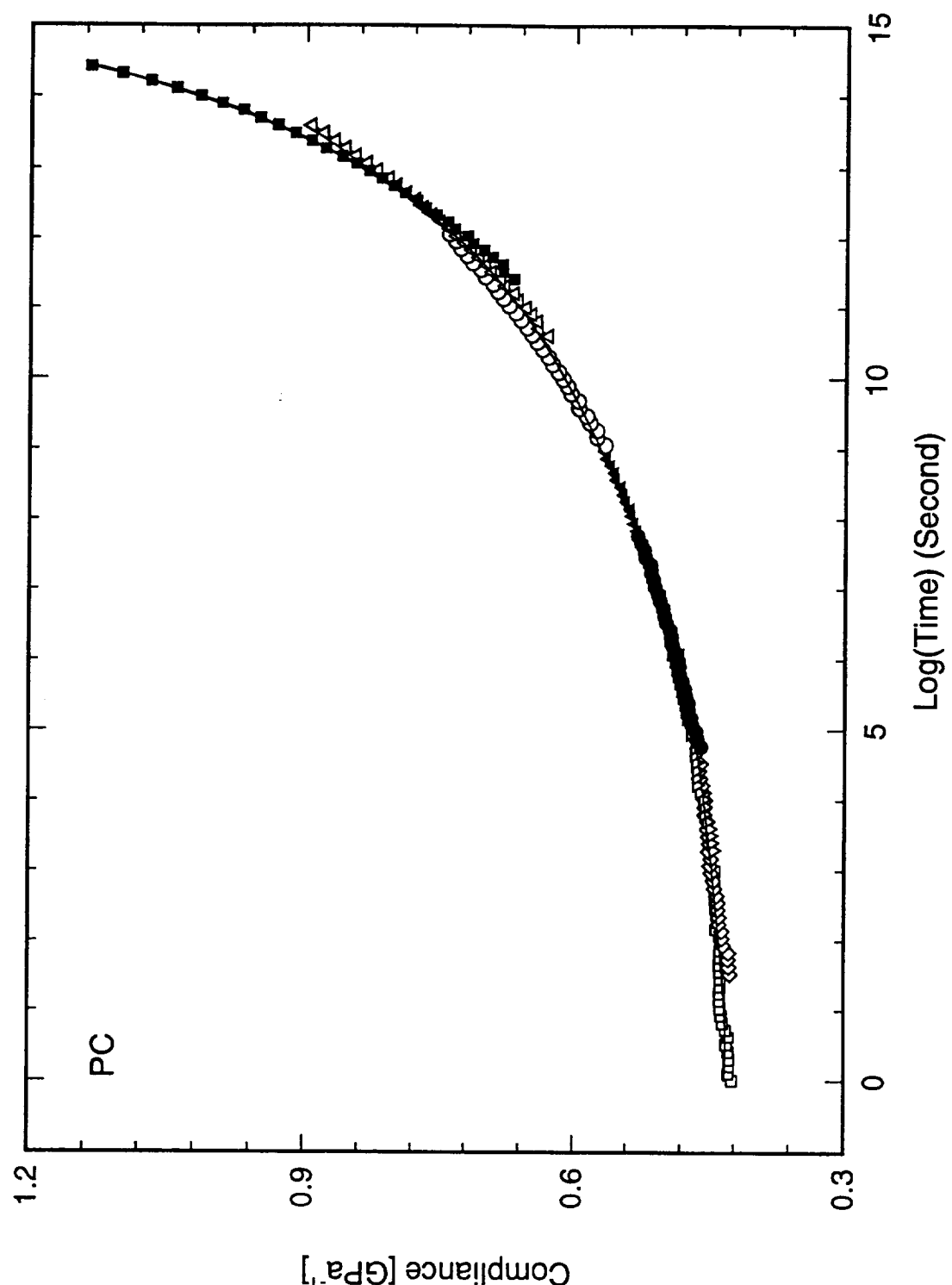
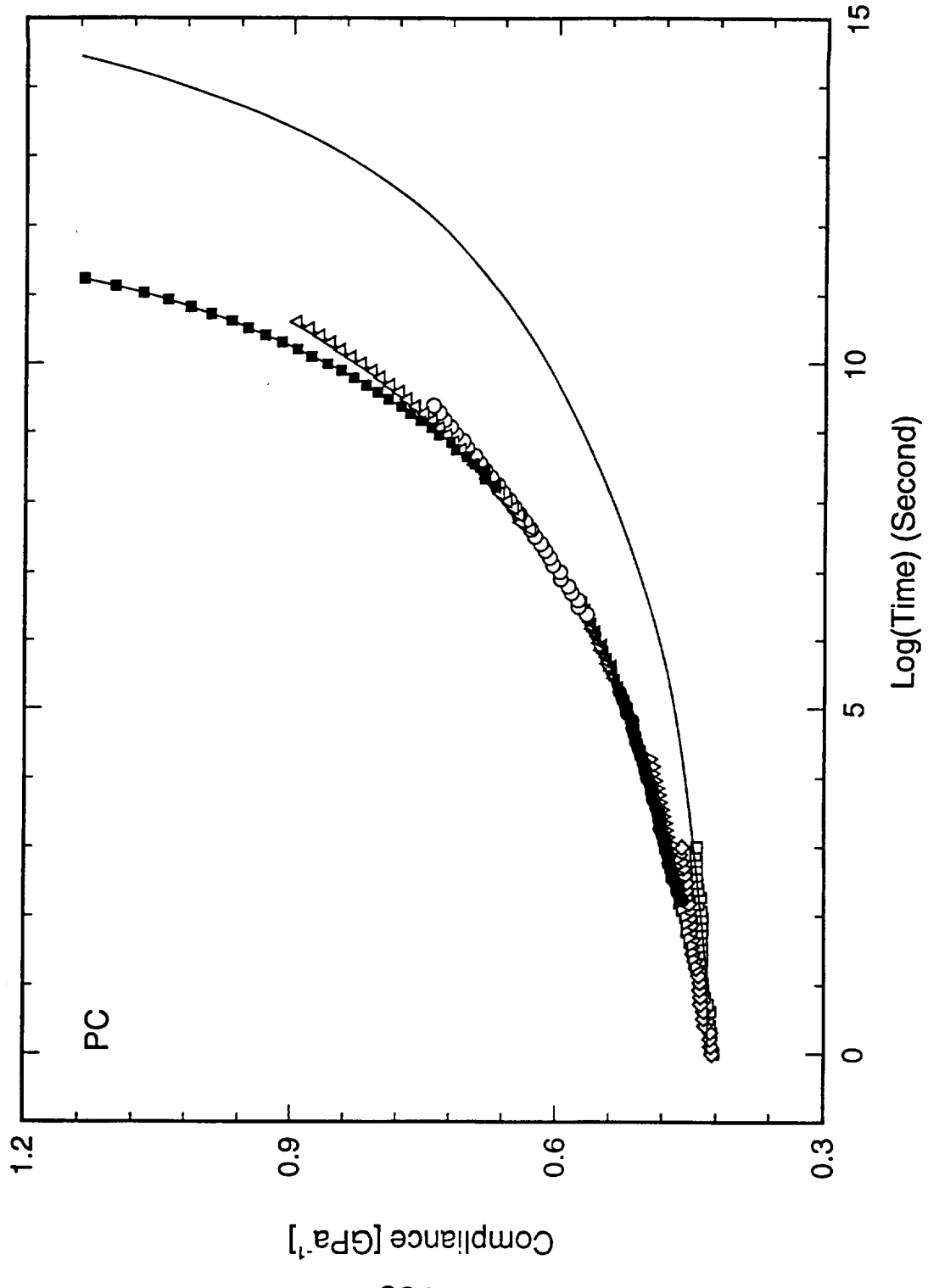


Figure 4.7 Model Results for Variation in Straining Rates on Specimen of 65mm Gauge Length.

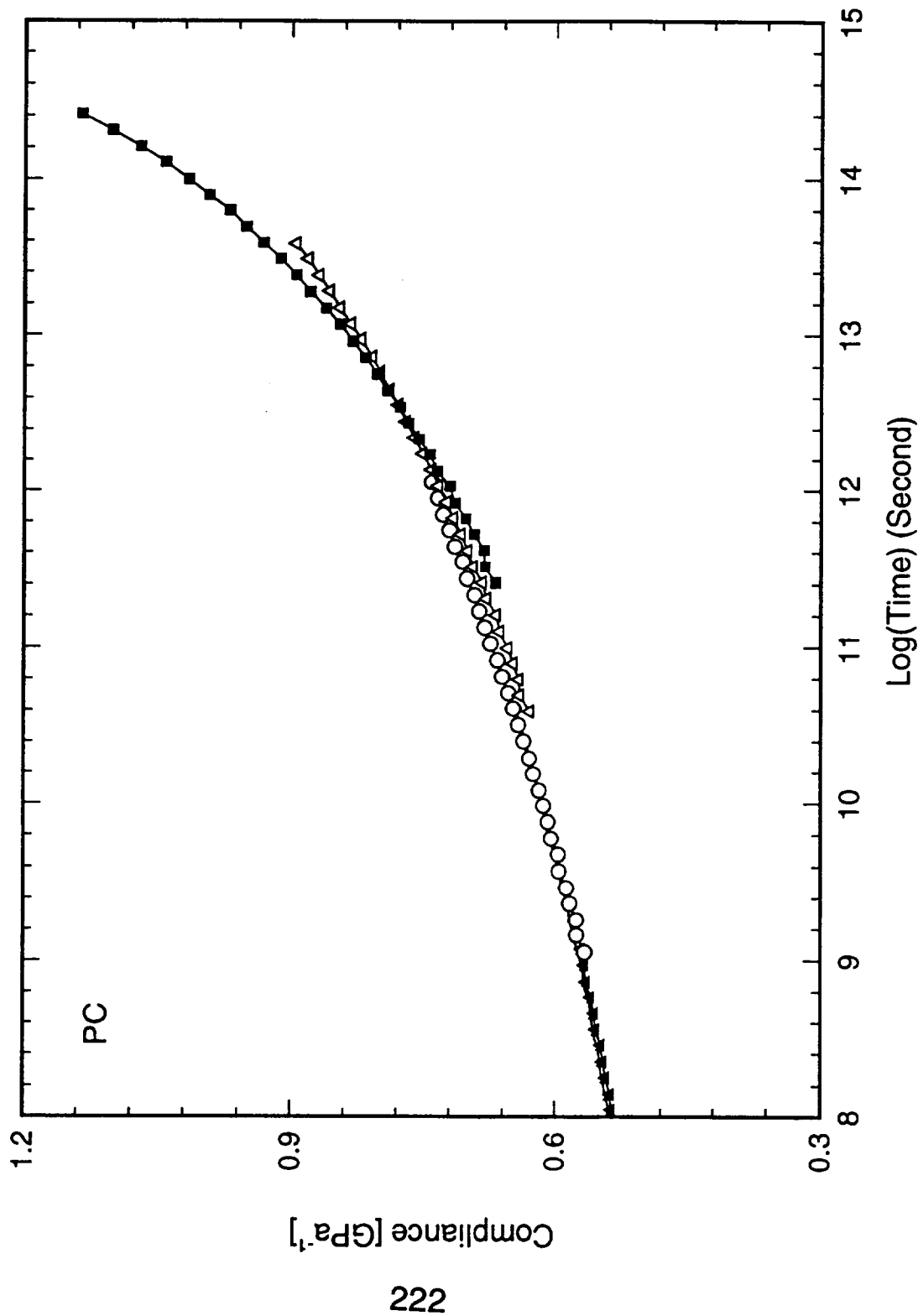


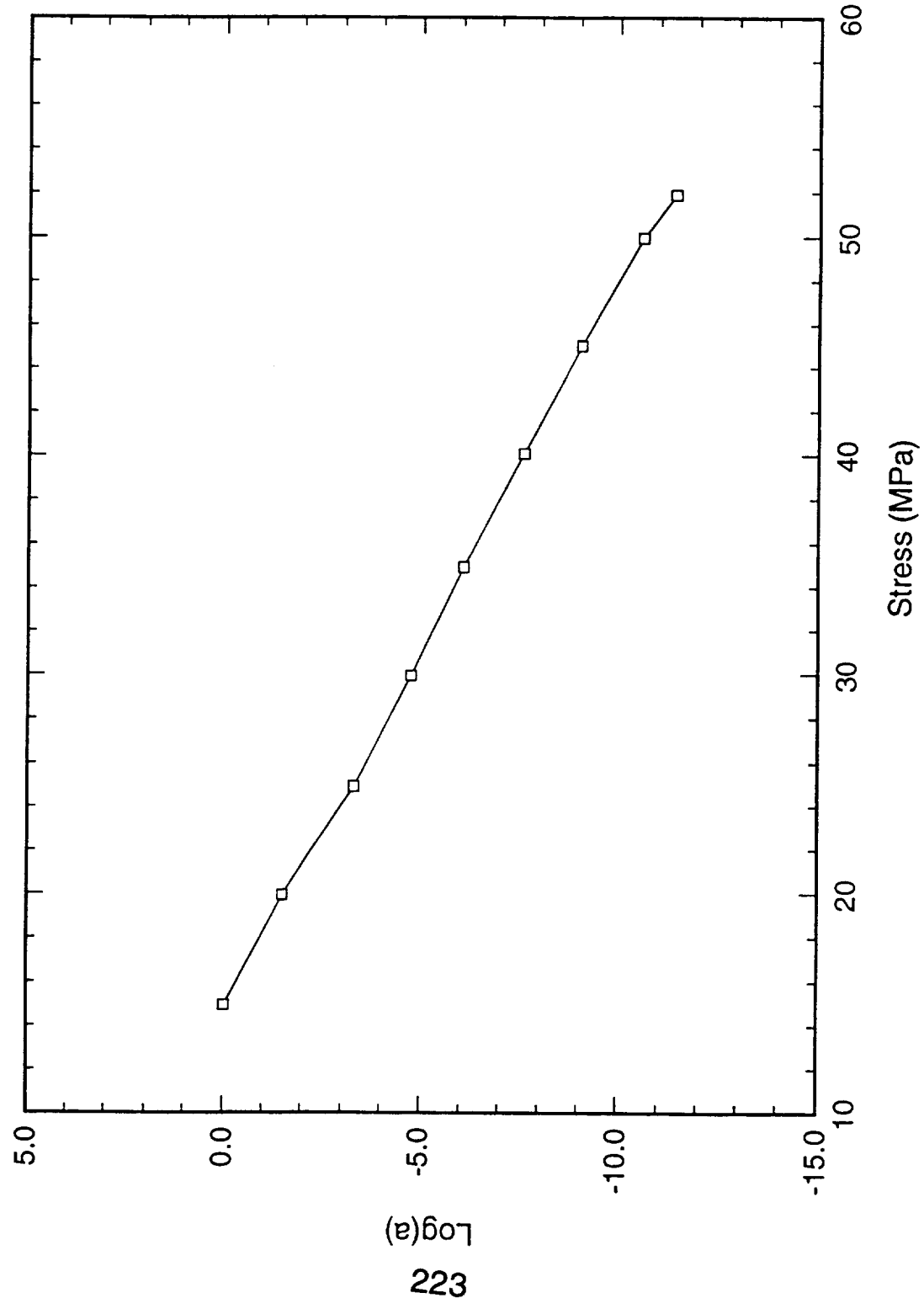


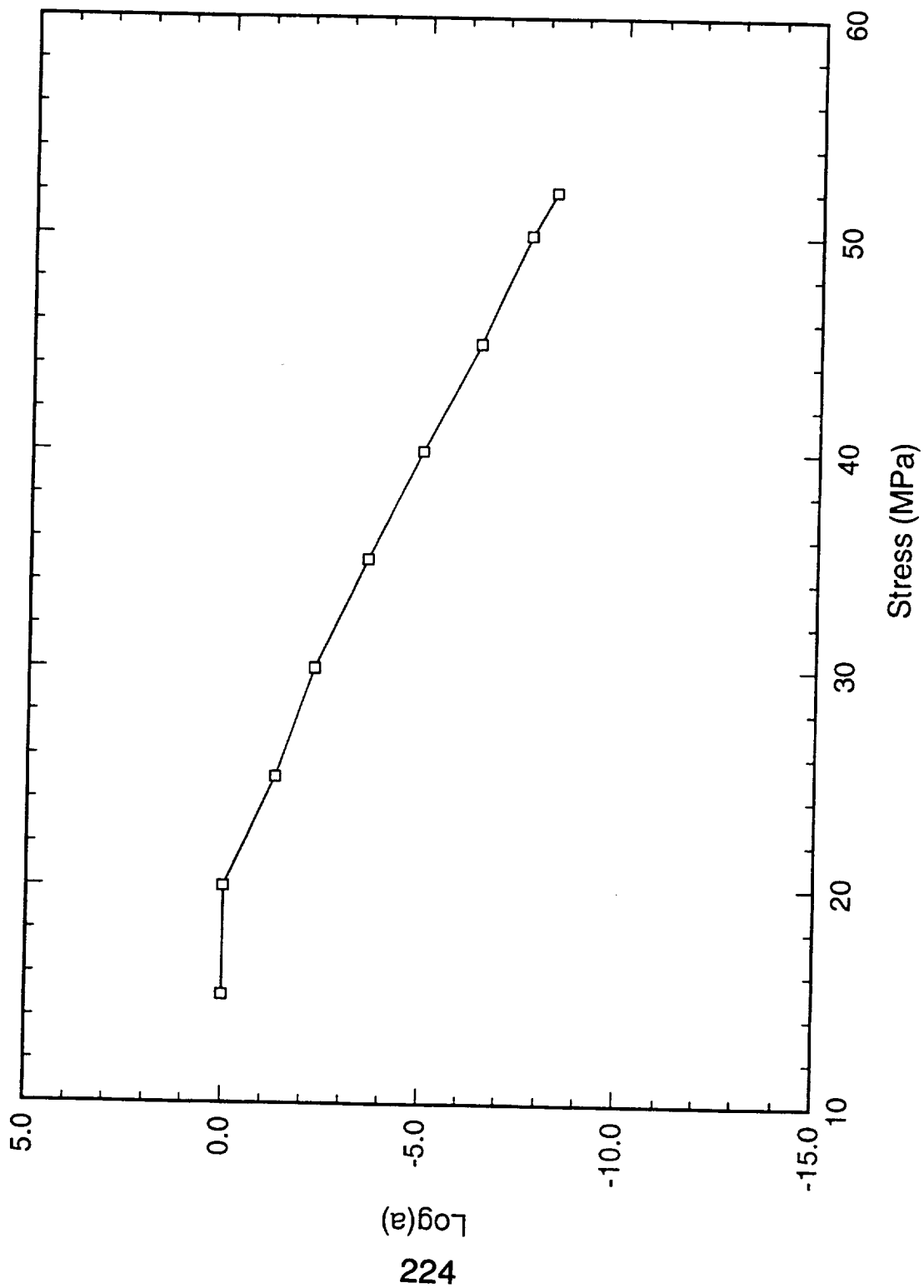
220



221







Displacement Resolution of the Method

A typical field of view is 25 mm (1 inch)

Pixel size: 50 microns/pixel side

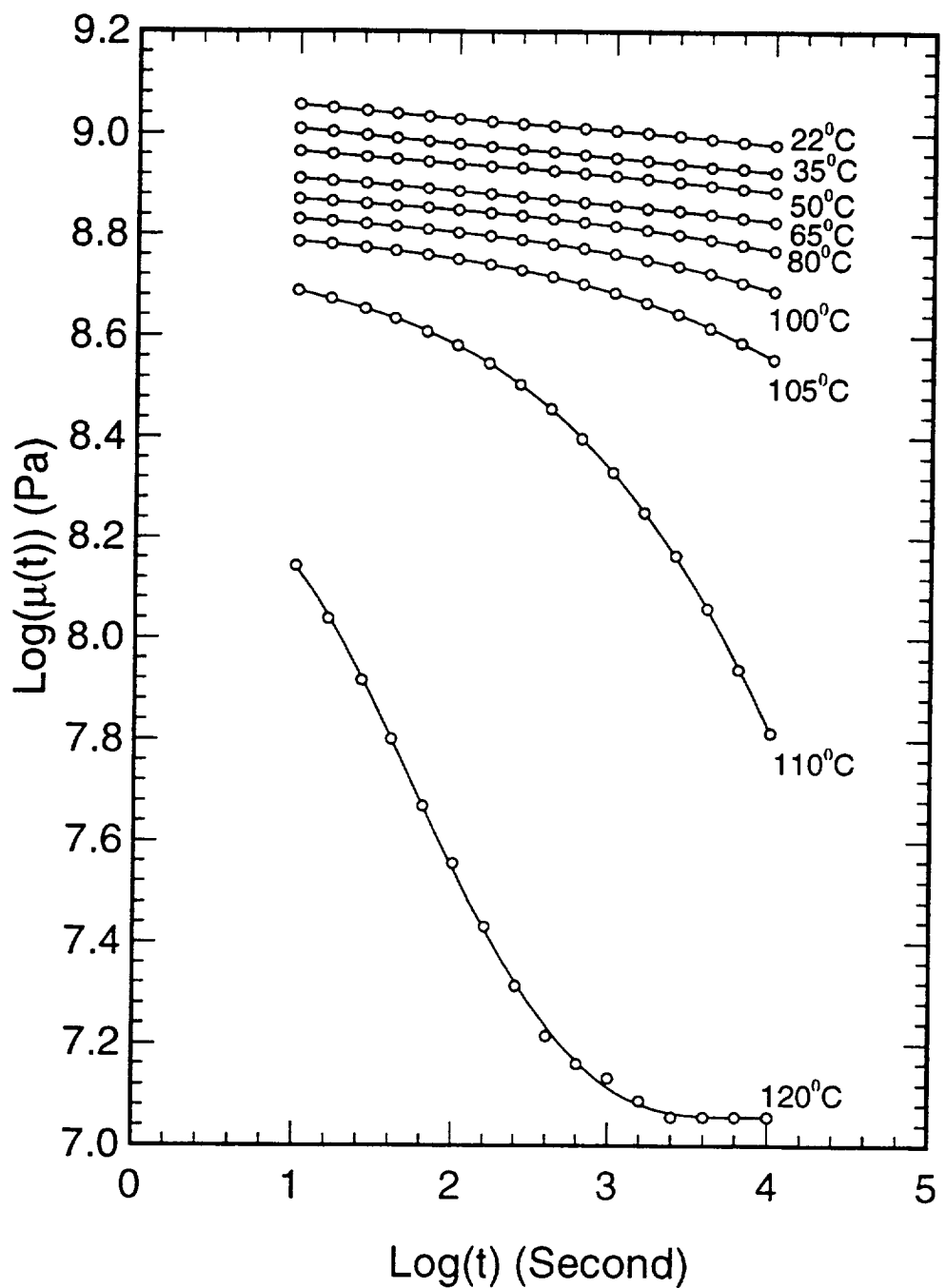
The resolution limit for displacements is 3 microns

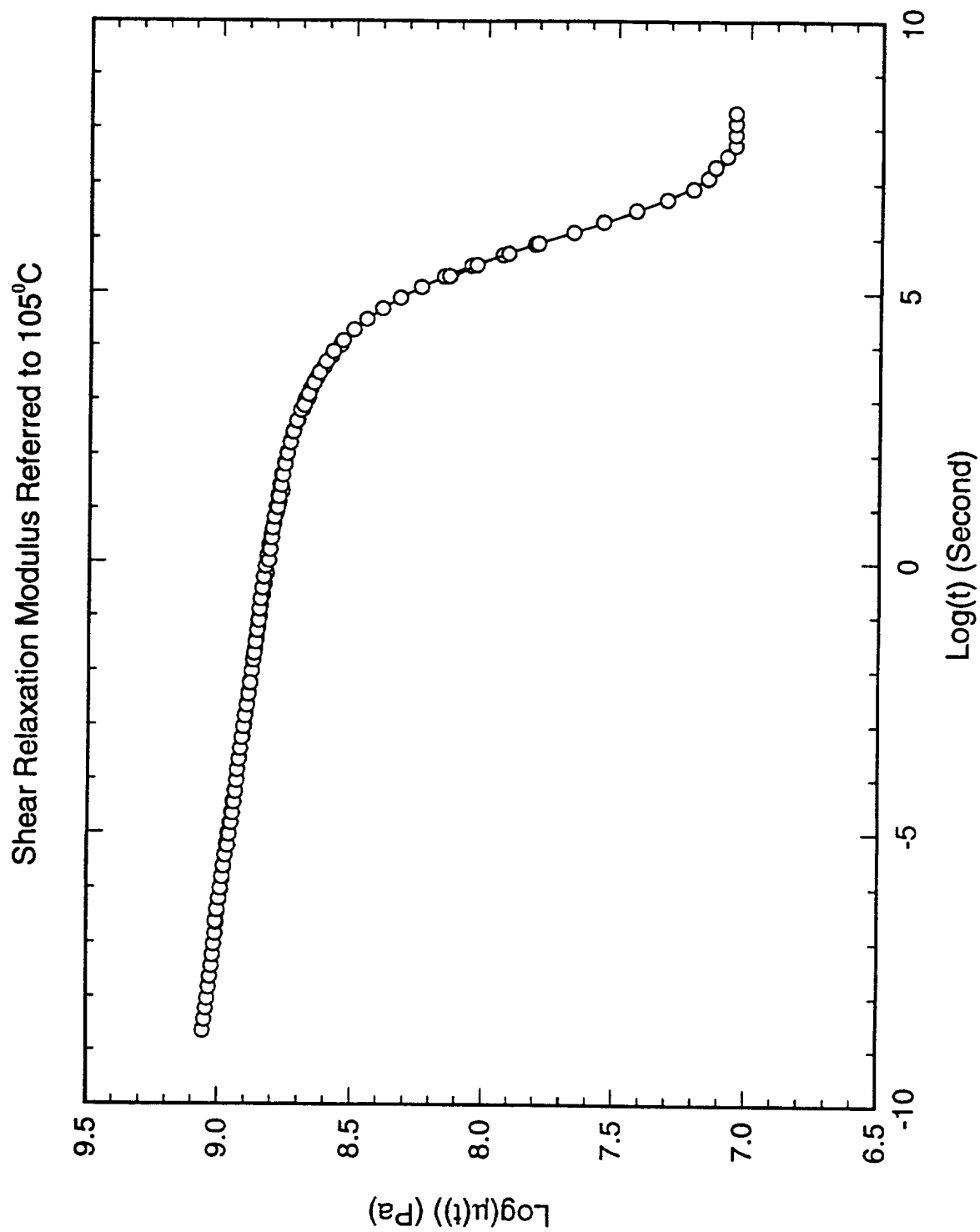
This translates into resolution of

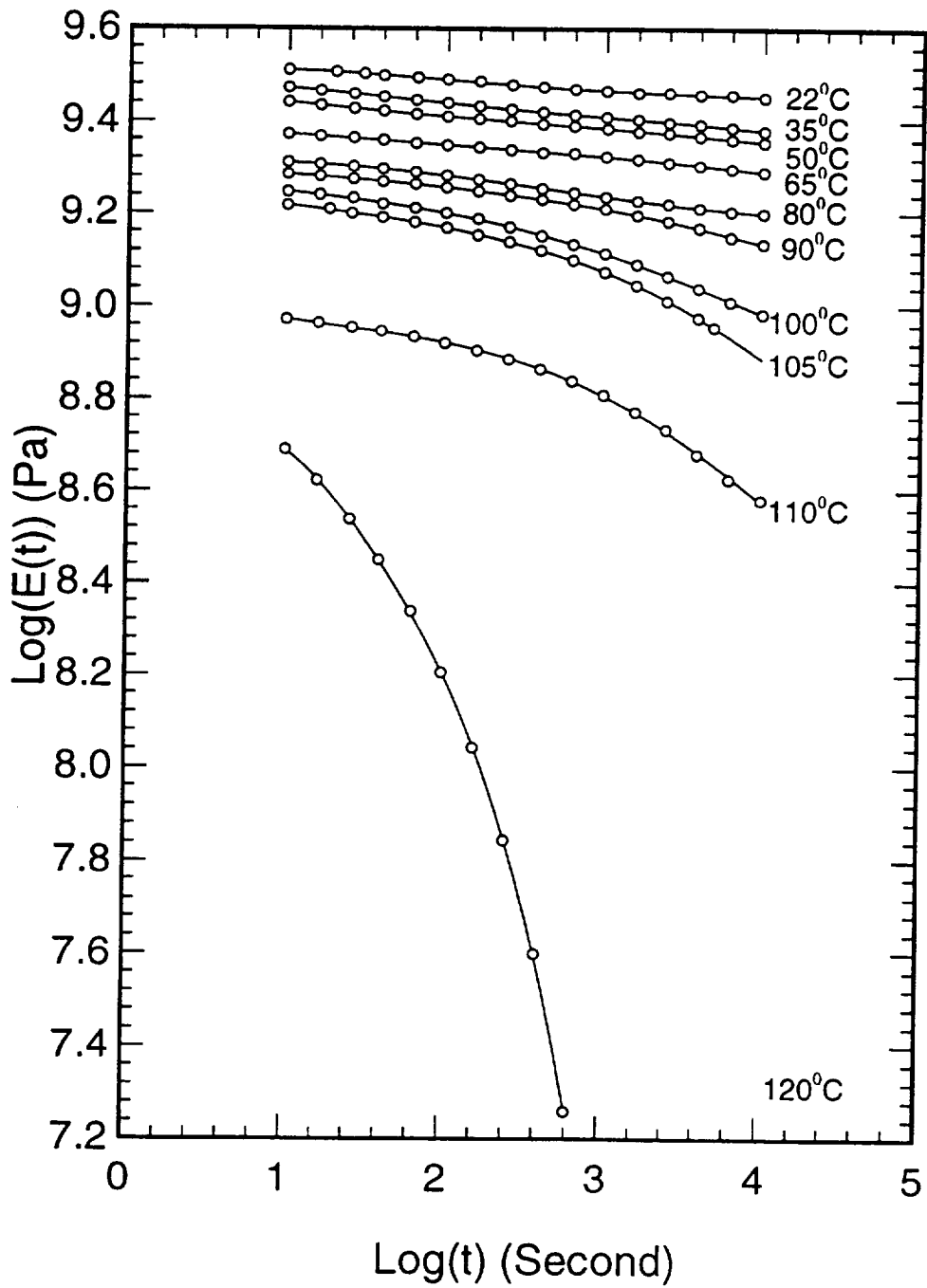
normal strains of 0.05%

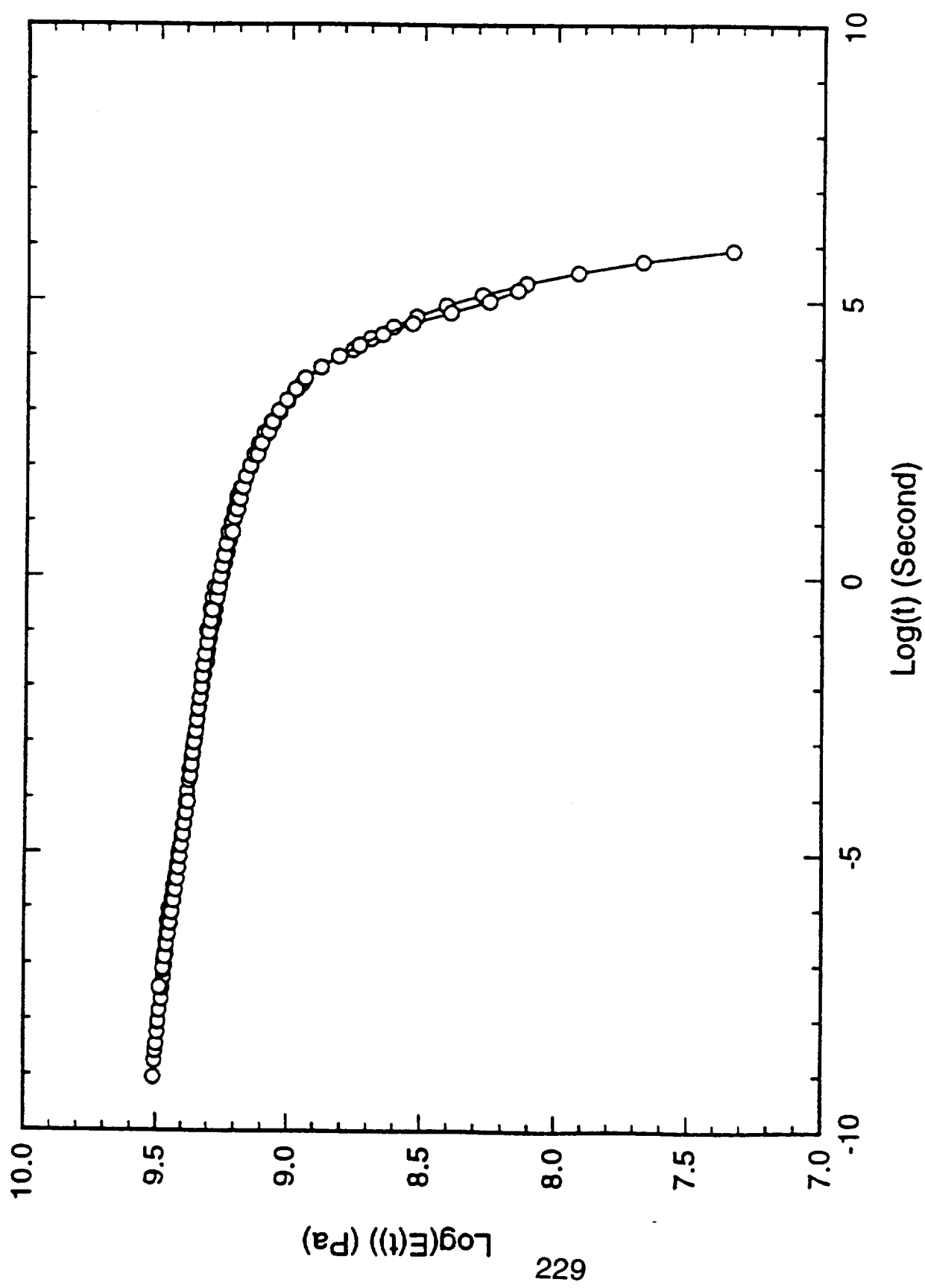
shear strains of 0.05%

circumferential strains of 0.08%



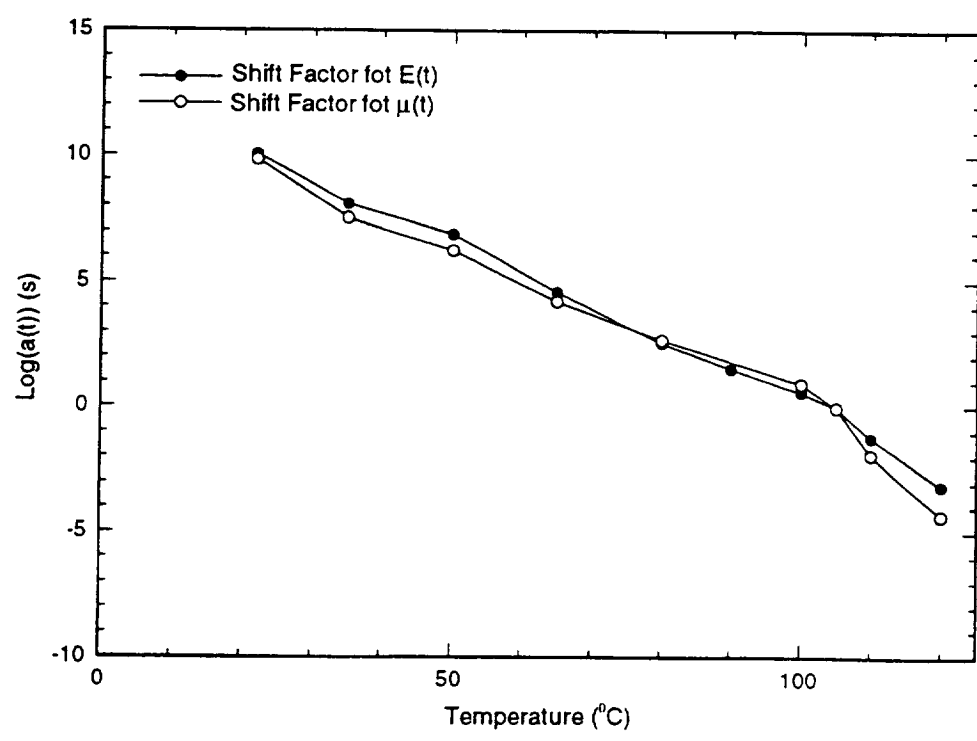




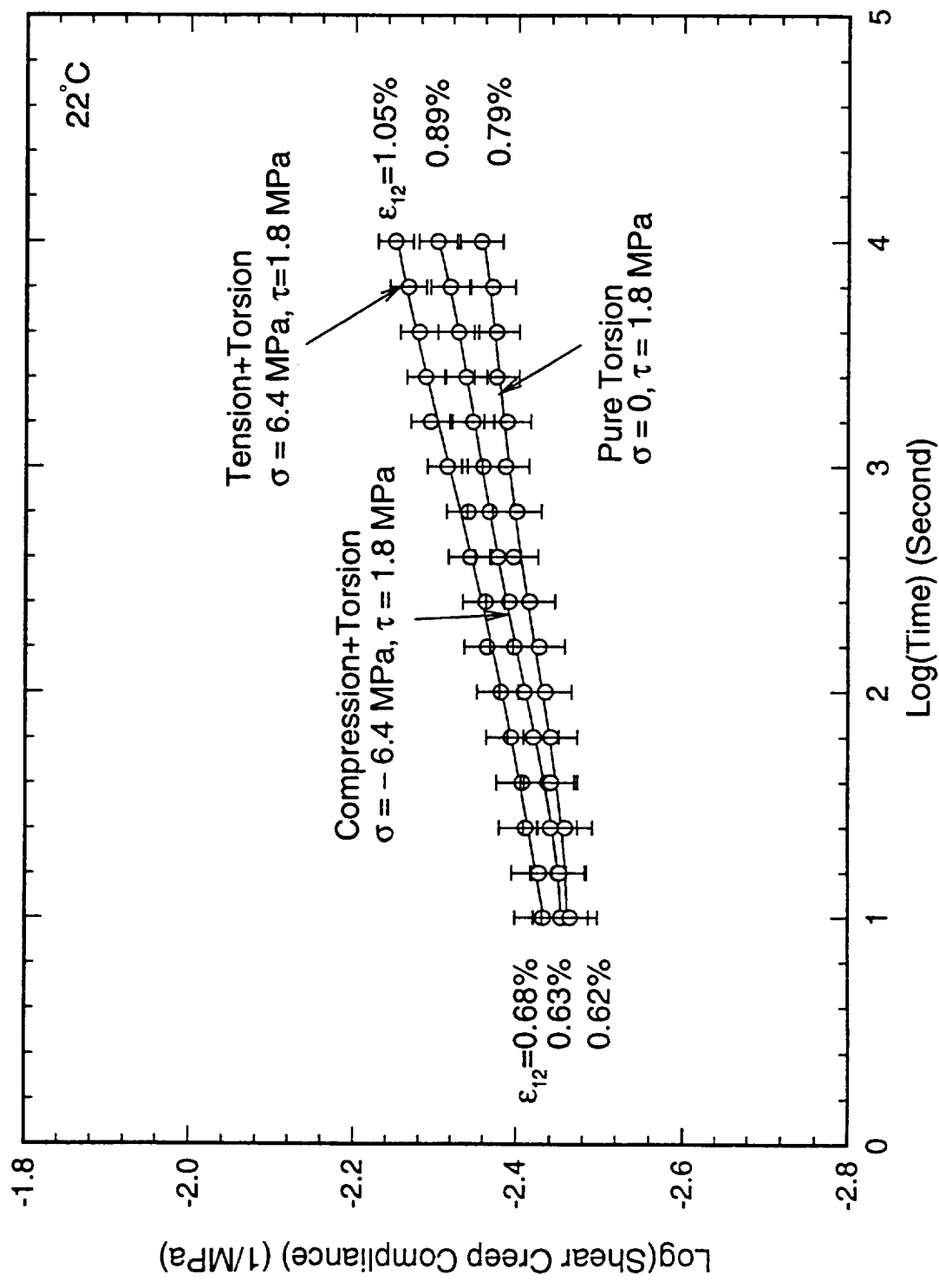


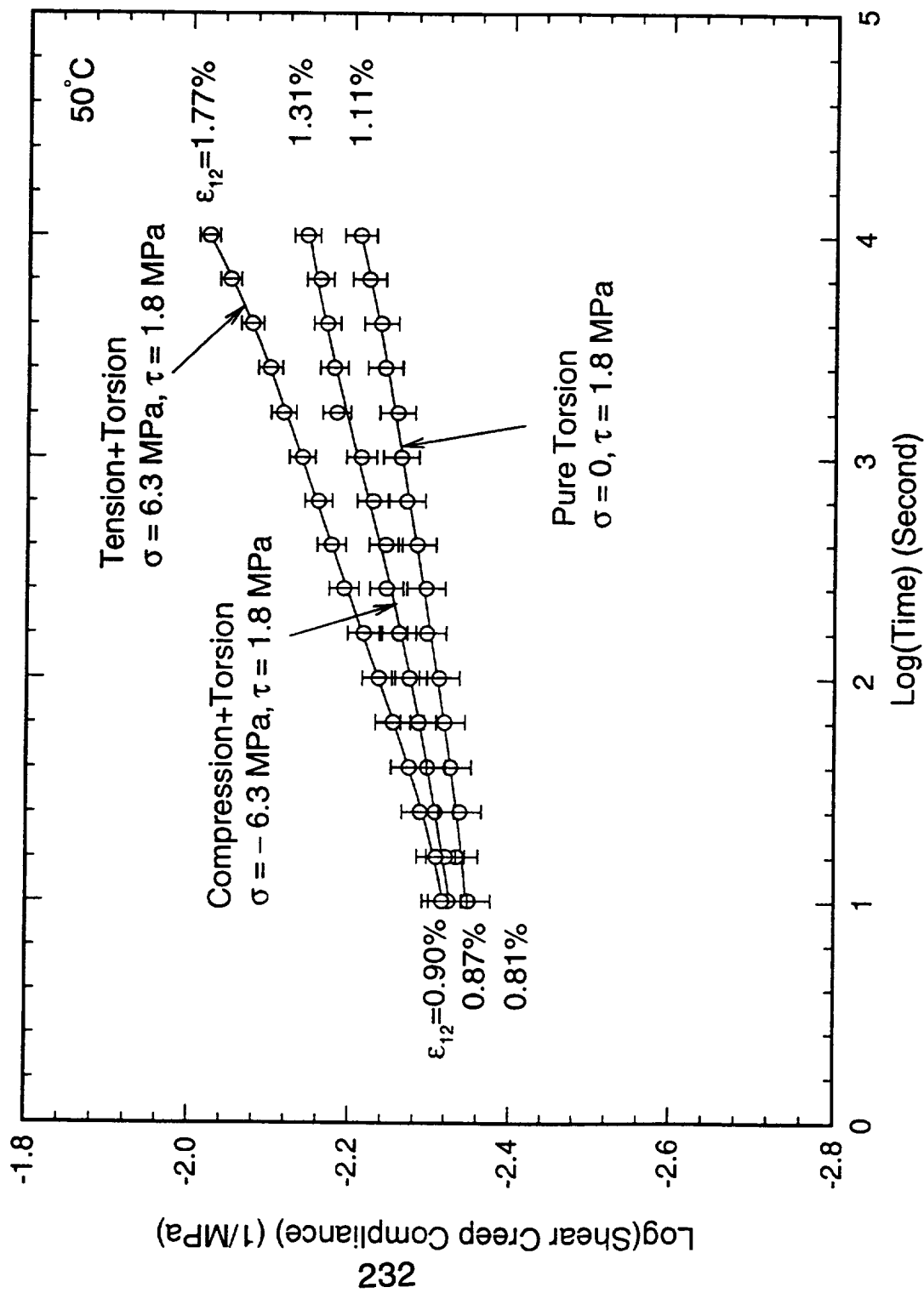
Log($E(t)$) (Pa)

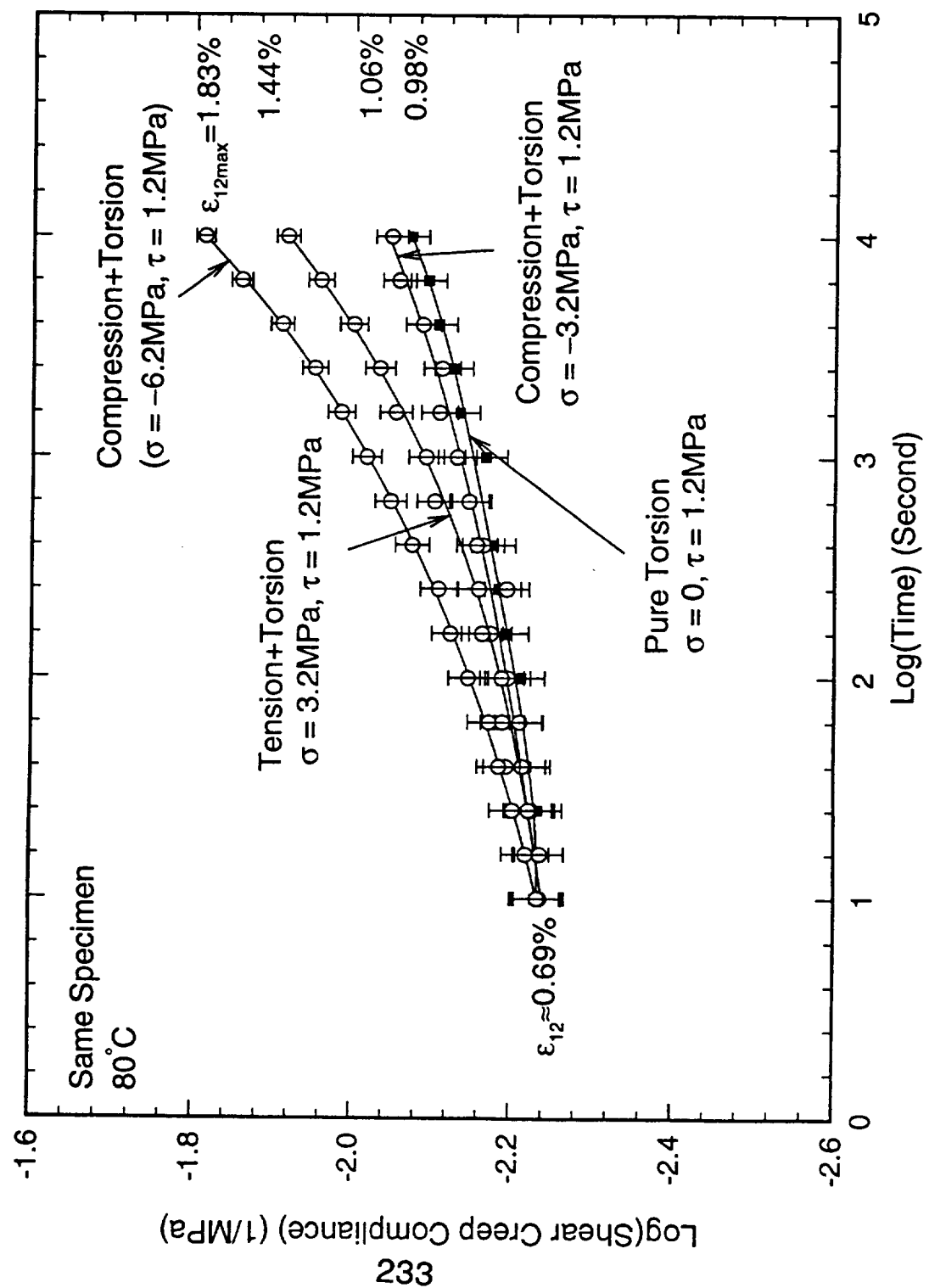
229

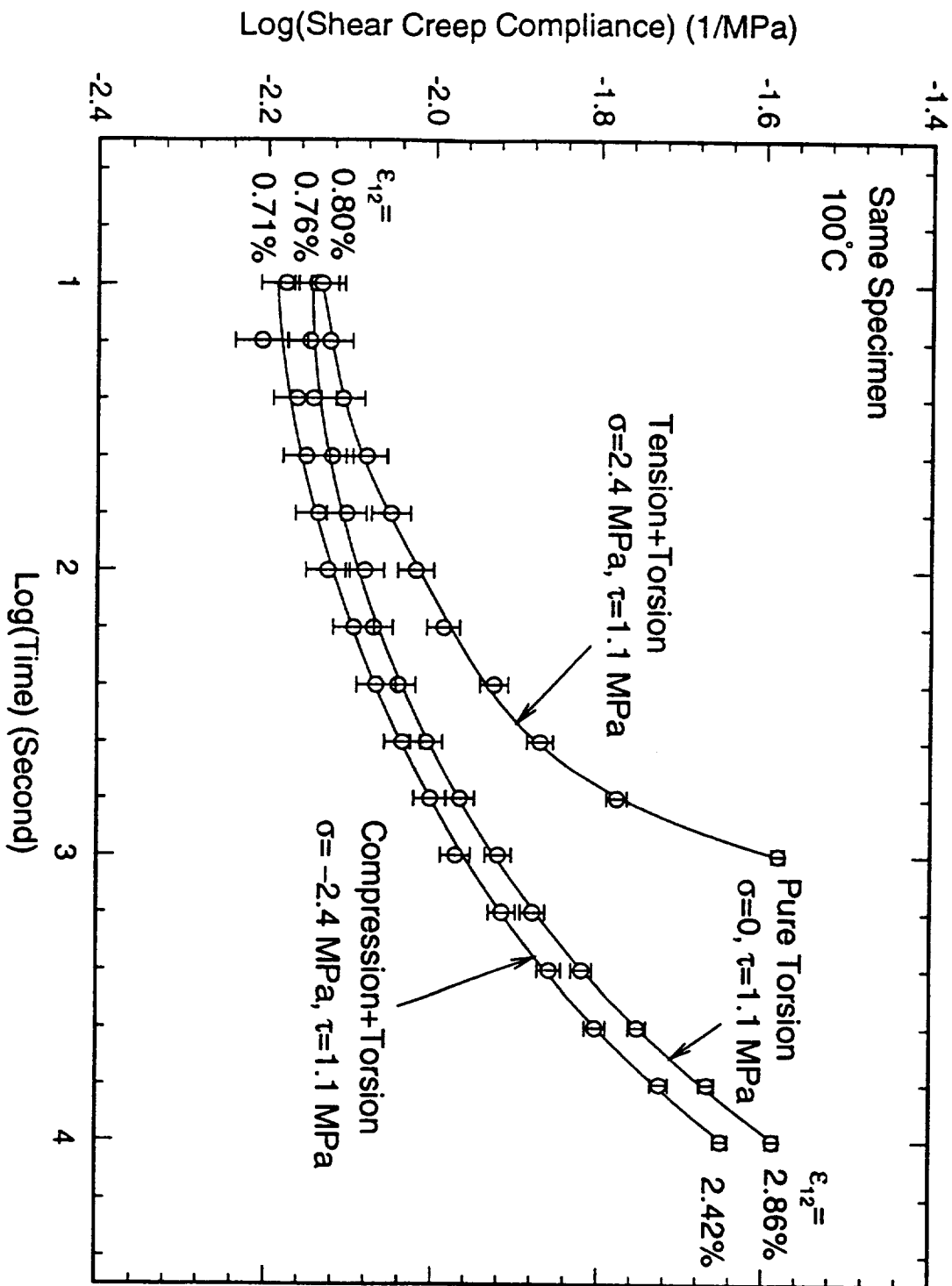


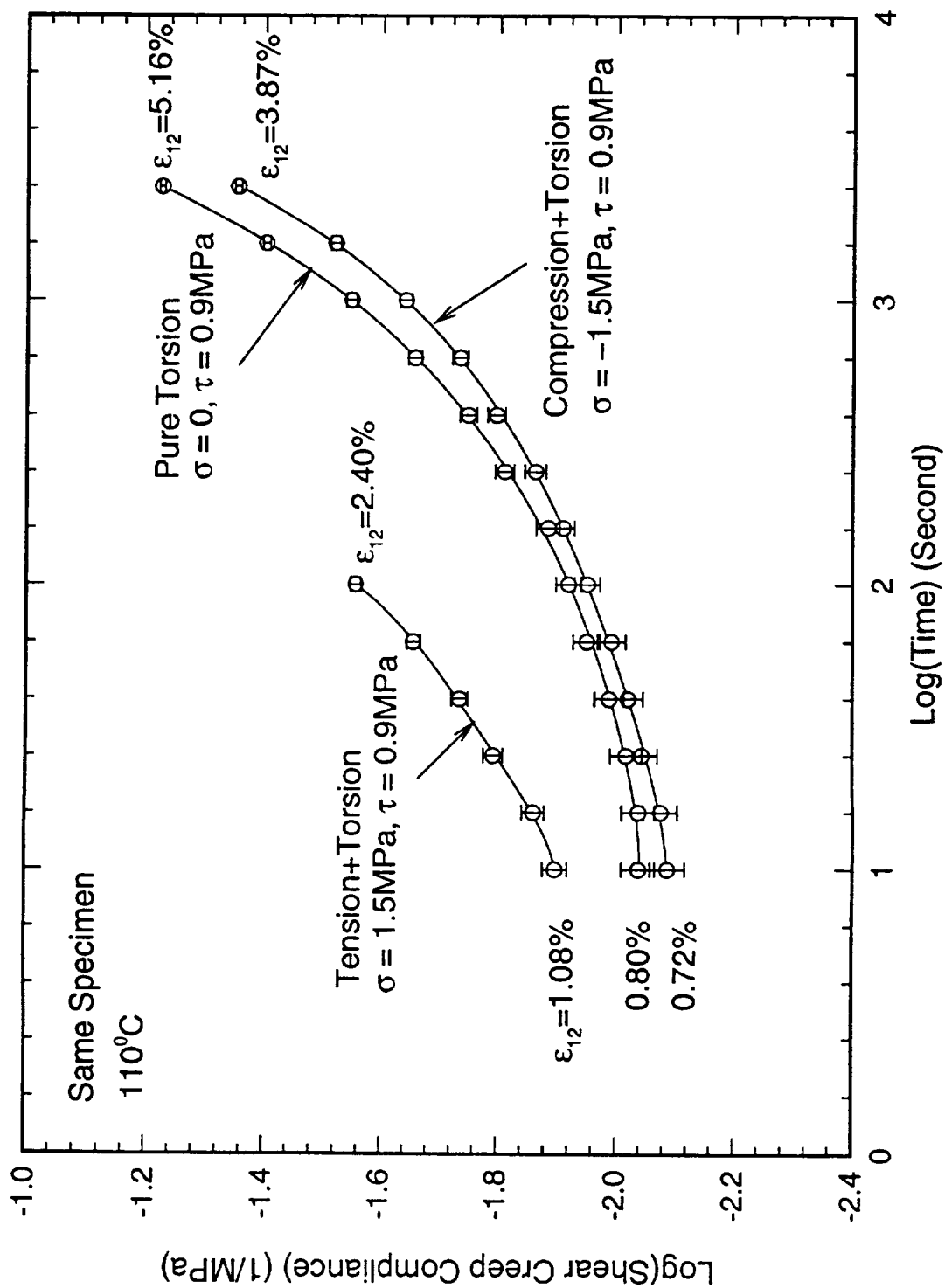
230

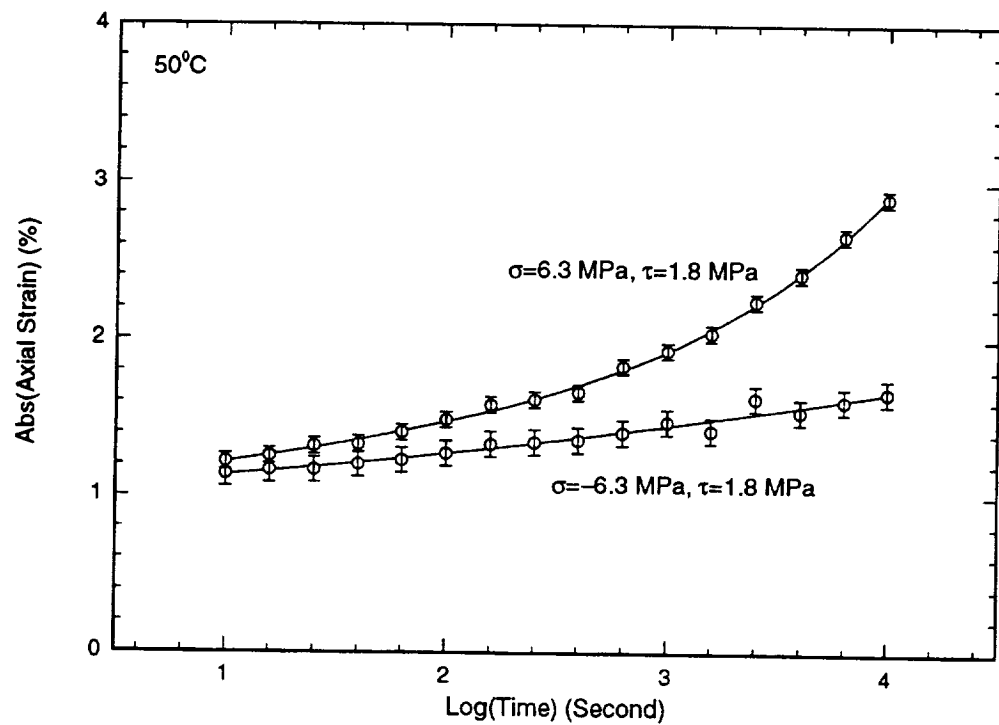












Coupling Between
Volumetric and Shear Response
as Based on an "Activation" Rate Model

$$\dot{\gamma}_n^{\pm}(\tau, \sigma_{ii}) = \pm A_n \exp\left\{-\frac{1}{RT} [\Delta E_n^* - |v_n^*(\tau)| - \sigma_{ii} \Omega_n]\right\}$$

Pool size

$$\dot{\gamma}_n^{\pm}(\tau, \sigma) = \pm A_n \exp\left\{-\frac{\Delta E_n^* - \sigma_{ii} \Omega_n}{RT}\right\} \cdot \exp\left\{\frac{|v_n^*(\tau) \cdot \tau|}{RT}\right\}$$

$$\dot{\gamma}_n = \dot{\gamma}_n^+ + \dot{\gamma}_n^- \doteq 2A_n \exp\left\{-\frac{\Delta E_n^* - \sigma_{ii} \Omega_n}{RT}\right\} \cdot \sinh\left\{\frac{|v_n^*(\tau) \cdot \tau|}{RT}\right\}$$

**volumetric
contribution**

**shear
contribution**

$$\dot{\gamma} = \sum_n \dot{\gamma}_n \doteq \sum_n 2A_n \exp\left\{-\frac{\Delta E_n^* - \sigma_{ii} \Omega_n}{RT}\right\} \cdot \sinh\left\{\frac{|v_n^*(\tau) \cdot \tau|}{RT}\right\}$$

Static and Viscoelastic Testing/Modeling
of LARC SI

Tom Gates
January 4, 1996

Objectives:

- Measure effects of :
 - 1) Molecular Weight
 - 2) Cross-link Density
- on the static and viscoelastic properties of LARC SI
- Develop analytical models to account for these effects
 - Elastic constants
 - Elastic/plastic constants
 - Fracture/strength
 - Viscoelastic constants, physical aging

Static Properties: RT to (T_g - 15°C) Elastic

Youngs Modulus (E), CTE

Poissons ratio (ν)

$$\text{Shear Modulus} \left(G = \frac{E}{2(1+\nu)} \right)$$

Plastic

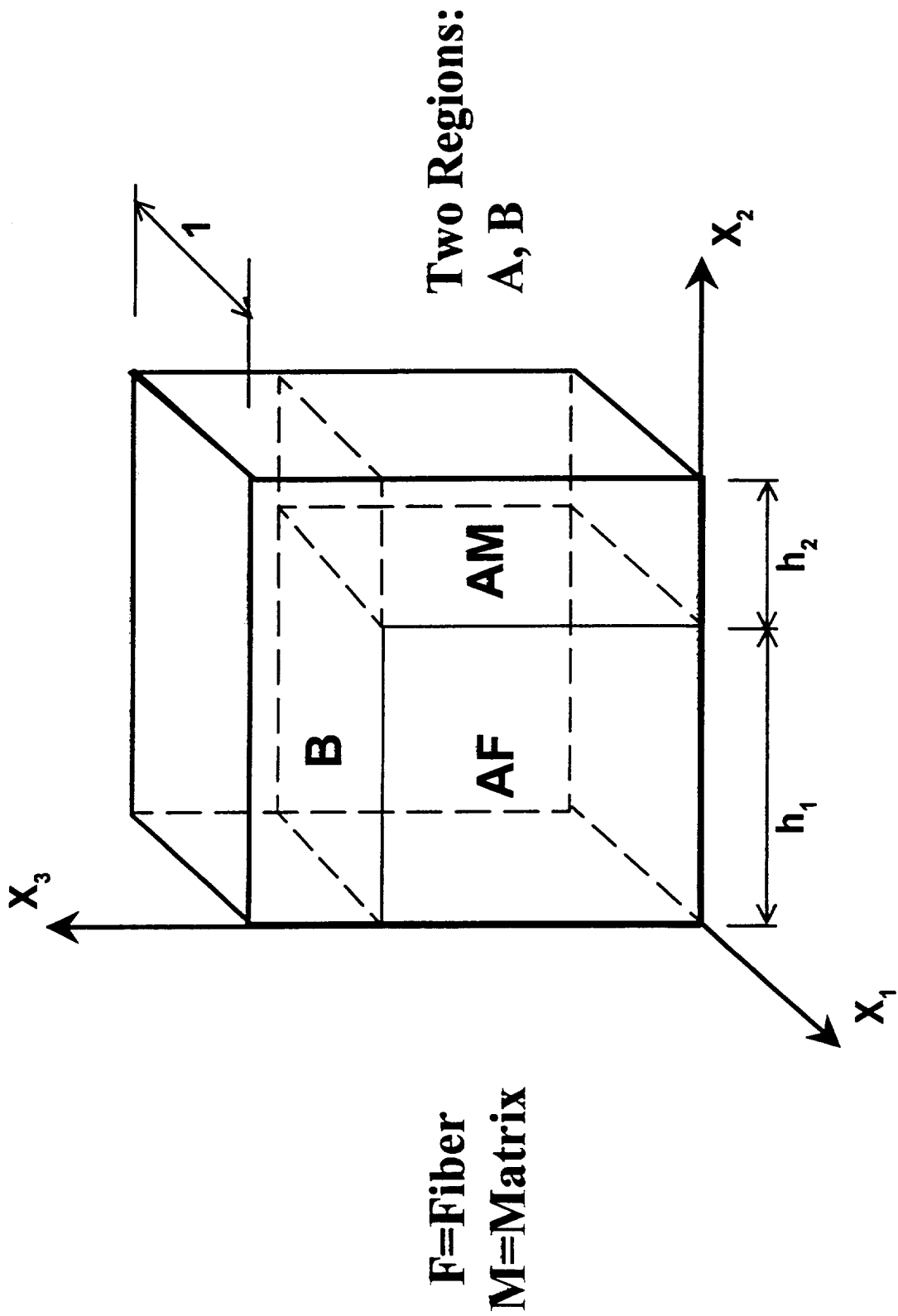
$$d\varepsilon_{ij}^p = d\lambda \frac{\partial J}{\partial \sigma_{ij}}$$

$$J = \frac{1}{3} [r_{11}(\sigma_{11})^2 + (\sigma_{22})^2 + 2r_{12}\sigma_{11}\sigma_{22} + 2r_{66}(\sigma_{12})^2]$$

$$\text{Effective Stress} \quad \bar{\sigma} = \sqrt{3J}$$

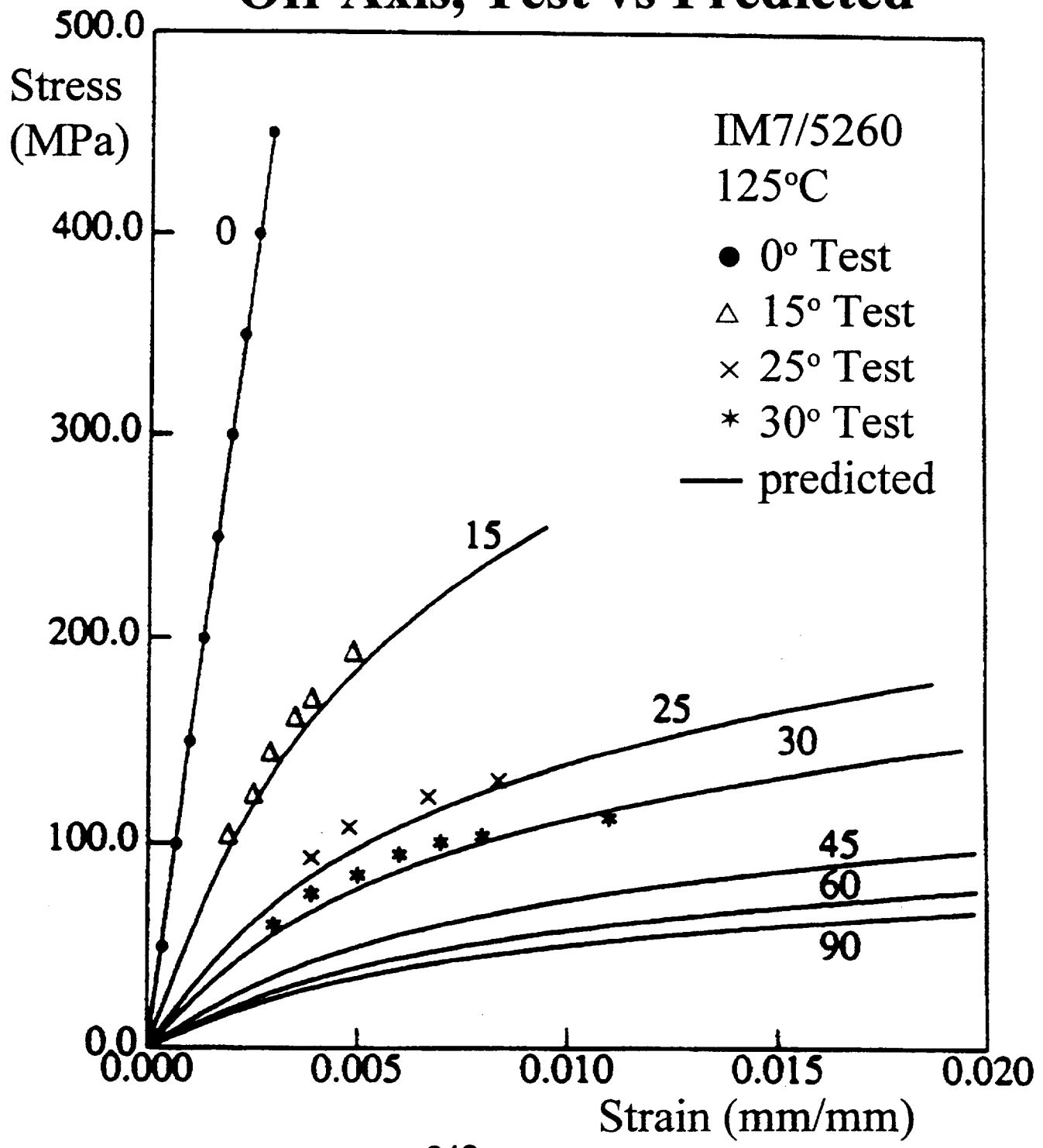
$$\text{Effective Plastic Strain} \quad \bar{\varepsilon}^p = \beta(\bar{\sigma})^\alpha$$

Geometry of Unit Cell



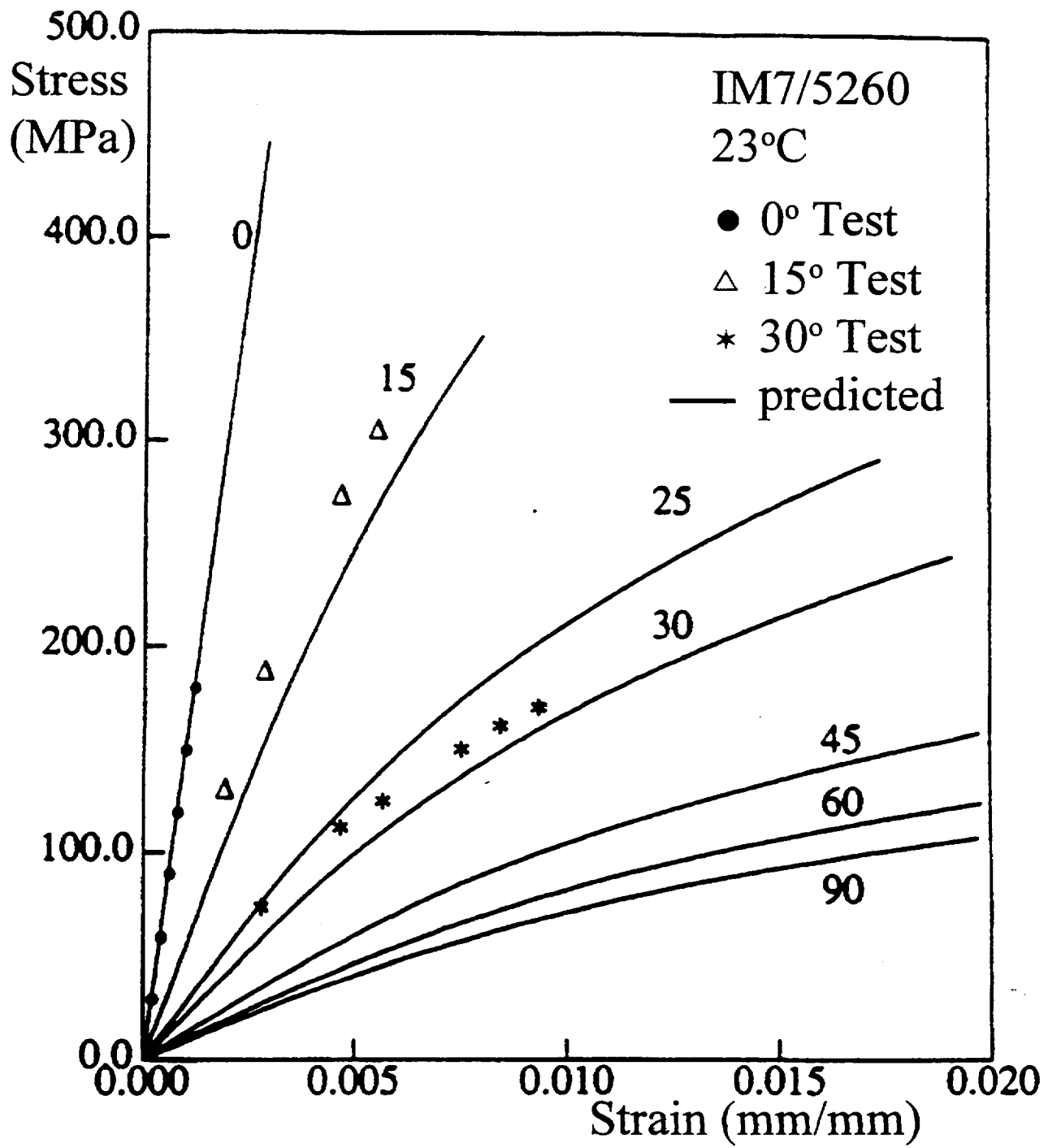
Micro-Model

Off-Axis, Test vs Predicted



Micro-Model

Off-Axis, Test vs Predicted



Fracture/Strength RT to (T_g -15°C)

- Edge Notched tensile tests
- Fracture surface morphology

Viscoelasticity, Physical Aging (T_g -15°,20°,25°C)

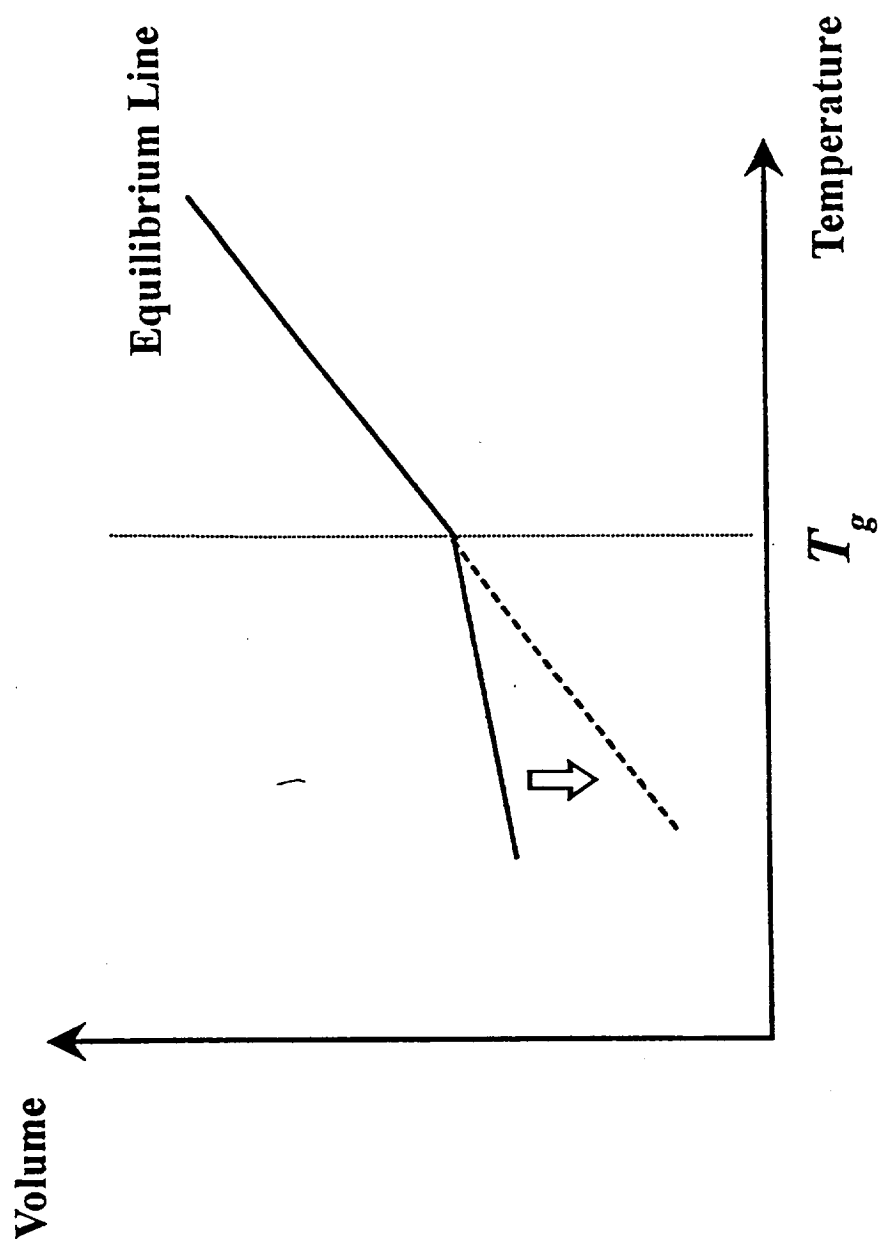
244

$$\varepsilon(t) = \int_{-\infty}^t S(t-\tau) \frac{d\sigma(\tau)}{d\tau} d\tau$$

$$Compliance \quad S_{ij}(t) = S_o e^{(N/\tau)^\beta}$$

$$Effective Time \quad d\lambda = a_{t_e}(t) dt$$

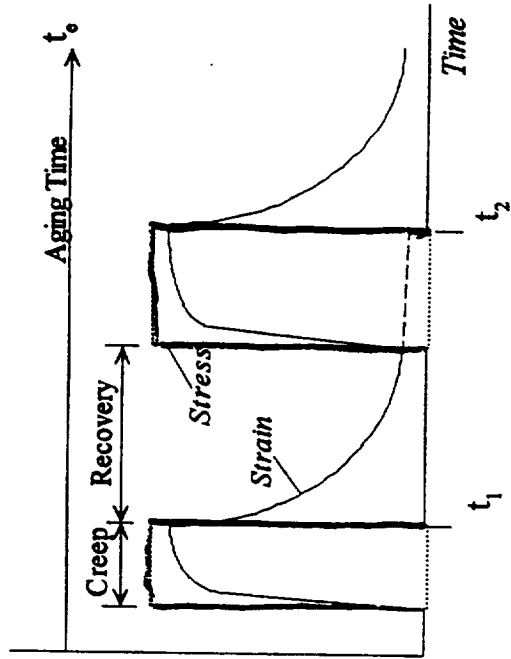
Free Volume Evolution During Aging



The Effects of Physical Aging on Creep Compliance

- Sequenced creep/recovery

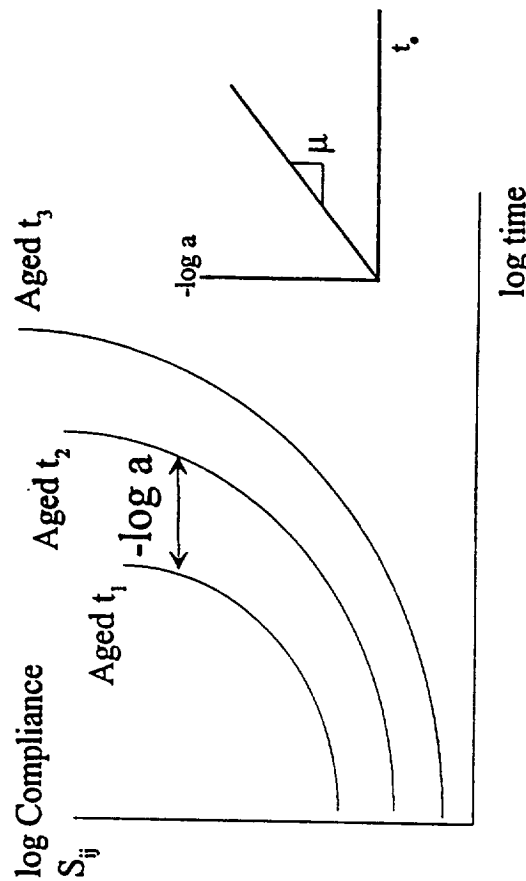
$$\text{For each sequence } \frac{\text{creep time}}{\text{aging time}} = \frac{1}{10}$$



- Measure compliance shifts and shift rates due to aging

aging shift factor $\equiv -\log a$

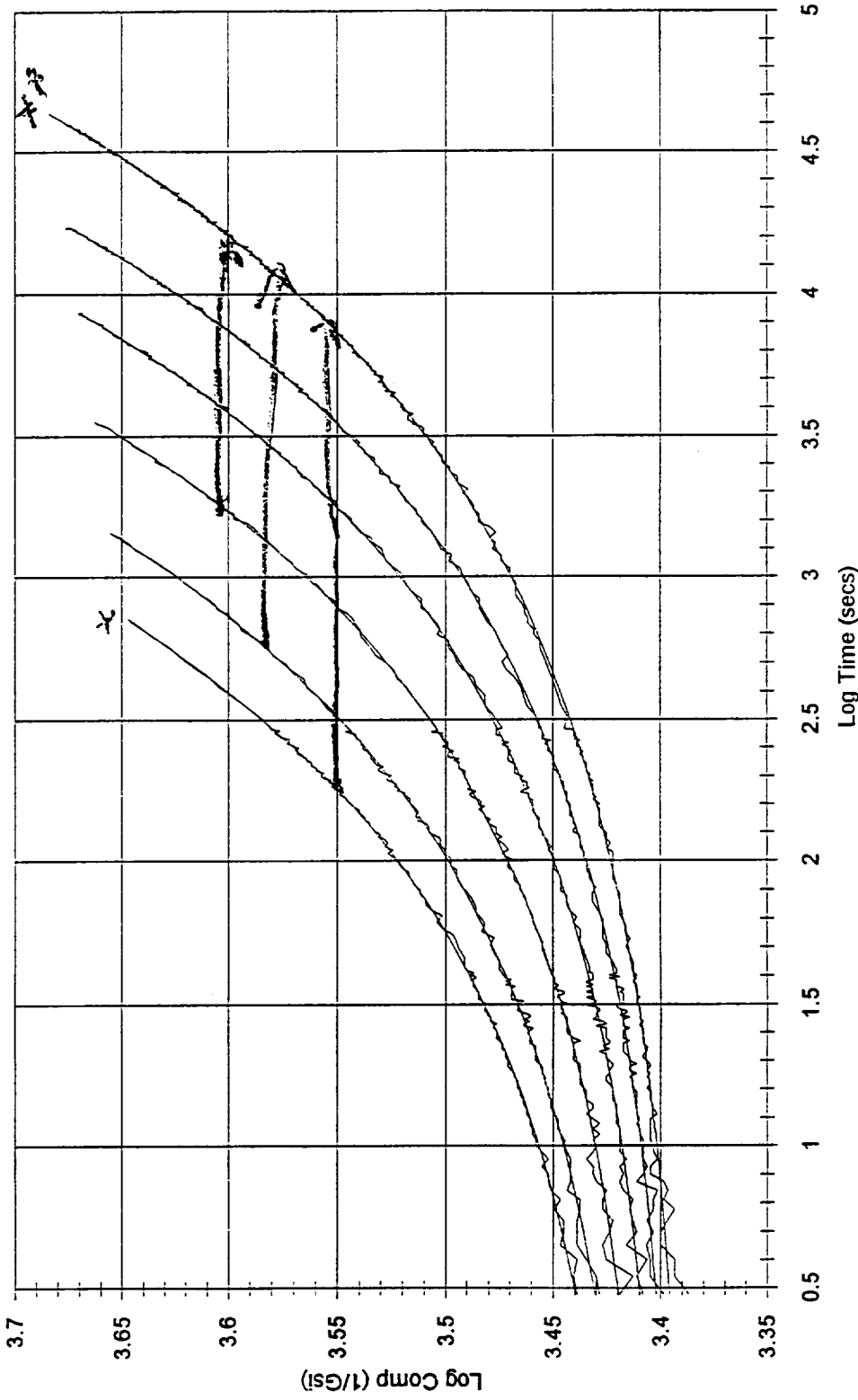
$$\text{aging shift rate } \equiv \mu = \frac{d \log(a_e)}{d \log(t_e)}$$



K3B-Resin Creep 8-14

Log Compliance vs Log Time

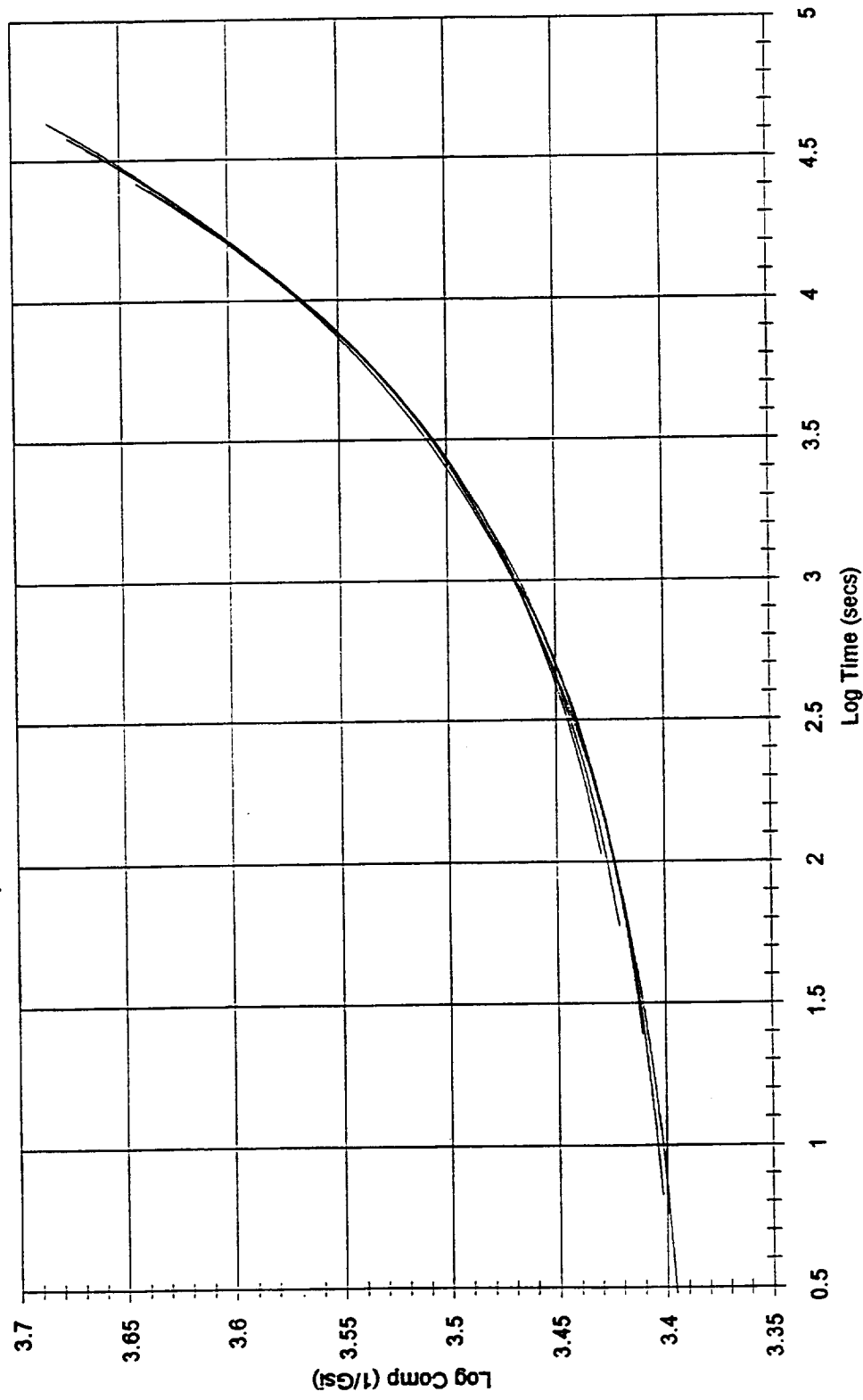
Resin Specimen 72-3 Test Temperature 215C Stress 387.6 Psi



K3B Resin Creep 8-14

Log Compliance vs Log Time

Resin Specimen 72-3 Test Temperature 215C Stress 387.6 Psi



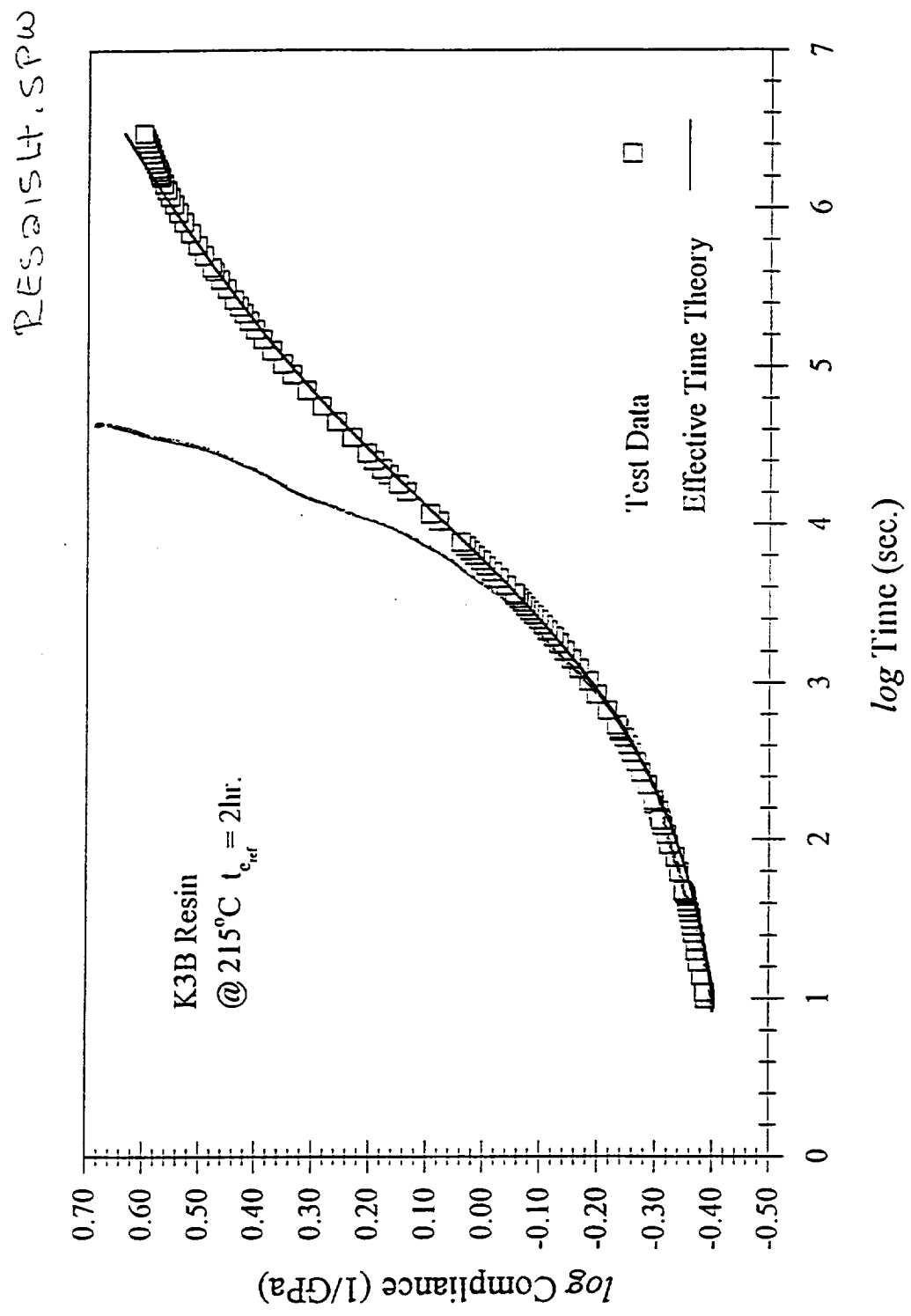


Figure XX: Long term 215°C resin data versus effective time theory prediction.

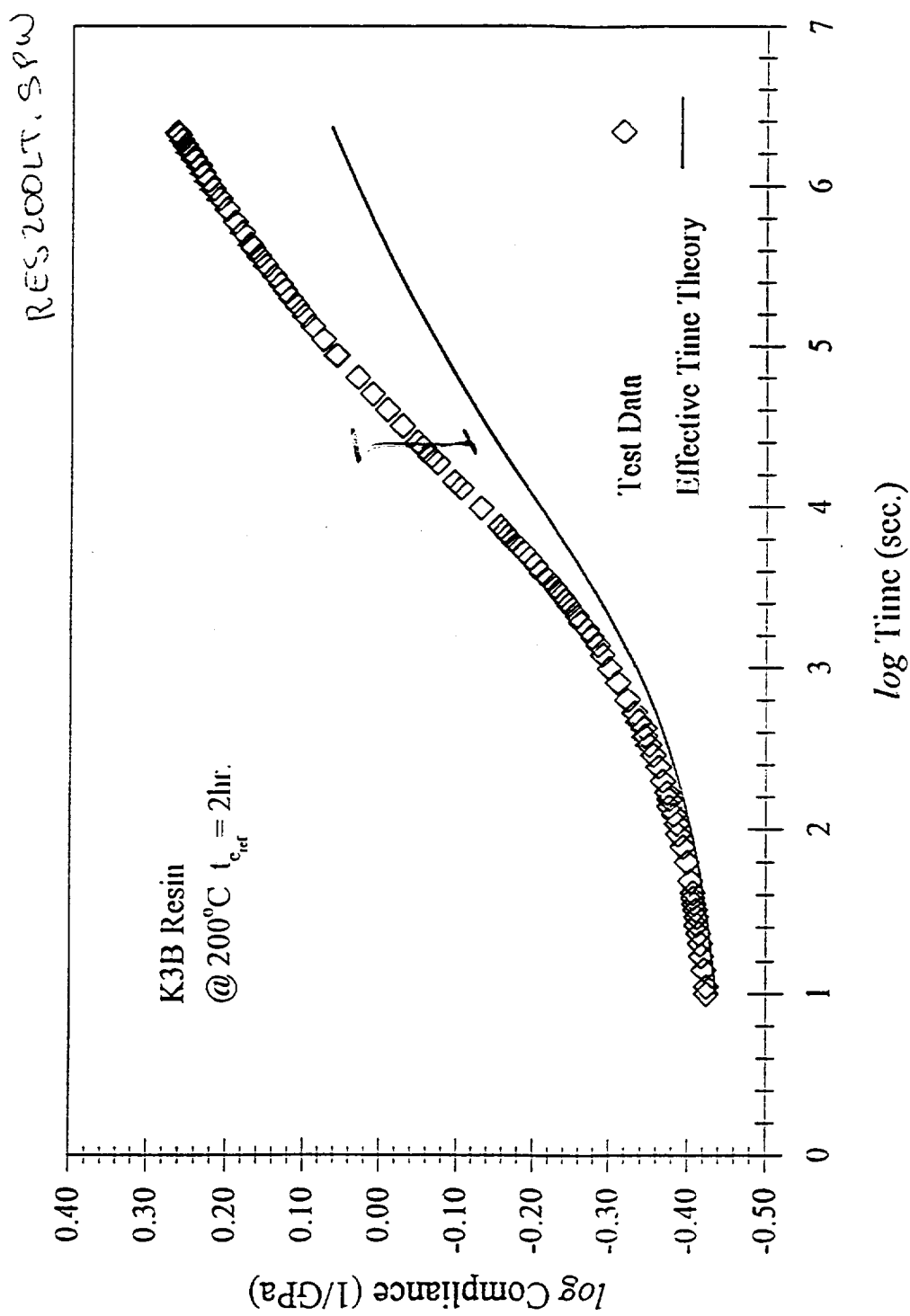


Figure XX: Long term 200°C resin data versus effective time theory prediction.

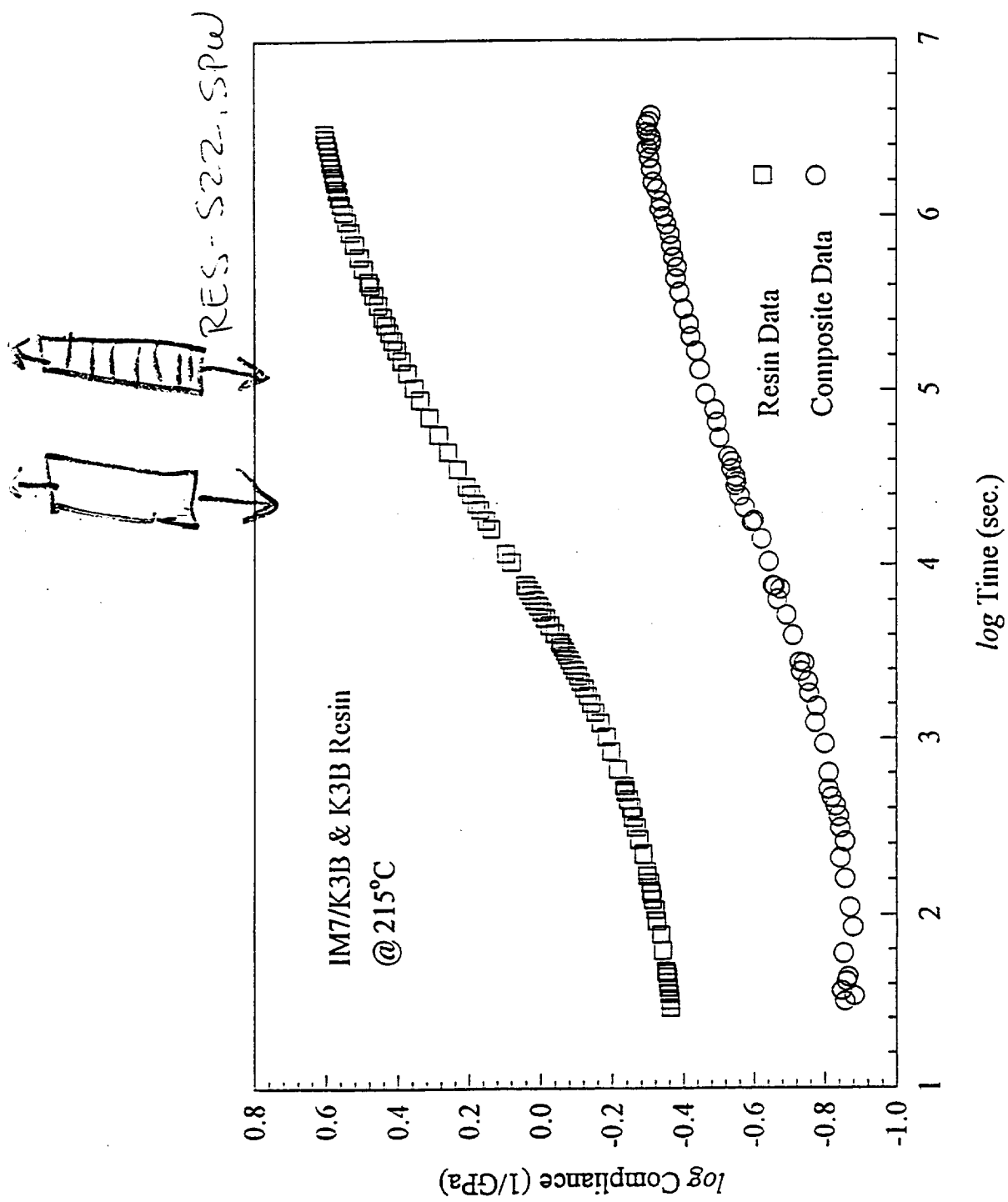


Figure: Comparison between resin and composite long term data at 215°C.

Computational Matl's. Related Issues

- Constituent Stiffness Properties $\not\Rightarrow$ Composite Properties
- Recovered Stiffness Properties $\not\Rightarrow$ Constituent Properties
- Can evaluate relative property differences between matl's.
- Unexplored material properties may correlate
eg. Strength, CTE, Interface, ?
- Alternative constitutive relations may be required
Need to expand beyond use of properties from macro level materials testing

| REPORT DOCUMENTATION PAGE | | | Form Approved OMB No. 0704-0188 |
|--|--|---|------------------------------------|
| <p>Public reporting burden for this collection of information is estimated to average 1 hour per response, including the time for reviewing instructions, searching existing data sources, gathering and maintaining the data needed, and completing and reviewing the collection of information. Send comments regarding this burden estimate or any other aspect of this collection of information, including suggestions for reducing this burden, to Washington Headquarters Services, Directorate for Information Operations and Reports, 1215 Jefferson Davis Highway, Suite 1204, Arlington, VA 22202-4302, and to the Office of Management and Budget, Paperwork Reduction Project (0704-0188), Washington, DC 20503.</p> | | | |
| 1. AGENCY USE ONLY (Leave blank) | 2. REPORT DATE | 3. REPORT TYPE AND DATES COVERED | |
| | November 1996 | Conference Publication | |
| 4. TITLE AND SUBTITLE | 5. FUNDING NUMBERS | | |
| Computational Materials Research | WV 505-63-50-18 | | |
| 6. AUTHOR(S) | | | |
| Jeffrey A. Hinkley and Thomas S. Gates, Editors | | | |
| 7. PERFORMING ORGANIZATION NAME(S) AND ADDRESS(ES) | 8. PERFORMING ORGANIZATION REPORT NUMBER | | |
| NASA Langley Research Center Hampton, VA 23681-0001 | | | |
| 9. SPONSORING / MONITORING AGENCY NAME(S) AND ADDRESS(ES) | 10. SPONSORING / MONITORING AGENCY REPORT NUMBER | | |
| National Aeronautics and Space Administration Washington, DC 20546-0001 | NASA CP-10190 | | |
| 11. SUPPLEMENTARY NOTES | | | |
| Proceedings of Workshop held January 4-5, 1996, at The College of William and Mary | | | |
| 12a. DISTRIBUTION / AVAILABILITY STATEMENT | | 12b. DISTRIBUTION CODE | |
| Unclassified - Unlimited Subject Category 27 | | | |
| 13. ABSTRACT (Maximum 200 words) | | | |
| <p>Computational Materials aims to model and predict thermodynamic, mechanical, and transport properties of polymer matrix composites. This workshop, the second coordinated by NASA Langley, reports progress in measurements and modeling at a number of length scales: atomic, molecular, nano, and continuum. Assembled here are presentations on quantum calculations for force field development, molecular mechanics of interfaces, molecular weight effects on mechanical properties, molecular dynamics applied to poling of polymers for electrets, Monte Carlo simulation of aromatic thermoplastics, thermal pressure coefficients of liquids, ultrasonic elastic constants, group additivity predictions, bulk constitutive models, and viscoplasticity characterization.</p> | | | |
| 14. SUBJECT TERMS | | 15. NUMBER OF PAGES | |
| Computational Chemistry, Molecular Mechanics, Monte Carlo Simulation, Constitutive modeling. | | 253 | |
| | | 16. PRICE CODE | |
| | | A12 | |
| 17. SECURITY CLASSIFICATION OF REPORT | 18. SECURITY CLASSIFICATION OF THIS PAGE | 19. SECURITY CLASSIFICATION OF ABSTRACT | 20. LIMITATION OF ABSTRACT |
| Unclassified | Unclassified | | |